AN ANALYTICAL AND EXPERIMENTAL INVESTIGATION OF HIGH PERFORMANCE SUSPENSION DAMPERS

Brian Warner

A Thesis
in
The Department
of
Mechanical Engineering

Presented in Partial Fulfillment of the Requirements
for the Degree of Doctor of Philosophy at
Concordia University
Montreal, Quebec
Canada

March 1996

ISBN 0-612-10908-9

Canada

ABSTRACT

AN ANALYTICAL AND EXPERIMENTAL INVESTIGATION OF HIGH PERFORMANCE SUSPENSION DAMPERS

Brian Warner, Ph.D.
Concordia University, 1996

Racing vehicle suspensions pose unique design requirements on dampers due to the performance criteria and excitations associated with quick lap-time and high speeds. The primary suspension requirement is the enhancement of traction, arising from the mechanical adhesion of the tire with the road and the aerodynamic downforce, to achieve maximum lateral and longitudinal acceleration of the vehicle. Isolation of the sprung mass constitutes the secondary requirement for the damper. An analytical and experimental study is performed to determine the influence of dampers on race-vehicle suspension performance, and to develop comprehensive analytical models. The dissertation research is carried out in seven sequential phases: (i) analysis and development of experimental test methods; (ii) development of analytical damper models; (iii) validation of damper models, using conventional test methods; (iv) development of quarter vehicle model and determination of performance criteria; (v) validation and response analysis of the candidate dampers in a quarter-car configuration; (vi) parametric analysis of damper parameters relative to performance criteria; and (vii) analysis of simplified models. Analytical models of three dampers are developed incorporating nonlinearities due to gas spring, friction, asymmetric multi stage damping valves, fluid compressibility and temperature dependence. The analytical models are thoroughly validated by comparison of responses with experimental measurements. A quarter-car simulator is designed and fabricated, an analytical model is developed, incorporating friction, tire and suspension spring, tire lift-off, and displacement

constraints, permitting validation of the analytical damper models under realistic vehicle excitations. The analytical response characteristics and the measured data are evaluated in terms of mechanical and aerodynamic traction, and oscillations of the sprung mass. A comprehensive parametric study is performed to study the influence of damper design on the performance criteria. The response behavior of simplified damper models are compared with those of the comprehensive model to demonstrate the significance of gas spring, temperature variations, valving, etc. From the study it is concluded that the damper and thus the vehicle suspension performance is specifically sensitive to temperature variations, and that the assymetric multi-stage valving provides a nonlinear tuning capability for performance enhancement.

ACKNOWLEDGMENTS

The author wishes to express his deepest thanks to Dr. S. Rakheja for his guidance and support prior to taking over supervision of this work, and his tireless efforts during the completion of this dissertation. The author would also like to thank Dr. S. Sankar, under whom this work was initiated, and who had the vision to provided the facility and environment for this research to be undertaken.

Thanks are due to the staff of CONCAVE Research Centre, who have assisted and supported this work over the years, particularly Dale Rathwell, Dan Juras and Arlene Zimmerman.

The support and assistance of various personnel at Chrysler Corporation is also gratefully acknowledged, particularly that of Dave Mienko, Tom Cowing and Darrel Hancock. The encouragement and support of ex-coworkers at Arvin Ride Control Products is also appreciated, especially Mark Lula, Tom Roll and Gwynne Williams.

The support and encouragement of my parents, Albert and Mary Warner, and my in-laws, John and Pat Firth, has been greatly appreciated.

I would also like to thank various engineers, racing personnel and friends, who over the years have taken the time to share their knowledge with me, these include, Geoff Burgess, Peter Dragffy, Peter Gibbons, Patrick Head, Will Moody, Ed Nathman, Terry Satchell, Gilles Vaincourt, Dr. Mark van Vliet, and John Webb.

Above all the author would like to thank his wife, Karen, and his children, Andrew and Lindsey for their love and patience.

To my wife and children I dedicate this work.

TABLE OF CONTENTS

CHAPTER 6

ANALYSIS OF CANDIDATE DAMPERS IN A QUARTER CAR CONFIGURATION

CHAPTER 7

CONCLUSIONS AND RECOMMENDATIONS FOR FURTHER WORK

LIST OF FIGURES

LIST OF TABLES

CHAPTER 1

INTRODUCTION AND LITERATURE REVIEW

1.1 INTRODUCTION

The performance characteristics of racing vehicles involved in competition sports are strongly related to their traction, directional control and stability properties. The race car performance, invariably evaluated in terms of lap time, is thus dependent upon the longitudinal and lateral acceleration developed by the vehicle. While the mechanical grip and aerodynamic down force determine the tire-road adhesion and thus the tractive effort at the tire-road interface, the lateral load transfer and vehicle roll determine the directional control and stability characteristics of the vehicle. The design and performance of vehicle suspension directly influences the road-holding, lateral load transfer and roll properties of the race vehicles. Developments in effective vehicle suspension springs and dampers have thus drawn increasing efforts from race car designers to enhance their lap-time performance.

Technological developments evolving from competition sports have been frequently implemented into conventional automobiles to improve their ride, handling, stability and safety performance. The rear view mirrors, seat belts, aerodynamic designs, four-bar motorcycle rear suspension, MacPhearson struts, disc brakes, etc. are examples of some of the developments which evolved from the race-car engineering during the past few decades. Developments in motocross suspension contributed to the design of compliant suspension with travel increased from approximately 100 mm to 300 mm to enhance the road-following ability of the wheel and ride quality. A suspension linkage with high wheel displacement ratio was realized to accommodate the increased rear wheel travel. Such suspension designs, however, posed high demand on the damping forces at

low speeds, which resulted in rapid fade and failures of the twin tube dampers. The extensive development efforts prompted by the strong desire to improve suspension performance contributed to the designs of monotube and remote reservoir dampers to enhance heat dissipation properties and reduce the oil foaming and the cavitation. Upon recognizing their performance benefits, these dampers were adapted to virtually every other form of racing, including: World Super Bike, Formula One, Indy Car, NASCAR, off-road truck, etc. While motocross suspension is designed to achieve a compromise between the impacts and vibration transmitted to the rider, and the road following ability of the vehicle, the race car suspension dampers are tuned to achieve improved traction performance. The race car suspensions are thus designed with relatively stiff spring and limited travel. The mechanical grip, aerodynamic down force, and the directional control performance characteristics of the race cars are attained through design and tuning of effective dampers.

Various active and adaptive suspension systems have been developed for the racing vehicles in the late eighties and early nineties. While the performance potentials of the computer controlled active suspension with rapid ride height and attitude control have been clearly demonstrated, the extensive development efforts and the associated costs have limited the use of such suspension. In view of the high development costs, the organizing body of Formula One competitions prohibited the use of such suspension following the precedent established by the Indy Car, NASCAR and various other racing organizations. This has prompted renewed development efforts in passive dampers, utilizing the knowledge gained from the developments in active and adaptive suspension.

Furthermore, it has been established that various active and adaptive suspension developed for passenger cars are not value added products and hence have been limited to a very small amount of passenger car production.

The developments in high performance dampers, have primarily, evolved from repetitive field testing and tuning. The need to develop effective analytical models and laboratory test methods for the different damper designs has been strongly emphasized by the race car teams and the automotive industries. The analytical models in conjunction with laboratory tests and limited field trials can enable the cost effective designs and performance analyses of the dampers. Although, a limited number of highly complex analytical models have been reported in the literature, the use of such models has been limited due to their high complexity and poor correlation with the measured data. The lack of efforts in development of affective analytical models, is perhaps attributed to the complexities associated with characterization of nonlinear low-and mid-speed compression and rebound valving, friction, temperature dependency, fluid compliance, etc.

In this dissertation, analytical models of different monotube and remote reservoir dampers are developed through systematic analytical and experimental characterization of their components. The analytical models of the gas spring, friction force, flows through rebound and compression valves, thermal expansion of the oil and components, and fluid compliance are developed and integrated to formulate the total damper models. Different test methodologies are investigated to characterize the various components and the total damper. The response characteristics of the models derived under varying harmonic and transient excitations are compared with those obtained from extensive experiments performed in the laboratory to demonstrate the effectiveness of the models. A performance criteria is formulated to facilitate the study of the influence of various design and operating variables of the dampers.

1.2 REVIEW OF RELEVANT LITERATURE

Studies on vehicle suspension encompass a diversity of subjects related to model development, development and analysis of different concepts, performance evaluations, etc. Extensive studies on race-car vehicle suspension, including those on simplified damper models, have been published in the literature. While the majority of these studies on race cars, focus on conceptual design details and field assessments, the studies on conventional road vehicles focus on development of analytical models, and analysis methodologies. The relevant published studies on both types of vehicle suspension are thus reviewed and grouped in sequence to develop the scope of the investigation.

1.2.1 Review of Studies on Race Car Suspension

The majority of published studies on race car suspension report the fundamental understanding of the race vehicle suspension kinematics and tuning methodologies for the dampers, springs and aerodynamic devices in order to achieve a competitive vehicle design [1,2,3,4]. The evolution of the current generation of race car dampers has been comprehensively described by Smith [5]. The study further presented the principles of operation of the damper, its interactions with the race car dynamics and traditional testing methodologies for the dampers.

The kinematic analysis of vehicle suspension linkage has been extensively analyzed and reported in many published studies. Crahan [6,7] presented comprehensive models for the kinematic analysis to study the steady-state handling performance of a race car. A race car model comprising a three-DOF (degree-of-freedom) vehicle model with Pacejka tire model, with look up tables defining roll height and stiffness from analysis of planar A-arm suspension, has been described by Jonash [8] to evaluate the handling and stability characteristics for synthesis of the suspension and determination of spring rates, based on

selected performance indices comparing the dynamic handling response of the vehicle. Case studies are presented along with a parametric study showing the sensitivity of coefficients with respect to vehicle response behavior. The dynamics of race car vehicles, together with the kinematics of the suspension, causes and effects of aerodynamic down force, tire models, suspension spring models, and the analytical models have been thoroughly described by Milliken and Milliken [9]. The authors further described the influence of damper force on the race car performance and emphasized the need for higher damping for race car suspension than that required for the conventional road vehicle suspension. Race cars utilize higher aerodynamic loading to generate cornering forces and thus require higher damping to reduce pitching motions and the magnitude of variations in the aerodynamic loading. The damping ratios of an Indy car, subject to high aerodynamic loads in an oval trim, have been computed as 0.938 and 0.747 respectively, for the front and rear axle suspension in the base line configuration.

The aerodynamic loading of a race car and thus the overall lap time is strongly influenced by the suspension design and tuning. It has been stated that a change in the ride height by 7.6 mm can lead to an additional 0.5 s to the lap time of an Indy car [10]. This is on a one mile oval track where aerodynamic loads play a critical role and the fastest lap times range from 21 to 22 s. The pitch dynamics of the vehicle suspension further effects the vehicles stability and its lap-performance time. The front wing of a Formula One car is particularly sensitive to pitch motions, which alters the magnitude of downforce significantly with only a small change in the attitude [11].

The effects of aerodynamic loads on the performance characteristics of the Formula One vehicles have been discussed by Wright [12]. The aerodynamic downforce directly affects the tire-load adhesion and thus the tractive and cornering effects developed at the tire-load interface. Race cars, in general, are able to generate aerodynamic downforce equivalent up to 2.5 g. The high downforce coupled with high cornering coefficients of

the tires (in excess of 1.5), permit the vehicle to generate transient cornering forces in the order of 4 g/s. The variations in the aerodynamic downforce, caused by ride height response of the suspension, therefore, affect the cornering and traction ability of the vehicles in a significant manner. It is thus vital to reduce the magnitudes of variations in the aerodynamic downforce by maintaining the clearance between the underbody and the track to a nearly constant value. The control of the ground clearance, however, necessitates the control of pitch and roll motions of the vehicle and its suspension. Relatively high stiffness suspension springs are thus frequently employed to reduce the pitch and roll oscillation of the vehicle. The combined heave and pitch motion, often referred to as "porpoising" and attributed to nonlinear variations in the downforce with the angle of attack, further contributes to excessive variations in the downforce. A high suspension damping ratio in the pitch mode is thus desirable to suppress such variations, which yields high damping in the bounce, as well as roll modes of oscillations of the vehicle. High suspension damping combined with relatively stiff suspension springs yield oscillation frequencies considerably larger than those of the conventional road vehicles. The typical resonant frequency associated with various modes of oscillation are as follows:

Frequency of Heave Mode: >5 Hz

Frequency of Pitch Mode: >8 Hz

Frequency of Roll Mode: >15 Hz

The race car suspension design and tuning thus form the most important tasks to achieve improved lap-time performance. The tuning of the suspension and dampers is frequently attained through repetitive field trials. Only limited studies have addressed the development of cost effective and efficient methods of suspension tuning through development and analysis of effective models. Kasprzak and Floyd [13] developed a simplified bicycle model of a race car to derive optimal damper parameters. The model

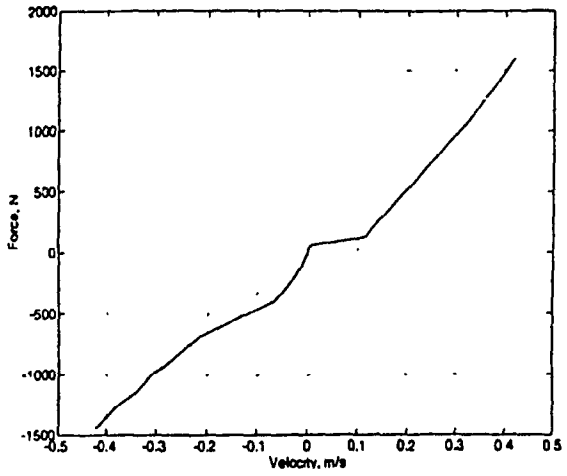

Figure 1.1 Force-velocity characteristics of a damper [13].

was used to tune the race car dampers through response analysis of the model, subject to the excitations generated by a four post shaker system. The vertical acceleration response measured at the front and rear of the sprung mass, the front and rear hubs and the exciters were used to determine transfer functions of the vehicle and suspension with different dampers. The relative performance evaluations of different dampers were carried out by comparing different transfer functions derived from the measured data. The study utilized linear models of the dampers, although the damper traces clearly revealed the nonlinear characteristics, as shown in Figure 1.1. The contributions due to the assymetric multi-stage valving, gas spring, hydraulic compressibility and the friction forces of the damper and the suspension were assumed negligible. A comparison of the transfer function derived from the model simulation and measured vehicle response characteristics revealed significant differences in the peak frequencies (4.8 vs. 5.8 Hz) and magnitudes, as shown in Figure 1.2. Although the simulator results revealed trends similar to those observed with the measured data, the results show considerable errors in the magnitude. The large errors are perhaps attributed to simplifying assumptions of the model associated with neglecting the assymetric multi-stage damping, friction and gas

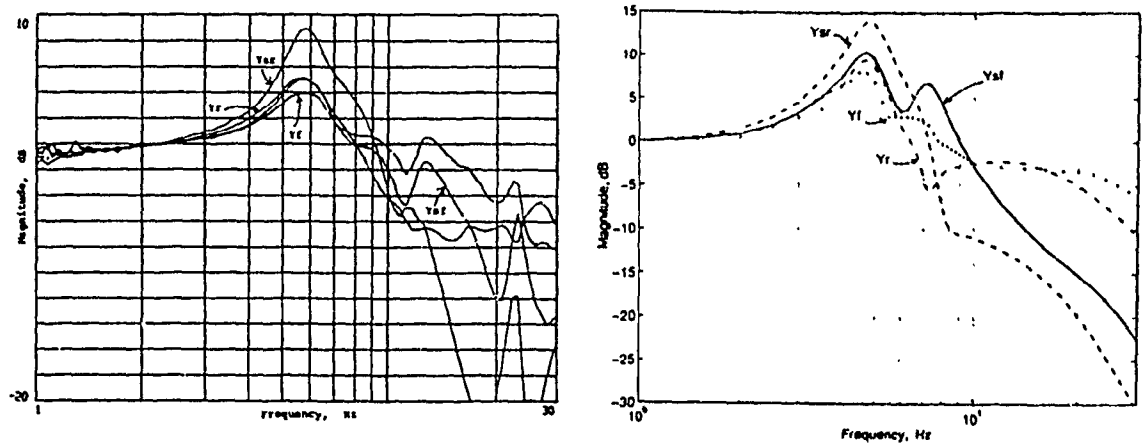

Measured Simulation

Ysf-front sprung mass, Ysr-rear sprung mass, Yf-front wheel hub, Yr-rear wheel hub

Figure 1.2 Acceleration transfer functions for a GTP car [13].

spring forces. Owing to the comparable trends, the simplified model has been used to select dampers to enhance the race car performance.

1.2.2 Review of Studies on Vehicle Suspension

While the developments in race car suspension have been mostly realized through field evaluations of the prototypes, the designs of road vehicle suspensions have evolved from systematic analytical and experimental studies. The systematic development efforts for the road vehicles has been prompted by the need to enhance ride, handling and stability of high production volume cars. It should be emphasized that the fundamental design concepts of production automobiles and their road vehicles frequently evolve from the efforts in the race car industry. The design objectives of the road vehicle suspensions, however, are considerably different from those of race vehicles. While the design objectives for the race vehicle suspension include high traction and cornering abilities, the road vehicle suspension designs involve a compromise between the ride comfort,

handling and directional control performance characteristics. To an extent, the methodologies developed to analyze and assess the road vehicle suspension can be applied to evaluate race car suspension.

The relevant published studies on automotive dampers, and suspension, and semi-active and active suspension are thus briefly reviewed to enhance an understanding of the similarities and differences between the race car and general road vehicle suspensions. The analytical methods are specifically reviewed for their potential applications to the race car dampers.

1.2.2.1 Automotive Dampers

The damper force, however, is a complex function of the design, valving, friction, operating temperature and gas spring. Analytical models of varying complexities have been developed to characterize the force-velocity behavior of the automotive dampers. Simanaltis [14] and Jackson [15] presented a comprehensive description of automotive dampers, including the history, operation of valves, effects of changes in valving components, testing, and manufacturing of typical passenger car units. The design of seals for the gas pressurized shock absorbers has been described by Yukimasa et al. [16]. Their study concluded that the frictional force of a particular seal design increases with both internal pressure and piston rod velocity, as shown in Figure 1.3. The study further revealed the time variant nature of the damper friction force, also shown in Figure 1.3.

A comprehensive study of twin-tube passive dampers has been reported by Lang [17] and summarized in the paper by Segel and Lang [18]. An analytical model of a twin tube damper incorporating orifice and blow off valving, compressibility of the oil, and vapor phase was developed to study the hysteresis and asymmetric multi-stage damping characteristics. The analytical model, validated using the experimental results derived

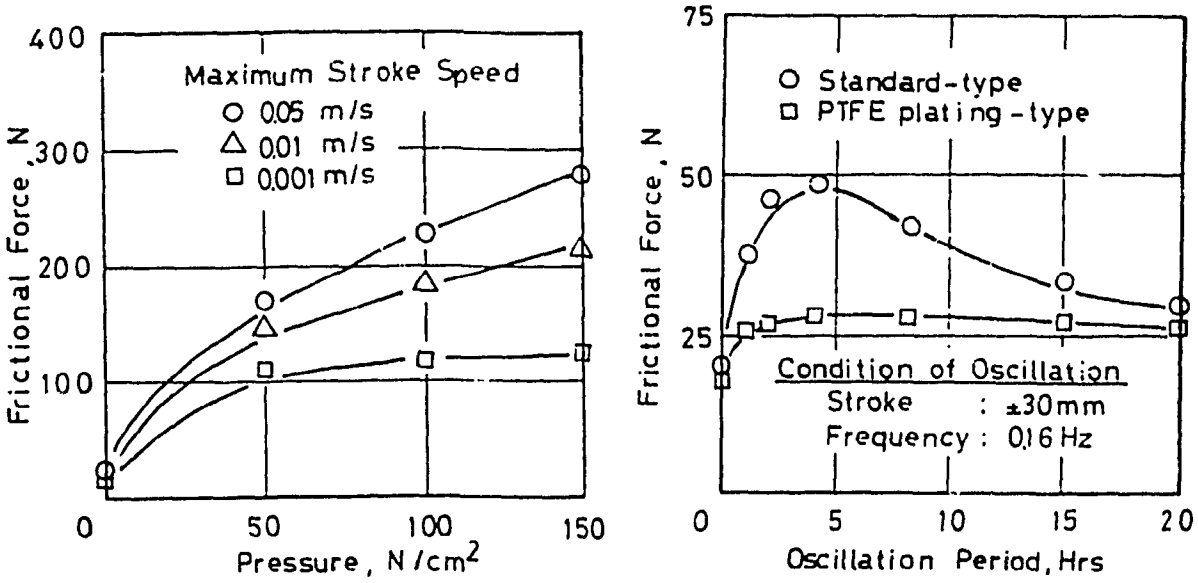

Friction-Internal Pressure Friction-Cycle Time

Figure 1.3 Variations in seal friction force with cycle time and internal pressure [16].

under deterministic square wave acceleration inputs, in the 1 to 10 Hz frequency ranges demonstrated an increase in damper hysteresis with frequency. The proposed model revealed excellent correlation with the experimental data under specified deterministic excitations, as shown in Figure 1.4. The validity of the damper model was demonstrated for deterministic inputs alone, while neglecting the compliance due to mounts and the effects of friction, bearing mounts, gas spring, and temperature variations. A suspension damper, in general, is subject to excitations caused by the relative dynamic motions of the sprung and unsprung masses. The performance evaluations of automotive dampers thus necessitate appropriate characterization of the dynamic motion of the vehicle. The analysis and validity of the proposed model has not been attempted under such realistic excitation.

The damping characteristics of a twin tube shock absorber incorporating the compliance due to the rubber bushings have been investigated by Anderson and Fan [19].

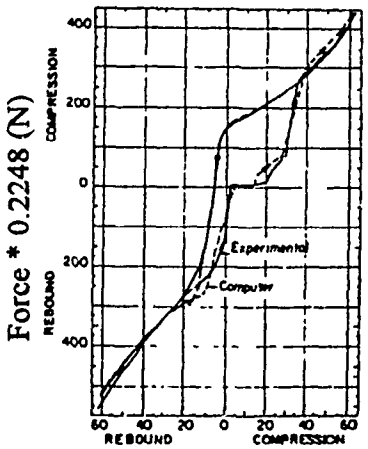

Figure 1.4 Comparison of analytical and experimental force-velocity characteristics of a damper configuration [19].

The damper valving is modeled using linear flow coefficients identified from the measured data and the effective compressibility due to gas, oil and dimensional changes in the damper body is incorporated within the model. While the contributions due to damper friction are considered negligible, the model revealed reasonably good correlation with the experimental data. The results of the study concluded that the rubber mounts increase the hysterisis of the damper particularly at higher frequencies. This is perhaps one of the reasons that the rubber bushings are not used in mountings of race car dampers. Karadyi and Masada [20] developed a nonlinear shock absorber model based upon the coefficients, determined from the experimental data. Describing function techniques are used to characterize the damping forces. The proposed model is developed to incorporate asymmetric damping, dry friction and hysterisis due to back lash and fluid compressibility. The damping model, however, does not describe the multi-stage damping properties of the damper. The model was validated using laboratory test data obtained under low velocity excitations (0.4 Hz), which explains the lack of

multistage damping. The simulation results show relatively poor correlation with the experimental data, when compared to those demonstrated in works presented by Lang [18] and [19]. The effects of fluid compressibility on the damper hysteresis was represented by an equivalent spring in series with the damping model. Modeling of the compressibility as a spring in series with the damping model is also used and validated by Moline et al. [21] under excitations ranging from 0.46 to 9.06 Hz. The details of the proposed model, however, are not fully described by the authors.

The experimental and analytical studies on automotive dampers have emphasized the strongly nonlinear force-velocity characteristics attributed to valving, friction, gas spring, fluid compressibility, and thermal expansion of oil and the damper components. Development of semi-empirical models of the dampers have thus been attempted to accurately describe the behavior within a specified operating range.

Reybrouck [22] present a semi-empirical damper model, where the coefficients were identified from experiments. While the fluid flow is assumed to be incompressible, a correction factor related to the damper acceleration is introduced to account for the effects of compressibility. The proposed model incorporates multi-stage valving. and friction force modeled as an offset, while the contributions due to thermal and displacement effects are assumed negligible. The gas spring force is modeled using the ideal gas laws, while the initial volume determined by measurement. The proposed model results revealed good correlation with the experimental data.

1.2.2.2 Suspensions

Increasing demands placed on the ride, handling, and stability performance of automobiles, and stability dynamics and pavement load characteristics of heavy vehicles have resulted in extensive theoretical and experimental investigations in the role of

vehicle suspension. The potential performance benefits of different concepts in semi-active and active suspensions have further prompted numerous theoretical developments for their analysis. The majority of theoretical studies on suspension concepts are carried out using a simplified quarter-car vertical dynamic model neglecting the inter-axle coupling, and roll and pitch dynamics of the vehicle. The quarter-car two degree of freedom (DOF) models have been extensively used to study the role of damping and to carry out relative performance analyses of different suspension concepts. The quarter-car model comprises a sprung mass supported on either linear or nonlinear suspension spring and damper, and an unsprung mass supported between the suspension components and a linear or nonlinear tire spring [23-26]. The performance characteristics of different suspension concepts in the simplified two-DOF models are evaluated for deterministic and stochastic excitations, characteristics are evaluated in terms of these three parameters: passenger discomfort, suspension deflection and tire load variations [23-26]. The quarter vehicle models, however, assume negligible influence of friction, bump stops, asymmetric damping, hysteresis in damping, changes in linkage geometry, etc. The mathematical relationships between the transfer functions for sprung mass acceleration (a measure of ride quality), suspension deflection and the tire deflection have been investigated by Hedrick and Butsuen [26]. The study concluded that the three performance functions are interrelated and that a gain in one of the functions is accompanied by the deterioration of the other performance functions throughout the entire frequency range, except near the wheel-hop frequency. The design of suspension thus involves a complex compromise among these performance functions.

The ride quality, tire loads and suspension deflection performance characteristics have also been investigated by Sharp and Hassan [27] using a linear quarter vehicle model subject to random excitations. The study of influence of varying damping and stiffness coefficients concluded the need for suspensions with variable damping and

stiffness coefficients to achieve an improved compromise. A quarter-vehicle ride dynamic model comprising a simplified twin-tube damper model derived from the study of Lang's work [17] has been investigated by Hall and Gill [28]. Although the response of their simplified damper model to square wave acceleration excitation showed reasonably good correlation with the experimental data (Figure 1.5), the degree of correlation is inferior to that demonstrated by Lang [17] and shown in Figure 1.4. The authors attribute the errors to inaccurate damping coefficients of the valves, or error in the experimental data. It should be noted that Hall and Gill [28] analyzed the damper model and the quarter-vehicle response using a digital computer, while Lang [17] performed the analysis of the damper alone using a analog computer. The quarter-car model, excluding the nonlinearities due to friction, bump stops, rubber mounts, suspension linkages, tire damping and wheel lift-off was analyzed for random road excitations to evaluate the ride performance of linear and bilinear damper models and the simplified nonlinear damper model based on Lang's work. The study concluded that linear and bilinear dampers yield better ride then the nonlinear damper.

Recognizing the potential performance benefits of variable coefficient dampers, numerous concepts in semi-active and sequential dampers have been proposed and investigated. A concept of a tunable sequential hydraulic passive damper has been proposed and analyzed by Rakheja et al. [29]. The study compared the performance characteristics of the proposed concept to those of a fixed orifice passive damper model and semi active sequential damper model. The analytical model developed in the study incorporated the nonlinearities due to orifice flows, gas spring and pressure relief mechanism. The ride response characteristics of the proposed models evaluated using a single-DOF model subject to harmonic excitations and a two-DOF quarter vehicle model subject to harmonic and transient excitations were compared to demonstrate the performance potentials of the proposed concept. While the sequential damper proposed

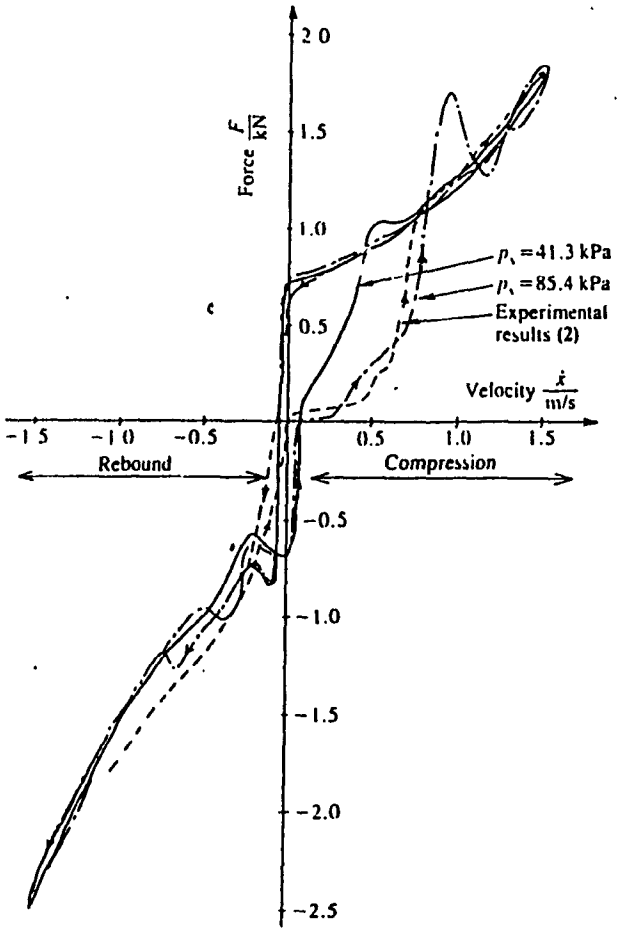

Figure 1.5 Comparison of analytical and experimental response of a twin-tube damper (Excitation; 38 mm amplitude at 5 Hz) [28].

in the study is similar to a conventional passive automotive damper, with multi-stage asymmetric damping, the control valves are proposed to be externally mounted to facilitate tuning.

The performance characteristics of a telescopic front fork and a remote reservoir rear dampers used in motorcycle suspensions have been experimentally and analytically investigated by van Vliet [30-32]. The analytical models comprising asymmetric damping due to orifice flows, check ball in series with spring and orifice blow-off valves, ball and plate one way valves, gas and helical springs, stiction and hydraulic bump stops

were analyzed for deterministic and stochastic excitations derived from field measurements using the equivalent linearization methods. The damper characteristics were experimentally validated using an equivalent mass laboratory tester. An analytical model of a passive, nonlinear hydropnematic suspension system compromising polytropic gas spring, orifice flows, coulomb friction, bump stops and hydraulic compressibility has been developed and analyzed by Joo [33]. The analysis of the suspension model under shock and harmonic excitations demonstrated significant ride performance gains for a multi-wheeled vehicle.

Although some of the damper models described above include the effects of friction, gas spring and fluid compressibility, only a few studies have quantitatively discussed the influences of such nonlinearities on the damper characteristics. The effects of suspension friction on the response characteristics of a simple linear quarter-vehicle model and a multi-DOF vehicle model, subject to random excitations arising from smooth and rough roads, have been discussed by Yabuta et al [34]. The nonlinear friction force is analyzed using a statistical linearisation technique, the study concludes that the suspension friction is detremental to the ride performance. The study further demonstrated that the effect of friction will depend not only on its magnitude but also the road surface, vehicle velocity and tire stiffness. Their conclusion have been further supported through a study conducted by Ilosvai and Szucs [35] on the effects of dry friction on the quarter-car model response. The study demonstrated the detremental effects of dry friction on the ride quality response, and that suspension friction was related to increased probability of wheel lift-off from the ground.

While most of the above reported studies are concerned primarily with the ride quality of the vehicle, the design of a suspension affects the handling performance in a significant manner, particularly in the case of high performance and racing vehicles. In some of the studies described above [23,25,27], the handling performance of a particular

suspension is evaluated in terms of the dynamic variations in tire load in a quarter-vehicle model. High magnitudes of variation in the tire load are related to poor handling performance. The subjective nature of most handling evaluations and the significance of the driver interactions have been emphasized by Sano [36]. Analysis of vehicle handling response is frequently performed through development of yaw-plane or three-dimensional vehicle models subject to steering excitations. Although a large volume of literature exists on handling response analysis, only few studies have analyzed the role of vehicle suspension in handling performance. Loos and Dodlblbacher [37] performed analysis of handling using an ADAMS computer simulation model with over 100 degrees-of-freedom, nonlinear large scale displacements and suspension bushing and tire models. The authors investigated the influence of various suspensions and design factors, including: McPherson strut geometry and compliance, shimmy, front suspension harshness, and comparison of rear suspension. The authors, however, do not describe the suspension damper model used in the study. The model response evaluated for a rapid (0.4 s) ramp steering input showed good correlation with the experimental data during the first cycle, and considerable divergence in the results in the later periods.

The studies on analysis of different suspension systems have been comprehensively reviewed by many researchers [38-40]. These articles discuss the analytical techniques, suspension and vehicle models, semi-active and active suspension and performance analysis. These studies further identify the further studies needed in the discipline. In a review article, Morman and Giannopoulus [38] concluded that 'more realistic models for shock absorber behavior need to be developed' along with studies on the characterization and role of dry friction. The article further concludes that most of the studies on active suspensions are based on linear assumptions, which are supported by only limited experimental verifications. A comprehensive review of studies on semi-active and active suspensions has been reported by Sharp and Crolla [39]. It was concluded that the 'study

of behavior and design influences under discrete event excitation is comparatively undeveloped, especially in relationship to subjective performance.' Furthermore, most of the developments in the area are of theoretical and conceptual nature, which need to be proven through hardware realization and laboratory and road testing. Bernard et al [40] review developments in active suspension, multi-body dynamic models, rear steer and aspects of commercial vehicle dynamics. It was further established that most developments are of a theoretical nature, and that one case of experimental verification was hindered by the nonlinearities of the actuators.

1.3 SCOPE OF INVESTIGATION

Various analytical and experimental studies, reported in the literature and briefly reviewed in the above sections, have established that the ride quality and handling performance of the vehicle is strongly related to its suspension damper. The race car performance, evaluated in terms of lap-time, and longitudinal and lateral traction, has been related to the damping properties of the suspension. Although a number of semi-active and active damping concepts have been shown to enhance the vehicle performance, their banning by virtually all governing bodies of competition vehicles ensures the further development of passive race car suspensions. These developments continue to focus on realization of effective suspension dampers, mostly through inefficient and costly repetitive field trials. A need to develop effective analytical models of the modern dampers has been strongly emphasized by various racing teams and automotive companies. Although, validated analytical models of twin-tube dampers employed in passenger cars have been developed, only limited efforts have been made to develop effective analytical models of high performance monotube and remote reservoir dampers.

While the strong dependency of the damping forces on variations in operating temperature have long been identified, no attempts have been made to include this

dependency. Furthermore, a need to accurately characterize the damper friction, gas spring forces, and compliance has been identified to develop effective models.

The overall objective of this thesis research is thus formulated to derive comprehensive analytical models of high performance suspension dampers through systematic parameter identification. The specific objectives of the dissertation research are as follows:

a. Develop analytical models of the various damper components to characterize the contributions due to gas spring, Coulomb friction, non-linear multi-stage and assymetric damping valves, fluid compressibility and thermal expansion for the candidate race car dampers.

b. Develop test methodologies for characterization of component behavior, specifically, the gas spring, Coulomb friction, valving, fluid compressibility, and thermal expansion.

c. Perform laboratory tests and identify component model parameters and coefficients through analysis of the experimental data.

d. Validate the component models using the experimental data, and integrate the different component models to derive total models for the monotube and remote reservoir dampers.

e. Investigate the damping characteristics of candidate dampers under varying levels of harmonic excitations and operating temperatures using a conventional test stand. Investigate the validity of the damper models for a wide range of excitation velocities, displacements and operating temperature, using the experimental data.

f. Develop a quarter vehicle test stand and associated analytical model to study the damper performance under more realistic excitations. Investigate the validity of the

total damper and quarter-vehicle model under sinusoidal and step excitations of varying amplitudes.

g. Formulate performance criteria to asses the damper performance in a quarter vehicle configuration relating to the requirements of race car suspension.

h. Perform a comprehensive parametric variation study to investigate the influence of design and operating parameters on the proposed performance criteria.

i. Develop simplified models of a candidate damper and compare the response characteristics of the quarter-car model with the simplified damper models, and the comprehensive damper model to the measured response, to demonstrate the significance of the various component nonlinearities.

1.3.1 Organization of the Thesis

In Chapter 2, design details and performance characteristics of the candidate racing vehicle dampers are briefly described, and two different constructions are identified based on the location of the gas chamber relative to the damper body, and the design of the valving. Two experimental methodologies to characterize the force-velocity and force-displacement properties of the dampers are discussed in view of their benefits and limitations. Selected experimental results are discussed to enhance an understanding of the damper characteristics and the role of multi-stage assymetric damping, compressibility effects, friction, gas spring and the thermal effects on the damping, friction and the gas spring forces.

Analytical models of various damper components, such as gas spring, friction, multi-stage valving, thermal expansion and fluid compressibility are developed in Chapter 3. Extensive laboratory tests are performed and the data is analyzed to identify the different model coefficients. A comprehensive Coulomb friction model is developed

as a function of the sign of velocity, damper displacement, and operating temperature. A test methodology is proposed to characterize the low-speed gas spring and friction force properties of the candidate dampers. Gas spring models are developed using the ideal gas laws and the thermal expansion of oil. The characteristics of different compression and rebound valving mechanisms are modeled using the fundamental flow and pressure equations. Analytical models defining the multi-stage characteristics of the valving are developed based on combined parallel and series flows through valving mechanisms. The effects of fluid compressibility are analyzed and two different compressibility models are derived; pressure independent and pressure dependent. The influence of variations in the operating temperature on the damping properties is represented by considering the thermal expansion of oil and damper components. The components models are integrated to derive the total damper models.

In Chapter 4, the various coefficients for the component models are identified through analysis of the experimental data. The response characteristics of the analytical model are compared with those derived from the experimental data to demonstrate the validity of the models. The friction force is characterized as a function of the displacement using the data derived from the static force measurements. The data is further used to compute the initial gas volume and pressure. The experimental data derived from very low speed harmonic excitations at varying temperatures is used to determine the dynamic and temperature coefficients of the friction model, the polytropic coefficient of the gas spring, and the effective thermal volumetric expansion of the oil. The valving and fluid compliance coefficients are derived from the test data attained under sinusoidal inputs of varying frequency and displacement amplitudes. The coefficient of thermal expansion of oil is also identified from experimental data obtained over a range of operating temperatures. The total damper models are thoroughly validated for harmonic excitations of varying amplitudes and frequencies.

In Chapter 5, the quarter-car test stand is developed to study the damper performance under realistic excitation. The quarter-car simulator is analytically modeled incorporating the friction between the sprung and unsprung masses, and the input, nonlinear relative displacement limit constraints, and loss of tire ground contact. An additional quarter car model is developed that more closely approximates a racing vehicle suspension, for usage in the parametric variation study. The methodology used to determine the coefficients of friction of the links in the quarter vehicle model is also presented.

In Chapter 6, the damper models in a quarter-vehicle configuration are analyzed for harmonic and transient excitations. The damped and undamped quarter-vehicle models are thoroughly validated using the results derived from experiments performed in the laboratory. Methods of analyzing the suspension performance related to requirements of the race cars in the frequency and time domain are developed. Analysis in the frequency domain is performed using two different amplitudes in order to observe the effects of the nonlinearities. A parametric study of a candidate damper model is performed in the frequency domain using the quarter vehicle model to enhance an understanding of the influence of different design and operating variables on the performance. Two simplified damper models are further developed and their response characteristics are compared with those of the comprehensive model to demonstrate the significance of various component models.

The highlights of the dissertation research are finally discussed in Chapter 7 together with the major conclusions and the recommendations for future work.

CHAPTER 2

DAMPER CHARACTERISTICS AND TEST METHODS

2.1 INTRODUCTION

The total dynamic force developed by a hydraulic damper is the resultant of the hydraulic, gas spring and frictional forces, which are complex functions of the fluid compressibility, valving, velocity, acceleration, temperature, etc. Although numerous analytical models of varying degrees of complexities and simplifying assumptions have been developed and analyzed, the majority of these models are considered valid only under specific operating conditions. A number of models have utilized equivalent linearization techniques for response analyses [30,41]. While such methods provide the response characteristics in the frequency domain under specified conditions, the nonlinear time-domain behavior of the damper cannot be characterized using these methods. Many other models are considered valid for low acceleration levels, while the acceleration dependent lag caused by fluid compressibility is assumed negligible [18]. Analytical models, derived from the analysis of various damper components, are known to provide good correlation with the measured data in the frequency as well as time domain [18,30]. Such models however, are quite complex and require prior knowledge of numerous design constants.

The lack of an appropriate analytical model is perhaps attributed to the strong dependence of the damping characteristics on various design and operating conditions, and the complexities associated with development of the accurate analytical representations. It is thus desirable to establish a thorough understanding of the static and dynamic contributions of the various design and operating factors, through a series of laboratory tests, prior to developing an analytical model of the damper. Such a study will enable the identification of the most significant design parameters to be incorporated in the model.

In this chapter a brief review of hydraulic dampers is presented and three candidate dampers are selected for the thorough experimental investigation. The test methodologies used to measure damping, gas spring and frictional forces over a range of excitation amplitudes, frequencies and operating temperatures are described. The test data is analyzed and the relative significance of various test parameters is discussed for the candidate dampers.

2.2 DESCRIPTION OF DAMPERS

The design and performance criteria of suspension systems for high performance racing vehicles are significantly different from those of conventional automobiles. Performance criteria for automobile suspensions, in-general, include: isolation of the occupants from road induced vibration and noise; suspension rattle space; handling and directional stability [27]. The performance characteristics of racing vehicles are primarily evaluated in terms of the lap time which, is a function of the acceleration that can be generated laterally and longitudinally [42]. The acceleration performance of a vehicle is strongly dependent upon the traction arising from mechanical or aerodynamic grip [1]. The aerodynamic grip is directly related to the component of the normal force acting on the tire due to aerodynamic loads. The position of the vehicle body relative to the road surface is known to be one of the major factors contributing to the aerodynamic grip, and thus provides a measure of the suspension's performance. Mechanical grip refers to the tractive forces which are not attributable to aerodynamic downforce, arising from the tire-road adhesion properties, and is determined from the road holding abilities and the dynamic weight transfer. While ride comfort, suspension travel, and handling constitute the primary design criteria for conventional automobiles, the directional control and stability are primarily emphasized for the design of race vehicle suspension. The design and performance requirements of race vehicles are therefore considerably different, and vary from track to track. As an example, high performance race vehicles employ

suspensions with damping coefficients in the 0.6-0.8 range, while conventional automobile suspensions are designed to yield damping coefficients in the order of 0.25 [43].

Apart from the differences in damping properties, the dampers are subjected to varying levels of excitations dependent upon the application. For road racing vehicles, the damper is expected to control the unsprung and sprung masses at relatively low velocities. The relative velocity across the damper of a Formula 1 car suspension remains below 0.025 m/s for 90% of the time [11], while the peak velocity across an Indy race car damper approaches 0.38 m/s [44]. In the case of a road racing super-bike, peak velocities of 1 m/s can be frequently experienced [45]. A typical family sedan damper may experience velocities up to 3 m/s, and damper velocities of 4.3 m/s have been reported for off road racing trucks [46]. Unlike conventional automobile dampers, the design and performance evaluations of racing car dampers are primarily concerned with low velocity operation.

Dampers are also subject to other evaluation criteria, which differ considerably between racing and passenger vehicles. These performance criteria include: operating temperature (-40°C to 95°C for the family sedan, typically 10°C to 150°C for most North American racing vehicles), endurance (160,000 km for the sedan vs. the finish of the race for racing vehicles), noise (as little as possible for the sedan, of no concern for the racing cars), light weight (while important for the sedan, it is extremely important for the race car), and cost (approximately $5 to $20 for the sedan vs. $400 to $10,000 for the racing car). The different performance criteria and factors for race cars and conventional automobile dampers are summarized in Table 2.1.

2.2.1 Damper Characteristics

Since the design details and operating principles of hydraulic dampers have been extensively dealt with in the literature [15,17,47], only the important and relevant design

TABLE 2.1
PERFORMANCE CRITERIA FOR RACING CARS AND CONVENTIONAL AUTOMOBILE DAMPERS

Criteria	Passenger Car	Race Car
Operating Temperature	-40°C to 95°C	10°C to 150°C
Expected Life	160,000 km	160 to 800 km
Subjective Noise	Very Low	No Concern
Weight Concern	Slight	Very High
Compressible Medium	Air at atmospheric or nitrogen at low pressures	Nitrogen at 0.7 to 2.6 MPa, separated from oil
Approximate Cost	$5 to 20	$400 to 10,000
Approximate Damping Coefficient	0.25	0.6 - 0.8
Permissible Variation in Force	+/- (8.8% + 20N) to 30%	0 to 10 N
End Mounts	Rubber Bushings	Spherical Bearings

aspects of the dampers are discussed in this section. The hydraulic dampers, invariably, dissipate thermal energy generated by restriction of oil flows. Pressurized nitrogen gas is frequently used as a co npressible medium to allow for the displacement of oil by the differential rod volume. The hydraulic resistance in the damper is controlled using various combinations of valving mechanisms, which are effective over different speed ranges. The hydraulic resistance of a damper is frequently tuned for three distinct ranges of velocity, in both rebound and compression, in order to achieve the optimal vehicle response. These velocity ranges are termed as low, mid and high as illustrated by the typical characteristic curve of a damper in Figure 2.1. The low and mid speed results presented in the Figure have been derived from the laboratory tests performed on a Koni

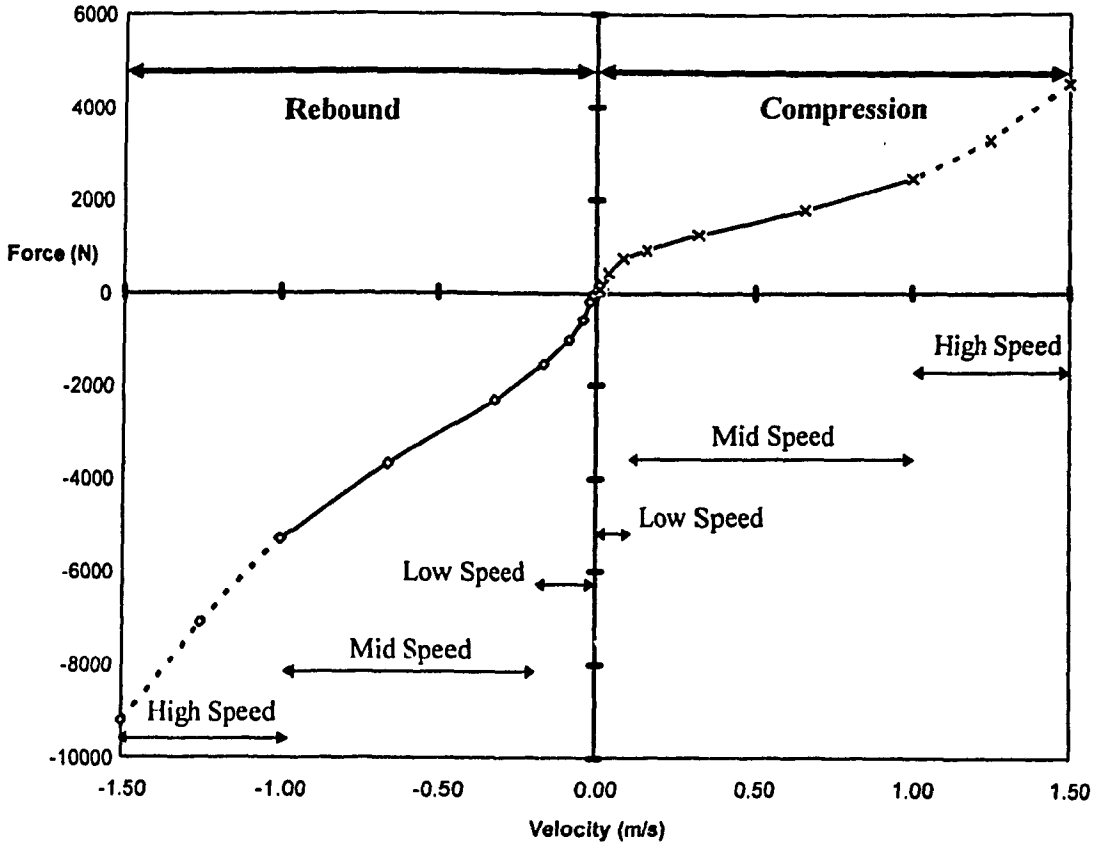

Figure 2.1 Force-velocity characteristics of a damper.

damper, while the force data in the high speed range is slightly altered to enhance the illustration, as illustrated by the dashed line. The characteristic curve describes the relationship between the measured peak force and peak velocity generated by sinusoidal excitations of varying periods and/or amplitudes.

For illustrative purposes the working of the compression valving across the piston alone is described. The principles of damping force associated with hydraulic flows across the base valve during the compression stroke or across the piston during the rebound stroke are quite similar, and are described in more detail in references [15,17,47]. The force-velocity characteristic curve reveals high damping coefficient (rate of change of the peak force with respect to the peak velocity) in the low velocity range, which is developed by the fluid flows through orifice restrictions, often referred to as the "bleed orifice". Figure 2.2 illustrates a schematic of the low speed compression operation of a

typical hydraulic damper piston with a bleed orifice and deflection disc valving. The hydraulic fluid displaced due to piston motion will flow from the high pressure side of the piston to the low pressure side. During the compression stroke the low pressure side of the piston is normally the side with the rod. The pressure differential developed across the piston is strongly dependent upon the piston velocity relative to the cylinder. At low velocity, fluid flow occurs through two paths: *(i)* through the bleed orifice(s) - the size and number of bleed orifice(s) are selected to tune the low speed characteristics of the damper; and *(ii)* leakage flows through the piston/wall clearance, which can alter the damper performance significantly. The deflection discs remain closed due to relatively low pressure differential developed at low velocity.

The mid speed damping control is achieved by another valve with established preload, and deflection characteristics. These valves are typically either deflected disk or blow off spring valves, which are tuned by varying the preload to obtain the desired transition velocity from low to mid speed control, while the stiffness of the valve determines the damping coefficient through the mid range speed [5,14,15,47]. The mid speed damping control valve works in parallel with the low speed bleed in most racing dampers, and in series with the low speed bleed in most passenger car dampers. Figure 2.3 illustrates a schematic representation of hydraulic flow through the compression valve corresponding to mid speed. As shown, the mid speed flow consists of leakage flow, bleed orifice flow, and flow through the deflection disc stack. The flow areas for leakage and bleed flows are relatively small in comparison with that for the deflection disc stack. The flows through the deflection disc stack, thus, dominates the mid speed damping characteristics. Changes in valve preload are normally achieved by changes in the curvature of the piston/disc stack interface, with increasing concavity in the piston causing increased preload. The valves comprising different number of discs of varying thickness, diameter, and material properties are used to achieve desired stiffness characteristics.

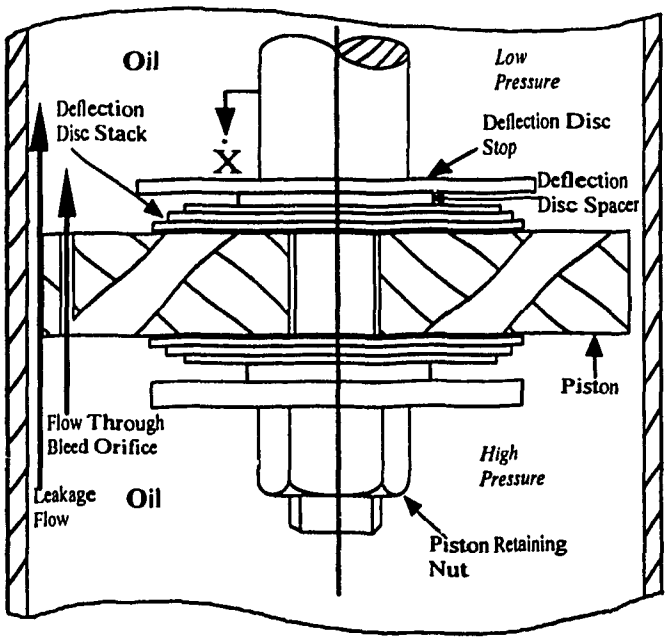

Figure 2.2 Schematic of low speed compression valve flow.

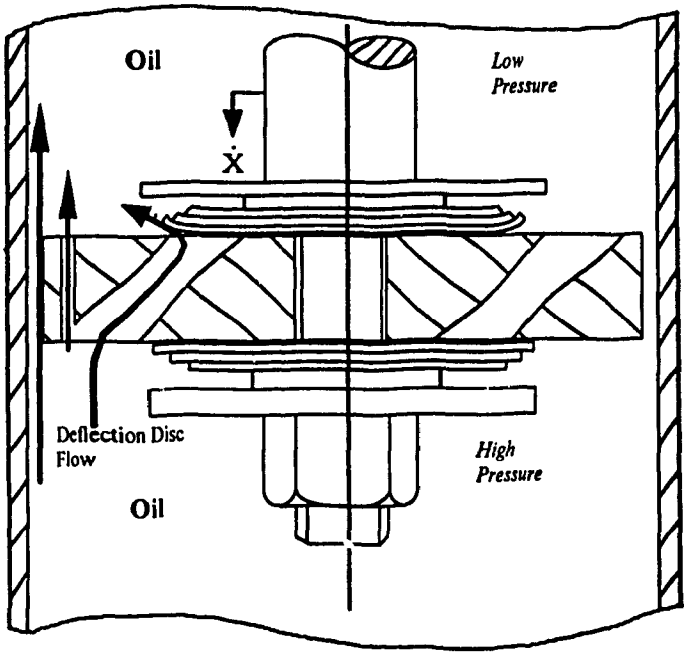

Figure 2.3 Schematic of mid speed compression valve flow.

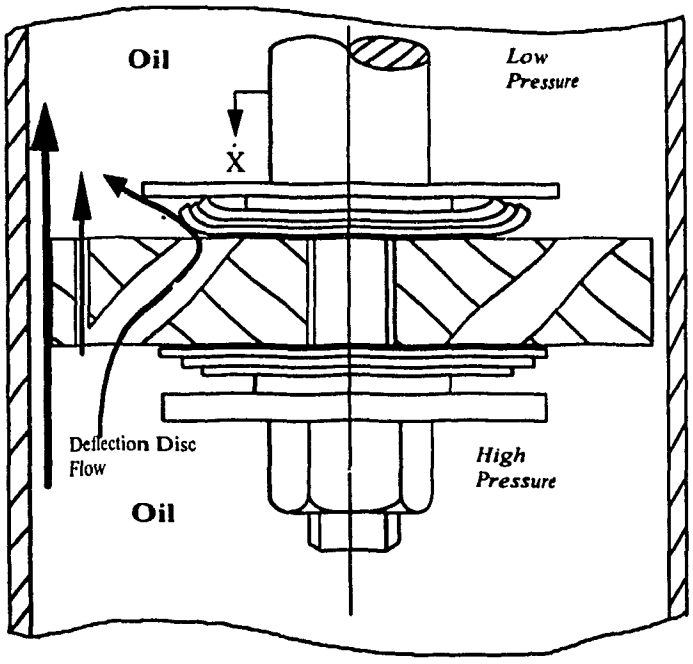

Figure 2.4 Schematic of high speed compression valve flow.

At high velocities the flow is restricted either by the limits in the opening of the valve or through a restriction in the flow passage leading to the valve [14,15,17,47]. Figure 2.4 illustrates a typical deflection disc stop, which serves to limit the opening of the valve and controls the high speed damping flow. In passenger car dampers, the high speed restriction is normally tuned for large excursions. This restriction in most racing car dampers, however, becomes effective at velocities considerably higher then the usual operating range. The damping characteristics corresponding to high velocity range are thus often neglected for racing vehicle dampers.

In order to allow for differential rod volume entering the damper, a compressible medium, such as air at atmospheric or nitrogen at higher pressures, is incorporated within the dampers [5,14,15,17,47]. Most passenger car dampers are designed without a separator between the oil and gas media, which can lead to foaming of the oil and significant loss of damping. In race car dampers, the pressurized nitrogen (pressure = 0.7 to 2.6 MPa) is separated from the oil using either a floating piston or a bladder, in order

to reduce the gas entrapment in the oil. The pressurized nitrogen further serves to reduce the possibility of cavitation on the low pressure side of the piston (rod side) during the compression stroke. In order to eliminate cavitation the pressure on the high pressure side of the piston must be higher then the pressure drop across the piston. In a conventional damper, with a foot valve between the high pressure side of the piston and the compressible medium, this is normally achieved by having a larger pressure drop across the foot valve. The dampers with monotube design and the conventional dampers with a foot valve, which is not tuned for a higher pressure drop, require high pressure gas as the compressible medium to balance the pressure drop across the piston. The pressurized gas medium also helps to replenish the fluid flow during the rebound stroke when a foot valve is used.

The contribution due to the gas spring force is often neglected or inadequately incorporated in the experimental and analytical studies of dampers reported in the literature. In experimental studies, the gas spring force is frequently assumed as a bias, and its value measured corresponding to the mid stroke is subtracted from the measured total force [48,49]. The resulting force, when interpreted as the damping force may result in significant errors. The error is attributed to the contributions from the gas spring effects, particularly when the damping is relatively light and the gas spring is relatively stiff. Furthermore, the gas spring effects are known to be strongly dependent upon the operating temperature [50], and no other reported work has attempted to study this effect. As the damper acts in parallel with the suspension springs, a change in gas pressure caused by variation in operating temperatures can result in significant change in the vehicle ride height, affecting the vehicle's performance. In the case of Indy race cars, it has been stated that a change in the ride height of 0.76 mm can result in a loss of 0.5 s per lap [10] on a 1.6 km oval track, which is quite significant since lap times track are in the low 20 s range. In this dissertation research, extensive laboratory measurements are performed at different operating temperatures in order to enhance understanding of its

effects on the damper force. The measured damping force of the Koni Indy car damper is illustrated in Figures 2.5 (a) and (b), to illustrate the influence of operating temperature. The force-displacement characteristics measured at very low frequency (0.5 Hz) clearly illustrate the influence of temperature on the gas spring force, (Figure 2.5 (a)), as evident from the changes in the bias and the slope of the curves. A change in the temperature from 94°C to 149°C corresponds to an increase of 250 N in the gas spring force at mid stroke. For a typical 1990 Indy race car rear suspension designed with leverage ratio of 1.087, and approximate spring rate of 133 kN/m for road racing and 266 kN/m for 1.6 km oval track racing [44], a change of 250 N in the gas spring force would correspond to change in the ride height of 1.88 mm and 0.94 mm, respectively for road and oval track racing. This change in the ride height tends to deteriorate the vehicle performance considerably [10]. Figure 2.5 (b) illustrates the measured force-displacement response at a higher cycling speed (2 Hz). The effect of variations in temperature on the gas spring bias and slope changes are difficult to discern, due to the increase in the damping force. On first inspection, it would appear that the rebound damping decreases and that compression damping increases with increase in temperature. This is not the case, and it will be shown that the damping in both compression and rebound decrease with increase in temperature, when the friction and gas spring force components are removed.

2.2.2 Description of Candidate Dampers

The road racing vehicle dampers can be grouped into two basic configurations, based upon their construction and the location of the compressible medium, the monotube and remote reservoir. In a monotube damper, the gas reservoir is located in the same tube as the piston rod and piston, as shown in Figure 2.6 (a). The remote reservoir dampers employ the compressible medium in an auxiliary tank with a flow passage to the main body on the compression side of the piston, as shown in Figure 2.6 (b). Typically monotube dampers integrate all the valves across the piston, while the remote reservoirs

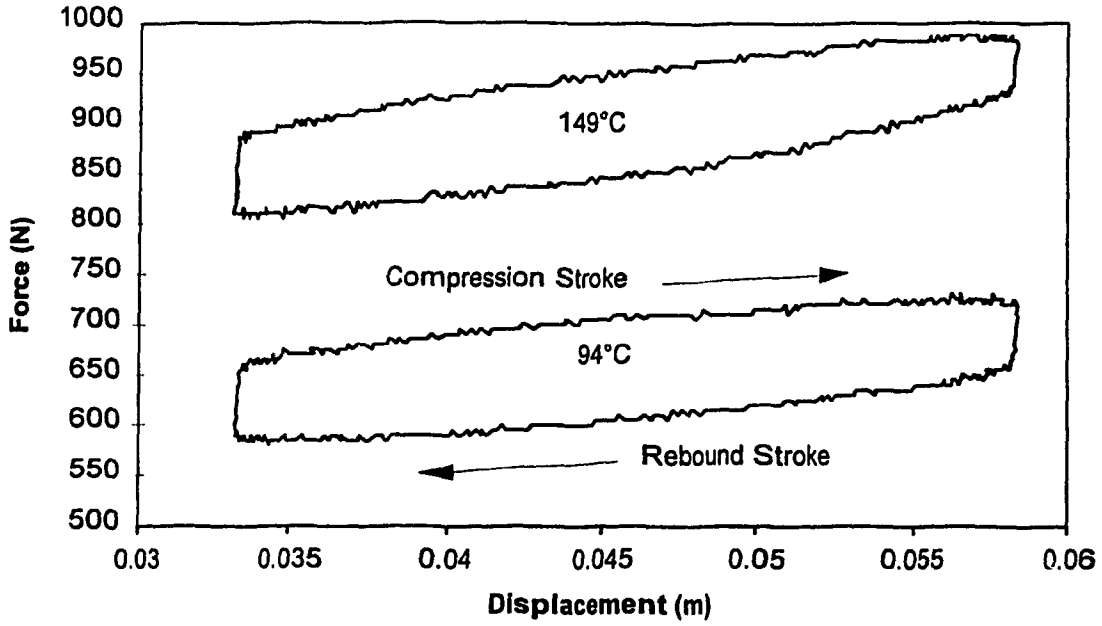

(a) Low speed, excitation frequency = 0.5 Hz.

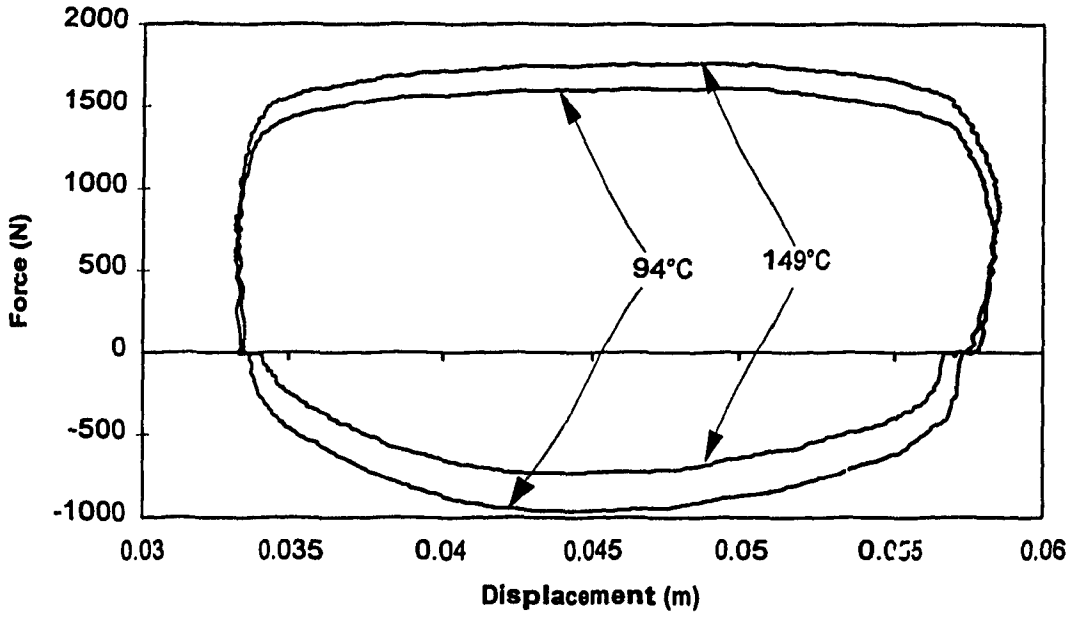

(b) Mid speed, excitation frequency = 2.0 Hz.

Figure 2.5 Influence of temperature variations on low- and mid-speed force-displacement characteristics.

dampers also incorporate a compression head (foot valve). The flows through the compression head contribute to some or all of the compression damping.

Figure 2.6 (a) illustrates the schematic of two of the popular monotube dampers, developed by Bilstien and Koni. Both the damper designs use deflected disc valves across the piston, in parallel with the bleed circuits, as shown in Figure 2.2. Different valves are used in compression and rebound strokes to generate the desired asymmetric damping forces. High pressure nitrogen (approximately 2.4 MPa) is used as the compressible medium, which is separated from the oil by a floating piston. The valving can be adjusted by disassembling the unit and changing the size and/or number of the orifice, preload deflection of the disks and/or size and number of deflection discs. Further, the Koni damper permits the external adjustment of the preload on the disc stacks.

The remote reservoir type dampers are quite similar to the monotube dampers except that the compressible medium is located in a separate cylinder with a separator (floating piston or bladder), as illustrated by Figure 2.6 (b). The separated reservoir is either directly attached to the main body (referred to as 'piggy back' configuration) or connected to the main body through a hydraulic pipe (referred to as 'hose connection configuration'). The remote reservoir type dampers have been manufactured by Fox, Penske, Ohlins, White Power, Kayaba, Showa and Mechformance.

With the exception of the Mechformance unit, the remote reservoir dampers employ valving across the piston in a manner similar to that of the monotube dampers. These dampers typically provide two external damping adjusters. The first adjuster permits the adjustment of orifice flow across the piston in the rebound stroke, which may also effect the compression damping in some cases. The second adjuster, located in the passage from the main body to the reservoir, permits the control of a portion of the flow during the compression stroke. This latter device commonly used in conjunction with valves mounted across the piston, can either be a bleed orifice, preload adjustment or

combination of both. The influence of the second adjuster on the damping properties is considerably smaller then that of the piston orifice adjuster.

The Mechformance damper with "piggy back" reservoir configuration comprises five different externally adjustable valving mechanisms. Two of the adjuster control the fluid flows across the piston in the rebound stroke by varying the low speed orifice and mid speed blow off valve. Three adjusters control the fluid flow to the reservoir during the compression stroke, two vary the stiffness of reeds which are placed on the flow ports, and the last controls the flow area of one of the ports. The flow across the piston in the compression stroke is relatively unrestricted, thus preventing cavitation [51].

All the dampers in this study use spherical bearings for their mounting. While most of the mountings are designed with bearings with minimal clearance (0 - 0.040 mm), some of the bearings (particularly the Koni) exhibit a noticeable amount of radial clearance (approximately 0.040 - 0.082 mm).

The design and construction of various dampers were reviewed in an attempt to select candidate dampers for the study. The damping characteristics of various dampers manufactured by Koni, Bilstien, Fox, Penske, Ohlins, Galles (modified Penske), and Mechformance were established through laboratory tests. While all the dampers revealed quite similar force-displacement and force-velocity characteristics established from the experimental data, the various dampers revealed differences in damping curves dependent primarily on the applications. As a criterion for selection of dampers for further analytical and experimental investigations, it was established to include at least one monotube and one remote reservoir construction due to their distinct construction and modeling differences. While a monotube damper involves study of pressure drop across the piston alone, a remote reservoir damper involves pressure drops across the piston and the compression head. For the candidate monotube type damper, a Koni Indy race car damper was selected, so the effect that variation in temperature has on the gas spring, could be studied relative to ride height, and damper performance. The Fox damper was

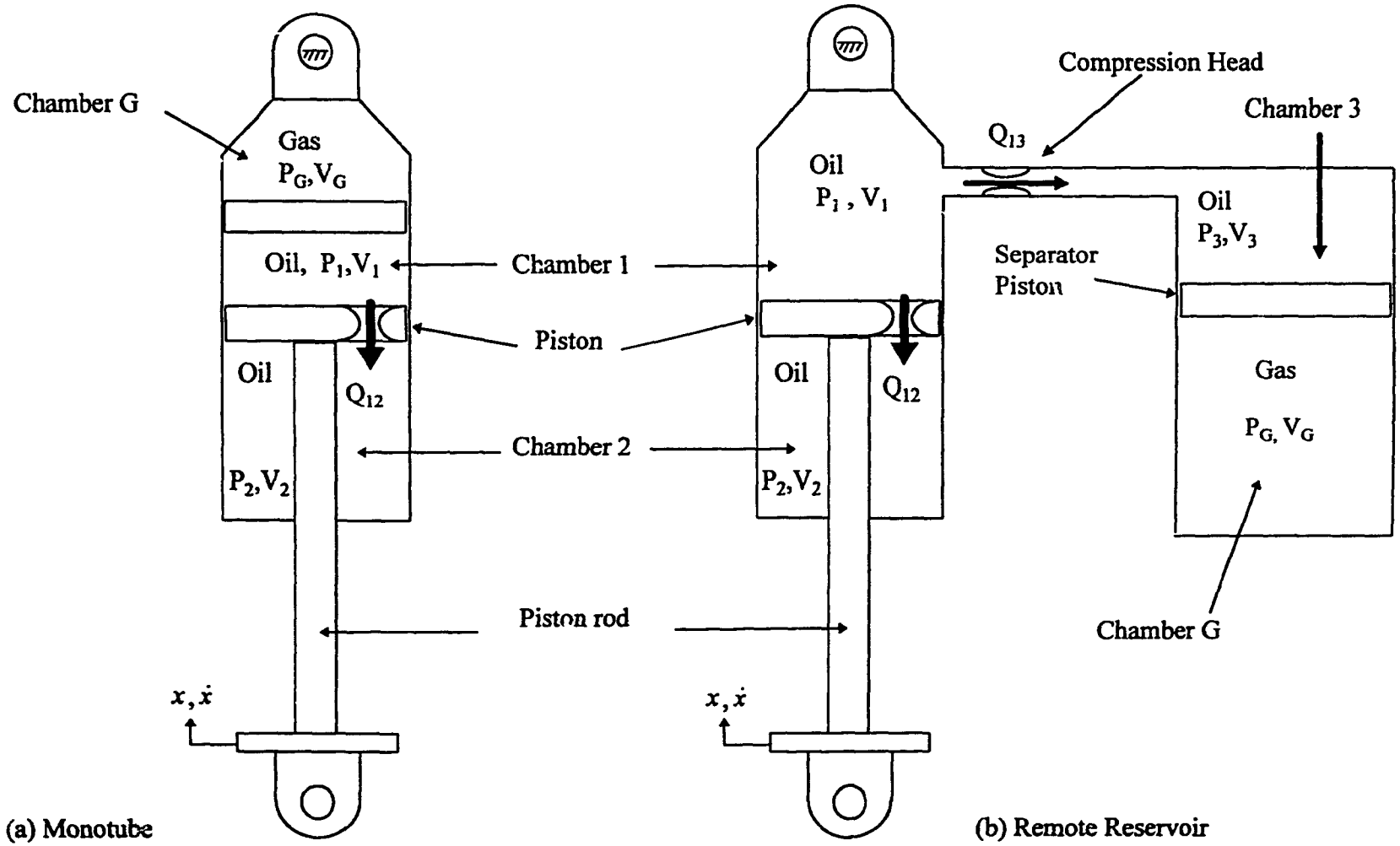

Figure 2.6 Schematics of monotube and remote reservoir dampers.

chosen as being representative of the remote reservoir units, due to its wide range of external damping adjustments, which allows the study of both very stiff and soft damping characteristics. A Mechformance remote reservoir damper, was also selected for further investigation due to its different valving mechanisms. Furthermore, this Mechformance damper revealed strong displacement dependent friction characteristics and poor sealing performance on a one way valve across the piston, resulting in unique damper characteristics which require further refinements of the models. This latter unit was set up to exhibit stiff rebound and soft compression damping in comparison to the other units.

The candidate damper developed by Koni (model B53), considered for the study, was previously used in an Indy race car. This damper is typically charged with nitrogen at a pressure of 2.41 MPa. The candidate Mechformance damper, used on a number of F2000 cars, operated at a pressure of 2.07 MPa. The valving for the candidate Fox damper was adjusted for usage on a Superbike and was charged with gas at a pressure of 1.90 MPa. While the Koni damper was not rebuilt, the Fox and Mechformance dampers were carefully rebuilt with new oil, in a manner that would minimize the amount of entrapped air in the oil. The Koni and Mechformance bodies and Mechformance reservoir are hard anodized aluminum, while the Fox damper uses a steel main body and hard anodized aluminum reservoir. All the three candidate dampers employed a floating piston to separate the nitrogen gas from the oil.

The candidate dampers were extensively tested in the laboratory under different operating conditions to characterize their properties and to identify the most significant operating factors to be incorporated into the associated models. The Fox damper was investigated with minimum and maximum damper settings to establish the significance of these settings for damper modeling, and their affects on quarter-car performance characteristics. The initial gas volume and charge pressure were set at room temperature for all the three dampers, while the damper's piston rods were fully extended. The test

methodologies employed to investigate the performance characteristics of different dampers are described in the following section.

2.3 EXPERIMENTAL STUDY OF DAMPER PERFORMANCE CHARACTERISTICS

Since the damper performance is a complex function of asymmetric bleed orifices and valving, variations in operating temperature, gas spring force, seal friction, etc., industry practices invariably include repetitive road testing and damper tuning in an interactive manner. Alternatively, laboratory tests are performed to characterize the damper behavior under specific controlled conditions. The performance characteristics of the damper are evaluated in the laboratory using two methods: conventional and quarter-car test fixtures.

Conventional testing of dampers is accomplished by placing a damper between a fixed reference and an excitation source. While this method yields the damping characteristics under preset levels of excitations, in a convenient manner, the interactions between the damper and the dynamics of the sprung and unsprung masses is neglected. The test results can thus be considered valid for idealized conditions. The quarter-vehicle model testing involves testing of dampers installed within a two-degree-of-freedom (DOF) vertical mode vehicle simulator. The two-DOF test stand, comprises two guided masses representing the equivalent sprung and unsprung masses of a quarter vehicle, coupled through an equivalent suspension spring. The damper is placed in parallel with the suspension spring, and a spring representing the elasticity of the tire is mounted between the unsprung mass and the excitation source. Unlike the conventional method of testing, this method permits the damper testing under more realistic damper excitations, when the quarter-vehicle model is adequately tuned. In this study conventional damper tests are initially performed to characterize the behavior of the candidate dampers under known excitations and to identify the most significant modeling considerations. Quarter-

vehicle testing is later performed to validate the damper models and to carry out more thorough performance evaluations.

2.3.1 Conventional Damper Testing

In a conventional damper test method the damper is mounted between a fixed inertial frame and an electro-hydraulic vibration exciter. Although conventional damper tests have been performed under deterministic excitations of varying waveforms, sinusoidal excitations are most commonly used for damper evaluations. The test objectives, in-general, are classified as either performance or endurance evaluations. While endurance testing is extremely important for dampers designed for passenger car applications, the endurance of racing car dampers is normally not an issue, due to the relatively short duration of the race. The endurance tests are performed under varying excitations, such as sinusoidal, ramp displacement waveforms, displacement time histories acquired from road tests, and dual superimposed sine waves. Standard endurance testing of dampers mostly employ sinusoidal input of 0.2 to 1 m/s peak velocity for one million cycles [48].

Performance testing is important for both racing and passenger car dampers. While standard test specifications do not exist for racing dampers, it is generally accepted that the racing dampers need to comply to tighter tolerances then those used for the passenger car dampers. The inputs used for performance testing are normally sinusoidal, although constant velocity and other waveforms are sometimes substituted. The performance curves, in general, include; peak force-peak velocity characteristics, force at peak velocity-peak velocity, and force-displacement or force-velocity characteristics measured during the cycling of the damper. Figure 2.7 illustrates a family of curves for the Fox damper with heavy damping settings subjected to sinusoidal excitations of varying displacements at a frequency of 8 Hz. The composite peak force-peak velocity curve, presented in the Figure 2.7, is derived from the values of peak force and peak velocity for

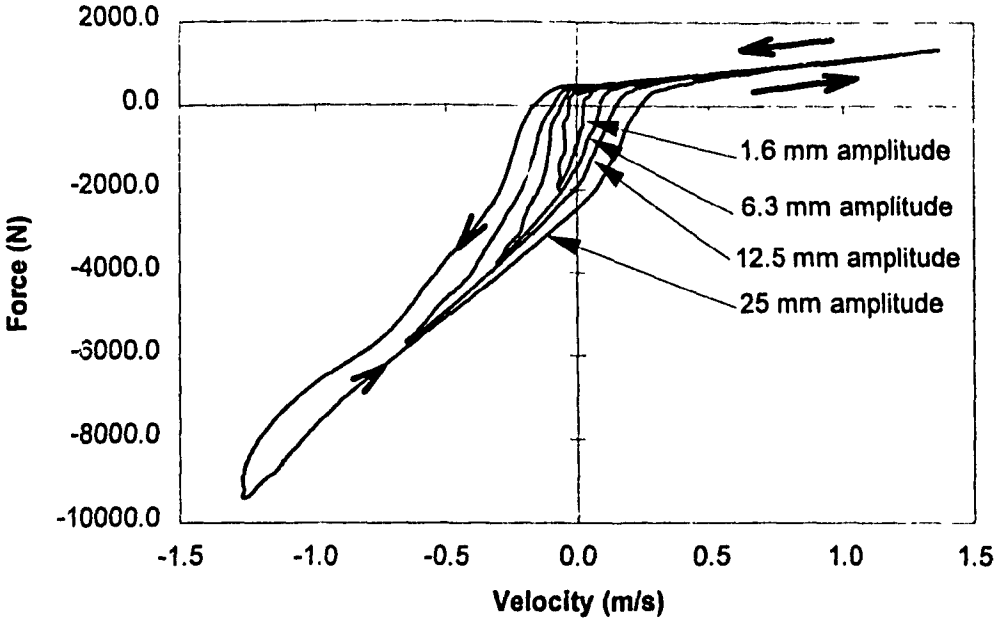

Force-velocity characteristics.

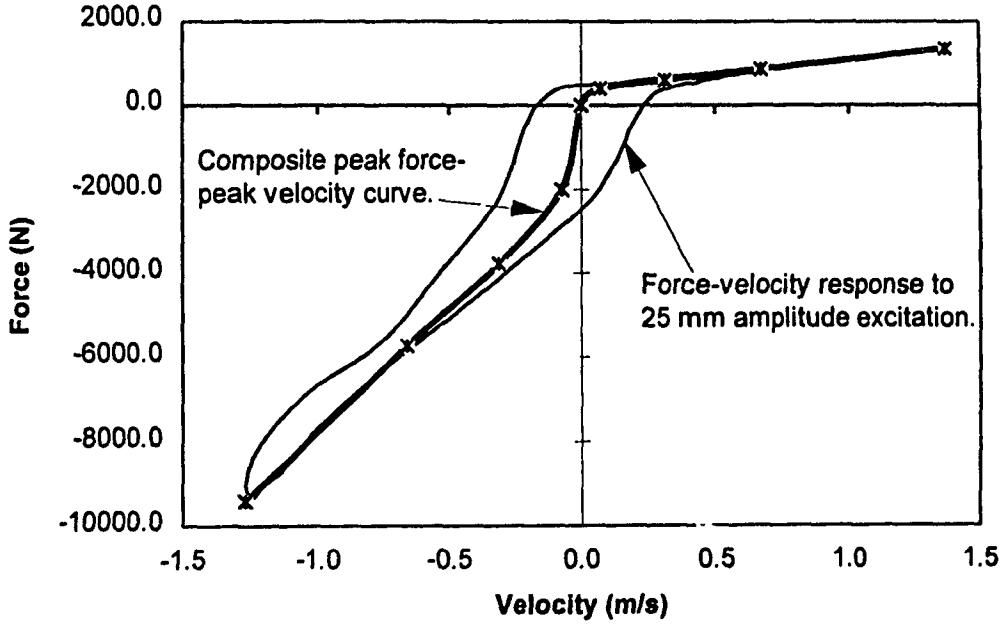

Composite peak force-peak velocity characteristics.

Figure 2.7 Force-velocity and composite peak force-peak velocity characteristics of the Fox damper with stiff settings, subject to sinusoidal displacement excitations (8 Hz).

a family of force velocity curves. At sufficiently low cycling speeds, the force-displacement characteristics permit evaluation of gas spring and friction force characteristics of the damper. Low speed force-velocity curves can also be used to study the friction characteristics of the damper.

The measurement of peak force for a given sinusoidal input is commonly used to compare different units built by the same manufacturer with the same valve code. The force-displacement and force-velocity loops, however, provide the most significant information on the performance characteristics and relative evaluations of different dampers. The force-velocity properties permit the characterization of the fluid compressibility effects in a highly effective manner. The force-displacement characteristics further enhance understanding of the influence of operating temperature on the damper performance, as illustrated in Figure 2.5 (a) and (b). The displacement in these figures is measured relative to the fully extended position of the unit, and the dynamic traces are clockwise. The force corresponding to the upper portion of the curve is generated during the compression stroke and the bottom portion of the curve represents the extension or rebound stroke.

The operating temperature is known to affect the dampers performance quite significantly [50]. The experimental investigations in this study were performed in the temperature range of 20°C to 135°C, which is representative of the operating range of race car dampers. In normal applications, the dampers initially operate at ambient temperature, and approach working temperature with increase in local ambient temperature and dissipation of energy. In motocross applications dampers operate near the ambient at the start of the race, but quickly reach an operating temperature between 105°C to 150°C due to the severity of the inputs. Since the excitations to the formula type racing cars are not as severe, the dampers used in these vehicles operate at a moderate temperature differential from their surroundings. The front suspension dampers normally operate at a relatively lower temperature when compared to the rear suspension

dampers, which are exposed to the heat generated by the engine and the exhaust. Although no exact data has been published, it is known that the temperature in the vicinity of the rear suspension tends to vary substantially during the race, due to frequent interruptions, stoppage (pit stop), and variations in local ambient temperature [44].

2.3.1.1 Test Apparatus And Procedures

The test apparatus for the conventional damper testing comprises: a 35 kN electro-hydraulic actuator to generate the desired excitation; servo controller to operate the actuator in displacement feedback control; waveform generator to deliver the desired command signal to the servo controller; a feedback displacement sensor (LVDT); and a reaction frame to provide a fixed reference for the damper. The actuator used in the study is capable of achieving peak velocity of over 1.5 m/s for sinusoidal displacement excitations. While the bottom mount of the damper was attached to the actuator piston rod, the upper mounting was fixed to the reaction frame through a force transducer, as shown schematically in Figure 2.8. Linear velocity (LVT) and displacement (LVDT) transducers were mounted in parallel to the damper, to monitor the relative velocity and displacement, respectively, across the damper. Although the internal feedback LVDT is normally used in industry to derive the displacement and velocity of the damper, the external LVDT and LVT are used to eliminate the errors associated with the time delays built into the feedback signal and the flexibility of the reaction frame. Initial testing performed with the feedback LVDT built into the actuator, showed a time delay of 4 ms, which results in a skewed force-displacement plot, with distortion increasing with increase in the frequency. The force transducer, mounted between the damper and the reaction frame, was used to measure the force generated by the damper.

A pressure transducer was mounted on the Mechformance unit to measure the gas pressure during the tests. During earlier tests, pressure transducers were also fitted in different locations on the Mechformance damper to measure pressure differential across

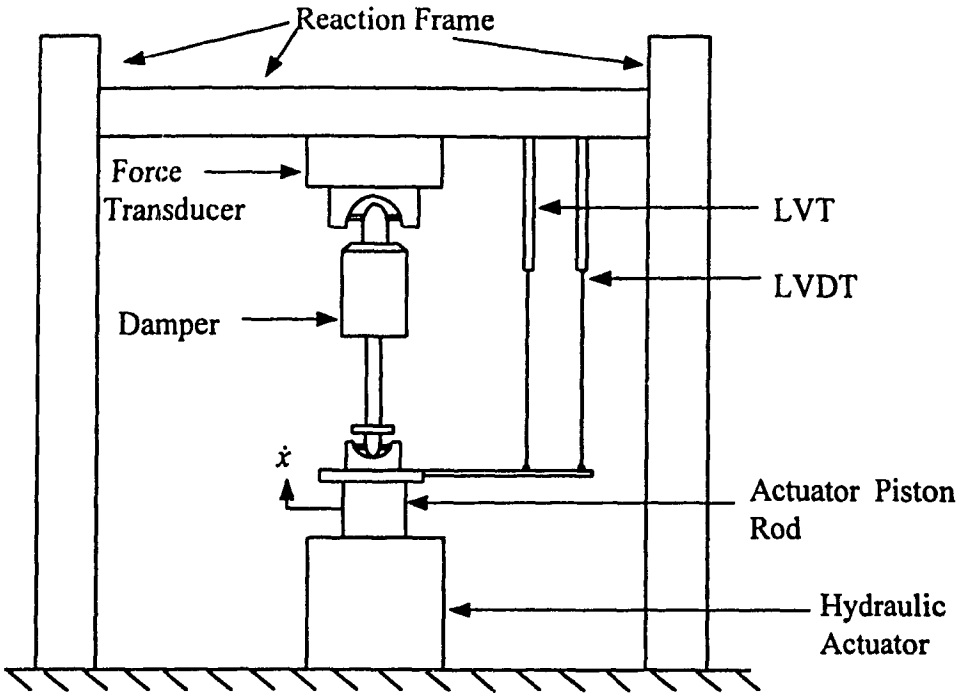

Figure 2.8 Schematic of a conventional damper test stand.

the floating piston, across the compression head, and between the main body and reservoir. Thermocouples were mounted at different locations on the candidate dampers to attain an estimate of their operating temperature. On a monotube body, the temperature measurement was performed using one thermocouple mounted approximately 20 mm from the top of the body. On the remote reservoir units, one thermocouple was mounted on the main body in the same location, and another was mounted midway on the reservoir body. The small areas in the vicinity of the thermocouples were insulated in order to attain a closer approximation of the internal temperature. The measured signals were recorded using a data acquisition system for further processing and analysis of the data. The test data were acquired at a sampling rate ranging from 250 to 500 samples/cycle depending upon the frequency of excitation.

Each damper test was initiated at the normal laboratory temperature condition. The damper was subjected to varying levels of excitations until the temperature approached a

value slightly higher than the highest desired test temperature. The damper was then subjected to sinusoidal excitations that allowed the temperature to slowly decrease, such that the damper was almost in a state of thermal equilibrium, between the heat being generated and dissipated. The force, velocity, displacement, temperature and, in the case of the Mechformance unit, pressure data were recorded when the damper reached the desired temperature. The measurements were repeated at different discrete temperatures in the specified range, starting with the highest temperature and progressing to the lowest test temperature.

The candidate dampers were subjected to two series of tests. The first series of tests involved measurements at 9-10 different reservoir temperatures, ranging from approximately 150°C to 20°C, to determine the temperature sensitivity of the damper forces. At each discrete temperature, the damper was subjected to 12.7 mm peak sinusoidal displacement at frequencies of 0.5 and 2 Hz. The data acquired at 0.05 Hz excitation frequency was used to determine the temperature sensitivity of the gas spring and friction forces. The data corresponding to the excitation frequency of 2 Hz was used to determine the temperature sensitivity of the damping forces The polytropic exponent for the gas spring model was also determined from the 0.05 and 2 Hz data for the Mechformance unit.

The second series of tests, involved measurement of the force-velocity and force-displacement characteristics under sinusoidal displacement excitations of varying frequencies and displacement amplitudes. The damper temperature was monitored during each test and the data were recorded corresponding to desired temperature (within ±5°C). The tests were performed under different levels of peak displacement excitations (12.7, 6.4, 3.2 and 1.6 mm) and frequencies (16, 8, 4, 2 and 1 Hz). In addition to the above test conditions, the Fox unit was subjected to 25.4 mm peak displacement at frequencies of 8, 4, 2 and 1 Hz. The force, velocity and displacement data acquired

during these tests were analyzed to determine the coefficients for the damping and compressibility models.

2.3.1.2 Measurement Of Gas Spring And Friction Forces

The damper force, measured during the tests, comprises components due to friction, gas spring, and damping forces. The damper forces measured at low frequencies are often assumed to characterize the gas spring and friction force components, while the damping forces are assumed to be negligible. The rapid change in the magnitude of the damper force in the force-velocity or force-displacement curves is considered to represent the static friction of the damper as illustrated in Figure 2.9. While this methodology yields a reasonably accurate estimate of the static friction force within a variety of dampers, the method yields significant errors in dampers that deliver considerable damping force at low velocity. The evaluation of the gas spring and friction force components, thus, becomes a complex task for race car dampers, which generate large damping forces at low velocities.

The force-velocity and force-displacement characteristics of the candidate dampers were measured under sinusoidal and ramp displacement waveforms at frequencies of 0.005 to 1 Hz and varying amplitudes up to 25 mm. The test results revealed poor repeatability in some instances, and relatively high magnitudes of low speed damping. Figure 2.9 illustrates the force-displacement characteristics of the Fox damper corresponding to two different settings: *(i)* adjusters set to minimal damping; *(ii)* adjusters set to maximum damping. The displacement off-sets of the two test are different, both however are referenced to the damper displacement at full extension. It should be noted that the adjusters primarily control the low speed flow through the bleed orifice. The test speed was selected as 0.05 Hz, which is well within the traditional test speeds used for most gas spring tests [49]. The results corresponding to light damping setting reveal only minimal damping force component. Although a detailed analysis of

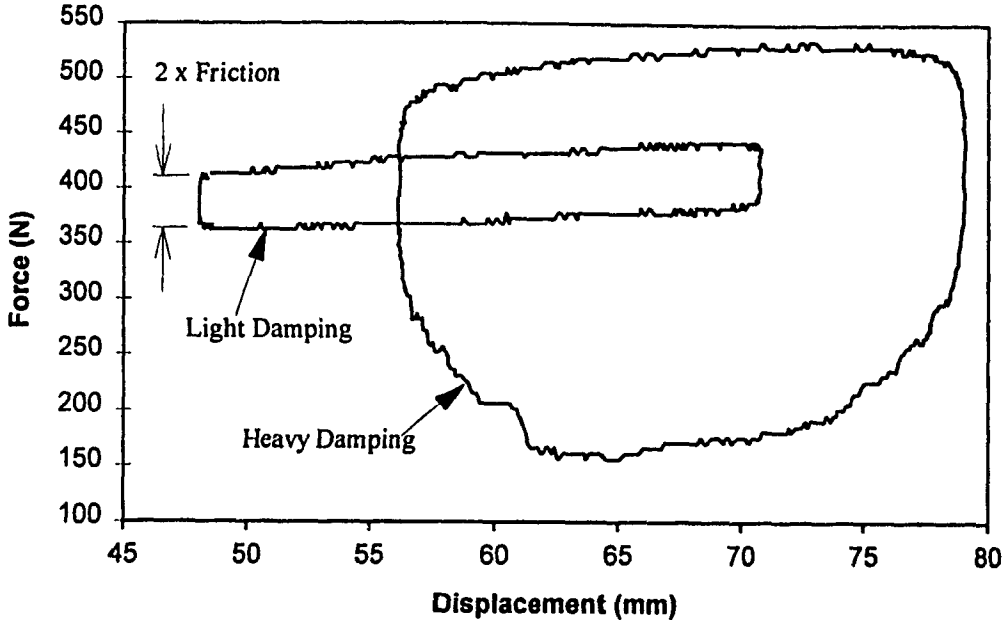

Figure 2.9 Force-displacement characteristics of the Fox damper corresponding to light and heavy damping settings (0.005 Hz).

the measured data is presented in Chapter 3, a rapid change in the measured forces corresponding to stroke reversal is quite apparent. The change in the damper force, the difference between the upper and bottom curves, is equal to approximately 2 times the breakaway friction force. With light damping, the rate of change of damper force with respect to displacement provides an estimate of the gas spring constant. The slopes of the upper and lower curves corresponding to light damper setting are observed to be quite similar. The results presented in Figure 2.9 further reveal that the damping force corresponding to the high setting, obscures the effect of the gas spring and friction, which are evident at the lighter damping setting.

Ideally a pressure transducer may be used to study the time history of the gas pressure and thus the gas spring force. Installation of a pressure transducer on a damper, however, may pose many complexities. Alternatively, gas spring force characterization can be carried out through measurement of rod reaction or damper force under discrete

deflections of the damper. The measurements were performed using different methods and the data examined for its repeatability. Rod reaction force and the damper deflections were first measured on the conventional damper test setup under static command signals. The results showed inconsistencies due in most part to the pump noise and the displacement feedback loop forcing the damper from the compression to rebound state and vice versa. The results also revealed poor repeatability. The tests were next attempted on a hydraulic press with an inertia frame. Although the measured data was observed to be more consistent and repeatable, it revealed a displacement drift with time caused by leakage flows across the hydraulic press's piston. The final test set up consisted of a universal milling machine, modified to accept a force transducer and height gauge, as shown in Figure 2.10. This setup was found to have good repeatability, with no possibility of displacement drift. The damper was mounted vertically between the vertical spindle and the force transducer located on the milling machine table. A precision height gauge was used to measure damper deflection, since the table crank showed appreciable backlash. The measured force was adjusted for the damper weight, and the data was recorded for further analysis.

The damper force was established using discrete displacements of the damper and measurement of the rod reaction force. During initial tests the damper was held at discrete displacements over an extended period of time (up to 12 hours) and rod reaction measurements were taken and plotted against time to identify the steady-state forces. Preliminary measurements revealed changes in damper force of 1 to 4 %, occurring in an exponential fashion during the first 15 minutes, approaching a constant value beyond this time. The data were thus recorded at a lapse of 20 minutes to determine the gas spring and static friction forces, and to determine the initial gas pressure and volume by modeling the gas spring using the ideal gas law.

Figure 2.11 illustrates a comparison of the static force displacement characteristics of the Fox damper derived from the universal milling machine apparatus with those

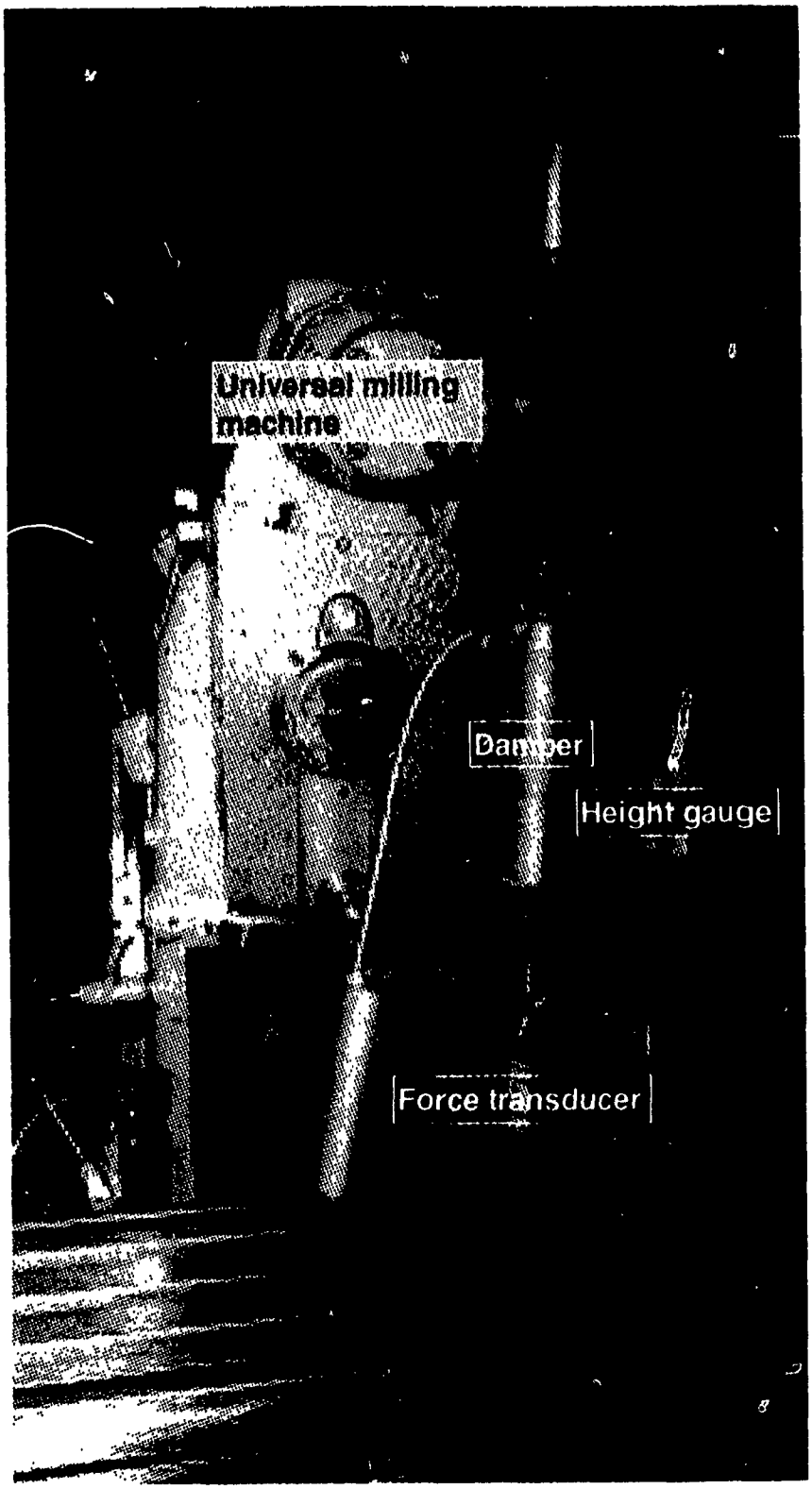

Figure 2.10 A pictorial view of the static friction and gas spring force measurement setup.

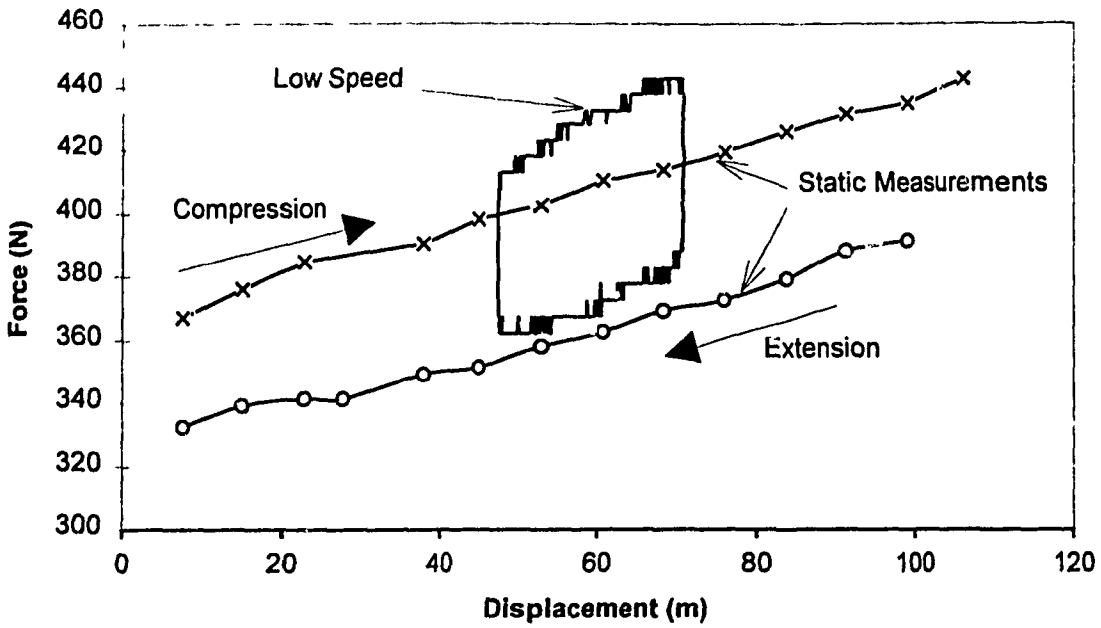

Figure 2.11 A comparison of the static and low speed force-displacement characteristics (Fox damper with light damping settings).

established from low speed test. Although the two measurement methods exhibit similar trends, discrepancies arise due to isothermal and adiabatic processes associated with static and low speed tests, respectively.

2.3.2 Quarter Car Simulator

While a conventional inertia frame tester provides repeatable inputs and measurements under laboratory conditions, it does not accurately simulate the realistic damper excitations encountered in a vehicle. Although 'hardware-in-the-loop' simulation tools have been recently proposed to test dampers under a more realistic relative motion between the sprung and unsprung masses [52], the time delays associated with the hardware in the loop limit the application of the tool, specifically at higher frequencies [53]. Furthermore, the validity of the tool has not yet been established as is evident from the limited number of reported studies in the area. Alternatively, the damper characterization may be carried out through either road or laboratory tests performed on a

vehicle with the candidate damper. The road test methods, however, pose many complexities due to poor repeatability caused by variations in the vehicle-road and vehicle-driver interactions, and various environmental conditions. The test method further necessitates excessive instrumentation and high costs associated with tuning and installation of dampers. While the laboratory testing of the vehicle under controlled conditions can yield good repeatability of the test results, an excessively large test facility is required to undertake the tests. Alternatively, the vertical mode dynamics of a vehicle can be effectively simulated using a quarter car simulator, with equivalent sprung and unsprung masses, and tire and suspension springs. Quarter car test methodology permits the realistic vertical excitations caused by relative deflections across the suspension, and tuning and installation of dampers in a convenient manner.

2.3.2.1 Test Apparatus And Procedures

Various designs of quarter car simulators used in the industry were reviewed in terms of their complexities and limitations in order to configure the design for the current study. One of the designs considered was a four bar type in which the quarter vehicle system is restrained by a relatively long lever arms pivoted in a horizontal plane. The tester, however, necessitated relatively large space and the resulting motion did not characterize the vertical response of the traditional quarter-vehicle model accurately [44]. A number of quarter-car simulators have been developed in the industry based upon the analytical models reported in the literature [47,54,55]. The analytical models, invariably, consist of a tire model, suspension damper and spring models, as well as, sprung and unsprung masses constrained to move along the vertical axis, as shown in Figure 2.12.

A quarter car simulator was developed using the experience gained from the design of an earlier single-degree-of-freedom (SDOF) test system, illustrated in Figure 2.13 [30]. The test system, designed to simulate the equivalent sprung mass acting on a motorcycle fork, provided good correlation with the theoretical and field results. The equivalent

sprung mass in the test apparatus comprised of two vertical shafts coupled through a cross member and the top of the motorcycle fork was coupled to the cross-member. The bottom of the fork was connected to the hydraulic actuator, and the motion was constrained along the vertical axis by the linear bearings mounted in pillow blocks attached to an inertia frame. Since the motorcycle fork was designed to resist high side loads and deflections, it served as a good guide. Although the candidate dampers are not designed to resist high side loads and thus do not serve as guides, the concept of the SDOF tester is used to design the quarter-vehicle tester shown in Figure 2.14. Equivalent sprung and unsprung masses, and tire and suspension springs, are integrated within the test system as shown. The sprung mass is represented by the two vertical shafts tied to a cross member. The vertical shafts provide the necessary guidance of the sprung and unsprung masses, while additional cross members may be integrated to achieve desired sprung mass, ranging from 150 to 252.5 kg.

The unsprung mass is also guided by the two vertical shafts and a pair of Teflon impregnated bronze bushings (DU material, commonly used in suspension struts), resulting in relative friction between the masses, as encountered in a real vehicle suspension system. Two different unsprung masses (27.2 & 45.4 kg) are available along with the provision to bolt on 9 kg of additional mass. The sprung mass shafts are also guided by a set of DU material bushings mounted in a cross member attached to the hydraulic actuator's piston, providing an unwanted friction between the input and the sprung mass. The damper is mounted between the sprung and the unsprung masses, with provision to mount a load cell between the damper and either of the masses. Two springs are mounted between the sprung and unsprung masses, on either side of the damper, to represent the suspension spring. The tire is modeled by a parallel combination of one to three helical springs, installed between the unsprung mass and the input. The system was setup with masses and springs that approximate those of a large racing sedan, such as a Trans-Am, and the corresponding parameters are given in Table 2.2.

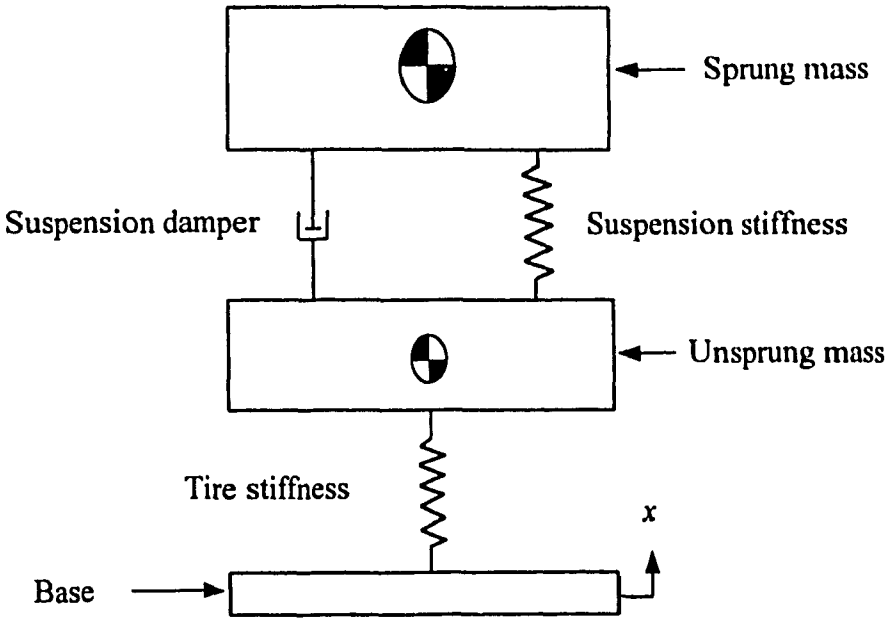

Figure 2.12 Schematic of two degree of freedom model.

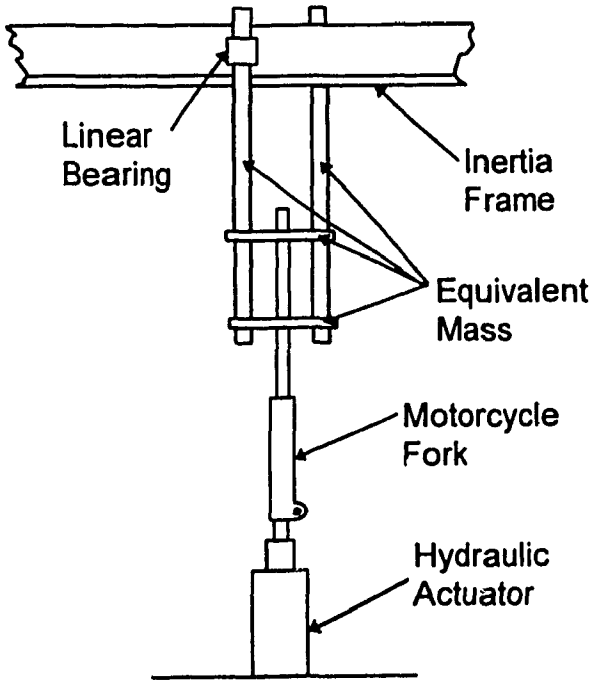

Figure 2.13 Illustration of single degree-of-freedom telescopic fork tester.

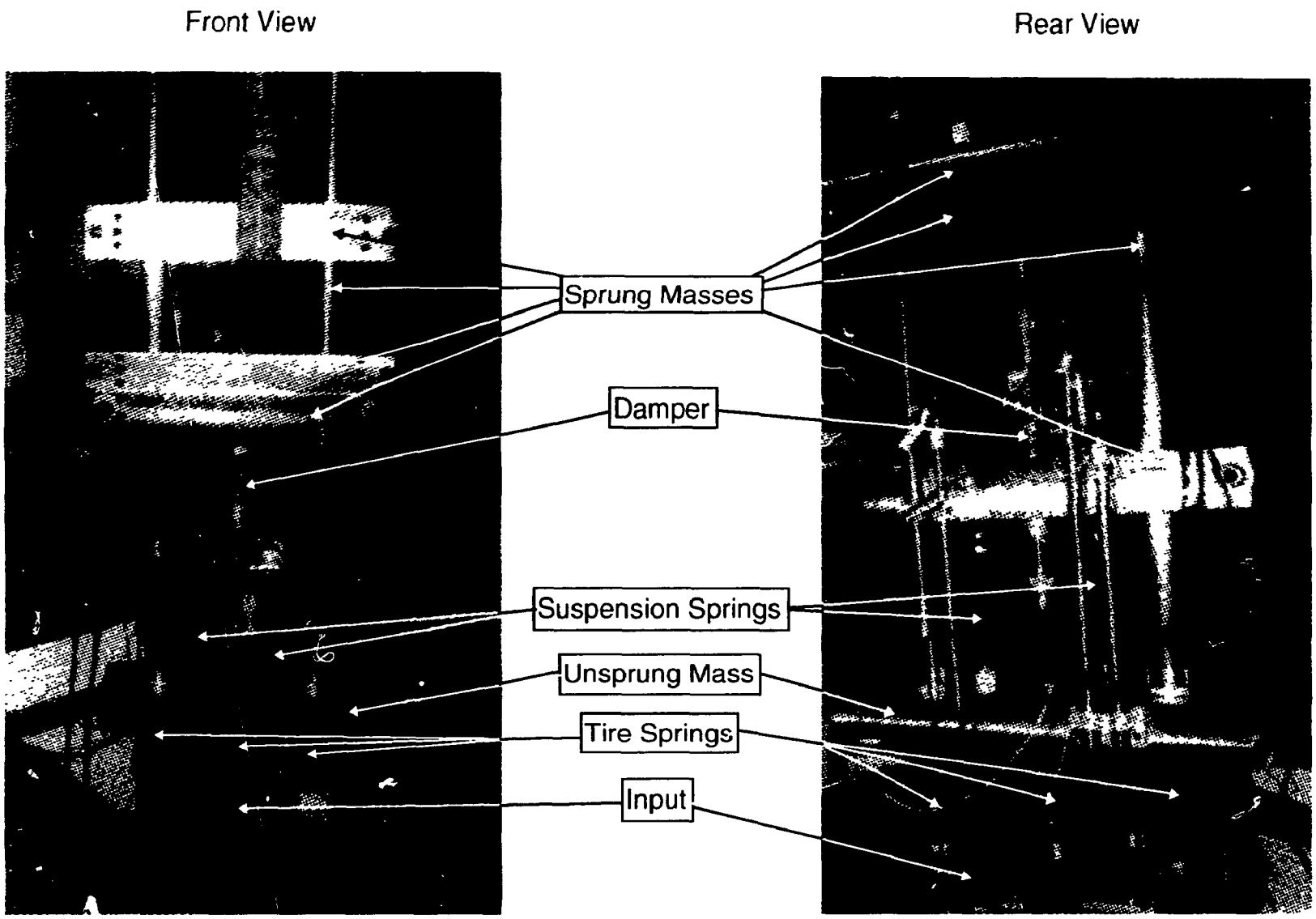

Figure 2.14: Pictorial views of the quarter-car test system

TABLE 2.2
QUARTER-CAR SIMULATOR PARAMETERS

Sprung Mass	252.5 kg
Suspension Spring Stiffness	70 kN/m
Unsprung Mass	45.4 kg
Tire Stiffness	350 kN/m

Although the quarter-vehicle test stand is designed for a wide variety of excitation, such as sinusoidal, step, ramp, random and measured road roughness, the inputs studied were sinusoidal and step displacements. Sinusoidal excitations of different amplitude (0.32, 0.63, 1.27, 2.54, 5.04 cm peak to peak) and discrete frequencies in the 1-20 Hz range were used for studying the damper and quarter-car frequency response. The transient response was investigated under step inputs of different amplitudes (1.27, 2.54 and 5.08 cm peak to peak) at a frequency of 0.1 Hz.

The quarter-car test stand was instrumented to measure the input acceleration, and response accelerations of the sprung and unsprung masses. Three sets of LVDT's and LVT's were installed to measure the displacement and velocity, respectively, at the unsprung mass, sprung mass and hydraulic actuator. Thermocouples were mounted on the external damper body and the remote reservoir surfaces to monitor the operating temperature. The damper force was measured using a force transducer mounted between the damper and the cross-member forming the part of the sprung mass. The data acquisition unit described in the conventional test was used for collection of data from the two DOF tests. While sampling rates from 250 to 400 samples per cycle were selected for tests performed under sinusoidal excitations, sampling rates of 1 and 2 ms were selected for damped and undamped systems, respectively, under step excitations.

The first series of tests were performed on the undamped quarter-car system to identify the friction forces arising from the linear bearings. Lightly damped, the test apparatus revealed excessive motion and/or jumps near the sprung mass resonance and wheel-hop frequencies. The test frequencies and amplitudes were, therefore, appropriately selected to ensure that the system remained stable.

The second series of tests were performed on the damped quarter-car simulator, and the tests were repeated with each of the candidate dampers. Similar to the temperature tests run on the conventional test stand, the damper was brought up to a temperature slightly higher then the desired test temperature, by varying the input excitation. The outside body temperature of the dampers was carefully monitored during the tests, and measurements were recorded corresponding to relatively constant desired temperature. A temperature variation ±5°C was allowed for the Koni and Mechformance dampers, and 9°C for the Fox damper. The body of the Koni damper was maintained near a nominal temperature of 95°C, while the temperatures of Mechformance and Fox reservoirs were held near 44°C and 46°C, respectively. The above test temperatures were selected due to the fact that the monotube Koni damper operates at a more uniform temperature throughout the damper, than the Mechformance and Fox dampers, due to its relatively smaller surface area, and the proximity of the gas chamber to the piston. In the case of remote reservoir dampers (Fox and Mechformance) it is difficult to maintain a uniform and consistently high temperature. It was thus decided to maintain the reservoir temperature near 45°C, while permitting larger variation in the body temperature ranging from 64 to 100°C. As in the case of conventional damper test, two series of tests were performed on the Fox damper corresponding to two damper settings.

2.4 SUMMARY

The force-velocity and force-displacement characteristics of different dampers and test methodologies were described. The construction and operation of monotube and

remote reservoir racing car dampers were described in terms of design, low-, mid-, and high-speed valving, gas spring and friction forces. Three candidate dampers were selected for the analytical and experimental studies, based upon their different design and performance characteristics. Typical damping characteristics were described to illustrate the effects of asymmetric multi-stage valving, friction, gas spring, fluid and temperature variations. Different test methodologies to identify the force components due to gas spring, friction and hydraulic flows were reviewed for their suitability for the study.

CHAPTER 3

DEVELOPMENT OF ANALYTICAL MODELS

3.1 INTRODUCTION

The use of analytical models in assessing performance characteristics has been limited primarily due to three factors: (i) associated complexities and determination of numerous coefficients to characterize a damper; (ii) inability to predict the performance for a wide range of operating conditions, such as variations in temperature and oil compressibility; and (iii) lack of a universal model to analyze different dampers with varying designs of valves, such as deflection discs and blow off valves.

Analytical models of automotive dampers of varying complexities and simplifying assumptions have been developed and reported in the literature [13,17,19-22,27,28,30]. A simplified model, based upon viscous and asymmetric damping, has been successfully used and published by Ahmed et al. [56]. Although this conceptual model can be generally applied for different configurations of dampers, the contributions due to gas spring, friction, temperature effects, and compressibility of the oil and damper components, are assumed to be negligible. The damper model developed by Segal and Lang [18] has established the significance of friction and compressibility effects, while the importance of temperature and gas spring effects, specifically in high performance applications, has been demonstrated by Warner and Sankar [50]. The significant influence of gas spring temperature, friction and compressibility effects is further illustrated in the laboratory test results presented in Chapter 2.

In this Chapter, an analytical model of the candidate dampers is developed to asses the performance characteristics over a wide range of operating conditions. The model of the damper is developed through systematic characterization of various components of the damper force. These components include; asymmetric multi-stage damping, friction, gas spring, fluid compressibility, and temperature sensitivity. An analytical model of

each component is then developed, and the associated coefficients are derived from the experimental data. Each model is validated using the experimental data for all the candidate dampers. The validated component models are then integrated with the hydraulic damper model, derived from fluid continuity and compressibility laws, to develop a total damper model.. The modeling technique proposed in the study eliminates the tedious and potentially erroneous task associated with disassembling the damper and performing various measurements of the components.

3.2 DEVELOPMENT OF GAS SPRING AND FRICTION FORCE MODELS

While the contribution due to damping can be minimized, by testing at very low speeds, the dynamic force developed by a damper invariably is comprised of components due to gas spring and friction, hence, these two components are identified simultaneously.

Although the gas spring force can be derived from the gas laws assuming a polytropic process and known initial conditions of gas pressure and volume [33], the strong dependency of the gas spring and oil volume on temperature can lead to significant errors. Alternatively, the gas spring force may be determined through measurement of gas pressure. The installation of a pressure transducer, however may pose certain complexities in some damper designs. The gas spring force of the Mechformance damper was determined from both the pressure and static force measurements described in Chapter 2. This force component for other dampers, however, was derived from the static force measurements alone. The measured pressure data is used to establish the polytropic exponent and to validate the gas spring force identified from static measurements. The measured force-displacement data is also analyzed to yield initial gas pressure and volume, assuming extremely low speed (static) and symmetric friction properties. The assumption of symmetric friction force is quite reasonable, since the magnitude of friction force is relatively small. The difference in compression and extension force can thus be equated to twice the magnitude of friction force, as shown in Figure 3.1.

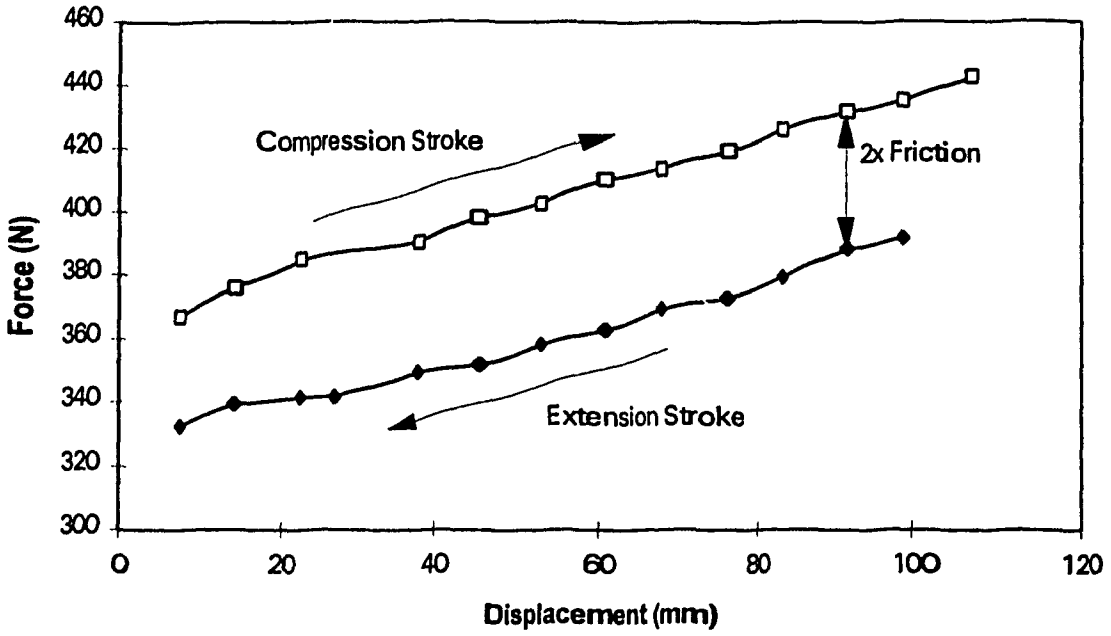

Figure 3.1 Measured static force-displacement characteristics of the Fox damper.

The gas spring force can be derived from the mean value of the two forces. A number of studies have established friction force models independent of the damper displacement [17,20,22,28,30,33-35]. Analysis of the test results, however, revealed that the magnitude of symmetric friction of the Mechformance and Koni dampers, and the gas spring characteristics of all the candidate dampers are strongly related to the damper displacement. The two components are thus identified as a function of the damper displacement. While the computed friction force corresponding to different displacements is arranged in a look up table, a regression analysis is performed on the gas spring force-displacement data to estimate the initial gas volume and charge pressure.

The data acquired from low speed dynamic testing is analyzed at the points of discontinuity in the force-displacement curves to determine: (i) the ratio of 'static' friction force to the 'dynamic breakaway' friction force, (ii) temperature sensitivity of the friction force, (iii) the polytropic exponent, and (iv) effective thermal expansion coefficient for the oil and other components that affect the gas volume. In order to simplify the analysis it is assumed that a thermal balance is achieved within the range of

operating temperature. Although the points of discontinuity, for the compression and rebound segments are quite distinct and easily identifiable for dampers with light damping, it is quite difficult to establish such points of discontinuity for heavy damping, as shown earlier in Figure 2.9. An algorithm is thus developed to estimate these points of discontinuities in the measured data.

3.2.1 Development of Friction Force Models

Many analytical and experimental studies have illustrated the significant influence of friction force on the damper performance characteristics [17,20,30]. All these studies, however, assume constant magnitude friction force irrespective of the displacement and velocity excitation amplitudes. The dependence of frictional force magnitude on the excitation amplitude has not been addressed in any published study on damper performance, except in the case of external loading where Bastrow [57] developed a mathematical model for strut friction. The laboratory tests performed in this study clearly illustrate the dependence of the friction force on the damper displacement, specifically for Koni and Mechformance dampers. This dependence of frictional force, attributed to misalignments and varying tolerances along the damper stroke, can be quite significant, particularly at low damper speeds. Variations in the friction force with displacement can also be attributed to small bearing overlap, particularly when the unit is subjected to side loads [57]. Bearing overlap is commonly defined as the distance between th[illegible] of the piston band and the bearing in the seal head at the unit's full extension. The [illegible] of changes in the side load on friction decreases with larger overlap. The candidate dampers, are, invariably, mounted concentric with helical wound springs which, when bowing of the spring occurs, can produce considerable side loads on the dampers. The influence of side loading on the dampers is not investigated since the quarter car fixture did not have the suspension springs mounted coaxial with the dampers, although this effect could be readily modeled using the methodology presented here. The methodology

described below yields variations in friction force with displacement that can be attributed to variations in cylinder bore and bent piston rods.

The magnitude of friction force (F_{sx}) is thus determined as a function of displacement derived from the static test described in Chapter 2. The friction force corresponding to discrete displacements is arranged in a look-up table, and integrated within the damper model using linear interpolations in the following manner:

$$F_{sx} = F_1 + \frac{(F_2 - F_1)}{(X_2 - X_1)}(x - X_1) \qquad x < X_1$$

$$F_{sx} = F_i + \frac{(F_{i+1} - F_i)}{(X_{i+1} - X_i)}(x - X_i) \qquad X_i \le x \le X_{i+1} \qquad (3.1)$$

$$F_{sx} = F_n + \frac{(F_n - F_{n-1})}{(X_n - X_{n-1})}(x - X_n) \qquad X_n < x$$

where F_1 and F_n are the measured friction forces at and smallest and largest damper displacements, X_1 and X_n , respectively. F_{sx} is the magnitude of static friction corresponding to displacement x at a temperature of 20°C. F_i (i=1, ..., n) is the magnitude of static friction tabulated corresponding to deflection X_i.

The velocity dependent friction, which is a complex function of the friction arising from piston-cylinder, rod-guide, and rod-seal interfaces, is further characterized to study the damper performance. The seal friction is known to vary considerably with operating temperature and the hydraulic pressure developed during damper operation [16,33] in a highly complex manner. In order to minimize the contributions due to hydraulic pressure drops, the damper valves were removed. An additional flow path across the piston was introduced, such that the flow area was approximately 1/5 of the piston area. The resultant damper force is then considered to constitute the components due to gas spring and friction. Figure 3.2 illustrates the measured force-displacement characteristics of the

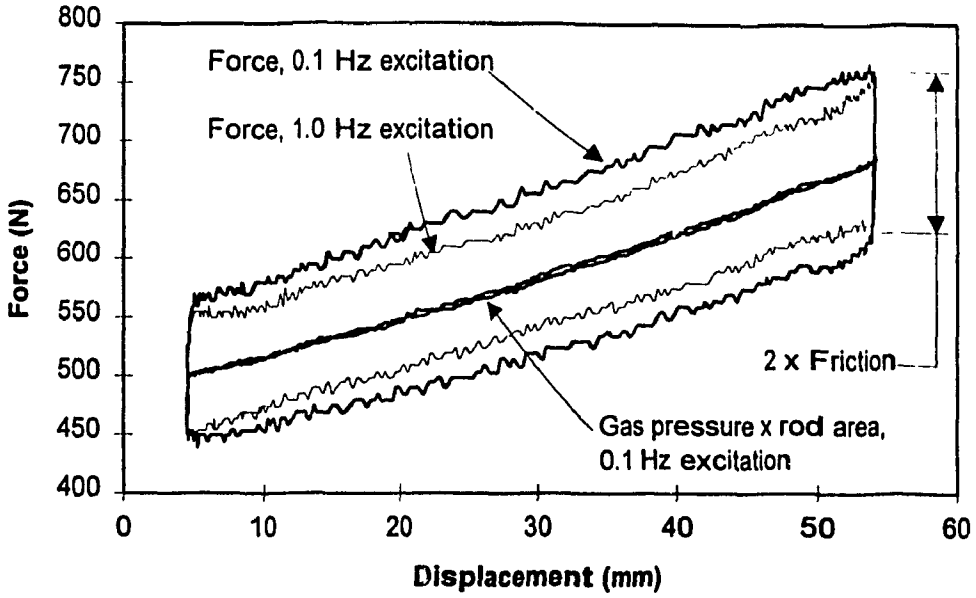

Figure 3.2 Friction and gas spring effects in a damper with no valving and minimal hydraulic drag.

Mechformance damper for different excitation frequencies (velocities). The gas spring force, derived from the measured gas pressure and rod area, is relatively insensitive to changes in the velocity. The magnitude of friction force, decreases with increasing velocity as can be seen in the Figure. The seal friction, however, will increase with increasing velocity when the damper valving is included, due to the effect of increased hydraulic pressures [16]. This combined with the effects of piston-cylinder and rod-guide, friction, under different operating conditions, makes it extremely difficult to characterize the combined dynamic friction. Therefore the development of a dynamic friction model is not attempted. A friction force model based upon the measurements of static and dynamic breakaway forces is formulated. The errors associated with this simplification are partially corrected through the coefficients of the hydraulic model.

A friction model comprising the effects of displacement, temperature and variations between the static and dynamic breakaway measurements, based upon linear correlation is proposed. The linear model is developed assuming linear thermal expansion of the

materials in the temperature range of interest. The corresponding changes in clearances thus cause proportional changes in the friction force. While all the three units use steel pistons, the bodies of the Koni and Mechformance units are aluminum, and the Fox damper has a steel body The measurements performed at different operating temperatures revealed a decrease in static friction force with an increase in temperature (results presented in Chapter 4), in the case of the Koni and Mechformance dampers. The test data for the Fox damper (with steel body) was observed to be more scattered, with no clearly defined variations with temperature.

For the damper model, the ratio, R_{fxT},of the magnitude of dynamic breakaway(F_{bxT}) to static (F_{sxT}) friction forces corresponding to displacement x and temperature T, is defined as:

$$R_{fxT} = \frac{F_{bxT}}{F_{sxT}} \tag{3.2}$$

The damper force measured at different temperatures is analyzed and the ratio R_{fxT}, as a function of the displacement and the temperature difference, computed. The ΔT is expressed with reference of a temperature of 20°C, such that $\Delta T = T-20$. A linear regression is performed. The damper friction model is then expressed in terms of the resultant coefficients, temperature differential and static friction:

$$F_{mext} = F_{sx}\left(C_{sfT}\cdot\Delta T + C_{ifT}\right)\cdot sgn(\dot{x}) \tag{3.3}$$

where C_{sfT} defines the sensitivity of friction force with variations in temperature, primarily attributed to the different thermal expansion coefficients of the components. C_{ifT} is the intercept or the ratio R_{fxT} at zero temperature change and is the derived ratio between the dynamic breakaway and static measurements at zero temperature change (T = 20°C), sgn(x) defines the sign of the relative velocity.

The friction force model, described in Equation (3.3), does not include the friction force due to floating piston separating the gas from the oil. The friction force arising

from the floating piston of the Mechformance damper was investigated through measurement of the pressure drop across the floating piston for a range of test conditions. The test data revealed that the values of pressure differentials were relatively small, in comparison with the gas spring and force, and thus may be neglected. As an example, the pressure differential across the floating piston at an operating temperature of 93°C subject to excitations at frequencies of 0.5 and 3 Hz can be equated to forces of 1.7 and 2.5 N, respectively.

3.2.2 Gas Spring Models

The gas spring force, defined as the piston rod cross section area multiplied by the gas pressure, can be a significant factor in the forces generated by the damper. Simple analytical models based on the ideal gas laws have been employed in the studies of motorcycle dampers [30] and hydropneumatic suspension [33]. These models have proven to be accurate, while not being overly complex. An analytical model based on Rubin Webber equation has been shown to correlate very well with the experimental results [58] for a gas charged accumulator. Els and Grobbelaar [59] developed a model of the hydrodynamic suspension using the Benedict-Webb-Rubin equation. The study demonstrated good correlation between theoretical and experimental results derived under 80 mm amplitude displacement excitation at 0.1 Hz. The model validity corresponding to more representative suspension excitations, however, is not demonstrated. Further, the contributions due to friction forces were assumed negligible, even at the at the relatively high charge pressure (2-40 Mpa) used in the study.

The gas spring model for the candidate models is developed using ideal gas law for its simplicity and due to relative low gas pressures. The assumption of low pressures is further supported by experimental studies and literature [5,30,49,50]. The gas spring model based upon real gas laws, however, has been validated for higher gas pressure [60].

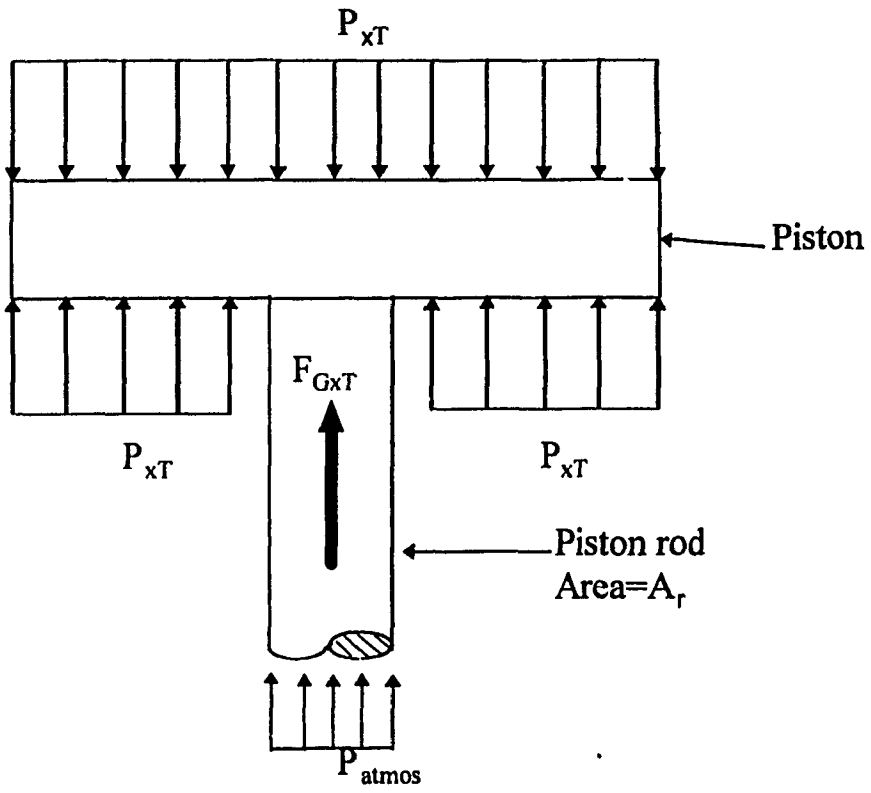

Figure 3.3 Representation of the forces acting on the piston and the rod.

Assuming negligible pressure drop across the flow restriction valves, the gas pressure approaches the fluid pressure throughout the damper. The gas spring force, derived from Figure 3.3, can be expressed as:

$$F_{GxT} = (P_{xT} - P_{atmos}) \cdot A_r \tag{3.4}$$

where F_{GxT} and P_{xT} are the gas spring force and pressure, respectively, corresponding to rod displacement x from full extension and temperature T measured on the damper body. A_r is the cross section area of the piston rod, and P_{atmos} is the atmospheric pressure.

3.2.2.1 Development of Static Gas Spring Model

The force-displacement data derived from the static test stand experiments, described in section 2.3.1.2, is used to determine the initial gas pressure and volume of

the unit at an initial temperature T_0. An analytical model of the static gas spring is then developed by curve fitting the test data, assuming incompressible hydraulic fluid, and a rigid container. The constant temperature ideal gas process under static conditions yields:

$$P_x V_x = P_0 V_0 \tag{3.5}$$

where P_0 and V_0 are the initial gas pressure and volume, respectively, corresponding to full extension. V_x is the gas volume corresponding to rod displacement x, which is derived from the volume of oil displaced by the piston rod:

$$V_x = V_0 - x(A_r) \tag{3.6}$$

The corresponding gas pressure P_x is then derived from Equations (3.5) and (3.6):

$$\frac{1}{P_x} = -\frac{A_r}{P_0 \cdot V_0} \cdot x + \frac{1}{P_0} \tag{3.7}$$

Equation (3.7) is solved to determine the initial gas pressure and volume, using linear regression analysis.

3.2.2.2 Temperature Dependent Gas Spring Models

The gas spring force is strongly dependent on the operating temperature, primarily due to thermal expansion of oil and other components, and the variations in volume and pressure. These two factors are additive, both increasing the gas force with an increase in temperature. The change in gas volume in sealed damper designs is primarily attributed to thermal expansion of the oil, while the contributions due to thermal expansion of the components is relatively small. The changes in fluid volume in the Mechformance unit are computed to demonstrate the relative effects of variations in temperature. An oil volume of 270 cc with coefficient of thermal expansion of 0.00072/°C [61] yields a 16.7 cc volume increase resulting from an 86°C increase in temperature. A simplified model employed to compute the volume increase due to body and reservoir expansion resulted in 2.3 cc volume increase for the same temperature change, which is considerably

smaller. Such secondary effects, however, can be readily incorporated within the model based on effective thermal coefficient of expansion of oil, derived from the experimental data. The volume change is then derived from:

$$\Delta V_{oilT} = \Delta T \cdot K_{oil} \cdot V_{oil} \tag{3.8}$$

where K_{oil} is the coefficient of thermal expansion of oil and V_{oil} is the initial oil volume. The volume of gas at full extension, corresponding to temperature T, can thus be expressed as:

$$V_{0T} = V_0 - \Delta V_{oilT} \tag{3.9}$$

The resulting gas volume corresponding to a rod displacement x and temperature T, can be then derived by substituting V_{0T} for V_0 in equation (3.6):

$$V_{xT} = V_0 - x(A_r) - \Delta V_{oilT} \tag{3.10}$$

Equations (3.8) and (3.10) yield the gas volume as a function of ΔT and K_{oil}:

$$V_{xT} = V_0 - x(A_r) - (\Delta T \cdot K_{oil} \cdot V_{oil}) \tag{3.11}$$

Upon substituting for the gas volume, V_{xT} , in the ideal gas law, gas pressure as function of T and K_{oil} is derived as:

$$P_{xT} = P_0 \cdot \frac{V_0}{V_0 - x(A_r) - (\Delta T \cdot K_{oil} \cdot V_{oil})} \cdot \frac{T}{T_0} \tag{3.12}$$

The gas pressure P_{xT} can also be expressed in terms of rod reaction force from equation (3.4):

$$P_{xT} = \frac{F_{GxT}}{A_r} + P_{atmos} \tag{3.13}$$

Equation (3.12) and (3.13) yield the following expression for oil volume change in terms of rod reaction force and operating temperature:

$$\Delta T \cdot K_{oil} \cdot V_{oil} = V_0 - x \cdot A_r - \frac{P_0 \cdot V_0 \cdot T}{\left(\frac{F_{GxT}}{A_r} + P_{atmos}\right) \cdot T_0} \tag{3.14}$$

It should be noted that the thermal expansion coefficient and the oil volume of a damper design are not readily available. The model, however, necessitates the determination of the product of the two variables. From equation (3.14), it is apparent that the variables ΔT, T, x and F_{GxT} can be easily derived from experiments. The product $K_{oil}\, V_{oil}$ is then conveniently derived using linear regression analysis, and known damper geometry. An effective coefficient of thermal expansion is defined to incorporate the change in oil volume caused by expansion of body and the reservoir, such that the left side of equation (3.14) can be expressed as:

$$\Delta T \cdot K_{oil} \cdot V_{oil} = \Delta T \cdot K_{voil} + K_{voint} \tag{3.15}$$

where K_{voil} the slope of the linear regression curve, represents the effective thermal expansion coefficient and K_{voint}, the intercept, accounts for the experimental errors. Equations (3.4), (3.12) and (3.15) yield the following temperature dependent gas spring force model for an ideal gas process:

$$F_{GxT} = \left(\frac{P_0 \cdot V_0 \cdot T}{\left(V_0 - x \cdot A_r - \Delta T \cdot K_{voil} + K_{voint}\right) \cdot T_0} - P_{atmos} \right) \cdot A_r \tag{3.16}$$

3.2.2.3 Development of Polytropic Gas Spring Model

Equation (3.16) yields the gas spring force under static test conditions, where the gas process can be accurately characterized by the ideal gas equation, or as a reversible isothermal polytropic process. The gas spring force under dynamic conditions, however, is accurately modeled as a reversible, approximately adiabatic, polytropic process, by:

$$P_{xT\gamma} = P_{xeT} \cdot \left(\frac{V_{xeT}}{V_{xT}} \right)^{\gamma} \tag{3.17}$$

where $P_{xT\gamma}$ is the gas pressure, corresponding to a rod displacement x from full extension and temperature T, assuming a polytropic process, γ is the polytropic exponent to be determined from the pressure measurements performed on the Mechformance damper. In application the gas compression involves a complex combination of isothermal and approximately adiabatic polytropic gas processes. In most cases, the damper is at rest prior to excitations. during which time the heat build up from the nearly adiabatic compression process is dissipated, resulting in a pressure equal to that obtained under isothermal compression from the initial volume and pressure conditions. P_{xeT} is the gas pressure corresponding to temperature T and displacement x_e , which refers to a point in the damper displacement curve at which the pressure can be equated to the initial conditions under an isothermal process using equation (3.12). In damper testing, this point will normally refer to the damper position at the start of the test, assuming that a sufficient rest period is allowed to dissipate the heat generated during damper motion. V_{xeT} is the corresponding gas volume, which can be related to gas V_{xT} at damper displacement x and temperature T, in the following manner:

$$V_{xT} = V_{xeT} - (x_e - x) \cdot A_r \tag{3.18}$$

Assuming quasi steady-state heat transfer, the gas spring force corresponding to a polytropic gas process, $F_{GxT\gamma}$, can be derived from equations (3.4), (3.17) and (3.18):

$$F_{GxT\gamma} = \left(P_{xeT} \cdot \left(\frac{V_{xeT}}{V_{xeT} - (x_e - x) \cdot A_r} \right)^{\gamma} - P_{atmos} \right) \cdot A_r \tag{3.19}$$

3.3 DAMPING AND COMPRESSIBILITY

The development of damping force model involves appropriate considerations of flow rate and pressure dependent valving mechanisms, interactions between the valving, the fluid compressibility and temperature dependency. In view of the complexities associated with all of these factors, a systematic building block approach is utilized to

develop component models. Different valving mechanisms are initially modeled, followed by development of valve systems and fluid compressibility models. The above component models are integrated to derive distinct damper models, characterizing the forces due to two different damper designs: *(i)* monotube design, where the entire pressure drops occur across the piston; and *(ii)* remote reservoir design, where pressure drops occur across the piston and compression head. The valving and damper models are also developed for incompressible flow in order to determine initial approximations for the valving model coefficients. These coefficients are achieved by curve fitting the experimental data obtained under low levels of acceleration, where the compressibility effects are considered negligible. The damper valving model incorporating the compressibility coefficients is derived using an iterative methodology. The temperature dependence of damper force is finally derived through identification of temperature sensitive oil density coefficients. The mass due to oil, floating piston and valving components is assumed negligible in the modeling process.

3.3.1 Valving Models

3.3.1.1 Individual Valving Models

Dampers invariably employ valving in the form of one or more orifices and/or pressure relief valves. Such valves are analytically modeled, while the associated coefficients are determined experimentally. Although the flow through valves may occur under either laminar or turbulent conditions, the experimental and analytical studies conducted by van Vliet [30] have demonstrated that an assumption of turbulent flow under all conditions yields an accurate model. This due to the relatively low damper forces produced at the low speeds that would be associated with steady state, laminar flow, hence the error in the assumption of turbulent flow is minimized. Further, in application, the damper response typically changes rapidly, resulting in turbulent flow.

Based on the assumption of turbulent flow, the characteristic equation for flow rate (Q) through an orifice is given by:

$$Q = C_d \cdot A_{eff} \cdot \left(\frac{2 \cdot \Delta P}{\rho}\right)^{1/2} \tag{3.20}$$

where ΔP is the pressure drop across the valve or the orifice and A_{eff} is the effective flow area. The flow area is constant for orifice flows and can be measured. In case of pressure relief valves, the flow area is computed from the limiting flow area of the valve, which is controlled by ε load-deflection device. ρ is the density of the fluid, which can be determined either experimentally or from the fluid properties. C_d is the discharge coefficient of the valve, which is a complex function of fluid pressure, valve design, geometry, etc. Lang [62] developed a comprehensive analytical passenger car shock absorber model and analytical and empirical expressions for discharge coefficients. The study resulted in a highly complex damper model and "concluded that flow rate prediction can not be made with an accuracy of better then 10%." While the experimental study demonstrated the strong dependence of discharge coefficient on the Reynolds number, acceleration number, geometric properties of the parts, and other design factors, a constant value of 0.7 resulted in good correlation and reduced complexity. In this study, the flow constants defined in modeling the valving are combined to yield effective flow impedance, in order to simplify the experimental-iteration process used to identify various constants.

Orifice Flows

Equation (3.20) can be rearranged to yield the pressure drop across the orifice:

$$\Delta P = \left(\frac{Q}{C_d \cdot A_{eff}}\right)^2 \cdot \frac{\rho}{2} \tag{3.21}$$

For constant values of area orifice, discharge coefficient, and fluid density, the ΔP can be related to the flow rate in the following manner:

$$\Delta P = C_{orr} \cdot Q^2 \tag{3.22}$$

where $$C_{orr} = \left(\frac{1}{C_d \cdot A_{eff}}\right)^2 \cdot \frac{\rho}{2}$$

Since ΔP and Q are related to force and damper velocity, respectively, by the area constants, equation (3.22) can be directly used to describe the low and high speed portions of the damper force-velocity characteristic curves, where orifice flow is dominant.

Flow Compensation

The response in the mid-speed range is dominated by a flow compensating valve, comprised of a spring and one-way valve. The spring is installed with a predetermined amount of preload, such that when the pressure differential across the valve exceeds the cracking pressure, defined as the preload force times the working area, the valve opens, permitting fluid flow. Typically the valve operates in a manner such that the force velocity curve is linear, throughout its effective range, as is illustrated by the force-velocity characteristic of the damper presented in Figure 2.1. Since ΔP and Q are directly proportional to force and velocity, this linear force-velocity behavior establishes the linear relationship between ΔP and Q. Referring to equation (3.21) with density and coefficient of discharge assumed constant, this would require that for the flow compensating valve, the effective orifice area is proportional to the square root of the flow rate:

$$A_{eff} = K_v \cdot \sqrt{Q} \tag{3.23}$$

where K_v is the constant for the flow compensating valve. Substituting for the effective area in equation (3.21) yields the following linear relationship:

$$\Delta P = Q \cdot \left(\frac{1}{C_d \cdot K_v} \right)^2 \cdot \frac{\rho}{2} \tag{3.24}$$

Alternatively, ΔP may be related to the flow rate in the linear mid-speed range by

$$\Delta P = C_{lin} \cdot Q \tag{3.25}$$

where $$C_{lin} = \left(\frac{1}{C_d \cdot K_v} \right)^2 \cdot \frac{\rho}{2}$$

Polynomial Model

Equations (3.22) and (3.25) reveal that the pressure drop is proportional to the square of the flow rate, through a fixed restriction and directly proportional to the flow rate through a flow compensating valve. A number of damper tests performed in this study revealed the predominance of flows through either orifice or the compensating valves in limited speed ranges. The force-velocity characteristics in certain speed ranges are best described by flows through both orifice restriction and the flow compensating valve. The pressure drop can thus be related to a polynomial function of Q combining the flows through orifice and compensating values:

$$\Delta P = C_{orp} \cdot Q^2 + C_{linp} \cdot Q \tag{3.26}$$

where C_{orp} and C_{linp} are the orifice and compensating coefficients respectively, in the polynomial model.

The above relationship also offers potential to compensate for internal leakage and laminar flows. Experimental results further revealed that addition of a constant into the above flow models yields improved correlation between the analytical and experimental data. The need for this constant may be attributed to residual errors associated with curve

fitting the data with gas spring and friction forces removed. The need for the constant may be further attributed to flow through preloaded valves which permit flows when the pressure differential approaches a preset value. The pressure differential due to orifice compensating valve and combined flows, described in equations (3.22), (3.25) and (3.26), are thus expressed as:

orifice flows: $$\Delta P = C_{orr} \cdot Q^2 + C_{iorr} \tag{3.27}$$

compensating valve flows: $$\Delta P = C_{lin} \cdot Q + C_{ilin} \tag{3.28}$$

combined flows: $$\Delta P = C_{orp} \cdot Q^2 + C_{linp} \cdot Q + C_{ip} \tag{3.29}$$

3.3.1.2 Flows Through the Valving Systems - Incompressible Fluid Flow

The candidate dampers employ different configurations of valving resulting in asymmetric damping characteristics in compression and rebound. Development of the damper model thus necessitates appropriate consideration of different flow models. The flow through one way valves employed in some dampers can be described by equation (3.28), since the valve operates at small pressure drops allowing nearly unrestricted flow in one direction. The majority of the damper designs, however, employ two parallel flow paths, where one of them remains functional at all times, while the second path requires a pressure differential to be activated. At low speeds (low pressure differential) the flow is best described by one of the three models (orifice, flow compensating or combined), while the mid speed flow is modeled using the low speed circuit in parallel with a flow compensating circuit, which is activated at a preset pressure differential. Although high speed flow circuits exist in many damper designs the racing car dampers typically do not operate in this speed range. The flow through the valving system, illustrated schematically in Figure 3.4, can be expressed in the following manner:

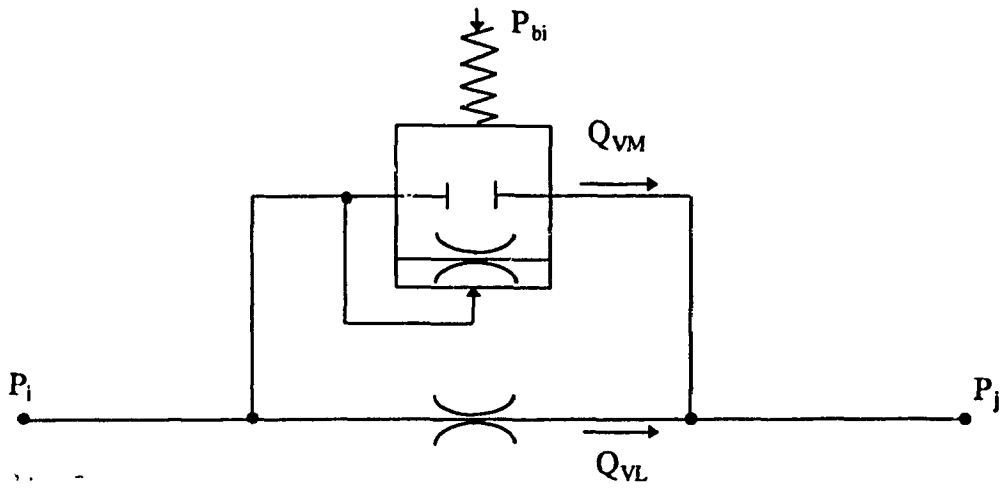

Figure 3.4 A schematic representation of hydraulic flows through the valves.

$$Q_{ij} = Q_{VL} \quad ; \quad \Delta P_{ij} \le P_{bi}$$

$$Q_{ij} = Q_{VL} + Q_{VM} \quad ; \quad \Delta P_{ij} > P_{bi} \tag{3.30}$$

where Q_{ij} is the flow through the valving system from chamber i to chamber j, and ΔP_{ij} is the pressure differential between chambers i and j. Q_{VL} and Q_{VM} are the flow rates through the low and mid speed valving, respectively, and P_{bi} is the preset pressure at which the mid speed valve between chamber i and chamber j opens. For compressible flows, the flow rate can be easily computed from the damper geometry and velocity. The pressure drop across the valving system is then derived from equation (3.30) in combination with equations (3.27) to (3.29). Figure 3.5 illustrates the methodology to solve for the pressure drop for known flow rate. Alternatively, the above formulations can be used to derive the flow rates when the pressure drop is known, as illustrated in Figure 3.6.

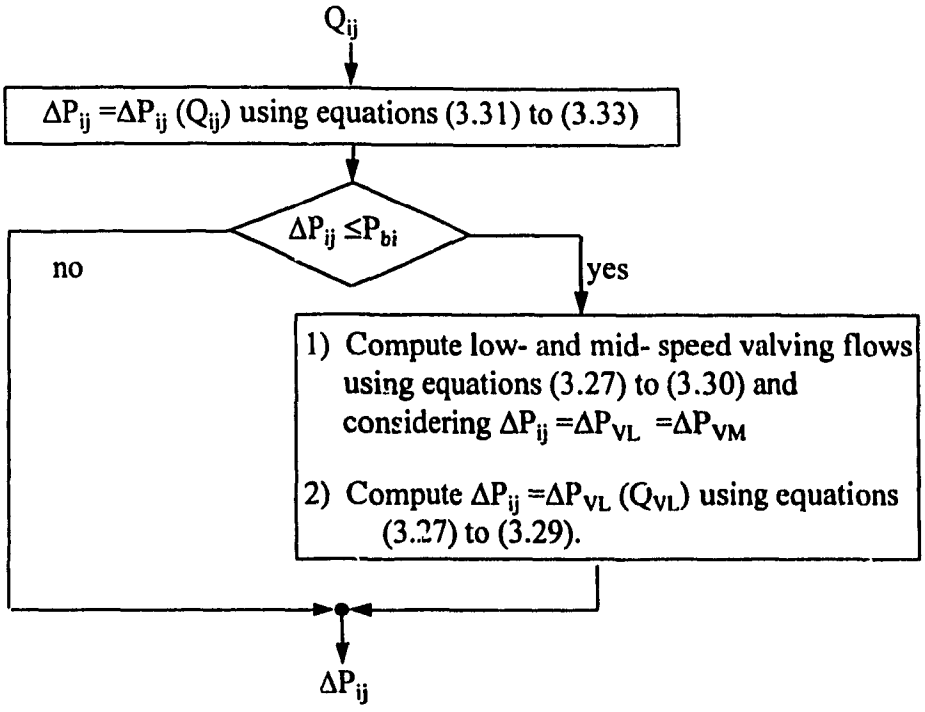

Figure 3.5 Determination pressure drop off as a function of known flow rate.

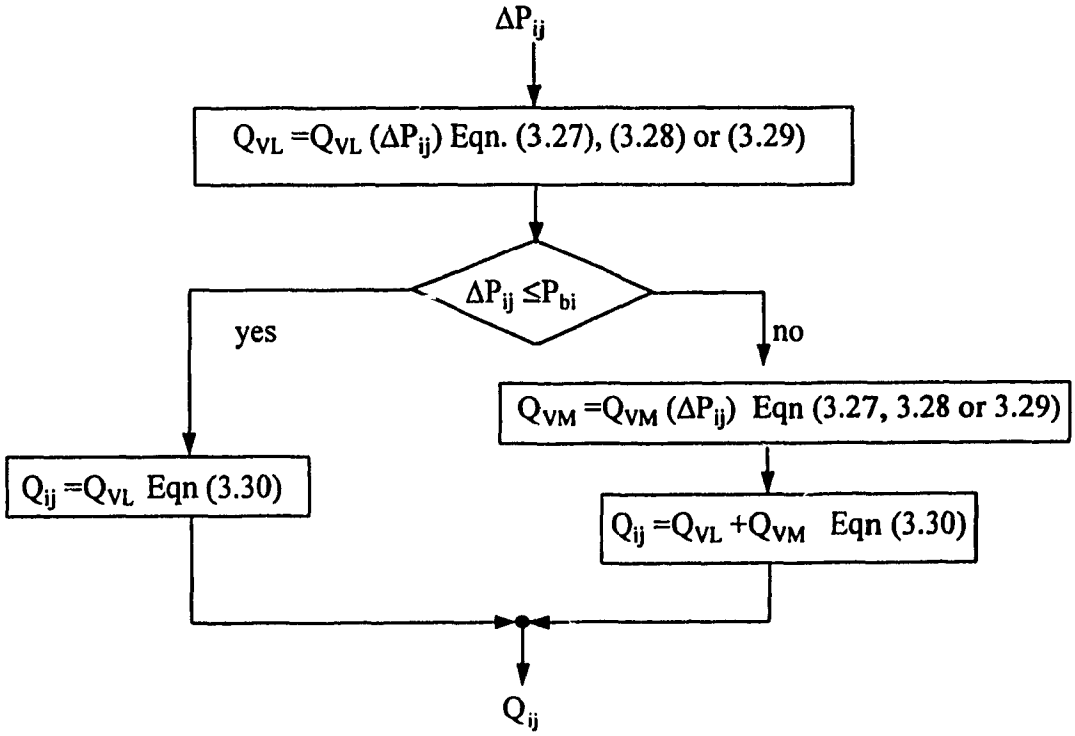

Figure 3.6 Determination of flow rate as a function of known pressure drop.

3.3.2 Compressible Fluid Flows

The peak force-peak velocity characteristics of dampers correlate very well with the results derived for incompressible fluid flows. The significance of fluid compressibility, however, becomes apparent when the time-histories of force and velocity, and the associated force-velocity data for one cycle are examined. The measured force-velocity characteristics presented in Figure 2.7 demonstrate that the magnitude of damping force is considerably smaller on the segments of the curves where the magnitude of acceleration is decreasing then on the segments where it is increasing, while the composite peak curve in general lies in-between. This is particularly true in the segments where the rate of change of acceleration is the highest. For compressible flows during the decreasing magnitude of acceleration segments of the cycle, the flow restriction yields pressure build up on the high pressure side of the piston and results in storage of energy in the oil. The resulting flow through the valves and thus the damping is smaller than that encountered with incompressible flows. The compressible fluid flow, however, is larger than the incompressible flow during the segment of the cycle where the magnitude of acceleration increases, which is attributed to gradual pressure reduction causing the release of stored energy in the form of increased oil volume, hence flow. The resulting damping force under increasing magnitude of acceleration is thus larger when compared to that achieved with incompressible flows. The development of a comprehensive damper model thus necessitates appropriate consideration of the fluid compressibility, specifically when time history of damping force is desired. The expansion and contraction of the cylinder walls and damper components caused by variations in chamber pressures also contributes to the change in fluid volume. This effect, although being similar to the fluid compressibility, is of second order. The combined effect of fluid compressibility and compression/expansion of the cylinder, however, can be effectively incorporated using a coefficient modified to include oil and cylinder wall effects [63]. Many studies have employed the modified coefficient in terms of an

effective compressibility or bulk modulus [17,33,64]. The fluid compressibility can be expressed as:

$$dP = -\frac{dV_c}{\beta \cdot V} \tag{3.31}$$

where β is the compressibility of the liquid, V is the chamber volume, P is the chamber pressure, and $d V_c$ the change in volume due to compressibility.

In this, as in the works of others, the temperature sensitivity of the oil compressibility is assumed negligible. This assumption is validated, over the temperature range applicable to race cars, by the validation of the damper models over a range of temperatures and operating conditions. The compressibility of the fluid, relative to pressure changes, has been often assumed constant in majority of the reported studies [17,19,33,64]. Although this assumption resulted in good correlation with the experimental data of some dampers used in this study, the need to derive a more complex compressibility model as a function of the pressure was identified to achieve good correlation between the experimental and analytical results, for the dampers with higher levels of damping. The dependency of β on the pressure may be attributed to a number of factors: *(i)* the compressibility of oil decreases with increase in pressure [65]; *(ii)* any air volume entrained in the oil results in an increase of the effective compressibility [66,67]; and *(iii)* variations in effective fluid compressibility caused by nonlinear deformation of rubber O-rings and other components with fluid pressure. Among these factors, the entrained air is known to affect the fluid compressibility most significantly.

An effective compressibility model is thus developed to study the effects of air entrainment. The model comprises a cylinder with a closed end and a piston at the other, with a known volume of gas entrained in the oil at standard conditions. Pressure is applied to the gas-oil volume through the piston, resulting in relatively rapid changes in the air volume with only slight changes in the oil volume. Assuming constant bulk

modulus of oil (1.37 x 10^9 Mpa) and polytropic process to describe the compression of entrained gas, the effective compressibility is computed as a function of the fluid pressure using equations (3.5) and (3.31). Figure 3.7 illustrates the effective fluid compressibility of the mixture as a function of the pressure for known air to oil volume ratio. It is evident that the effective compressibility varies significantly with pressure and initial volume of air entrained. The results further reveal that the effective compressibility can be approximated as a linear function of pressure, up to a minimum value (β_{min}) beyond which it is insensitive to the increase in the pressure, such that:

$$\begin{aligned} \beta &= P_i \cdot C_{s\beta} + C_{i\beta} \qquad & \beta \geq \beta_{min} \\ \beta &= \beta_{min} & \beta < \beta_{min} \end{aligned} \tag{3.32}$$

where P_i is the pressure in the *i*th chamber, $C_{s\beta}$ is the slope of the effective compressibility approximation model, and $C_{i\beta}$ is the intercept of the effective compressibility approximation model. The constants in equation (3.32) are determined

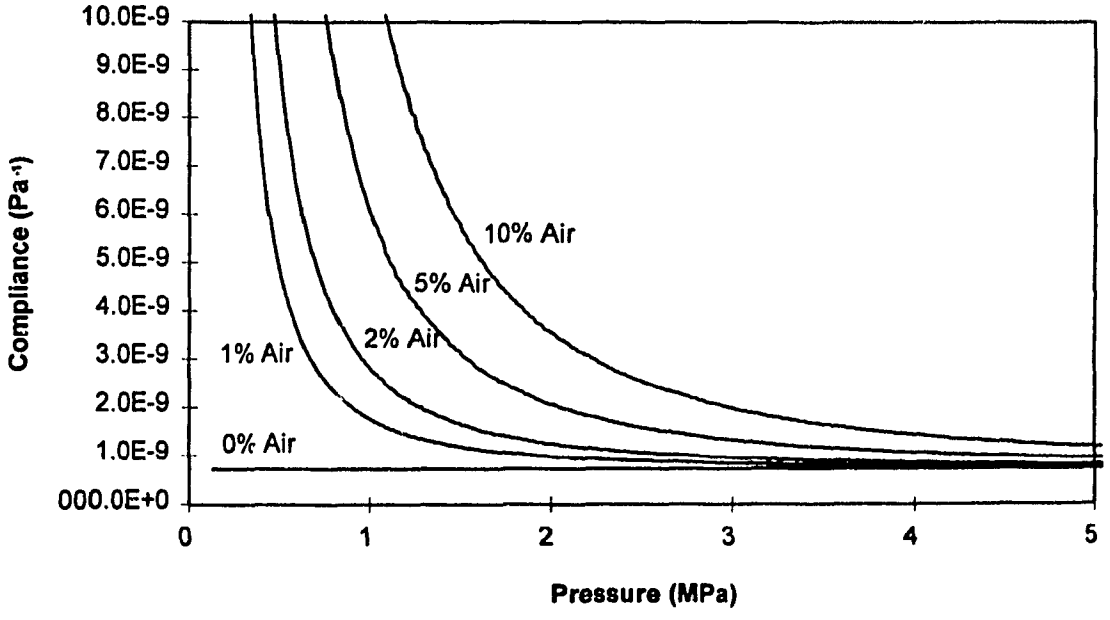

Figure 3.7 Effective compliance of oil as a function of pressure and entrained air.

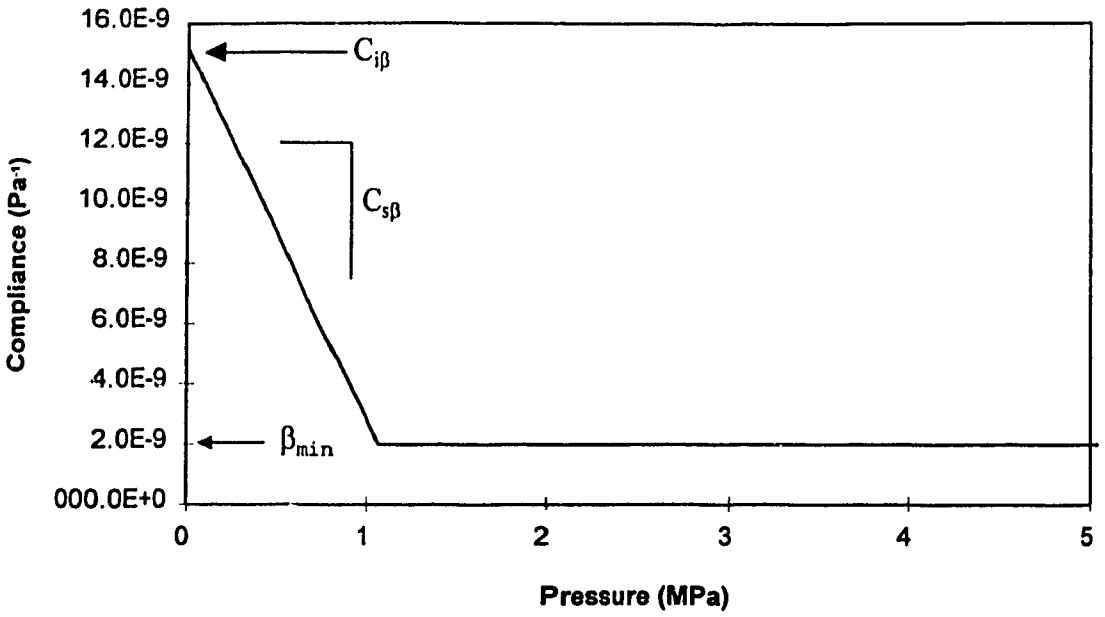

Figure 3.8 Effective compliance-pressure, characteristics of the Mechformance damper.

from the experimental force-velocity characteristics for different sinusoidal excitations, using an iterative procedure. Figure 3.8 illustrates the piecewise linear compressibility model described in equation (3.32). A comparison of Figures 3.7 and 3.8 reveals that the simplified model yields trends similar to those observed with the compliance model with entrained air.

3.3.3 Analytical Model of the Monotube Damper

Analytical models of the candidate dampers are derived upon combining the friction force, gas spring and the valving system models described in the previous sections, using the flow and pressure balance. A schematic of a monotube damper is shown in Figure 3.9. Chambers 1 and 2, referred to as 'compression' and 'rebound' chambers, respectively, contain oil, and chamber G is charged with nitrogen gas. Piston movement yields fluid flow from chamber 1 to 2 or from 2 to 1, depending on the

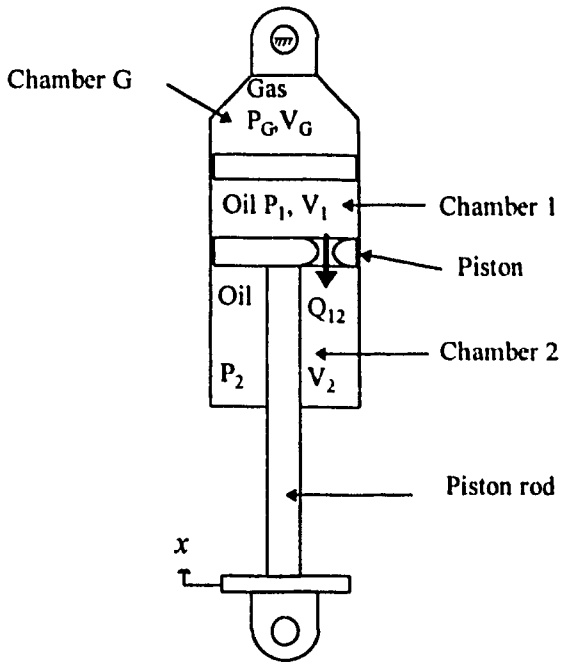

Figure 3.9 Schematic of a monotube damper

direction of motion. For incompressible fluid, the flow from chamber 1 to 2 can be expressed as:

$$Q_{12inc} = \dot{x} \cdot \left(A_p - A_r\right) \tag{3.33}$$

where Q_{12inc} is the flow rate from chamber 1 to 2 assuming incompressible fluid, and $\dot{x}$ is the piston velocity. The flow rate associated with compressible fluid assuming relatively rigid chambers can be expressed as:

$$Q_{12} = Q_{12inc} - \frac{dV_{C1}}{dt} + \frac{dV_{C2}}{dt} \tag{3.34}$$

where V_{C1} and V_{C2} are the volumes of fluid in chambers 1 and 2, respectively. Assuming negligible friction losses due to the separator piston, the pressure in the gas chamber can be equated to that of chamber 1, $P_G = P_1$. Since the gas is considerably more compressible than the oil, the rate of change of fluid volume in chamber 1, $\frac{dV_{C1}}{dt}$, can be assumed negligible, resulting in:

$$\frac{dV_{C2}}{dt} = Q_{12} - Q_{12_{inc}} \tag{3.35}$$

The volume of chamber 2, V_{C2}, is related to the piston displacement and geometry in the following manner:

$$V_{C2} = V_{C20} - [x \cdot (A_p - A_r)] \tag{3.36}$$

where V_{C20} is the initial volume of chamber 2 with the rod at full extension. It should be noted that the compressibility of oil in chamber 2 affects the pressure and volume of gas in chamber G and thus the effective gas spring force. The gas spring model, derived in section 3.2.2.3, assuming incompressible flows, thus needs to be refined to account for changes in volume of chamber 1 caused by compressibility of fluid in chamber 2. The change in chamber 1 volume due to compressibility of fluid in volume 2 (ΔV_{12}) can be derived from:

$$\Delta V_{12} = \int_0^t dV_{C2} dt \tag{3.37}$$

The effective gas volume, derived from equations (3.18) and (3.37), is then expressed as:

$$V_{xT}^c = V_{xeT} - (x_e - x) \cdot A_r - \Delta V_{12} \tag{3.38}$$

The corresponding gas pressure is derived assuming polytropic process:

$$P_{GT}^c = P_{xeT} \cdot \left(\frac{V_{xeT}}{V_{xT}^c} \right)^{\gamma} \tag{3.39}$$

where the superscript c refers to the gas pressure and volume corresponding to compressible flow conditions.

The rod reaction or damper force can be derived from the free body diagram of the piston rod and piston, shown in Figure 3.10:

$$F = P_1 \cdot A_p - P_2 \cdot (A_P - A_r) - P_{atmos} \cdot A_r + F_{fricxT} \tag{3.40}$$

By letting $\Delta P_{12} = P_1 - P_2$, the damper force can be expressed as:

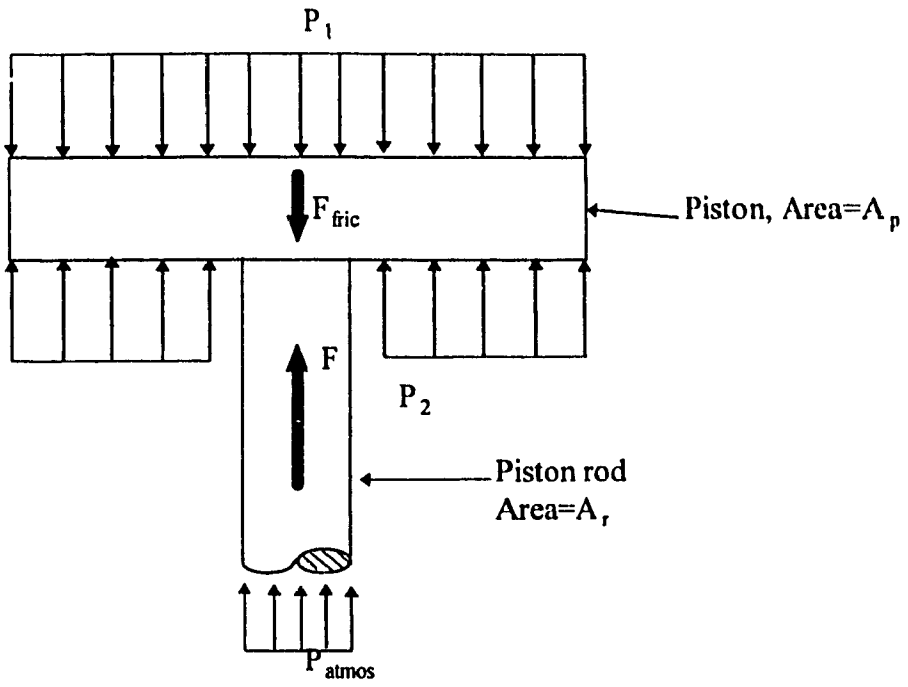

Figure 3.10 A free body diagram of the piston and rod assemblies illustrating the various force components.

$$F = \Delta P_{12} \cdot (A_P - A_r) + (P_1 - P_{atmos}) \cdot A_r + F_{fricxT} \tag{3.41}$$

Since $P_1 = P_g$, the term $(P_1 - P_{atmos}) \cdot A_r$ can be equated to the gas spring force, F_{GxT}, as described in equation (3.4). From equation (3.41), it is apparent that the damping force (F_d) is related to the pressure differential across the piston:

$$F_d = \Delta P_{12} \cdot (A_P - A_r) \tag{3.42}$$

The total damper force is thus expressed as a combination of forces due to damping, gas spring, and friction:

$$F = F_d + F_{GxT} + F_{fricxT} \tag{3.43}$$

The damping and gas spring forces for incompressible flows are directly derived from equations (3.4), (3.33) and (3.42). The pressure in chamber 1 is equal to the gas pressure determined from equation (3.18). Figure 3.11 presents the algorithm for solution

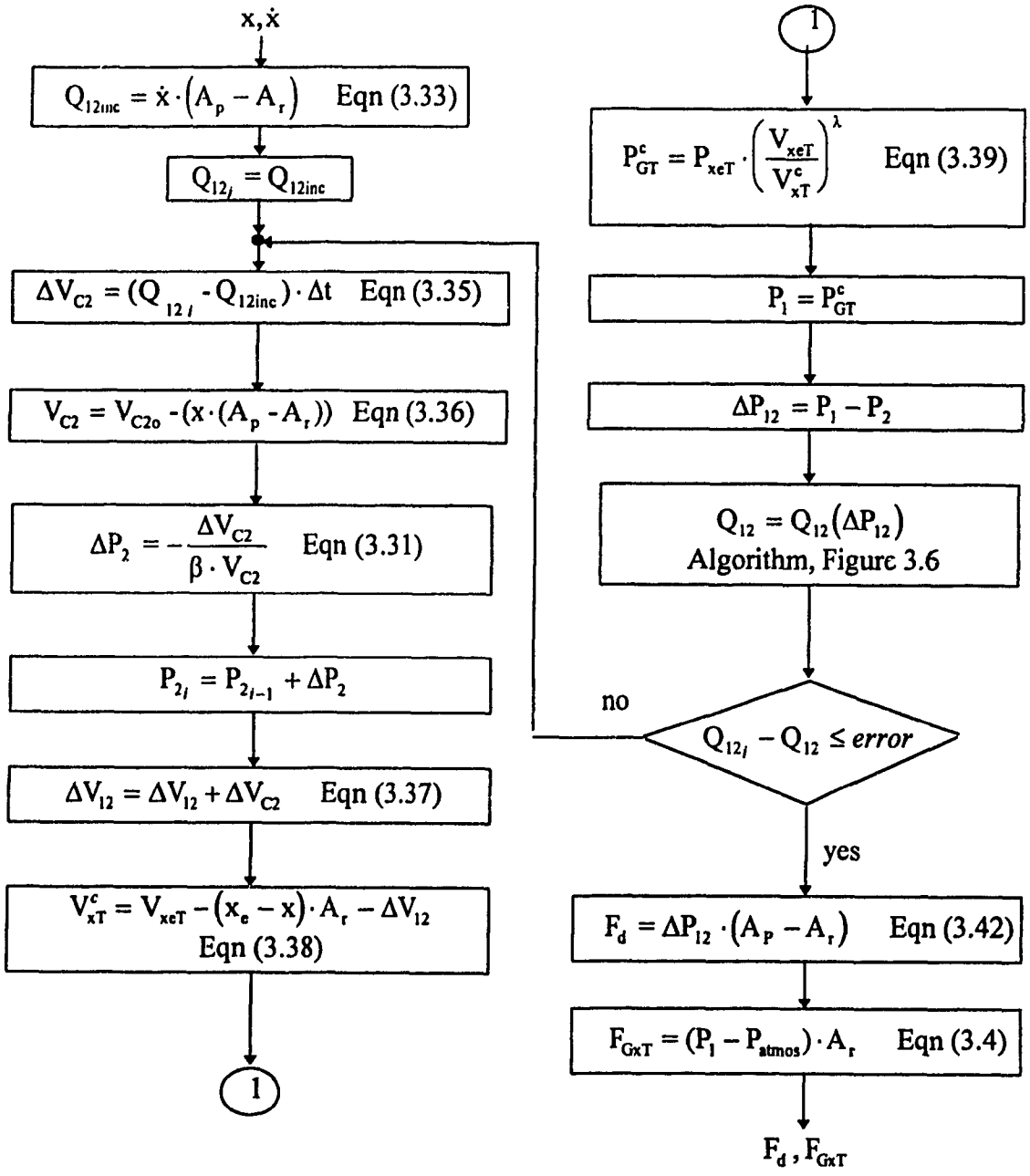

Figure 3.11 The computation of damping and gas spring forces of a monotube damper with compressible flows.

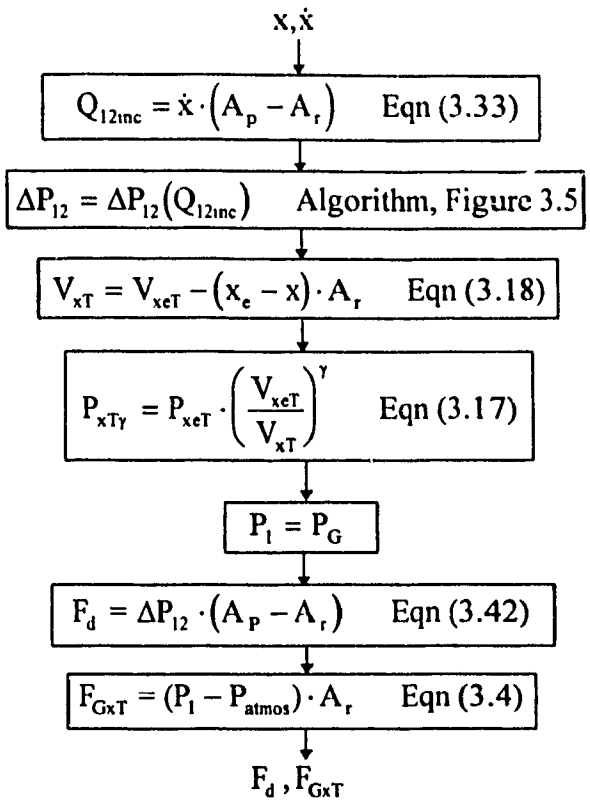

Figure 3.12 The computation of damping and gas spring forces of a monotube damper with incompressible flows.

of gas and damping forces for incompressible flow in a monotube damper. For compressible flows, however, the flow rate, pressure, and gas spring and damping forces are interrelated by the fluid compressibility, as evident from equations (3.35) to (3.41). An iterative algorithm is thus formulated to determine the force components through solution of equations (3.31) to (3.42), as illustrated in Figure 3.12.

3.3.4 Analytical Model of the Remote Reservoir Damper

Figure 3.13 illustrates a schematic of the remote reservoir damper, which differs from the monotube design. The remote reservoir damper comprises an additional chamber (3) connected to the gas chamber and a compression head located between chambers 1 and 3. The compression head consists of a set of valving including a check

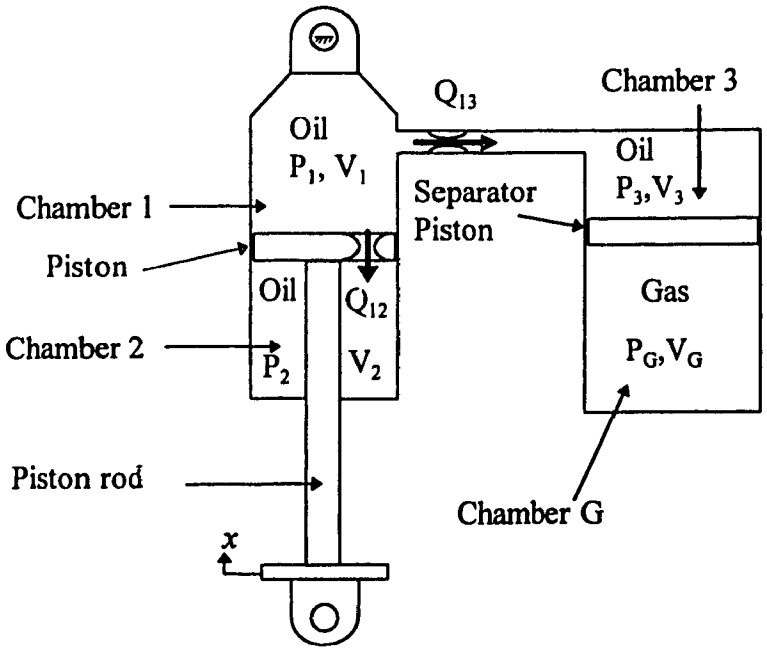

Figure 3.13 Schematic of a remote reservoir damper.

valve which permits nearly unrestricted flow during the extension stroke, and significant pressure drops during the compression stroke. Chambers 1, 2 and 3 contain oil while G is charged with nitrogen gas. As with the monotube design, the piston rod motion causes fluid flows across the piston and the compression head. For incompressible fluid flow, the flow rate across the piston is directly related to piston and rod areas, and piston velocity, as described earlier in equation (3.33) for the monotube design:

$$Q_{12inc} = \dot{x} \cdot \left(A_p - A_r \right) \tag{3.44}$$

The fluid flow rate through the compression head, (Q_{13inc}) can be directly related to the piston velocity through the rod area, and given by:

$$Q_{13inc} = \dot{x} \cdot A_r \tag{3.45}$$

For compressible flows, the flow rate across the piston can be derived upon incorporating the changes in fluid volumes in different chambers:

$$Q_{12} = Q_{12inc} - \frac{dV_{C1}}{dt} + \frac{dV_{C2}}{dt} \tag{3.46}$$

The fluid flow through the compression head is derived in a similar manner resulting in:

$$Q_{13} = \dot{x} \cdot A_r - \frac{dV_{C1}}{dt} + \frac{dV_{C2}}{dt} + \frac{dV_{C3}}{dt} \tag{3.47}$$

where dV_{C3} is the change in chamber 3 fluid volume, due to compressibility of the fluid. Assuming negligible friction losses due to the seals in the separator piston, and negligible inertial force due to the piston mass, the pressure in the gas chamber can be equated to that of fluid in chamber 3:

$$P_G = P_3 \tag{3.48}$$

Since the gas is significantly more compressible than the oil in chamber 3, and both media are subject to identical pressure, the effects of compressibility on the change in fluid volume in chamber 3 can be considered negligible. The flow through the compression head can thus be expressed as:

$$Q_{13} = \dot{x} \cdot A_r - \frac{dV_{C1}}{dt} + \frac{dV_{C2}}{dt} \tag{3.49}$$

From equations (3.46) and (3.49) it is evident that the compressibility of oil in chambers 1 and 2 affects the fluid volume in chamber 3, and the volume and pressure of the gas in chamber G. The change in fluid volume in chamber 3 due to variations in fluid volumes in chambers 1 and 2, can be derived from:

$$\Delta V_{312} = \int_0^t dV_{C1}dt + \int_0^t dV_{C2}dt \tag{3.50}$$

where ΔV_{312} is the change in fluid volume in chamber 3 caused by compressibility of fluid in chambers 1 and 2. This change in fluid volume directly influences the volume and pressure of gas in chamber G, given by:

$$V_{xT}^c = V_{xeT} - (x_e - x) \cdot A_r - \Delta V_{312} \tag{3.51}$$

$$P_{GT}^{c} = P_{xeT} \cdot \left(\frac{V_{xeT}}{V_{xT}^{c}} \right)^{\gamma} \tag{3.52}$$

where the superscript c refers to the gas pressure and volume corresponding to compressible flow conditions. The total dynamic force developed by the damper can be derived by considering the free body diagram of pressures and forces working on the piston rod and piston shown in Figure 3.10:

$$F = P_1 \cdot A_p - P_2 \cdot (A_P - A_r) - P_{atmos} \cdot A_r + F_{fricxT} \tag{3.53}$$

Letting $\Delta P_{12} = P_1 - P_2$ and $\Delta P_{13} = P_1 - P_3$, the damper force can be expressed in the following manner:

$$F = \Delta P_{12} \cdot (A_P - A_r) + \Delta P_{13} \cdot A_r + (P_3 - P_{atmos}) \cdot A_r + F_{fricxT} \tag{3.54}$$

where the term $(P_3 - P_{atmos}) \cdot A_r$ represents the gas spring, force, F_{GxT}, as described in equation (3.4), and F_{fricxT} is the friction force as described in equation (3.3). The remaining terms in equation (3.54) describe the damping force developed due to flows across the piston and compression head, given by:

$$F_d = \Delta P_{12} \cdot (A_P - A_r) + \Delta P_{13} \cdot A_r \tag{3.55}$$

The total dynamic force developed by the damper can thus be expressed as a combination of the force components:

$$F = F_d + F_{GxT} + F_{fricxT} \tag{3.56}$$

The components of forces developed by the damper can be directly computed from equations (3.4), (3.33) and (3.55), when incompressible fluid flow is considered. The pressure in chamber 3 is equal to the gas pressure determined from equation (3.17). Figures 3.14 and 3.15 illustrate the computation of gas spring and damping forces for incompressible and compressible flows respectively, in a monotube damper.

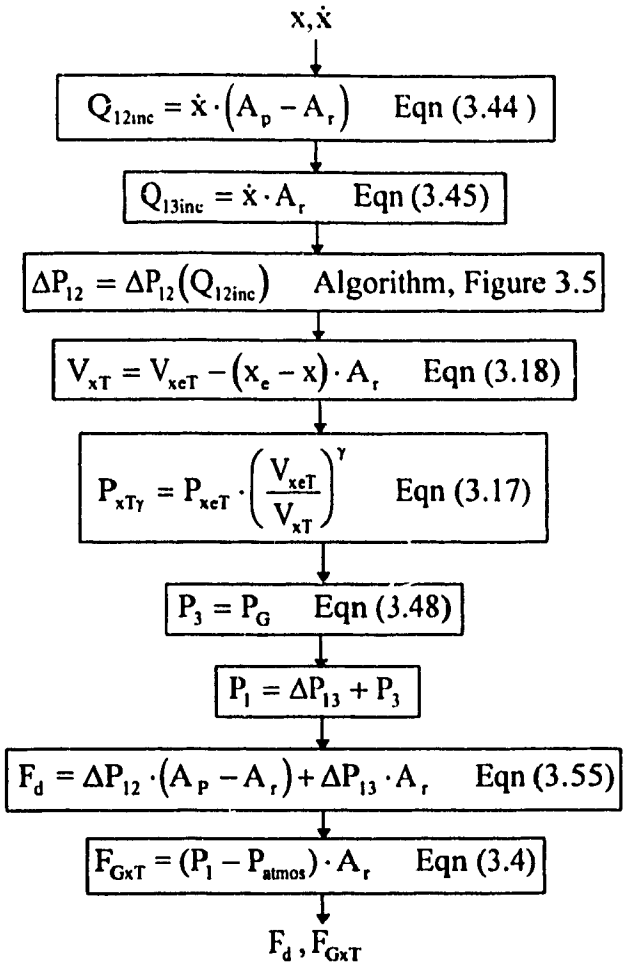

Figure 3.14 The computation of damping and gas spring forces of a remote reservoir damper with incompressible flows.

3.3.5 Temperature Sensitivity Model

The temperature sensitivity of the damping force can be characterized upon consideration of thermal expansion of the oil and the damper body. From equation (3.42) for the monotube and (3 55) for the remote reservoir designs, it is apparent that the damping force is related to the pressure drop. For a flow through a constant orifice valving, the damping force can be related to the flow rate using equations (3.21) and (3.42):

$$F_d = \left(\frac{Q}{C_d \cdot A_{eff}}\right)^2 \cdot \frac{\rho}{2} \cdot (A_P - A_r) \qquad (3.57)$$

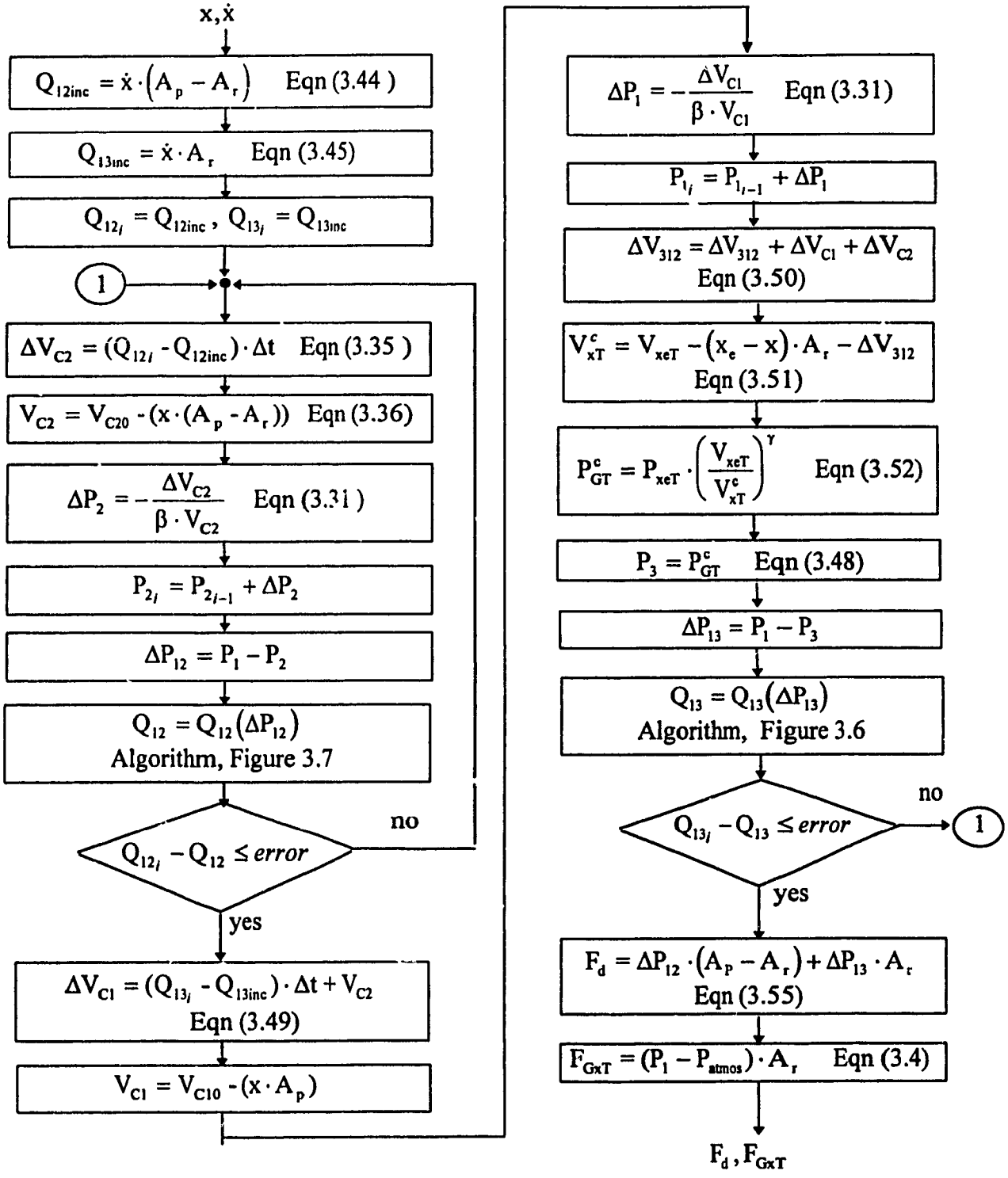

Figure 3.15 Computation of damping and gas spring forces of a remote reservoir damper with compressible flow.

Variations in the operating temperature affect the component dimensions and the fluid properties. In this study, the influence of temperature changes on the component dimensions is considered to be relatively small when compared to the thermal expansion of the fluid. Equation (3.57) clearly illustrates that a decrease in fluid density caused by an increase in the oil temperature yields reduced damping force. The ratio of damping forces developed at two different temperatures can thus be directly related to the inverse ratio of fluid volumes corresponding to the two temperatures, given by:

$$\frac{F_{dT}}{F_{dTref}} = \frac{V_{OILTref}}{V_{OILT}} \tag{3.58}$$

where $V_{OILTref}$ is the volume of oil at the reference temperature and V_{OILT} is the volume of oil at temperature T. Using a linear model for the thermal expansion of oil, V_{OILT} can be expressed as:

$$V_{OILT} = V_{OILTref} + \Delta T \cdot K_{oil} \tag{3.59}$$

where $\Delta T = T - T_{ref}$ and K_{oil} is the coefficient of thermal expansion of oil.

Substitution of equation (3.59) into equation (3.58) yields:

$$\frac{F_{dT}}{F_{dTref}} = \frac{1}{1 + \Delta T \cdot K_{Toil}} \tag{3.60}$$

where $K_{Toil} = \frac{K_{oil}}{V_{OILTref}}$ describes the temperature dependent thermal expansion of the fluid. Upon defining a correlation factor, f_{FT}, as:

$$f_{FT} = \cdot \frac{1 \cdot}{1 + \Delta T_d \cdot K_{Toil}} \tag{3.61}$$

The temperature sensitive damping force developed by the damper can be expressed as:

$$F_{dT} = F_{dTref} \cdot f_{FT} \tag{3.62}$$

3.4 SUMMARY

In this chapter, various models are derived to characterize different components of forces developed by the candidate dampers. The component models are developed to incorporate the influence of temperature effects, fluid compressibility and other dampers characteristics. The analytical models of different valving systems are also developed and integrated with the component models to yield the total damper models for incompressible and compressible fluid flows. An iterative algorithm is developed to solve the coupled flow and pressure relationships for compressible fluid flows. Two damper models are developed, for the monotube and remote reservoir designs to describe the friction, gas spring and multi-stage asymmetric damping forces, and the influence of fluid compressibility and temperature variations. The total damper force developed by both the designs is expressed as a combination of the component forces in the following manner:

$$F = F_{dT} + F_{GxT} + F_{fricxT} \tag{3.63}$$

The algorithm to solve for damper forces is presented in Figure 3.16

Various coefficients required to describe the force components are identified from the test data and the above equation is solved for specific valving configurations employed in candidate dampers in the following chapter.

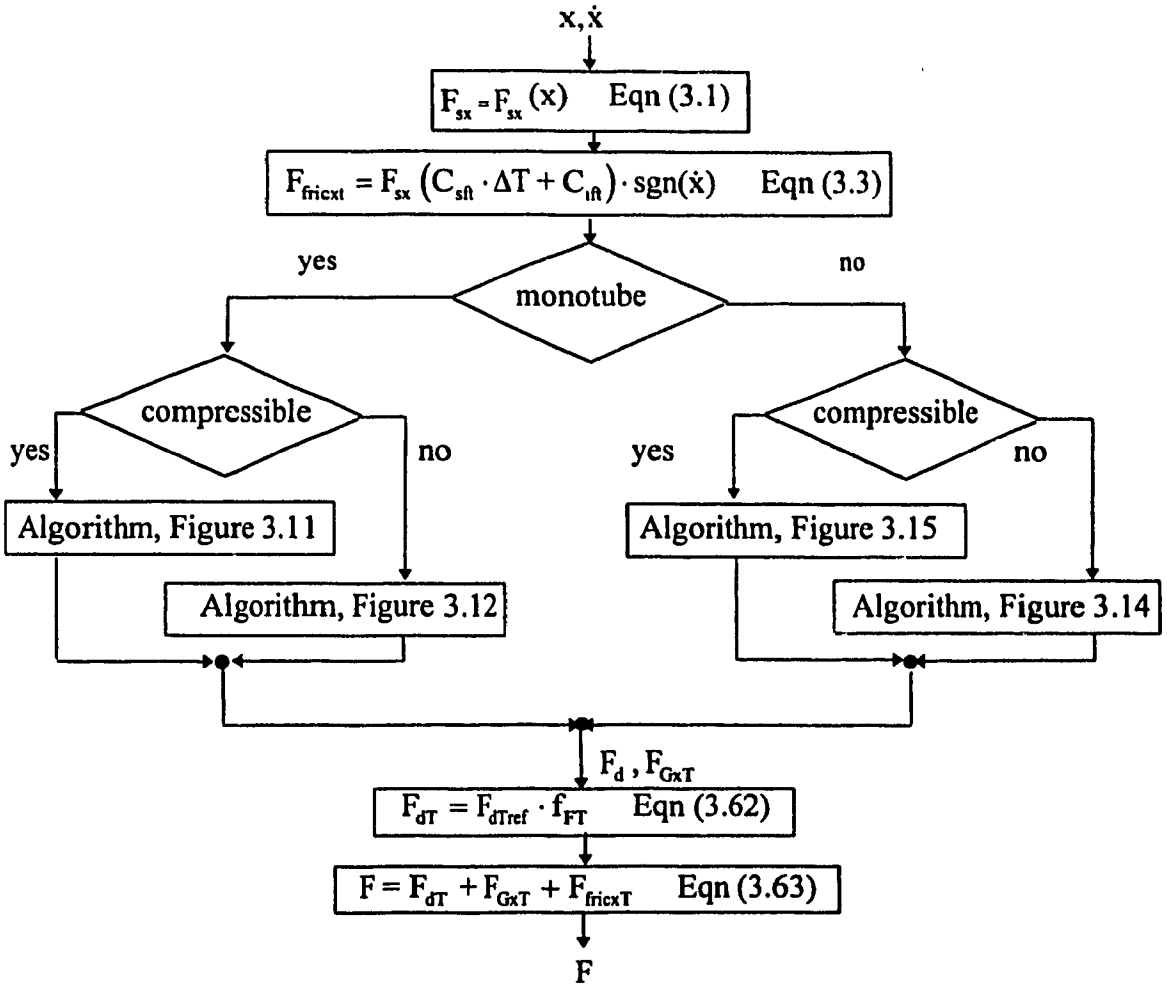

Figure 3.16 Computation of damper model force.

CHAPTER 4

IDENTIFICATION OF COEFFICIENTS AND MODEL VALIDATION

4.1 INTRODUCTION

Analytical models, in general, are formulated with a number of simplifying assumptions. The validation of analytical models is thus vital to develop reliable computer-assisted design and analysis tools. When validated the analytical models of certain general classes of dampers can be effectively utilized to evaluate various vehicle dynamic aspects, such as ride quality, dynamic pavement loads, handling and control performance. The validated models further provide a design tool for tuning of suspension for high performance vehicles, while minimizing costly and time consuming field trials.

The damper models, developed in Chapter 3, necessitate identification of various coefficients in order to incorporate the contributions due to valving, fluid compliance, entrained air, friction, gas spring, and temperature variation. The complexities associated with modeling of these contributing factors has been demonstrated in many published studies [15,17,19,20,22,30,33]. The associated coefficients, are identified from the results obtained from a series of systematic static and dynamic tests performed in the laboratory. The analytical models derived using these coefficients are then solved for a wider range of operating conditions to assess their validity.

4.2 ANALYSIS OF THE MEASURED DATA

The analytical models require a number of coefficients to be identified from the measured data. The static and dynamic test data is thus analyzed to determine various coefficients to describe the static and dynamic friction, gas spring, damping, fluid compliance and temperature sensitivity.

4.2.1 Analysis of Static Test Data

The results of the static test, described in section 2.3.1.2, are analyzed to determine static breakaway friction force as a function of the damper displacement, and initial gas pressure and volume. The static friction force is computed from half the difference between the compression and extension force of the damper. The static friction force corresponding to different discrete displacements is determined from the test data and arranged in a look up table, for usage in equation (3.1). The average of the two forces is assumed to be equal to the gas spring force corresponding to the specific test temperature (20°C under static conditions). The gas spring force and displacements are used to determine the initial charge pressure and the gas volume, using a regression analysis based on the pressure and force equations (3.7) and (3.4), assuming constant pressure throughout the damper.

Figure 4.1 illustrates the force-displacement characteristics of the candidate dampers derived from the static tests. The upper and lower curves represent the forces developed during compression and extension strokes, respectively. The mid-curve represents the force due to gas spring derived from regression analysis. The measured force-displacement characteristics of all the dampers reveal an increase in the static damper force with increasing displacement. The increase in the force is primarily attributed to increase in the gas pressure, while the dependency of the friction force on the displacement is apparent in the case of Koni and Mechformance dampers. The gas spring force of the Mechformance damper, derived from the measured gas pressure and equation (3.4), is also compared to that derived from the regression analysis, as shown in Figure 4.1 (c). The static characteristics of the Fox damper, presented in Figure 4.1 (a), reveal that the difference between the forces in compression and rebound does not vary considerably with the damper deflection. The differences in the forces near the extreme extension, however, is considerably higher, due to interactions with the rubber extension

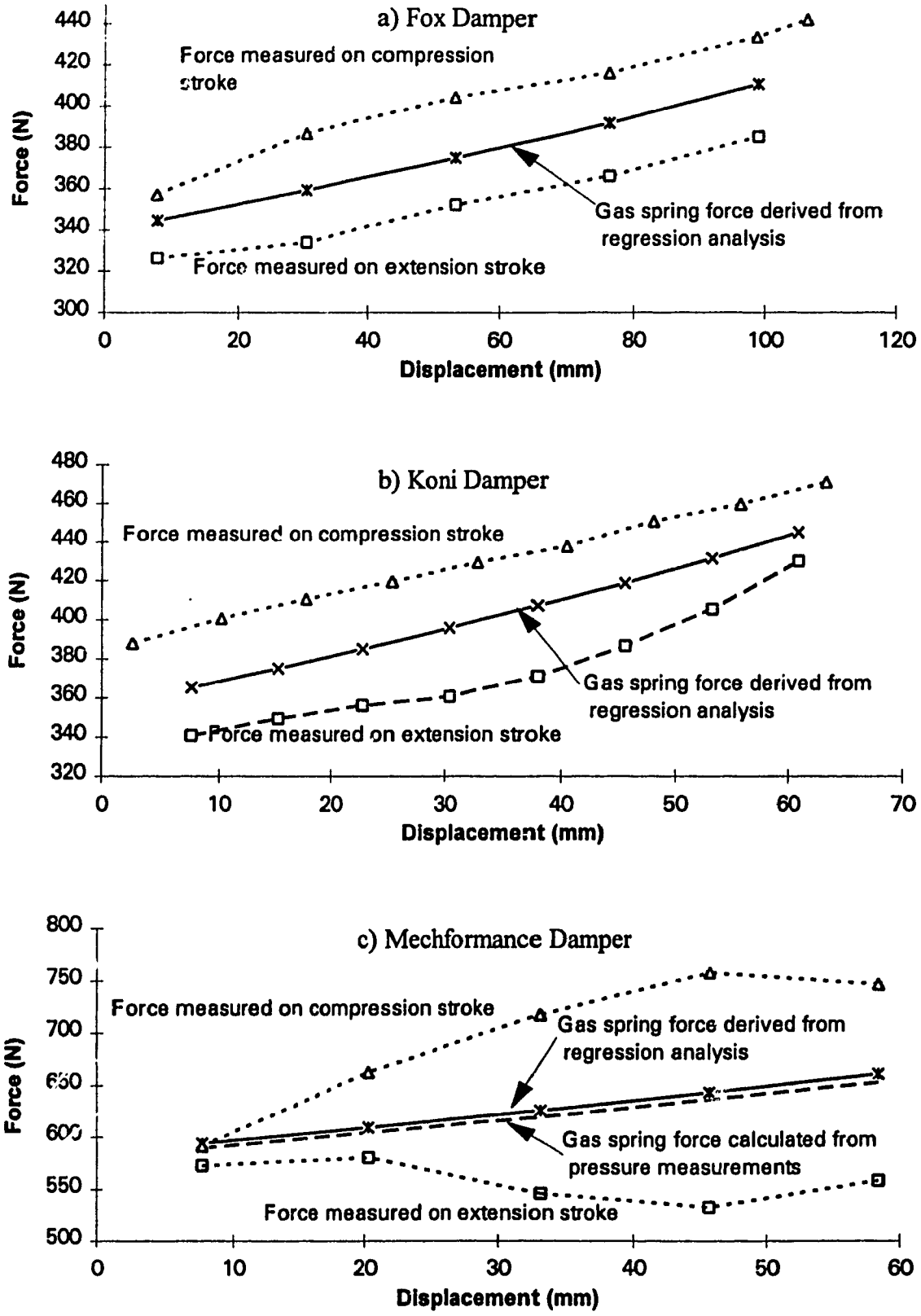

Figure 4.1 Static force-displacement characteristics of the candidate dampers.

limiter. While the force-deflection characteristics of the Koni damper (Figure 4.1 (b)) reveals somewhat larger variations in the difference between the compression and extension forces with deflection, the Mechformance damper (Figure 4.1 (c)) reveals excessive variations in the friction force with deflection. It is thus apparent from the test results that the static breakaway friction force is strongly dependent upon the damper displacement, which may be attributed to uneven cylinder bore, bent shaft, or misalignments. For the Koni damper discoloration and scratches on the piston rod surface were observed to coincide with the bearing, where the highest divergence in the forces was observed. The variation in friction force with displacement are thus most likely attributed to a bent shaft or misalignments. The Mechformance is a prototype damper with a bored body and it can be speculated that the variations in the friction force are due to unevenness in the cylinder bore.

The gas spring force of all the dampers varies with the damper deflection in a nonlinear manner. The gas spring force follows the trends demonstrated in the published studies, which utilize the gas laws based upon a polytropic process. A comparison of the gas spring forces derived from the measured gas pressure and the regression analysis, presented in Figure 4.1 (c), reveals that the error between the two forces is within 2%. The results further reveal a constant error irrespective of the displacement, indicating slightly larger friction during compression (approximately 3N) than during rebound. The measured gas spring force in compression is identical to that in extension indicating the absence of hysteresis.

The initial gas pressure and volume of each damper are calculated using the regression analysis in conjunction with equations (3.4) and (3.7). The results are compared with the true charge pressure in Table 4.1, and show only small errors between computed and actual initial pressures. The relatively larger error for the Koni unit, may

TABLE 4.1
COMPARISON OF COMPUTED AND ACTUAL VALUES OF INITIAL CHARGE PRESSURE AND VOLUME

	Fox Light	Fox Heavy	Koni	Mechformance
Computed				
P_0 (Mpa)	1.88×10^6	1.84×10^6	2.51×10^6	2.12×10^6
V_0 (m^3)	125.3×10^{-6}	116.3×10^{-6}	48.6×10^{-6}	151.2×10^{-6}
Actual				
P_0 (Mpa)	1.90×10^6	1.90×10^6	2.41×10^6	2.07×10^6
P_0 Error	1.1%	3.3%	4.1%	2.4%
V_0 (m^3)	125×10^{-6}	125×10^{-6}	not available	155
V_0 Error	0.2%	7.0%	-	2.5%

be attributed to loss of charge pressure, due to its being charged more than one year before the laboratory tests, while the other dampers were rebuilt shortly before the test.

4.2.2 Analysis of Low Speed Dynamic Test Data

The results of the tests performed at very low speeds are analyzed to determine the coefficients describing the dynamic friction, the temperature sensitivity, polytropic gas constant, and thermal expansion of the oil, as discussed in sections 2.3 and 3.2. The points of discontinuity at the extremities or stroke reversals are examined to determine the coefficients for the dynamic friction models, discussed in section 3.2.1. The magnitude of the breakaway dynamic friction force is derived using the methodology described for estimating the static friction and the gas spring force is computed from the average of the two forces at different operating temperatures.

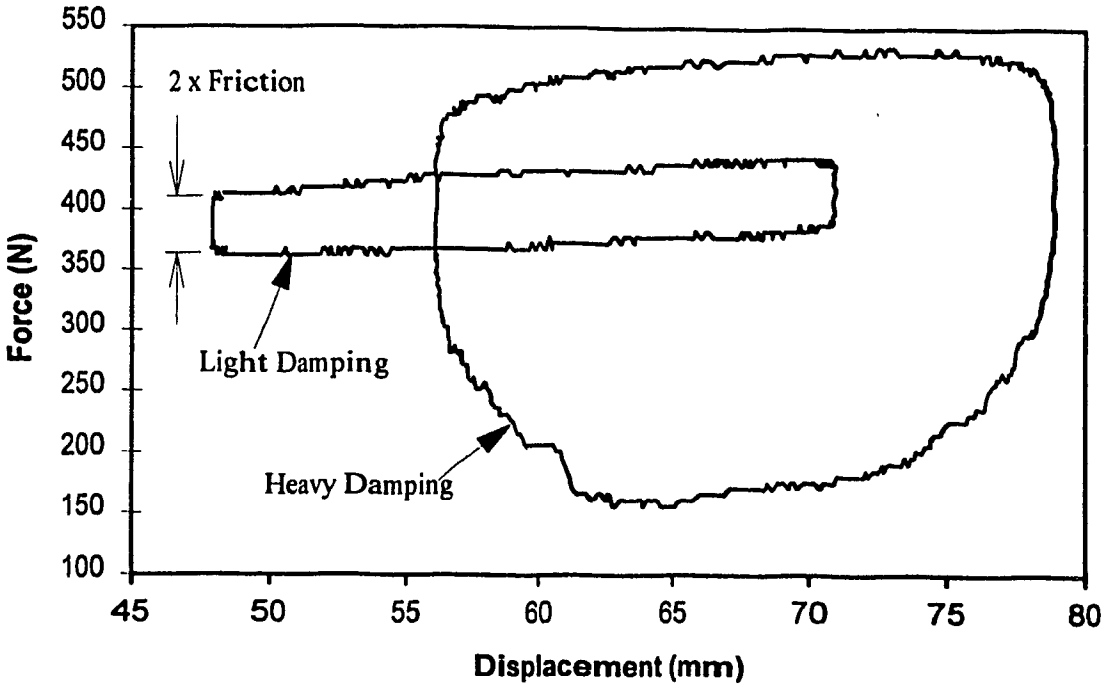

Figure 4.2 Force-displacement characteristics of the Fox damper corresponding to light and heavy damping settings (0.005 Hz).

4.2.2.1 Dynamic Friction Force

Although the friction force at very low speeds can be easily identified from the distinct points of discontinuities, in the case of light damped units, the presence of heavy damping force poses difficulties in identifying the friction force magnitudes as shown in Figure 4.2. The force-deflection properties measured for the Fox damper clearly demonstrate the presence of considerable rebound damping force in case of the heavy damper setting. An algorithm is thus developed to identify the points of discontinuity in the compression and rebound curves corresponding to minimum and maximum relative displacements (zero relative velocity) across the damper. The algorithm examines the rate of change of damper force with respect to the displacement and identifies the points of discontinuities when the slope approaches a very large value or changes sign. This approach, however, resulted in large errors due to occasional reversals of actuator motion near the extremities. Consequently, the data near the extremities was removed from the

analysis. The measured data in the range between the maximum/minimum displacement and 2.9 times the resolution of the data acquisition (approximately 0.37 mm) was eliminated from the analysis to ensure that the contributions due to irregular actuator motion were eliminated. A regression analysis was then performed on the 20 data samples following/proceeding the modified extremities corresponding to both compression and rebound force. The regression curves are then extrapolated to estimate the forces in compression and rebound corresponding to maximum and minimum displacements. The difference between the estimated compression and rebound forces at the stroke reversals is derived to compute the magnitude of dynamic breakaway friction force. It should be noted that the low speed dynamics introduces certain amount of hydraulic force, specifically for heavy damping as evident from Figure 4.2. The contributions due to hydraulic force, however, are assumed small due to low speeds. Furthermore extrapolation of the force-displacement curve to the point of stroke reversal (zero velocity) results in minimizing the contributions due to hydraulic damping effects.

Each candidate damper was tested in the laboratory at 0.05 Hz low speed excitation and 10 different temperatures, and the data was analyzed to identify the magnitude of dynamic breakaway friction and its sensitivity to variations in temperature, as described in section 3.2.1. Each measurement was performed twice and the data was examined for its repeatability. The measurements revealed good repeatability in terms of the sensitivity of gas spring and friction force to temperature variations. The data acquired for each damper was analyzed using the above algorithm to identify the magnitude of the dynamic breakaway friction. In order to isolate the temperature sensitivity of the friction force, from the affects of friction displacement sensitivity, the tests were performed for identical maximum and minimum positions of damper displacement. The measured dynamic breakaway friction, was normalized with respect to the static breakaway friction force determined at the same displacement, using equation (3.2) in section 3.2.1. The

normalized breakaway friction force (R_{fxTi}), as derived from the regression coefficients is:

$$R_{fxTi} = \left(C_{sfT} \cdot \Delta T + C_{ifT}\right) \cdot \mathrm{sgn}(\dot{x}) \tag{4.1}$$

where the coefficients C_{sfT} and C_{ifT} describing the temperature dependency of the friction force are determined from the linear regression analysis. The regression analyses are performed on the data acquired at minimum and maximum damper displacement, and on the data acquired for varying displacement in order to study the temperature sensitivity as a function of damper displacement. The resulting regression coefficients are presented in Table 4.2 together with the corresponding r^2 values.

Figure 4.3 illustrates the normalized values of breakaway friction of the candidate dampers as determined from the experimental data and Equation (3.2). The solid and dashed lines represent the results of the regression analysis corresponding to maximum and minimum damper displacements. The results demonstrate reductions in the friction force with increasing temperature, with a pattern that is quite difficult to establish, particularly for the Fox damper. The difficulty in establishing a pattern may in part be attributed to the measurement errors caused by the relatively low resolution of the force sensor (approximately +/- 5N), leading to significant variations in the relatively low magnitude friction force of the Fox damper (lower limit of static friction ≈ 19N). The Koni and Mechformance dampers with relatively high value of static friction (upper value ≈ 95 N) reveal a pattern of decreasing normalized breakaway friction with increasing temperature. The measurements, however, are expected to be influenced by the low resolution of the force sensor. Variations in the normalized values are also attributed to variations in the friction force due to misalignments, wear, and compression of the O-rings. The results show that breakaway friction properties of the Fox damper are less temperature sensitive than the Koni and Mechformance dampers, which is attributed to

TABLE 4.2
NORMALIZED FRICTION FORCE COEFFICIENTS

	Fox Light	Fox Heavy	Koni	Mechformance
Minimum Damper Displacement				
C_{sft} ($°C^{-1}$)	-2.778×10^{-3}	-3.956×10^{-3}	-4.771×10^{-3}	-5.191×10^{-3}
C_{ift}	1.707	2.731	1.526	1.111
R^2	0.097	0.128	0.743	0.876
Maximum Damper Displacement				
C_{sft} ($°C^{-1}$)	-1.74×10^{-3}	8.117×10^{-5}	-5.807×10^{-3}	-4.786×10^{-3}
C_{ift}	1.642	2.552	1.893	1.170
R^2	0.059	0.00003	0.563	0.687
Combined Data				
C_{sft} ($°C^{-1}$)	-2.260×10^{-3}	-1.937×10^{-3}	-5.289×10^{-3}	-4.989×10^{-3}
C_{ift}	1.675	2.641	1.709	1.141
R^2	0.078	0.022	0.469	0.727

their aluminum body and steel piston construction, while the Fox damper utilizes steel body and piston.

The values of the coefficients and r^2, derived from the regression analysis for Equation (4.1), corresponding to the minimum and maximum damper displacements are summarized in Table 4.2. The mean values of the coefficients are also presented in the Table. The results reveal poor correlation for the Fox dampers, and reasonably good correlation for the Koni and Mechformance dampers. The temperature and/or displacement sensitivity of the friction force of the Fox damper, therefore, cannot be concluded. The results derived for the Koni and Mechformance dampers, presented in Figures 4.3 (c) and (d), clearly illustrate the temperature dependency of the friction force.

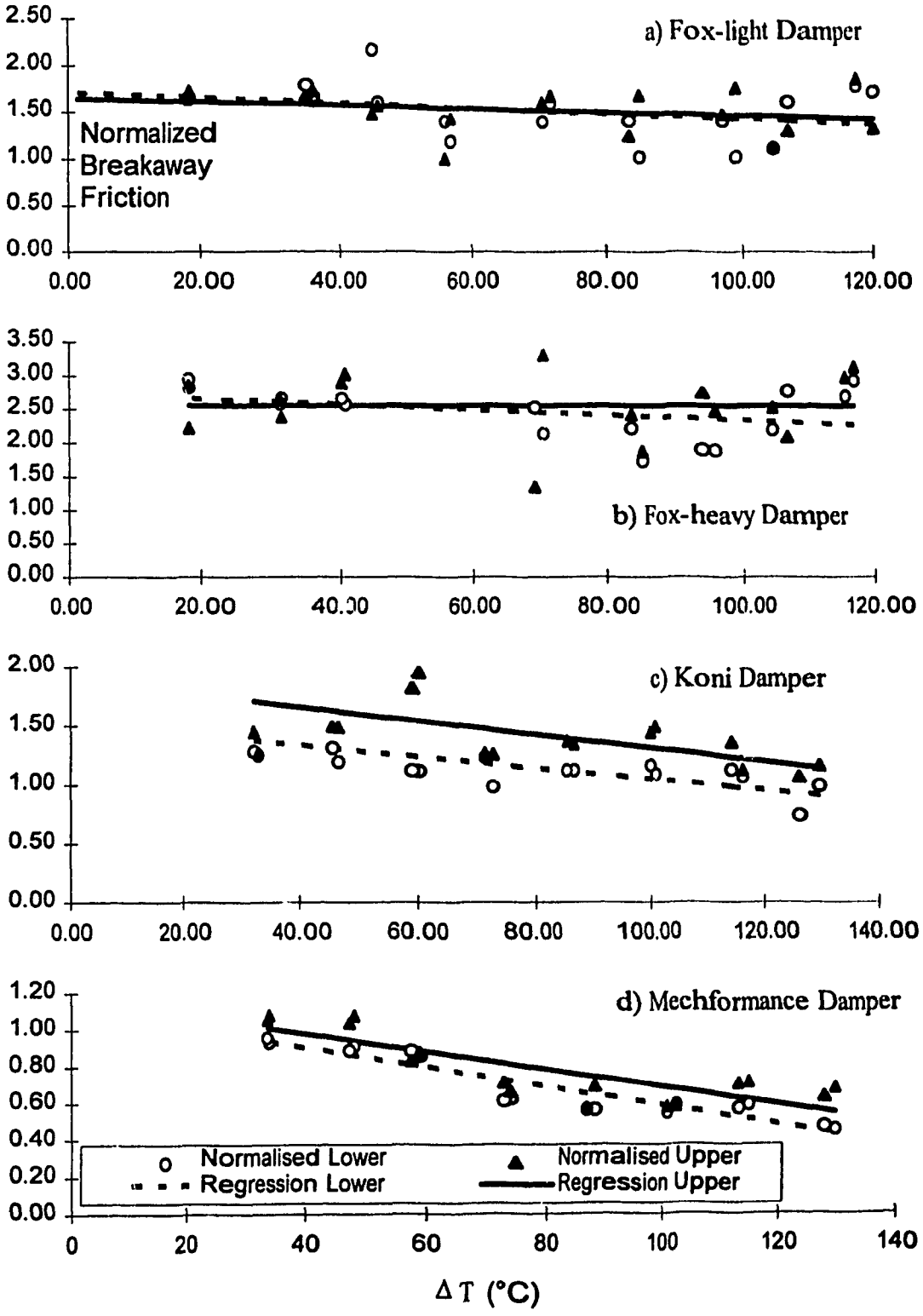

Figure 4.3 Normalized breakaway friction temperature characteristics of the candidate dampers.

The r^2 values range from 0.743 to 0.876 at minimum damper displacement and from 0.469 to 0.727 for the combined data. The temperature dependence of the breakaway dynamic friction of the Koni and Mechformance dampers is thus modeled using Equation (4.1).

Further the results summarized in Table 4.2 reveal different temperature coefficients corresponding to minimum and maximum damper displacement, indicating that the coefficients are position sensitive. A comparison of the slope coefficients for the Koni and Mechformance dampers derived at the maximum and minimum damper displacement reveal variations of 17% and 8%, respectively. The corresponding intercept coefficients, C_{ifT}, vary by 19.4% and 5%. Although these variations further support the displacement dependency of the temperature coefficients, it is quite complex to characterize the friction force as a function of the temperature as well as displacement. In light of the complexities associated with measurement and data analysis, and the lack of an identifiable pattern of displacement dependency, the enhancement of the damper model including displacement sensitive temperature coefficients is not attempted.

Although the breakaway friction for the Fox damper is not clearly temperature dependent, the considerable variations between the dynamic and static breakaway friction are evident from Figures 4.3 (a) and (b), which is also illustrated for both the Koni and Mechformance dampers in Figures 4.3 (c) and (d). While this variation is incorporated into Equation (4.1) to characterize the Koni and Mechformance dampers, the equation (4.1) yields poor correlation for the Fox damper.

Defining $\overline{R}_{fx}$, the mean normalized breakaway friction corresponding to the test temperature range, as:

$$\overline{R}_{fx} = \frac{\Sigma_0^n R_{xTi}}{n}; \quad i = 1,\ldots,n \tag{4.2}$$

TABLE 4.3
MEAN NORMALIZED BREAKAWAY FRICTION COEFFICIENTS

	Fox Light	Fox Heavy	Koni	Mechformance
$\overline{R}_{f_{xT}}$	1.52	2.50	1.26	0.74

where n is the number of measurements obtained at different temperatures. The mean normalized breakaway friction ratio, of the candidate dampers, summarized in Table 4.3 ranges from 1.52 to 2.5 for low- and high-damping setting of the Fox damper. These coefficients are larger than those obtained for the Koni (1.26) and Mechformance (0.74) dampers. The large difference in the coefficients for the Fox dampers may be attributed to its steel construction, contributions due to hydraulic forces specifically for high damping setting and increased seal friction due to the higher pressures generated. This model is used for the Fox damper, with coefficients determined from the damping setting.

4.2.2.2 Determination of the Gas Spring Force

As described in section 3.2.2, the damper force component due to gas operating about an equilibrium position x_e can be defined by Equation (3.19):

$$F_{GxTy} = \left(P_{xeT} \cdot \left(\frac{V_{xeT}}{V_{xeT} - (x_e - x) \cdot A_r} \right)^{\gamma} - P_{atmos} \right) \cdot A_r \qquad (4.3)$$

The above formulation was derived assuming a quasi-static thermal equilibrium of the damper, where heat generated equals the heat dissipated. The gas pressure and volume corresponding to this point of equilibrium can thus be related to the initial conditions in terms of the thermal expansion of the gas, oil and damper components, using an isothermal process, as was verified through laboratory measurements. Measurements revealed a rate of change of temperature less then 1°C/minute at higher operating

temperatures, and considerably lower rate of change of temperatures at relatively lower temperatures. The gas volume, V_{xeT}, corresponding to an equilibrium point and operating at temperature T, is related to the initial gas volume, rod displacement, and the thermal expansion of oil and other components:

$$V_{xeT} = V_0 - x(A_r) - (\Delta T \cdot K_{voil} + K_{voint}) \tag{4.4}$$

where the term $(\Delta T \cdot K_{voil} + K_{voint})$ describes the volume change due to thermal expansion of the oil and damper components, as described in equation (3.15). The corresponding gas pressure, P_{xeT}, can then be derived similar to Equation (3.13) as:

$$P_{xeT} = P_0 \times \frac{V_0}{V_0 - x(A_r) - (\Delta T \cdot K_{voil} + K_{voint})} \times \frac{T}{T_0} \tag{4.5}$$

where T_o is the reference temperature. Equations (4.3) and (4.4) can be solved to determine the gas pressure and volume, and thus the gas spring force, for known initial volume, rod displacement and operating temperature. The analysis, however, necessitates the determination of thermal expansion coefficients, K_{voil} and K_{voint} from the experimental data. From the measured sample results presented in Chapter 2 and equation (4.3), it is evident that the gas spring rate is strongly related to the polytropic exponent γ, which is determined from the measured data. The analysis of the measured data further revealed a predominant effect of the thermal expansion on the gas pressure (P_{xeT}) resulting in a significant temperature dependent bias in the force-deflection curve.

At each operating temperature, the model gas spring force is computed from equations (4.3) and (4.4), while the experimentally derived gas spring force is computed as the average of the compression and rebound forces at the points of discontinuity, corresponding to the maximum and minimum displacement.

The values of the polytropic constant is identified from the gas force derived from Equation (4.3) and the measured data for the Mechformance damper. Since the gas spring force is also dependent on the coefficients of thermal expansion, an iterative

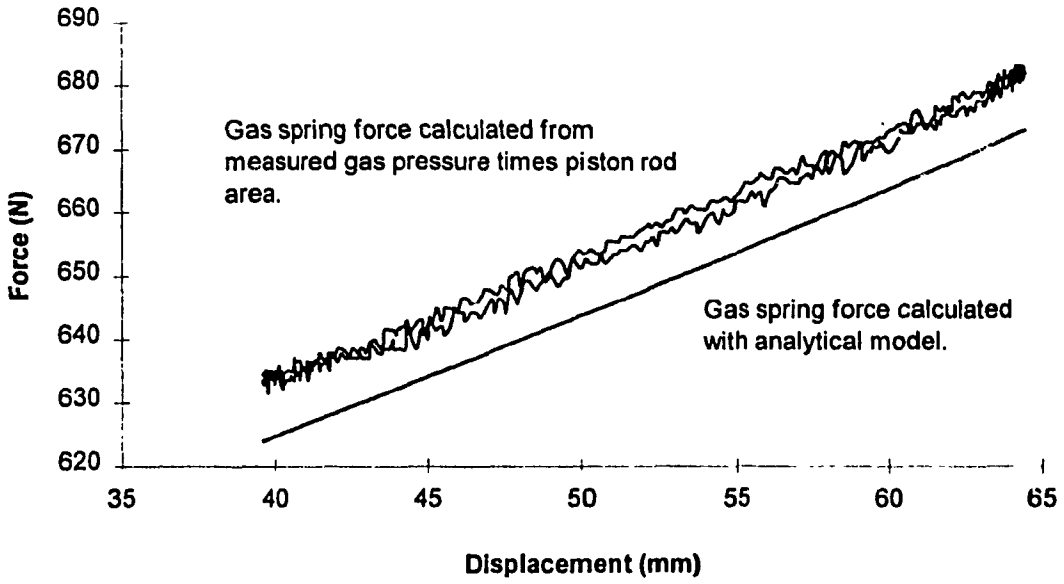

Figure 4.4 Comparison of computed and measured gas spring force of Mechformance damper (T= 38°C, γ=1.38, Frequency = 2 Hz).

estimation procedure was formulated to identify γ, K_{voil} and K_{voint} from the force-displacement curves. It should be noted that the value of γ relates to the slope of the force-deflection curve, while the thermal expansion coefficients relate to the bias. The iterative procedure is initiated by assuming the values of the above unknowns and the force-displacement characteristics of the gas spring are computed using Equation (4.3). A convergence criteria is formulated based upon the relative error in slopes of the analytical and experimental force-displacement characteristics. The procedure resulted in convergence in γ value as 1.38, which is quite close to the adiabatic value for nitrogen(1.40), frequently used in published studies [22,69]. The force-displacement characteristics derived using the identified value of γ revealed good correlation with the measured data acquired under sinusoidal excitation at 2 Hz and operating temperature of 38°C. The analytical results are compared to the measured force-deflection characteristics, where the spring force is computed from the measured pressure and the rod area, as shown in Figure 4.4.

The coefficients of thermal expansion affecting the gas spring force are derived from the measured data and the spring force model described in Equation (4.4). The change in gas volume can be related to the average gas spring force in the following manner:

$$\Delta T \cdot K_{voil} + K_{voiint} = V_0 - x_e \cdot A_r - \frac{P_0 \cdot V_0 \cdot T}{\left(\frac{F_{GxeT}}{A_r} + P_{atmos}\right) \cdot T_0} \qquad (4.6)$$

where F_{GxeT} is the gas spring at the mid-stroke position, derived as the average of measured forces corresponding to minimum and maximum damper displacement. The coefficients of thermal expansion are computed through the linear regression analysis performed on the left-hand side of Equation (4.6), which includes the measured average force.

Figure 4.5 illustrates the thermal expansion of oil derived from the regression analysis of the data obtained for the candidate dampers. The results of the regression analysis are compared with the measured data reveal good correlation over the entire temperature range. The values of thermal expansion coefficients are further summarized in Table 4.4, together with the thermal expansion of oil derived from a published value of the coefficient of thermal expansion (0.00072/°C) [61] and in the case of the Fox damper measured oil volume, while in the case of the Koni and Mechformance damper an estimated volume. A comparison of the regression coefficients reveals considerable variation in the coefficient of thermal expansion for the candidate dampers, which may be attributed to their different construction and material properties. The Fox damper with two different settings also reveals considerable variation in the thermal coefficients. The light damping setting yields an approximately 21% larger value of K_{voil} when compared to that for the heavier damping. This significant variation in the thermal coefficient is perhaps attributable to the relatively high value of damping (for the Fox with heavy

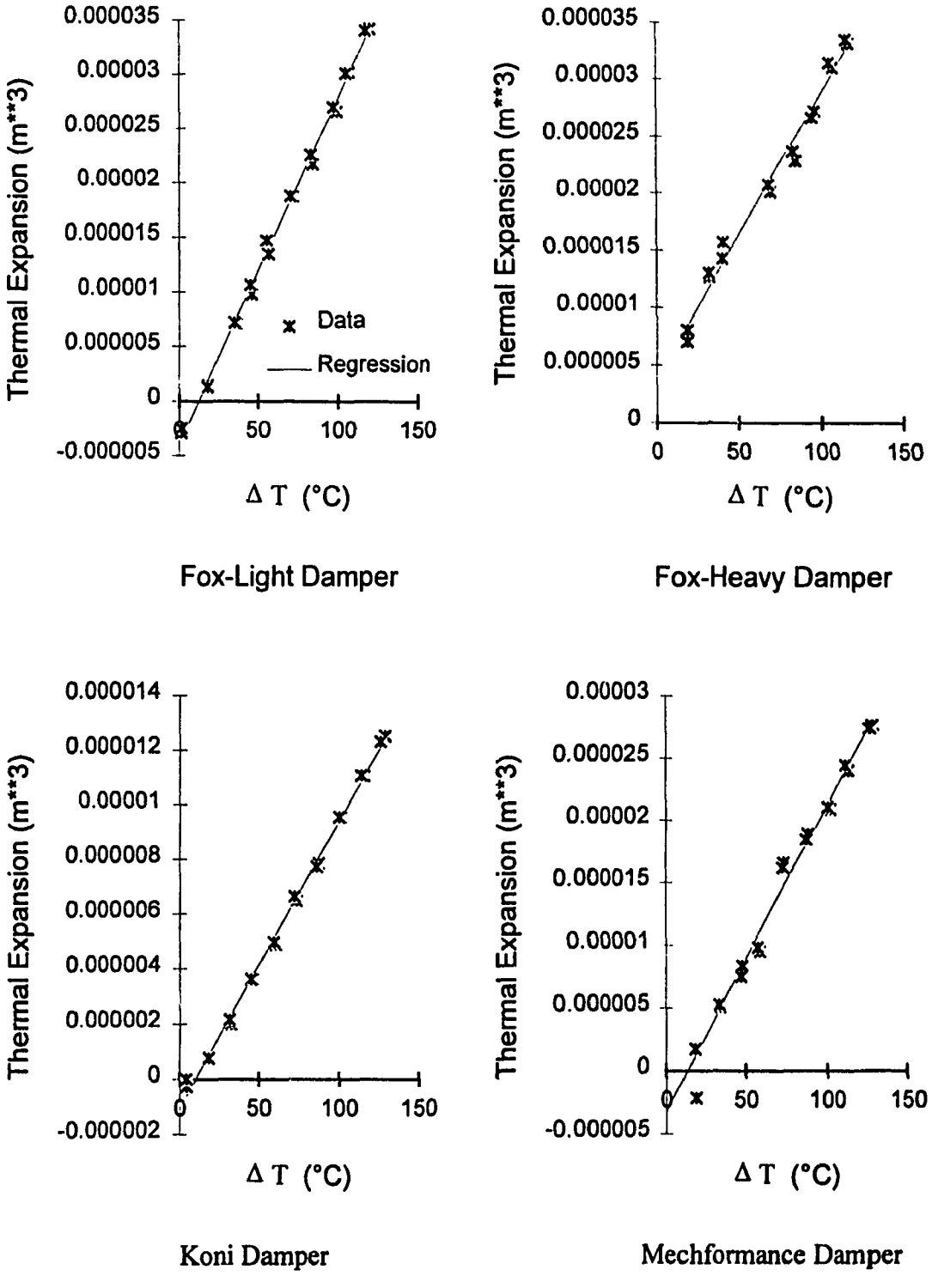

Figure 4.5 Effective thermal expansion of oil as a function of the temperature difference.

TABLE 4.4
COEFFICIENTS FOR THERMAL EXPANSION OF OIL MODEL

	Fox Light	Fox Heavy	Koni	Mechformance
K_{voil} (m^3 / °C)	3.17×10^{-7}	2.49×10^{-7}	1.04×10^{-7}	2.42×10^{-7}
K_{voint} (m^3)	-3.93×10^{-6}	3.88×10^{-6}	-1.05×10^{-6}	-3.17×10^{-6}
r^2	0.997	0.984	0.997	0.994
Theoretical Thermal Expansion of Oil				
Oil Volume (cc)	250	250	150 (est.)	220
Thermal Expansion (m^3 / °C)	1.8×10^{-7}	1.8×10^{-7}	1.08×10^{-7}	1.58×10^{-7}
Variation between K_{voil} and theoretical thermal expansion				
	43%	28%	4%	35%

damping) during the rebound stroke, which would result in lowering of the experimentally derived gas spring force, resulting in lower calculated temperature sensitivity. From both the Figures and the Table it is evident that the intercept, K_{voint}, for all cases, has a relatively insignificant effect on the volumetric thermal expansion, and that a model based on oil expansion, (constant times change in temperature) would be sufficient. Hence a comparison of the values of K_{voil} to theoretical thermal expansion of oil, in Table 4.4 would allow insight in to the effects that components other then oil have on the thermal expansion. In all cases except for the Koni damper, where the volume of oil is estimated, the experimental value of K_{voil} is much greater then the theoretical one, indicating that in addition to change in oil volume, there are contribution due to changes

in components, although the amount of variation being between 4 to 43% indicates that these contributions are secondary to that of the oil.

The gas spring force as a function of damper displacement and temperature is computed from Equations (4.3) and (4.4) using coefficients of thermal expansion summarized in Table 4.4 and $\gamma = 1.38$. The computed values are compared with those obtained from the experimental data corresponding to minimum and maximum damper displacements, as shown in Figure 4.6 The spring force derived from the model correlates very well with the measured data for all three dampers over the entire temperature range. The results reveal a nearly linear increase in the spring force with increase in temperature, which is primarily attributed to the linear thermal expansion of oil and damper components. The results further show higher spring force corresponding to maximum displacement. The difference between the spring forces at minimum and maximum damper displacements tends to increase slightly with increase in temperature, which is attributed to the polytropic gas process and decreased gas volume due to thermal expansion of oil and components. Figure 4.6 also includes for comparison the spring force computed from the measured gas pressure multiplied by the rod area for the Mechformance damper, which is in good agreement with both the calculated and experimentally derived gas spring forces. The results presented in Figure 4.6 clearly demonstrate the effectiveness and validity of the analytical gas spring model developed for three different candidate dampers.

4.2.3 Analysis of Multiple Speed Dynamic Test Results

The results derived from a series of laboratory tests performed under a wide range of damper velocities, as described earlier in section 2.3.1, are examined to identify various coefficients for development of the analytical models. The force-velocity characteristics obtained at low accelerations are analyzed to determine the suitability of

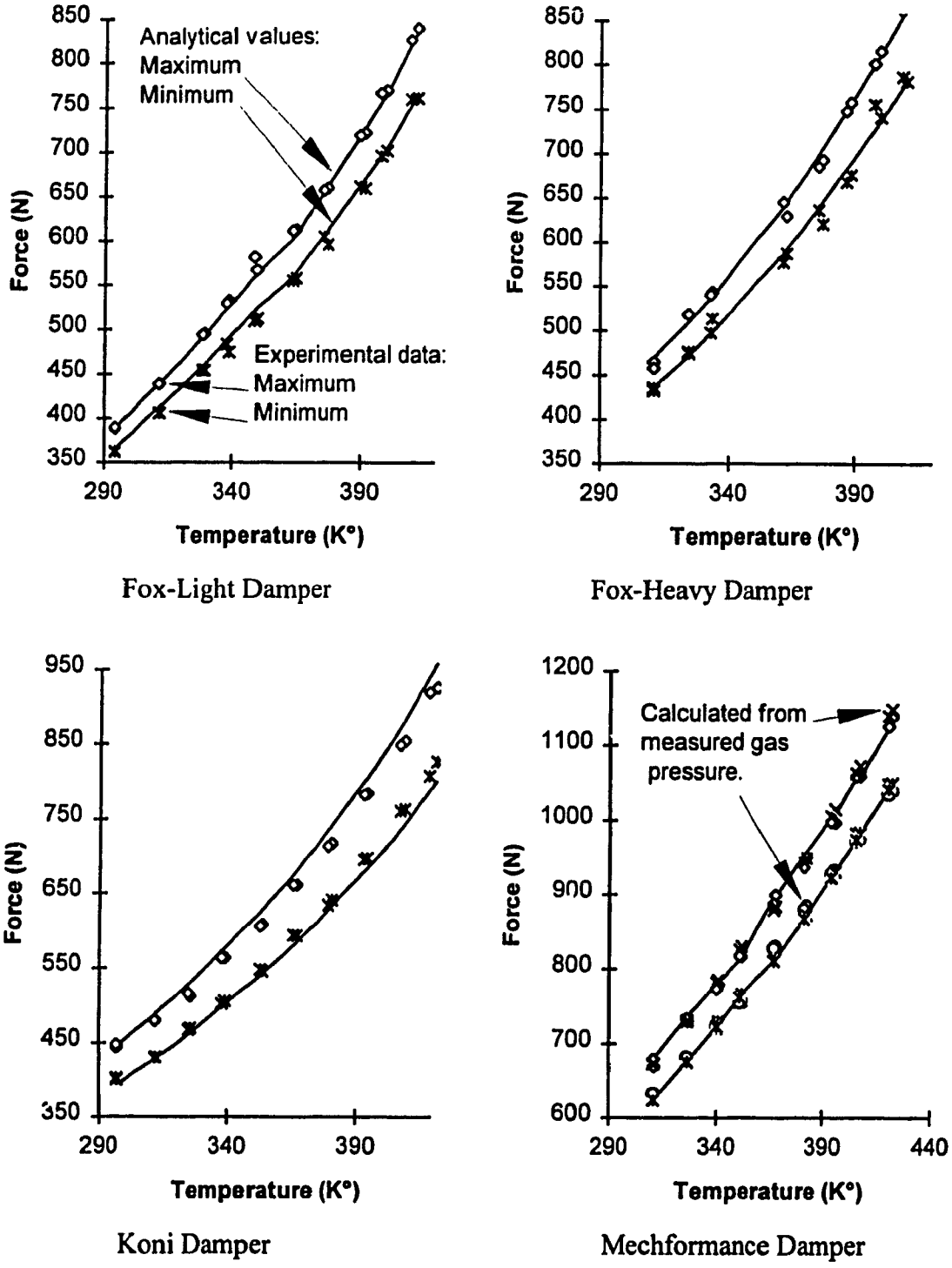

Figure 4.6 Comparison of analytical and experimental gas spring force of candidate dampers as a function of operating temperature, at maximum and minimum damper displacement.

the valving models discussed in section 3.3.1. The analysis allows for the selection of the valving model and initial approximation of the coefficients. The measured data is further analyzed to identify the compliance coefficients for the damper model, as described in section 3.3.2.

4.2.3.1 Determination of Coefficients for the Damper, Valving and Compliance Models

The analytical models of the candidate monotube and remote reservoir dampers were developed upon integrating the component models, such as friction force, gas spring force, valving and fluid compliance. Each component model involves identification of various coefficients to describe the motion and temperature dependency of the force components. While the gas spring and friction forces have been characterized from laboratory tests performed at static and low speeds, as described in sections 4.2.1 and 4.2.2, the coefficients describing the valve flows and fluid compliance need to be identified at different damper speeds. The test data acquired under different speeds is analyzed to derive the coefficients for the valving and compliance models, applicable to monotube and remote reservoir damper models, developed in sections 3.3.3. and 3.3.4, respectively. The coefficients are derived using a systematic iterative algorithm with an objective to minimize the errors between the test data and model results. The iterative process is initiated upon estimating the starting values based upon different observations made from the damper test data. From the tests performed in this study and the data reported in published studies [17,22,30], it has been established that valve flows are strongly related to damper velocity. The test results further illustrated the strong influence of acceleration on the damper force. In view of such complexities and the temperature dependency of the damper force, the test data obtained under different speeds and accelerations are analyzed to develop effective models.

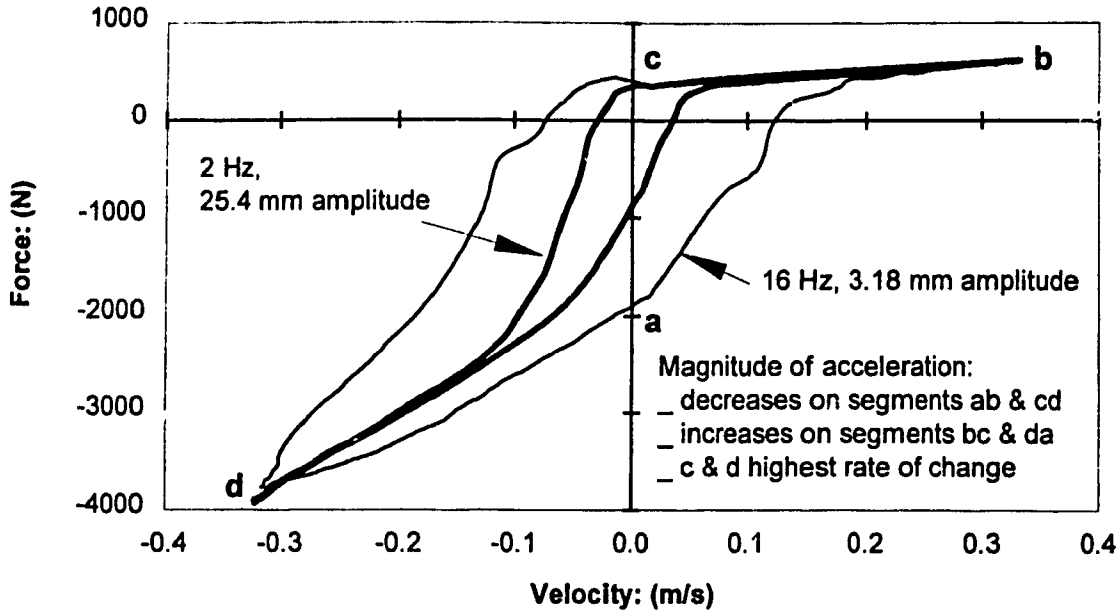

Figure 4.7 Measured force-velocity characteristics of the Fox-Heavy damper subject to harmonic excitation at frequencies of 2 and 16 Hz.

Acceleration Effects

Figure 4.7 illustrates the measured force-velocity characteristics of the Fox damper with high damping setting under excitations at frequencies of 2 Hz and 16 Hz. The damper displacement under the two excitations was selected to achieve identical peak velocity. The results clearly demonstrate significantly different hysteresis under the two excitations causing identical peak velocity. It should be noted that the friction force derived from the model presented in section 4.2.2.1 was subtracted from the measured force, leaving the gas spring and damping forces in the plot. In reference to Figure 4.7, although the two tests performed at 2 Hz and 16 Hz excitation frequencies yield identical peak velocity of 0.32 m/s, the force-velocity characteristics due to valve flow exhibit significantly less hysteresis under excitation at 2 Hz frequency, when compared to that developed at an excitation frequency of 16 Hz. This increase in hysteresis at a higher excitation frequency can be attributed to higher changes in the magnitude of acceleration and fluid compressibility. During the segments of the force-velocity curve in which the magnitude of acceleration decreases, the energy is stored due to fluid compressibility, and

released during the segments in which the magnitude of acceleration increases. At higher frequencies, the energy stored in the damper fluid, during the initial portion of the stroke, may not be released before the end of the stroke. This results in the shift in the crossing of the force axis at 0 velocities. This phenomenon may be illustrated through the definition of the fluid compressibility:

$$\beta = -\frac{dV_c}{VdP} \tag{4.7}$$

The rate of change of fluid volume may thus be related to the rate of change of pressure in the following manner:

$$\frac{dV_c}{dt} = -V \cdot \beta \cdot \frac{dP}{dt} \tag{4.8}$$

From the equations of fluid flow through valving, derived in Chapter 3, it is apparent that the fluid pressure is related to the damper velocity. Thus, the rate of change of pressure and the rate of change of volume of compressible fluid is related to the acceleration. The rate of change of fluid volume increases in magnitude with increase in magnitude of acceleration resulting in reduced flow through the valving and thus a reduction in the damper force, as seen in Figure 4.7. The results presented in Figure 4.7 demonstrate that the damper force developed under increasing and decreasing magnitude of accelerations is nearly identical when the magnitude of acceleration is low (for 2 Hz excitation the segments of the curve, $\dot{x} > 0.1$ m/s and $\dot{x} < -0.1$ m/s). As the effects of fluid compressibility under low level acceleration can thus be considered negligible, and based on an assumption of incompressible fluid flow, the starting values for the systematic iterative algorithm to determine the coefficients for the damping models of section 3.3, can be found by curve fitting experimental data at low levels of acceleration.

Low-Speed Valving Model

For incompressible flow the damping force can be related to the flow velocity and working area through the following relations derived from equations (3.27),(3.28) and (3.29):

$$F_d = (C_{orr} \cdot (\dot{x} \cdot A_w)^2 + C_{iorr}) \cdot A_w \tag{4.9}$$

$$F_d = (C_{lin} \cdot (\dot{x} \cdot A_w) + C_{ilin}) \cdot A_w \tag{4.10}$$

$$F_d = (C_{orp} \cdot (\dot{x} \cdot A_w)^2 + C_{linp} \cdot (\dot{x} \cdot A_w) + C_{ip}) \cdot A_w \tag{4.11}$$

where A_w is the working area derived as:

$A_w = A_r$; for flows through compression head.

$A_w = A_p - A_r$; for flows across the piston.

The damper force for a known valving model (constant working area) may be expressed in terms of weighted coefficients:

$$F_d = C_{orrw} \cdot (\dot{x} \cdot A_w)^2 + C_{iorrw} \tag{4.12}$$

$$F_d = C_{linw} \cdot (\dot{x} \cdot A_w) + C_{ilinw} \tag{4.13}$$

$$F_d = C_{orrpw} \cdot (\dot{x} \cdot A_w)^2 + C_{linpw} \cdot (\dot{x} \cdot A_w) + C_{ipw} \tag{4.14}$$

where the coefficients in the above equations with letter w added to the subscript are derived upon multiplying coefficients in equations (4.9) to (4.11) by the working area. Equations (4.12) to (4.14) describe the valving models for low speed and low magnitude of acceleration segments of the force-velocity curves in compression and rebound.

Mid-Speed Valving Model

The flow through valves corresponding to medium damper speed is a complex combination of flows through low and mid-speed valves. For low acceleration levels and

incompressible flows, the total flow rate can be estimated from the velocity and the working area, while assuming negligible flow rate through the low speed valves. This approximation yields an upper bound of the flow rate that may be considered valid for high damper speeds and stiff low speed valving. Furthermore, the experimentally derived force-velocity characteristics, presented in Figure 4.7 at 2 Hz., clearly demonstrate nearly linear relationship corresponding to mid-damper speeds, as is the case with the other dampers. Equation (4.13) can thus be used to characterize the mid-speed flow rates.

4.2.3.2 Validation of the Monotube Damper Valving Model (Koni)

The derivation of valving flow and compliance coefficients for the analytical model of the Koni damper with the monotube design is relatively simple, since the model involves only flow across the piston. The iterative procedure thus converged rapidly and revealed that the low speed valving flow for compression and rebound can be accurately characterized using the polynomial flow model of equation (4.14), with $C_{ipw}=0$. The results further revealed that the linear model of equation (4.12) provides good correlation with the mid-speed valving flows in compression as well as rebound, while the compliance effects are represented by a constant coefficient, $\beta=1.0\text{x}10^{-8}$. Various valving flow coefficients for the monotube damper model are summarized in Table 4.5.

The effectiveness of the monotube damper model is examined by comparing the response characteristics with the measured data corresponding to different damper speeds. The validity of the model is first examined in the low speed range by comparing force-time and force-velocity characteristics of the damper subject to sinusoidal excitations at low frequency (1 Hz) with the experimental data derived under the same excitations, as shown in Figure 4.8. The Figure demonstrates an excellent correlation between the analytical and experimental damping force characteristics, except for deviations near zero

TABLE 4.5
COEFFICIENTS FOR KONI DAMPING MODEL

		Rebound	Compression
Low Speed Coefficients	C_{orpw}	-280441	199028
	C_{linpw}	6889.5	3160.5
	C_{ipw}	0	0
Mid Speed Coefficients	C_{linw}	4684	1727
	C_{ilinw}	-1060	770
Bulk Modulus	β^{-1} (Mpa)	100	
Volume	V_{Total} (m^3)	145×10^{-6}	
	V_{20} (m^3)	6.7×10^{-6}	

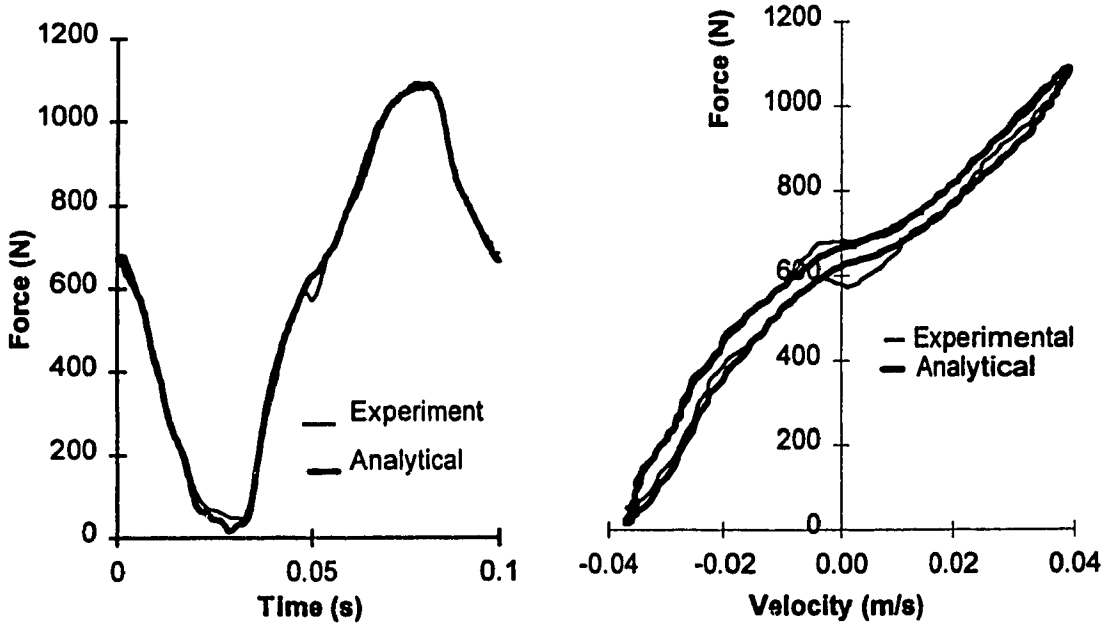

Figure 4.8 Comparison of analytical and experimental force-time and force-velocity characteristics of the monotube due to gas spring and damping (Excitation 12.7 mm, 1 Hz).

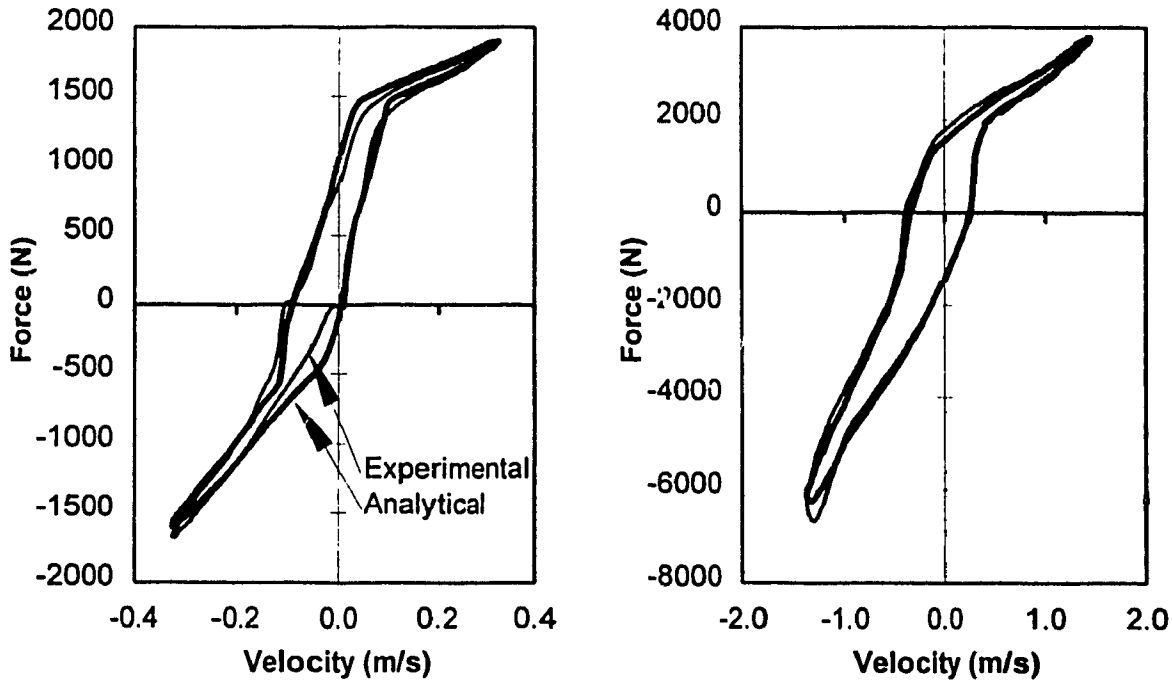

4 Hz 16 Hz

Figure 4.9 Comparison of analytical and experimental force-velocity characteristics of the monotube damper due to gas spring and damping.

velocity. These discrepancies are attributed to clearance within the mounting bearings resulting in a phase lag between the force and velocity near the zero-crossing, which is quite apparent in the time-history of the force.

Figure 4.9 illustrates comparison of the analytical model response with the measured data under medium to high speeds realized by increasing the frequency of excitation. The figures show good correlation between the model and experimental response at 4 Hz, with small deviations occurring primarily in the transition zone from low to mid speed. The damper model response, in general exhibits slightly larger hysteresis then the measured response. The measured force-velocity characteristics under an excitation of 16 Hz, however, reveal slightly larger hysteresis than the model response. The response under high damper speed further exhibits certain high speed restriction

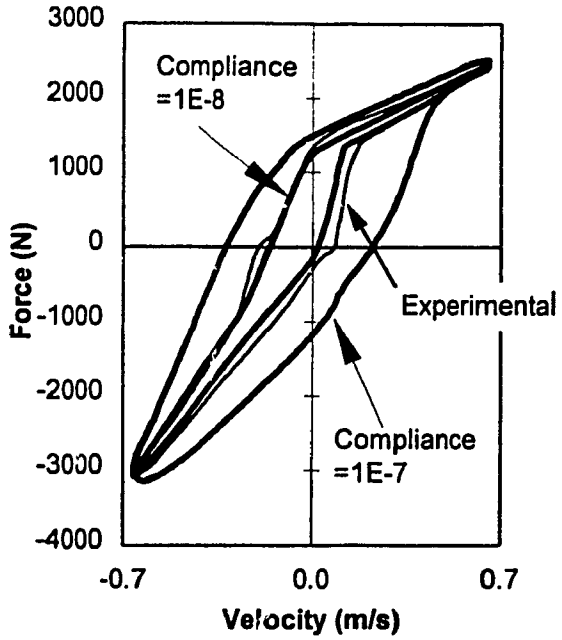

Figure 4.10 Influence of fluid compliance on the gas spring and damping force of the monotube damper (12.7 mm, 8 Hz excitation).

effects in the rebound part of the curve occurring at velocities below -1 m/s, which exceeds the reasonable speed expected for a race car damper.

The force-velocity characteristics derived from both the analytical model and experimental data reveal increase in hysteresis with increasing speed or excitation frequency. The measured data, however, illustrates a relatively larger increase in hysteresis with increasing frequency, which may be attributed to increase in inertia and compliance of the oil and damper components. The force-velocity characteristics of damper model are thus evaluated for different values of β in order to achieve better correlation between the analytical and experimental response. Figure 4.10 illustrates the influence of variations in β on the hysteresis properties of the damper model subject to sinusoidal excitations at 8 Hz. The results clearly demonstrate the strong influence of β on the damper hysteresis. A β value equal to 1.5×10^{-8} MPa yields better agreement with the measured data acquired under an excitation of 8 Hz, than the corresponding model

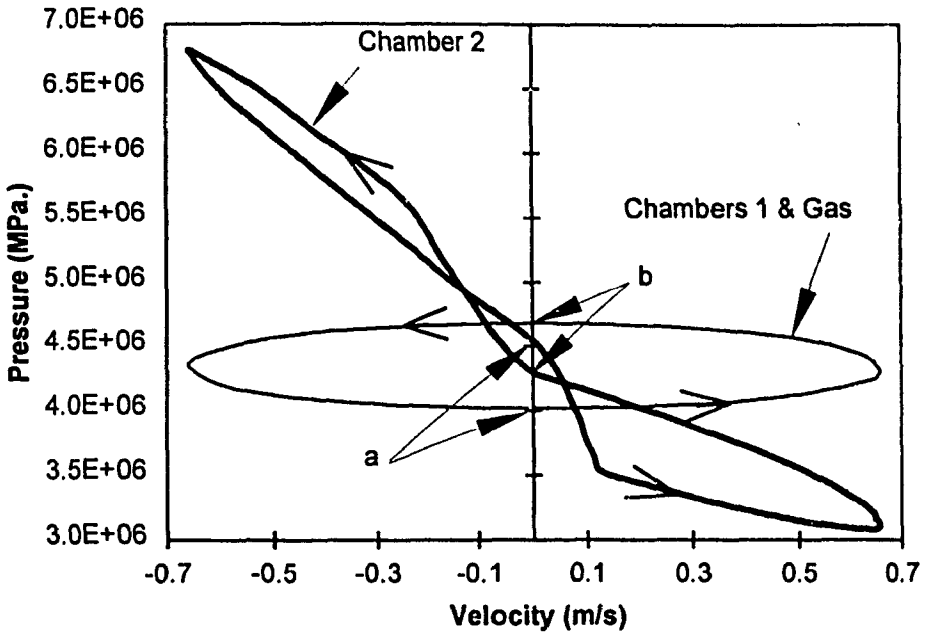

Figure 4.11 Pressure-velocity characteristics of monotube damper (12.7 mm, 8 Hz)

response under lower and higher speeds, however, it resulted in poor correlation with the measured data. The results showed an increase in the effective compliance with increase in the damper speed, which may be attributed to fluid inertia. A compromise was achieved by using $\beta = 1.0 \times 10^{8}$ Mpa in the current model., which results in improved correlation between the analytical and experimental data, as shown in Figure 4.9. The influence of fluid compliance on the damper performance is further investigated by studying the pressure-velocity characteristics of the two chambers from the simulation, whose force-velocity response presented in Figure 4.10, was computed under an excitation frequency of 8 Hz, and is presented in Figure 4.11. The results show slightly asymmetric pressure curve in chamber 1 (also equal to the gas pressure) due to variations in fluid flow caused by compressibility. The point 'a' refers to the extreme extended position of the damper, and thus low displaced volume of oil, high gas volume and low gas pressure.

The gas volume approaches its minimum and the pressure approaches its maximum value when the damper is compressed to its maximum displacement, which is indicated as point 'b' on the pressure-velocity curves. The effect of fluid compliance on the chamber pressure is quite apparent from the Figure. The pressure in chamber 2 is a complex function of velocity and compliance, as shown in the Figure. Since the damping force is a product of pressure difference across the piston and the working area, a thorough examination of the chamber pressure yields considerable insight into the behavior of monotube dampers. Starting from the fully extended position, indicated by point 'a' in the Figure, the pressure in chamber 2 changes rapidly during decreasing magnitude of acceleration segment of the cycle from 0 to approximately 0.11 m/s velocity (low speed compression). The fluid pressure in chamber 1, however, changes only slightly during the same segment resulting in a rapid change in the pressure differential and thus in the force, as shown in Figure 4.10. During the remainder of the compression stroke (mid speed) the fluid pressure in chamber 2 varies relatively slowly and gradually, and the corresponding pressure differential and damping force vary slowly with the speed. A comparison of the two segments of the chamber 2 pressure-velocity curve, at low speeds in the compression stroke, reveals considerably different pressure differential corresponding to decreasing and increasing magnitude of acceleration segments of the stroke resulting in large hysteresis in the force, as seen in Figure 4.10. This pressure differential between the positive and negative acceleration parts of the curve, however, is considerably smaller at velocities greater than 0.11 m/s resulting in relatively small hysteresis. The results further reveal relatively lower magnitude of pressure drop during the latter part of the compression stroke at velocities ranging from 0.11 m/s to 0 m/s, indicating that the damper force tends to follow the mid speed valving characteristics. The lower pressure differential during this part of the stroke is attributed to expansion of oil resulting in additional flow from chamber 1 to 2. The pressure-velocity curve

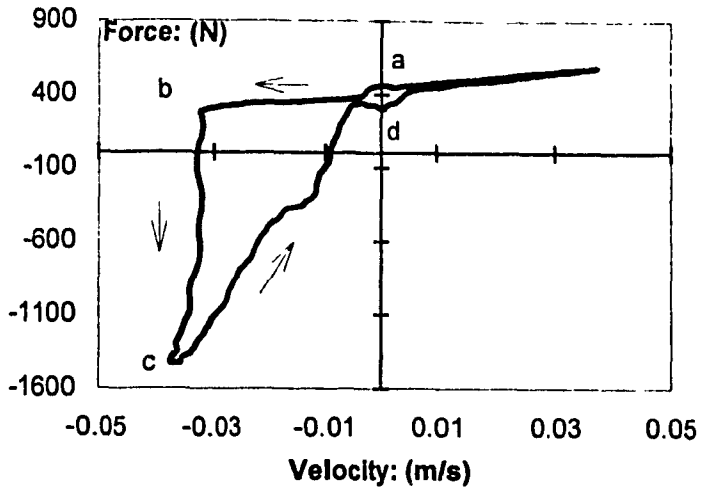

Figure 4.12 Force-velocity characteristics of the Mechformance damper due to gas spring and damping (Excitation 6.35 mm, 1 Hz).

presented in Figure 4.11 also reveals similar trends during the rebound stroke. The results also demonstrate the apparent advantages of the pressurized gas over the non-pressurized damper designs. From the Figure, it is apparent that a non-pressurized design would yield reduced pressure in both chambers, by approximately 4 Mpa. The fluid in Chamber 2 may thus approach vacuum conditions during the compression stroke, leading to cavitation process in the oil, and a loss of damping.

4.2.3.3 Validation of the Remote Reservoir Damper Valving Model

Mechformance Damper

The analytical models of the remote reservoir dampers, in general, involve increased complexities due to the increase in number of chambers and flow paths. The damping force is thus a highly complex function of flows associated with low-, mid- and high-speed asymmetric valves. The force-velocity characteristics of the candidate Mechformance damper exhibits highly nonlinear low speed rebound characteristics, as shown in Figure 4.12. Various attempts made to develop different low speed compliance models resulted in poor correlation with experimental data. Numerous additional

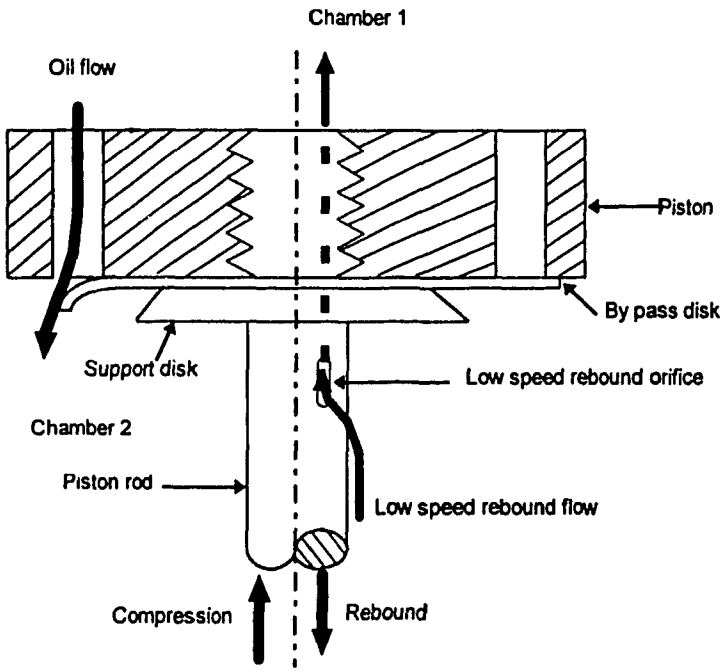

Figure 4.13 Schematic of the bypass valve used in the Mechformance damper.

laboratory tests were thus performed to enhance the understanding of low speed valves. The analysis of the data and physical examination of the valving mechanism revealed that the bypass valve was not seating properly, and a negative pressure differential was required for adequate sealing.

Figure 4.13 illustrates a schematic of this valve, which consists of a 0.2 mm thick spring steel disk pinched between the support washer and the piston and covers relatively large ports between chambers 1 and 2. When properly seated, the application of a relatively low positive pressure differential between chambers 1 and 2 causes the disk to deflect, permitting relatively unimpeded flow during the compression stroke. While the valve opens at a very low velocity during the compression stroke, it should remain closed during the rebound stroke, causing significant pressure drop to occur across the piston. Inadequate seating of the valve in the candidate damper, however, permitted unrestricted flow through the valve during the rebound stroke, as indicated by the segment a to b in Figure 4.12. The valve, however, tends to close when certain negative pressure is

achieved beyond point 'b'. The fluid flow is then controlled by the low speed recoil valve (segment c-d) at pressures below the mid speed blow off valve, and by the flows through parallel combination of low and mid speed valving above the blow off pressure. The bypass fluid flow is thus related to the pressure differential across chambers 1 and 2 in the following manner:

$$Q_{bypass} = \frac{\Delta P_{12}}{C_{seat}} \quad ; \quad \text{for} \quad \Delta P_{12} > \Delta P_{seat}$$

$$Q_{bypass} = 0 \qquad ; \quad \text{for} \quad \Delta P_{12} \leq \Delta P_{seat} \tag{4.15}$$

where ΔP_{seat} is the pressure required to achieve adequate seating of the bypass valve and C_{seat} is a coefficient relating the bypass flow rate to the pressure differential. The valve of this coefficient is derived assuming incompressible flow at low speeds with negligible flow through the low speed rebound valve. The fluid flow rate and the damping force can thus be related to the damper velocity in the following manner:

$$\dot{x} = \frac{F_d}{C_{seatw}} \tag{4.16}$$

where C_{seatw} is the coefficient weighted with respect to the working area. The damper valving model also involves the flows through low speed rebound valve, a passage through the piston rod allowing flows from chamber 1 to 2 in both rebound and compression. In compression the flow across the piston is modeled as a combination of flows through the low speed rebound and the bypass valves. The force developed by flow across the compression head, in compression and rebound (effectively a check valve), are characterized using linear equation (4.13). The effective compressibility of the damper is derived as a function of chamber pressure using the iterative algorithm and equation (3.32). The various coefficients derived for the damping and compliance models are summarized in Table 4.6.

TABLE 4.6
COEFFICIENTS FOR MECHFORMANCE DAMPING MODEL

		Rebound	Compression
By Pass Valve	$\Delta P_{seat} \cdot A_w$ (N)	-50000	same
	C_{seatw}	1800	same
Low Speed Coefficients	C_{linw}	56700	same
	C_{ilinw}	0	same
Mid Speed Coefficients	C_{linw}	17000	none
	C_{ilinw}	-2400	none
Compression Head	C_{linw}	30	3000
	C_{ilinw}	0	0
Bulk Modulus	β^{-1} (Mpa)	500	
	$C_{i\beta}^{-1}$ (Mpa)	66	
	$C_{s\beta}^{-1}$ (Mpa/Mpa)	81.25	
Volume	V_{Total} (m^3)	145×10^{-6}	
	V_{20} (m^3)	6.7×10^{-6}	

Figure 4.14 illustrates a comparison of the force-velocity characteristic of the candidate damper derived from the analytical model with that established from the laboratory tests at low speed range in which the blow-off valve operates. The damper force curves including the gas spring force reveals good correlation between the analytical and experimental results. The analytical model, however, exhibits considerably larger hysteresis during the rebound. The force-velocity characteristics

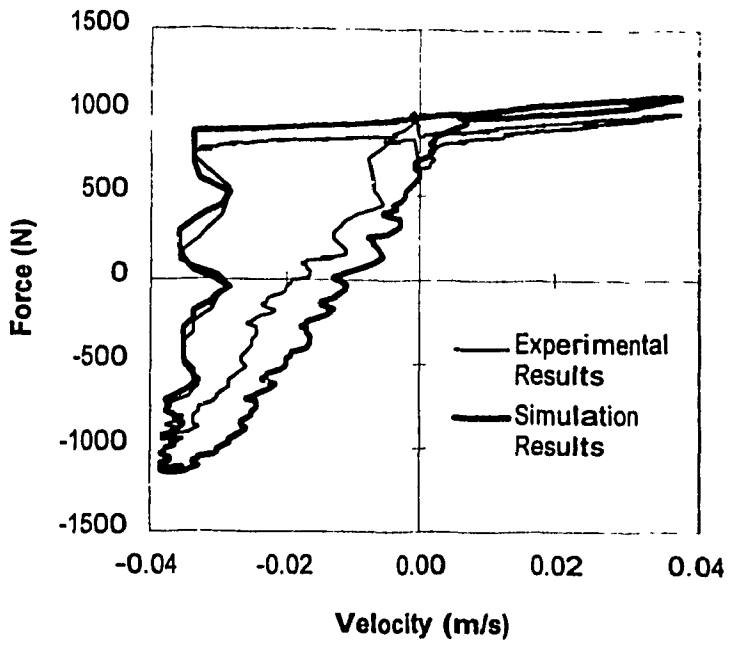

Figure 4.14 Comparison of analytical and experimental force-velocity characteristics of the Mechformance damper due to gas spring and damping (Excitation 6.35 mm, 1 Hz).

attained, corresponding to mid-speed to high-speed range, are compared with the test data obtained at excitation frequencies of 4, 8 and 16 Hz, with approximately the same peak velocity, in Figure 4.15. The results derived from the analytical model show reasonable correlation with the experimental data in the range of excitation considered in the study. An increase in hysteresis with increasing frequency is further observed in both analytical and experimental response characteristics similar to the case of the monotube damper designs.

The pressure response characteristics of the three chambers as a function of damper velocity are further analyzed to enhance an understanding of the valving and damping behavior. Figure 4.16 illustrates the pressure-velocity characteristics of the three chambers when the damper is subject to constant displacement sinusoidal excitation at a frequency of 8 Hz. The fluid pressures in chambers 1 and G (gas chamber) are observed to be slightly asymmetric due to fluid compressibility, similar to that observed for the

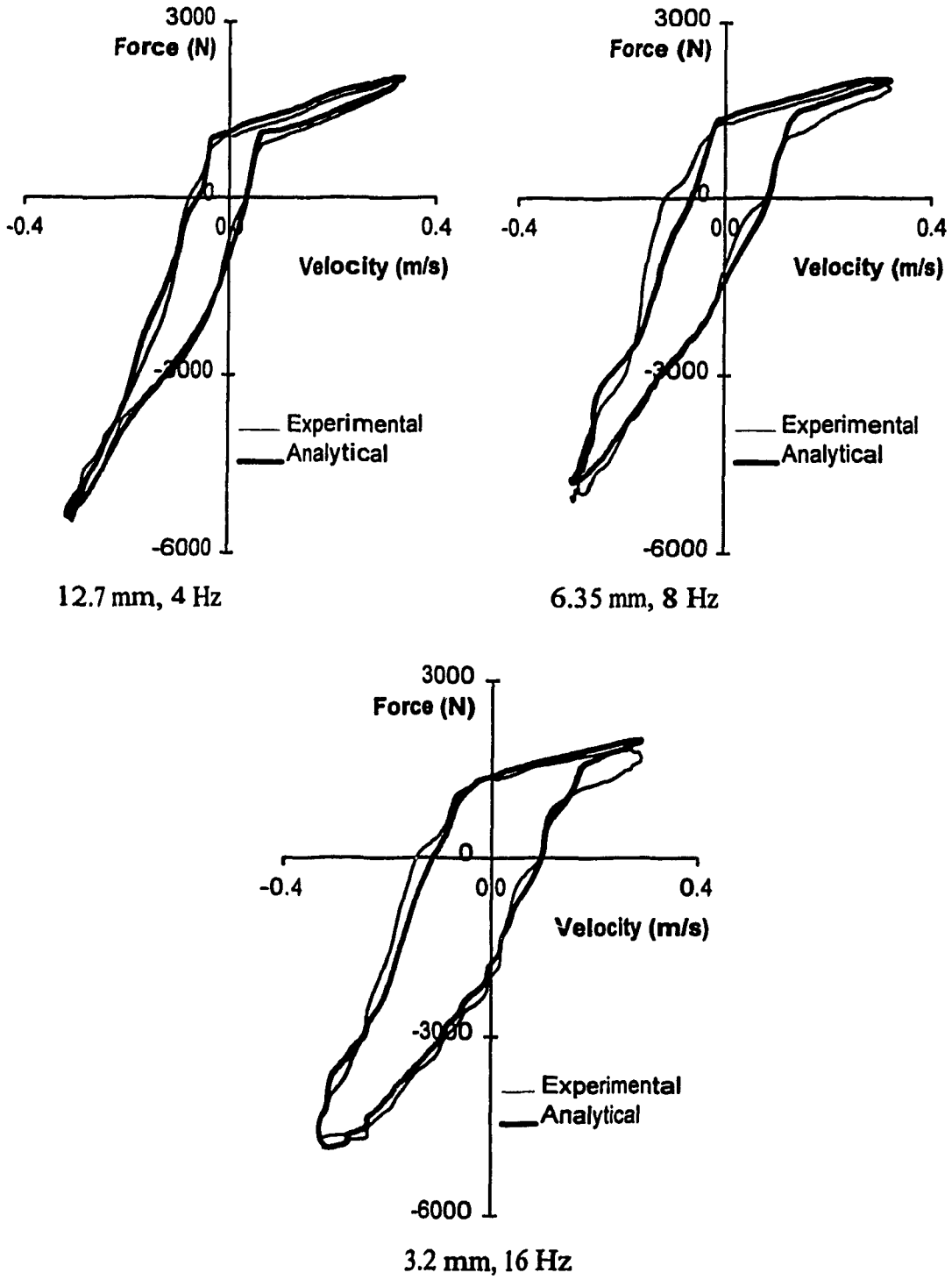

Figure 4.15 Comparison of analytical and experimental force-velocity characteristics of the Mechformance damper due to gas spring and damping.

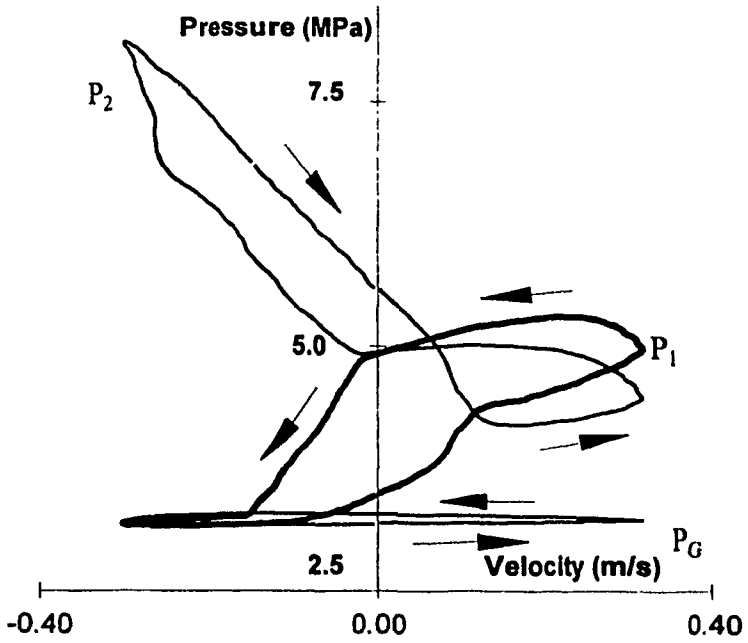

Figure 4.16 Pressure-velocity characteristics of the Mechformance damper (6.35 mm, 8 Hz).

monotube damper. The pressure differential between the two chambers is minimal during the rebound stroke due to relatively unrestricted flow between the chambers. A large pressure differential and thus damping force, however, develops during the compression stroke due to flow restrictions. The consistently large magnitude of pressure differential between chambers G and 2 is attributed to the valving restrictions, which do not permit sufficient bleed period between chambers 1, 2, and G resulting in the high differences in chamber pressures at zero velocity.

Fox Damper With Light Damper Setting

The remote reservoir Fox damper with light damper setting yields minimum low speed flow restrictions resulting in minimal pressure drop across the compression head and low speed piston valve during the compression and rebound strokes. The flows through both valves, however, are severely impeded when the damper is set for high damping. From the iterative algorithm used to identify the damper coefficients the

TABLE 4.7
COEFFICIENTS FOR FOX WITH LIGHT DAMPING MODEL

			Rebound	Compression
Low Speed Coefficients	C_{orrpw}	C_{linw}	-20935	1800
	$C_{lin\,pw}$	C_{ilinw}	558.10	0
	C_{ipw}		0	None
Mid Speed Coefficients	C_{linw}		8200	650
	C_{ilinw}		-2000	150
Compression Head	C_{linw}		10	17
	C_{ilinw}		0	0
Bulk Modulus	β^{-1} (Mpa)		200	
Volume	V_{Total} (m^3)		300×10^{-6}	
	V_{20} (m^3)		2×10^{-5}	

damper model was developed including: the constant compliance model of equation (4.7), the polynomial flow model for low speed flows through the rebound piston valve, linear flow model for low speed compression flow across the piston, liner models for both mid-speed compression and rebound damping across the piston, and linear models for flow in rebound and compression across the compression head. Various damper model coefficients identified from the study are summarized in Table 4.7.

Figure 4.17 illustrates a comparison of the force-velocity characteristics of the candidate damper derived from the analytical model with those established from the laboratory tests for a wide range of velocity inputs. The low-, mid- and high-damper speeds are realized through sinusoidal excitations at frequencies of 2, 4 and 16 Hz. The results presented in the Figure show good correlation between the analytical and

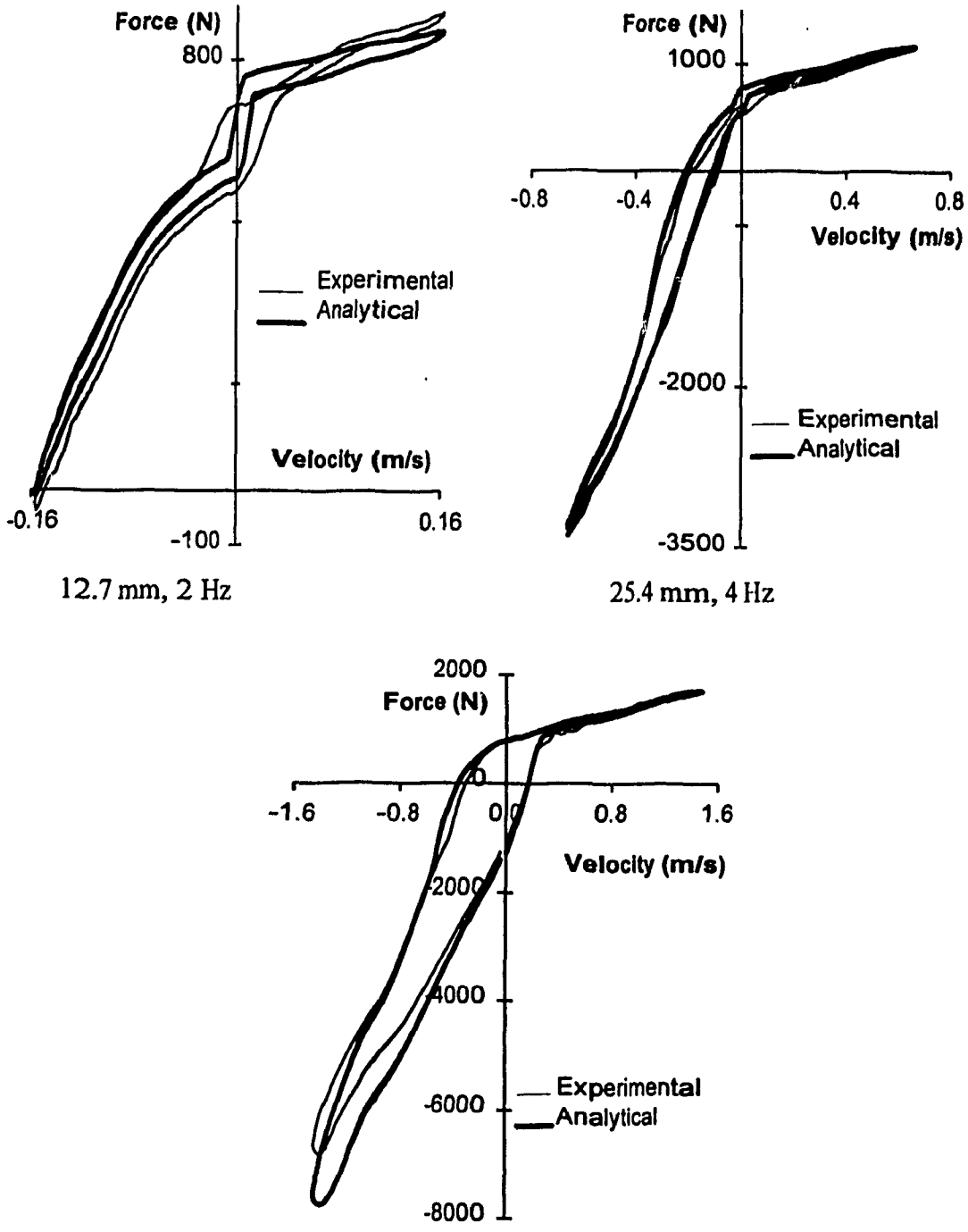

Figure 4.17 Comparison of analytical and experimental force-velocity characteristics of the Fox-Light damper due to gas spring and damping.

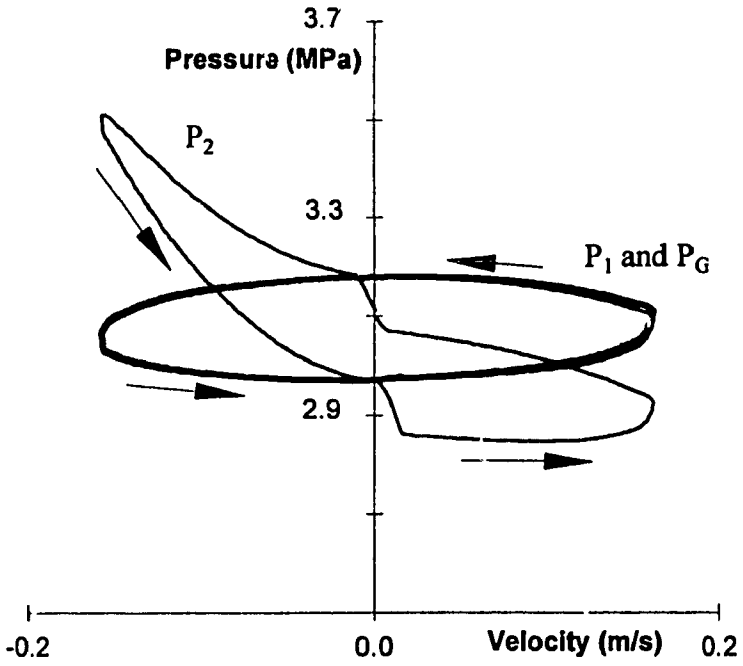

Figure 4.18 Pressure-velocity characteristics of the Fox-Light damper (12.7 mm, 2 Hz).

experimental response characteristics in the entire speed range. The results, however, show some divergence at high speed rebound attributed to the lack of a high speed rebound restriction in the model. The flows through high speed rebound valve were considered negligible assuming that peak velocity is well below the operating range of the valve. Figure 4.18 illustrates the pressure response of different chambers as a function of the velocity. The pressure-velocity curves exhibit only slightly asymmetric pressures in chambers 1 and 3, as illustrated earlier for the Mechformance damper. The pressure curves exhibit small pressure differential between chambers 2 and 3 during the compression stroke due to relatively low flow restriction, which is also apparent in Figure 4.17 for the low speed force-velocity characteristics. Low cycling speed and restrictions allow sufficient time for the flow of oil into and out of chambers 1, 2 and 3, such that the pressure in chamber 2 almost approaches that of the gas spring at the zero velocity crossing. During compression the light damping setting yields a low pressure drop across the compression head and the pressure in chamber 2 drops below the gas pressure, as

observed in the case of the monotube damper (Figure 4.11). A lower gas charge pressure in this damper configuration can thus cause cavitation.

Fox Damper With Heavy Damping Setting

When the damper valving is set for high damping, the low speed rebound and compression valving across the piston and the compression head, respectively, yield large pressure drops, increasing the damping through out the speed range, as shown in Figure 4.19. The increase in flow restriction results in the high speed rebound damping becoming effective at a considerably lower damper velocity. The analytical model of the Fox damper with heavy damping is thus developed to incorporate this additional valving restriction, which acts to limit the flow passing through the mid speed rebound valve in an orifice manner. A cross over point for flow rate is thus established and the mid-speed rebound valving model is replaced by a high speed restriction model when the flow rate exceeds this value. The damper coefficients for this restriction are initially established through curve fitting of the measured damper characteristics in a manner similar to that described for other valving models. The cross over point is established as the flow rate corresponding to the intersection of the mid speed and high speed rebound segments of the force-velocity plots. For low acceleration levels, the velocity at the cross over point can be estimated from the ratio of the flow rate to the working area (A_p-A_r), while the corresponding force is derived from the product of the pressure drop and the working area. The analytical model for the high damping setting further differs from that with light damping setting in that the low speed rebound flow is modeled using the linear model, equation (4.13), and that the compliance is expressed as a function of pressure, Equation (3.32). The damper coefficients established from the iterative procedure are summarized in Table 4.8. A comparison of damper coefficients derived for light (Table 4.7) and high damping setting reveal that the values for the mid speed compression across the piston are similar for both damper models, while the high damping model yields

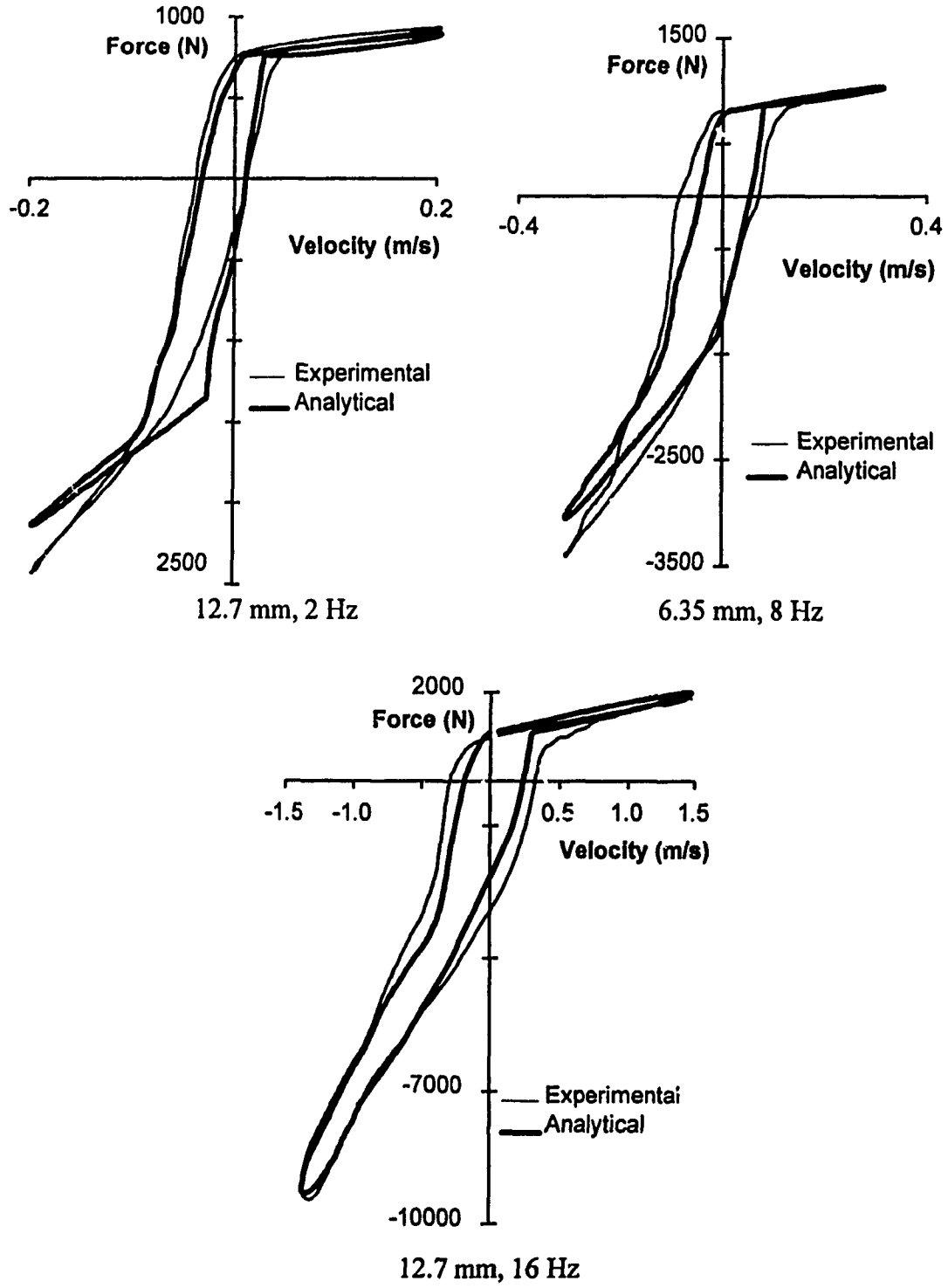

Figure 4.19 Comparison of analytical and experimental force-velocity characteristics of the Fox-Heavy damper due to gas spring and damping.

TABLE 4.8
COEFFICIENTS FOR FOX WITH HEAVY DAMPING MODEL

		Rebound	Compression
Low Speed Coefficients	C_{linw}	83000	22000
	C_{ilinw}	0	0
Mid Speed Coefficients	C_{linw}	20000	600
	C_{ilinw}	-1300	150
High Speed Coefficients	C_{linw}	6500	None
	C_{ilinw}	-1900	None
Compression Head	C_{linw}	10	150
	C_{ilinw}	0	0
Bulk Modulus	β_{min}^{-1} (Mpa)	250	
	$C_{i\beta}^{-1}$ (Mpa)	45.5	
	$C_{s\beta}^{-1}$ (Mpa/Mpa)	68.18	
Volume	V_{Total} (m^3)	300×10^{-6}	
	V_{20} (m^3)	2×10^{-5}	

considerably larger values of coefficients associated with flows through low speed valving and the compression head.

The force-velocity response characteristics of the analytical model of the Fox damper with high valving setting are compared to those derived from laboratory tests performed at different speeds, as shown in Figure 4.19. The Figure demonstrates good correlation between the analytical and experimental results over the entire speed range. A comparison of low-speed force-velocity characteristics of the dampers with light and

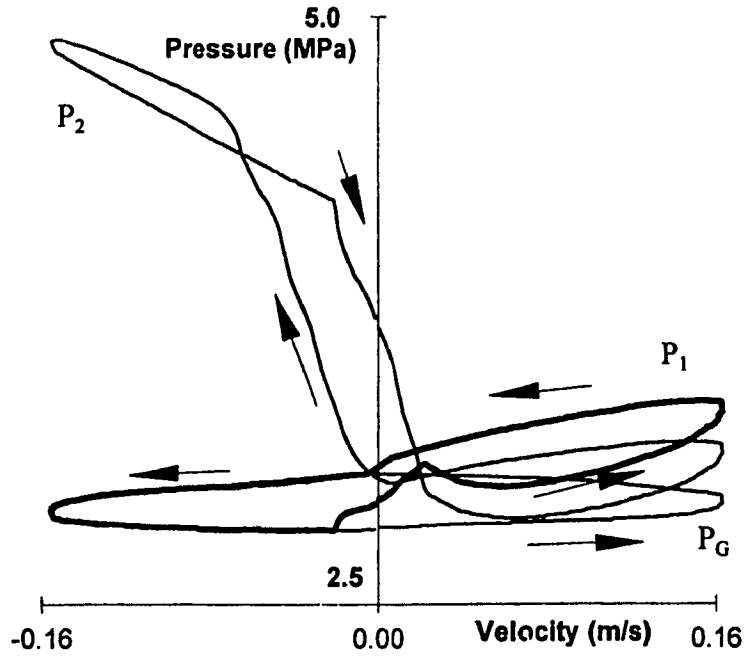

Figure 4.20 Pressure-velocity characteristics of the Fox-Heavy damper (12.7 mm, 2 Hz).

heavy setting (Figures 4.17 and 4.19) clearly illustrates the considerable increase in the rebound force caused by significant flow restrictions associated with the high setting. The comparison further reveals that with the high damping setting the mid-speed damping becomes effective at considerably lower velocity (below -0.05 m/s), while in the low damping setting the mid-speed damping occurs at nearly -0.3 m/s. The high speed rebound flow restrictions, in a similar manner, become effective at a lower speed (< -0.6 m/s), as shown in Figure 4.19. Although the analytical force-velocity response follows the pattern similar to that observed with the experimental results over the majority of the speed range, the model response corresponding to the low to mid speed transition in Figure 4.19, deviates significantly from the test data, indicating that improvements could be made in this part of the model.

The chamber pressure response characteristics of the damper model are evaluated under low speed excitations (frequency of 2 Hz), as shown in Figure 4.20. A comparison

with the pressure response behavior of damper with light setting (Figure 4.18) further illustrates the distinctly different performance of the two settings. The results show that the pressure of fluid in chamber 1 is similar to that of the gas pressure in rebound, and significantly higher in compression caused by increased pressure drop across the compression head. The fluid pressure in chamber 2 also increases during the compression stroke and remains higher then the gas pressure for majority of the compression stroke. The possibility of cavitation across the piston is thus greatly reduced in the event of the loss of gas charge. During the rebound stroke, the fluid pressure in chamber 2 remains significantly higher due to the increased pressure drop across the low speed rebound valve. The pressure-velocity curves for all three chambers are observed to be asymmetric in compression and rebound, similar to those observed for other candidate dampers. The gas pressure in chamber 3 reveals an increase in asymmetry, which may be attributed to increased pressure in the damper resulting in significant compressibility effects.

4.2.4 Identification of Damping Temperature Sensitivity Coefficients

The influence of temperature variations on the force developed by the candidate dampers is thoroughly examined in order to develop the damping temperature sensitivity models. A series of laboratory tests are performed under constant amplitude (12.5 mm) displacement excitation at 2 Hz, and the damping forces are measured at different discrete temperatures. The measured data is analyzed to derive the peak damping forces in compression and rebound in the entire temperature range. The temperature dependence of the normalized peak damping forces developed by the Koni and Mechformance dampers are illustrated in Figures 4.21(a) and 4.21 (b), while Figures 4.21(c) and 4.21 (d) illustrate the response behavior of the Fox damper with light and heavy damping settings. A regression analysis is performed to describe the normalized force as a linear function of the operating temperature. The coefficients derived from the linear regression and the

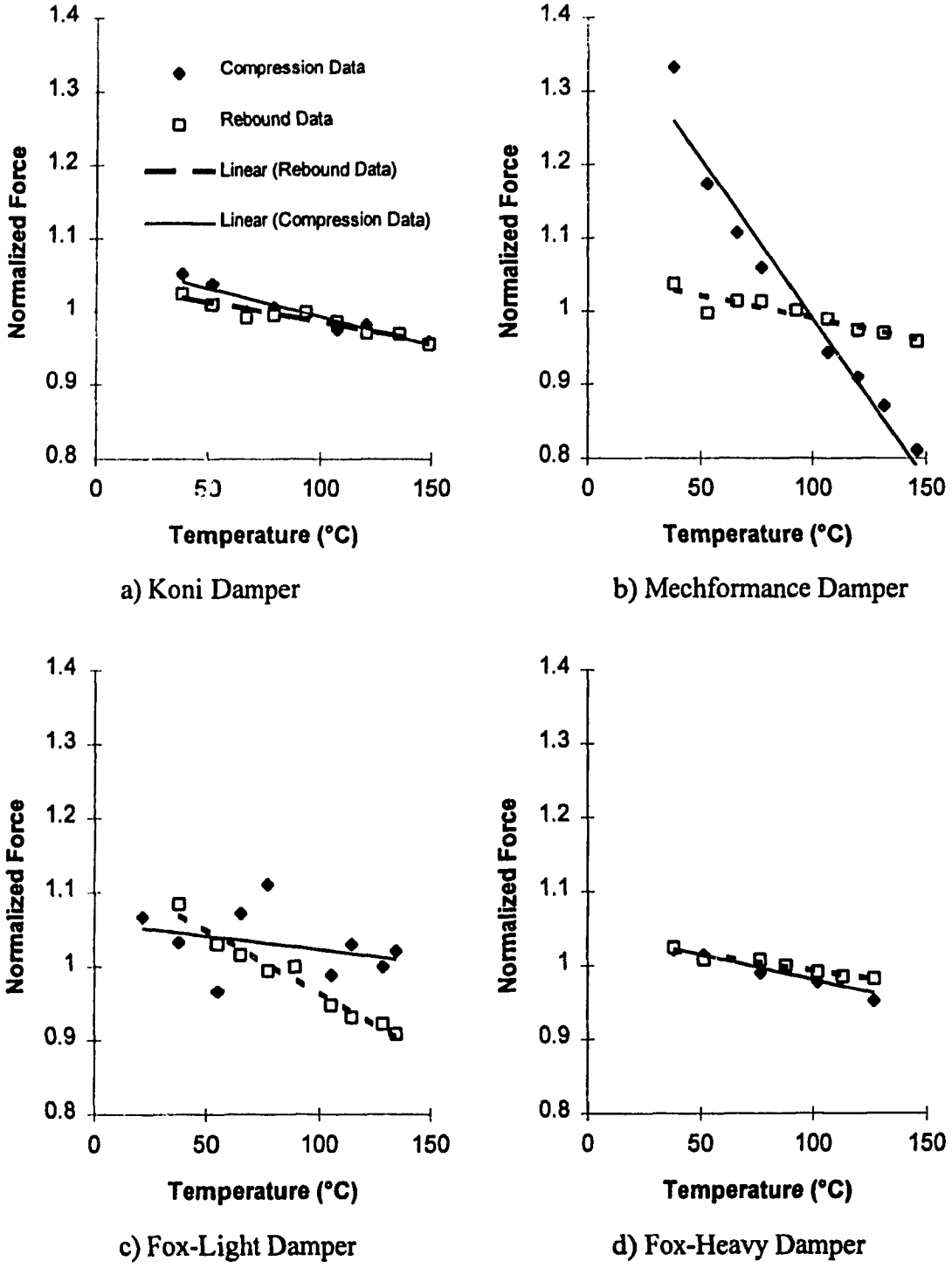

a) Koni Damper

b) Mechformance Damper

c) Fox-Light Damper

d) Fox-Heavy Damper

Figure 4.21 Normalized peak damping force as a function of operating temperature of the candidate dampers.

TABLE 4.9
TEMPERATURE COEFFICIENTS OF THE NORMALIZED PEAK DAMPING FORCE

	Koni	Mechformance	Fox - light	Fox - heavy
T_{ref} (°C)	93.5	93	89.2	91
		COMPRESSION		
Slope(10^{-3})	-0.77	-4.36	-0.37	-0.67
Intercept	1.07	1.43	1.06	1.05
r^2	0.90	0.96	0.10	0.87
		REBOUND		
Slope(10^{-3})	-0.55	-0.63	-1.69	-0.43
Intercept	1.04	1.05	1.13	1.04
r^2	0.91	0.85	0.96	0.94

corresponding r^2 values in compression and rebound are summarized in Table 4.9. The regression analysis yields good correlation with r^2 values ranging from 0.85 to 0.96 for all the candidate dampers, except for Fox damper with light damping, which may be attributed mostly to measurement errors associated with considerably lower compression damping. The normalized damping force decreases with increase in operating temperature, irrespective of the type and construction of the damper. The rate of change of normalized rebound damping with variations in temperature (slope) of the Koni, Fox with high damping and Mechformance is observed to be within a range of 31%, while the slopes of the compression curves for the Koni and Fox with heavy damping are just outside of this range. With the exception of the Mechformance in compression, the rate of change of the rebound normalized force with respect to the temperature for the Fox damper with light setting is considerably larger than those for the other dampers. This

may be attributed to the fact that at the peak velocity chosen, the damping is controlled by the slow speed circuit for the Fox with light damping, while with the exception of the Mechformance in compression, the damping force corresponds to their mid speed flow circuits. As the rate of change of the characteristic curve is observed to be greater in the slow speed range than that in the mid speed range, the Fox with light damping would be expected to have a higher rate of change in normalized force. For the Mechformance damper, the rate of change in normalized force is almost 7 times steeper in compression then rebound. This can be attributed to the fact that there is minimal damping in compression, hence the rate of change will be very sensitive to small changes in force.

While the results for the regression analysis presented in Table 4.9 may be used to develop a temperature sensitivity model for the damping, the model developed by analytical analysis of the thermal effects on flow, described in Equation (3.61), is used. The laboratory test is analyzed to determine the temperature sensitivity coefficients for the model, and the need for an additional coefficient (intercept) was identified to account for the experimental error. The temperature sensitive normalized damping force is thus expressed as:

$$f_{F_T} = \cdot \frac{1 \cdot}{1 + (K_{effoil} \cdot \Delta T_d + C_{fd})} \qquad (4.17)$$

where the constants K_{effoil} and C_{fd} are the slope and intercept, respectively, determined from the regression analysis, and ΔT_d is the temperature difference with respect to the reference temperature (T_{ref}) at which the tests are performed. The values of coefficients and the corresponding r^2 values derived from the analysis are presented in Table 4.10.

4.3 VALIDATION OF THE TOTAL DAMPER MODELS

The analytical models of the components, such as friction, gas spring, valving, fluid compressibility and their temperature dependence are developed upon identifying the

TABLE 4.10
TEMPERATURE SENSITIVITY COEFFICIENTS DERIVED FOR EQUATION (4.16)

	Koni	Mechformance	Fox - light	Fox - heavy
T_{ref} (°C)	93.5	93	89.2	91
		COMPRESSION		
K_{effoil} (10^{-3})	0.56	4.00	0.27	0.62
C_{fd} (10^{-3})	10.7	-3.35	-24.6	11.6
R squared	0.91	0.99	0.08	0.86
		REBOUND		
K_{effoil} (10^{-3})	0.77	0.61	1.54	0.45
C_{fd} (10^{-3})	2.50	5.76	20.8	2.91
R squared	0.91	0.84	0.95	0.93

various coefficients. These component models, validated in the previous sections, can be integrated to develop total damper model as described in equations (3.63). The analytical models of the candidate dampers, thus developed, are validated for different excitations ranging from low to high speeds, and different operating temperatures. The total damper models are validated for the following three types of excitations:

(i) Constant displacement amplitude (12.7 mm) sinusoidal excitation at a frequency of 2 Hz and operating temperature in the 38 - 39°C range.

(ii) Constant displacement amplitude (12.7 mm) sinusoidal excitations at a frequency of 2 Hz and operating temperature in the range of 133 - 149°C.

(iii) Constant displacement amplitudes (6.3 mm or 12.7 mm) excitation at a frequency of 8 Hz and operating temperature range of 89 - 94°C.

The analyses under excitations *(i)* and *(ii)* enable the verification of the model in terms of low speed damping characteristics, friction force and the gas spring force, as well as their temperature sensitivity. The analyses further provide the means to validate the gas spring, which is most sensitive to temperature variations. The last excitation will enable the verification of the mid-speed and high-speed damping characteristics together with the compressibility effects. The results of the simulations using the analytical models of the monotube and remote reservoir dampers, with coefficients identified from the analyses of the measured data, are compared with the experimental force-velocity characteristics to demonstrate validity of the models.

Koni Damper

Figures 4.22 (a) and (b) present a comparison of the force-velocity characteristics of the monotube damper derived from the analytical model and the experimental data under excitations *(i)* and *(ii)* at temperatures of 39°C and 149°C, respectively. The figures shows reasonable correlation between the analytical and experimental force-velocity characteristics over majority of the velocity range. The simulation results, however, differ considerably from the experimental data near two distinct velocities. Firstly, the analytical results deviate considerably from the experimental results near zero rebound force, when transition from low to high speed occurs. The experimental results exhibit discontinuous velocity response near zero force during the rebound stroke, irrespective of the operating temperature. This discontinuous response is attributed to the clearance within the bearing, as discussed earlier in section 2.2.2. Secondly, the analytical results exhibit relatively high damping force and significantly high change in the damping force in compression near the transition velocity (the velocity at which mid-speed valving becomes active). The experimental results show relatively less abrupt transition in the compression damping force, specifically at the operating temperature of 39°C. The analytical model further reveals slightly larger hysteresis at mid-speed range during the

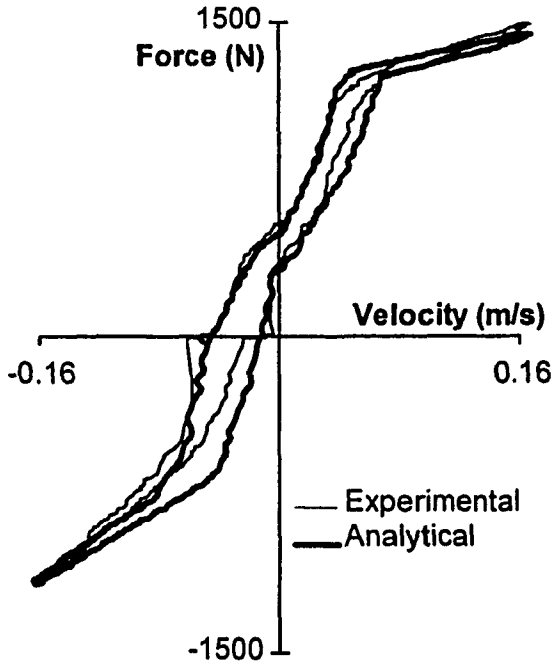

a) (2 Hz, 12.7 mm, 39°C)

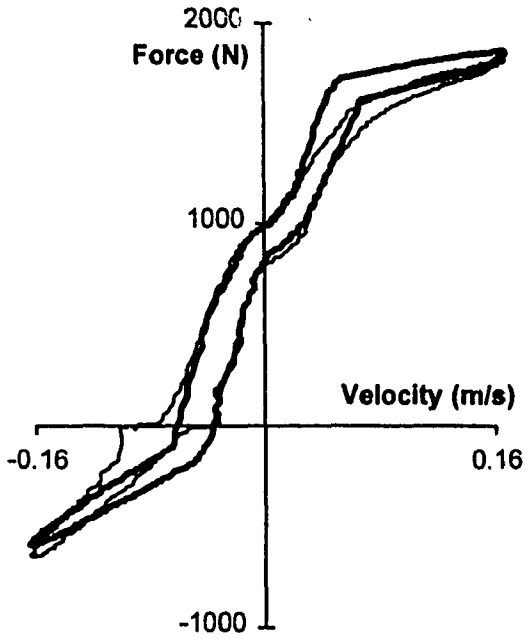

b) (2 Hz, 12.7 mm, 149°C)

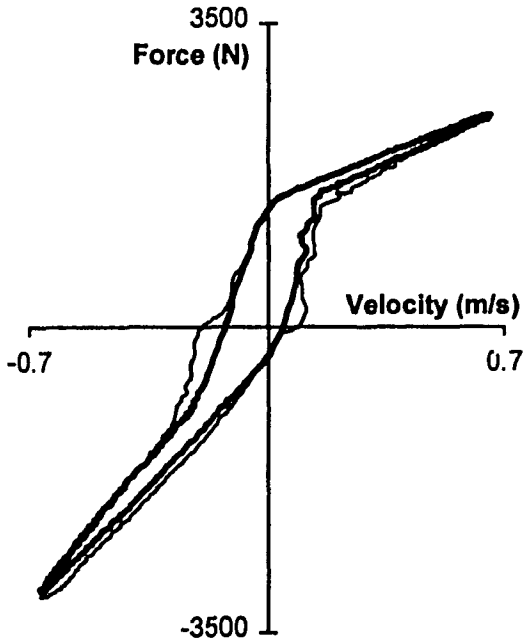

c) (8 Hz, 12.7 mm, 94°C)

Figure 4.22 Comparison of analytical and experimental total force-velocity characteristics of the monotube damper.

compression stroke. A comparison of damping forces presented at the two different temperatures exhibits an increase in bias in force of nearly 500 N, when the operating temperature is increased to 149°C. The analytical model characterizes the temperature dependency of the total damping force quite accurately.

The analytical model of the monotube damper is further validated for mid to high speed excitation *(iii)* at an operating temperature of 94°C, as shown in Figure 4.22 (c). The results derived from the analytical model correlate very well with the experimental force-velocity characteristics in the mid- as well as high-speed range during both compression and rebound strokes. The experimental results, however, exhibit somewhat larger hysteresis near low velocities, which is attributed to the bearing clearance. The results presented in Figure 4.22 clearly demonstrate the effectiveness of damper model in characterizing the compression and rebound forces in the entire speed range, and the temperature dependency of the damper force.

Mechformance Damper

The force-velocity characteristics derived from the Mechformance damper model under excitation *(i)* at 38°C and *(ii)* at 146°C are compared to the experimental response of the damper under identical excitations, as shown in Figure 4.23 (a) and (b). The experimental results show that increasing the temperature from 38°C to 146°C yields an increase in bias of the damper force by approximately 400 N, which is similar to that estimated by the analytical model. The results further illustrate that the gas spring of the Mechformance damper is less sensitive to temperature variations then the Koni damper, due primarily to larger initial gas volume. The results of the analytical model correlate well with the experimental data during the compression stroke, the model results deviate considerably from the experimental results in rebound stroke. The discrepancies between the analytical and experimental results can be primarily attributed to the errors in low- and mid-speed rebound valving models, and inadequate seating of the rebound valve

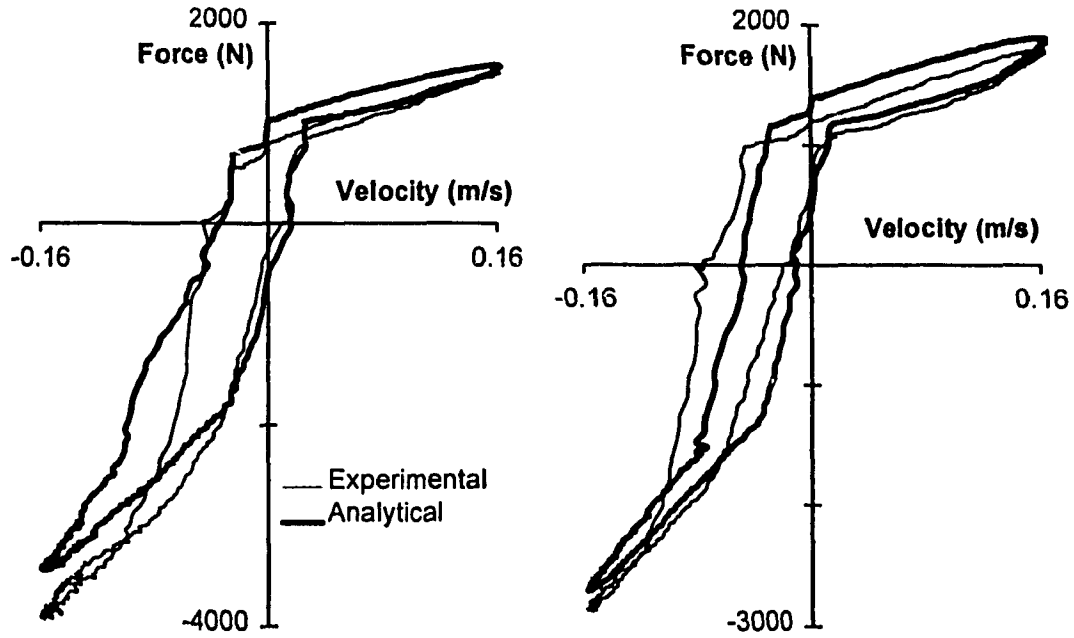

a) (2 Hz, 12.7 mm, 38°C)

b) (2 Hz, 12.7 mm, 146°C)

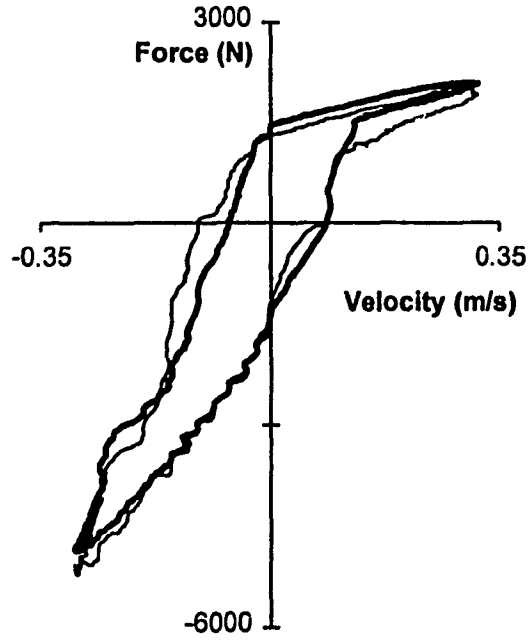

c) (8 Hz, 6.3 mm, 93°C)

Figure 4.23 Comparison of analytical and experimental total force-velocity characteristics of the Mechformance damper.

described earlier in section 4.2.3.3. The model, however, exhibits trends similar to those observed with the experimental data. The analytical model tends to provide better agreement with the experimental results obtained at higher operating temperature, specifically at mid- damper speeds in the rebound stroke. The analytical model also yields good correlation with the experimental results at higher speeds attained through excitation *(iii)* at an operating temperature of 93°C, as shown in Figure 4.23 (c). The results show slight discrepancies in damping during the decreasing magnitude of acceleration segments of the curve, which might be attributed to inertia effects of the fluid.

Fox Damper (Light Setting)

The analytical model of the remote reservoir Fox damper with light damping setting yields good correlation with the experimental force-velocity characteristics under low- to mid-speed excitations at two different temperatures (38°C and 135°C), as shown in Figure 4.24 (a) and (b). The analytical model, however, exhibits a rapid change in damper force in compression near zero velocity, while the experimental results show a gradual and continuous variation in the damping force. This discrepancy may be attributed to the errors in modeling the low speed compression valve. The results, however, exhibit correlation with the experimental data over almost the entire speed range and temperature range. The excellent correlation of the model with the test results is further demonstrated in Figure 4.24 (c) under high velocity excitations at an operating temperature of 92°C.

Fox Damper (Heavy Setting)

The analytical model derived for the remote reservoir Fox damper with high damping valving also yields reasonably good correlation with the experimental data at varying excitation velocities and operating temperatures. Figure 4.25 (a) and (b)

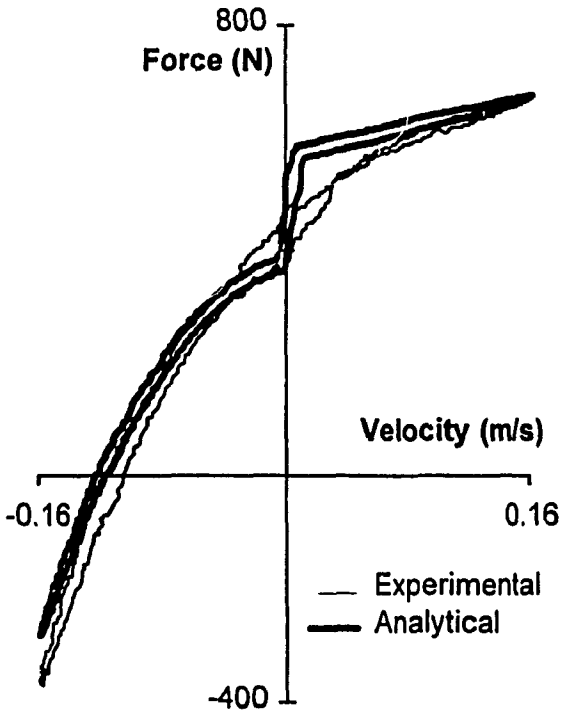

a) (2 Hz, 12.7 mm, 38°C)

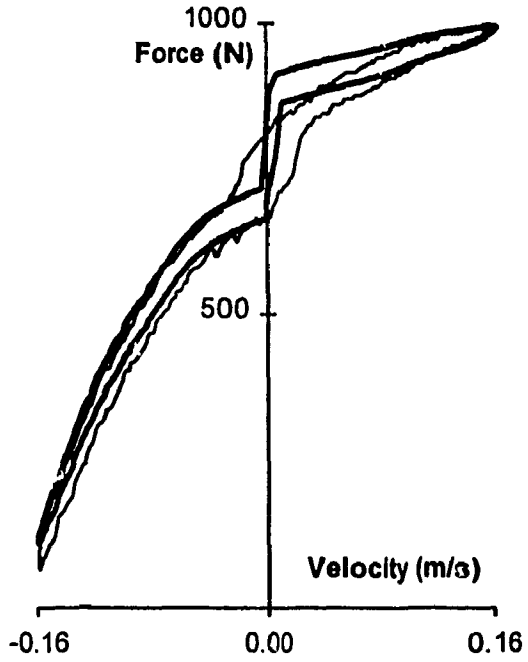

b) (2 Hz, 12.7 mm, 135°C)

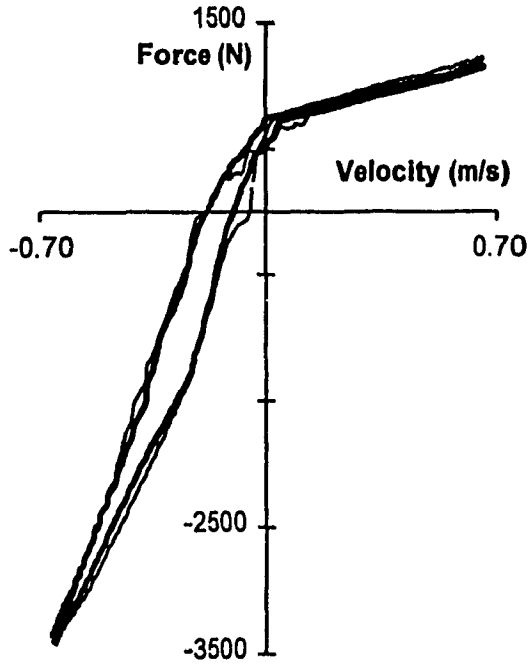

c) (8 Hz, 12.7 mm, 92°C)

Figure 4.24 Comparison of analytical and experimental total force-velocity characteristics of the Fox-Light damper.

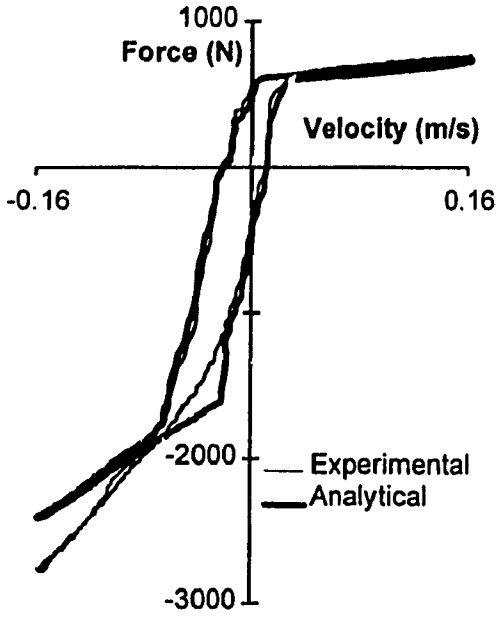

a) (2 Hz, 12.7 mm, 38°C)

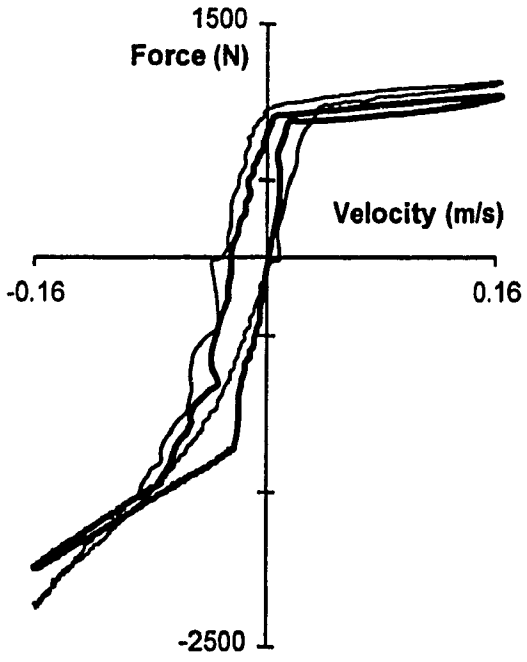

b) (2 Hz, 12.7 mm, 133°C)

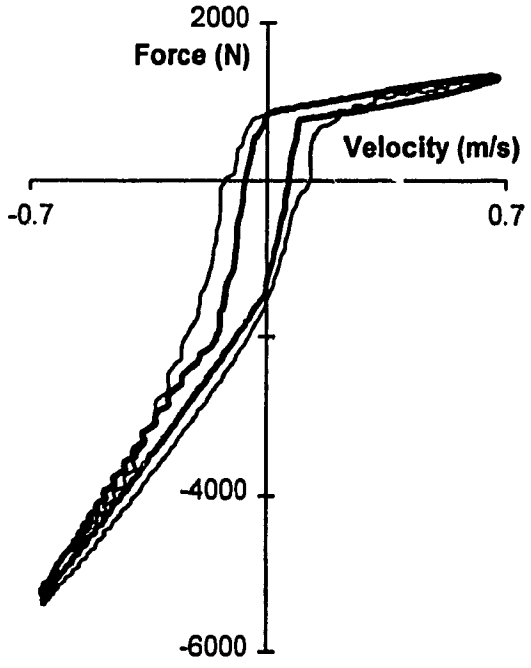

c) (8 Hz, 12.7 mm, 89°C)

Figure 4.25 Comparison of analytical and experimental total force-velocity characteristics of the Fox-Heavy damper.

illustrates a comparison of analytical and experimental force-velocity characteristics obtained under excitations *(i)* and *(ii)* at 38°C and 133°C, respectively. The figures show good correlation between the model and experimental results with some deviations in the rebound damping near the transition velocity. These deviations in rebound damping in the mid-speed range tend to decrease considerably when the operating temperature approaches 133°C. The mid-speed rebound damping model under such excitations can be easily improved through identification of coefficients to yield improved correlation. This approach was evaluated, resulting in improved correlation at low speed, however, correlation was poor between simulation and experimental results attained under mid- and high-velocity excitations. The proposed damper model represents a compromise in the validity of the model over the entire range of speed and operating temperature. The effectiveness of the model is further demonstrated by comparing the model results attained under higher velocity excitation *(iii)* with the corresponding experimental results, as shown in Figure 4.25 (c). The results show good correlation between the analytical and experimental plots, while the experimental results exhibit considerably larger hysteresis, particularly in the low speed response. This discrepancy can be attributed to the play within the bearings as evident near the zero force crossings and to the errors in the fluid compliance model.

4.4 SUMMARY

In this chapter, experimentally derived force-velocity and force-displacement characteristics are thoroughly analyzed to identify various coefficients for the component models. The analytical models of the gas spring, friction and valving components are validated under low-, mid- and high-speed excitations and at different operating temperatures. The component models are integrated to derive total models of the monotube and remote reservoir damper designs. The validity of the damper models is demonstrated for varying speeds and operating temperatures.

Static test results were used to characterize the displacement sensitive break away friction, and the initial gas volume and pressure of different damper designs. The dynamic breakaway and the thermal expansion of the dampers were identified from the test data obtained under low speed excitations. The component and the total damper models revealed reasonably good correlation with the experimental data in the entire range of operating speeds and temperatures. The effectiveness of analytical models under more realistic excitations will be further investigated in Chapter 6.

CHAPTER 5

DEVELOPMENT OF THE QUARTER CAR MODELS

5.1 INTRODUCTION

Although the analytical models developed in Chapter 3, and the experimental and model results described in Chapter 4 provide significant insight into the damper performance, the results derived from the simulation and laboratory tests performed using the fixed inertial reference, do not fully describe the damper performance under realistic road excitations. While the results attained under idealized excitations further demonstrate the validity of the models [17,19-22], the nonlinearities associated with the dampers, as demonstrated in analytical and experimental results in Chapter 4, require evaluations under realistic excitations to enhance their design and performance. The parametric sensitivity analyses, specifically, need to be performed under such realistic excitations, to evaluate the affect on the vehicles performance.

The quarter-car simulator test stand permits the study of damper characteristics as a function of realistic excitations arising from vertical dynamics of the sprung and unsprung masses, suspension and tire properties, road roughness and speed. The quarter-car simulator test stand developed in this study varies from the classic two-DOF vertical dynamics vehicle model, commonly found in the literature [27,28,54], due to friction between the sprung mass and the input. In this study a quarter-car model is developed upon integrating the damper models into an undamped two-DOF vertical dynamics model. Two quarter-car models are developed to evaluate the candidate dampers: (i) based on the quarter-car simulator test stand, to validate the damper models; (ii) a quarter race vehicle representative model to evaluate the damper performance. The latter model is used in conjunction with the validated damper models to study the influence of various damper design parameters, and compare the response characteristics with those of the simplified damper.

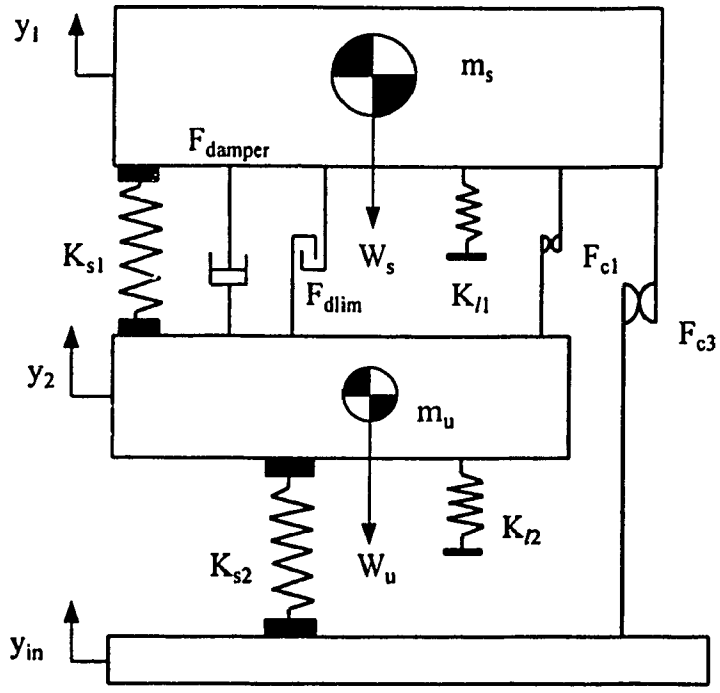

Figure 5.1 Schematic of the quarter car simulator test stand.

5.2 QUARTER VEHICLE MODELS

The uncoupled vertical dynamics of a single wheel suspension assembly can be effectively investigated using a two-DOF lumped parameter model shown in Figure 5.1. The masses due to wheel and tire assembly, and the brakes, are lumped together with portions of the steering and suspension masses, and represented as the equivalent unsprung mass, m_u. The unsprung mass includes approximately 2/3 of the suspension mass. The sprung mass, m_s of the vehicle model is derived upon subtracting the unsprung mass m_u from the total of the vehicle mass supported by a single tire. The suspension system is represented by its spring rate, damping forces, friction forces, and forces arising from the motion limiting stops. The tire is represented by a nonlinear spring in a point-contact manner, with asymmetric force-deflection characteristics to account for wheel-hop motions. The preload of the suspension spring is further

incorporated into the model to study the forces arising from wheel-hop motions and interactions with the bump stops.

5.2.1 Quarter Car Simulator Model

A quarter-car simulator comprising the unsprung and sprung masses, tire spring, suspension spring and a candidate damper is fabricated and installed on a electro-hydraulic vibration exciter. A pictorial view of the simulator has been presented in Figure 2.14. An analytical model of the simulator is developed to incorporate suspension preload, motion limiting stops, friction force and wheel hop motion. The static deflection of the suspension spring can be related to the sprung weight, the suspension spring rate and the gas spring force in the following manner:

$$Z_{pre1} = \frac{m_s \cdot g - F_{Gequil}}{K_{s1}} \tag{5.1}$$

where K_{s1} is the linear suspension spring rate, F_{Gequil} is the gas spring force developed by the damper at static equilibrium of the quarter car, g is the acceleration due to gravity and Z_{pre1} is the static deflection of the suspension system. In a similar manner, the static deflection of the tire spring, corresponding to static equilibrium, can be expressed as:

$$Z_{pre2} = \frac{(m_s + m_u) \cdot g}{K_{s2}} \tag{5.2}$$

where K_{s2} is the tire spring rate and Z_{pre2} is the static deflection of the tire. The equations of motion of the two-DOF quarter-car simulator are derived as:

$$(\ddot{y}_1 + g) \cdot m_s + \left[F_{damper}(z_1, t) + F_{dlim}(z_1, t)\right] + F_{fl}(z_1, t) + \left[F_{c1}(z_1, t) + F_{c3}(z_3, t)\right] + F_{s1}(z_1, t) = 0 \tag{5.3}$$

$$(\ddot{y}_2 + g) \cdot m_u - \left[F_{damper}(z_1, t) + F_{dlim}(z_1, t)\right] - \left[F_{fl}(z_1, t) - F_{f2}(z_2, \dot{z})\right] - F_{c1}(z_1, t) - \left[F_{s1}(z_1, t) - F_{s2}(z_2, t)\right] = 0 \tag{5.4}$$

where $z_1 = (y_1 - y_2)$, $z_2 = (y_2 - y_{in})$ and $z_3 = (y_1 - y_{in})$. The term $F_{damper}(z_1, t)$ in the above equations describes the total force developed by the damper, which includes the components of forces due to gas spring, friction, asymmetric damping, compressibility and thermal expansion. The analytical models of different candidate dampers, developed in Chapter 3, are integrated into the quarter-car simulator model to determine the total damper force comprising the above components. The damper force components are computed as a function of the damper coordinate z, which is related to the relative displacement z_1 in the following manner:

$$z = z_{install} - z_1 \tag{5.5}$$

where $z_{install}$ is the compressed length of the damper at static equilibrium of the quarter vehicle. Since all dampers are designed with a finite extended length they pose a motion limiting constraint on the relative displacement between the sprung and unsprung masses. In some instances, a relatively stiff elastic bumper (as with the Fox damper) or hydraulic absorber is built into the damper to reduce the impact when the damper reaches its full extension. All other designs, such as the Mechformance and Koni, comprise a rigid limit stop at full extension. The force arising from such limit constraint is derived using an asymmetric clearance spring model. The motion limiting constraint is represented by relatively stiff spring (K_{dlim}), in rebound, and the corresponding constraint force is given by:

$$\begin{aligned} F_{dlim}(z_1, t) &= K_{dlim} \cdot z \quad ; \quad z < 0 \\ F_{dlim}(z_1, t) &= 0 \quad ; \quad z \geq 0 \end{aligned} \tag{5.6}$$

The suspension spring or damper, and the tire springs, also yield a motion limiting constraint in compression arising from their minimum collapsed length. In the quarter-car simulator model, the constraint forces caused by minimal collapsed lengths of the

suspension and tire are represented by F_{l1} and F_{l2}, respectively. The constraint limit force in compression due to suspension spring or damper is given by:

$$\begin{aligned} F_{l1}(z_1,t) &= K_{l1}\cdot(Z_{l1}-z_1) \quad ; \quad z_1 < Z_{l1} \\ F_{l1}(z_1,t) &= 0 \quad ; \quad z_1 \geq Z_{l1} \end{aligned} \tag{5.7}$$

where K_{l1} is the equivalent spring rate due to the limit constraint and Z_{l1} is the permissible compression of the suspension components with respect to the static equilibrium. Z_{l1} is the larger of the collapsed lengths of the suspension spring or the damper. The limit force due to tire spring compression is derived in a similar manner:

$$\begin{aligned} F_{l2}(z_2,t) &= K_{l2}\cdot(Z_{l2}-z_2) \quad ; \quad z_2 < Z_{l2} \\ F_{l2}(z_2,t) &= 0 \quad ; \quad z_2 \geq Z_{l2} \end{aligned} \tag{5.8}$$

where K_{l2} is the equivalent spring rate due to the limit constraint and Z_{l2} is the permissible compression of the helical spring representing the tire, with respect to the static equilibrium. While the tire force, in its linear range, is represented by the force due to linear spring K_{s2}, the tire force reduces to zero under wheel-hop motion. The tire force $F_{s2}(z_2,t)$ is thus expressed as:

$$\begin{aligned} F_{s2}(z_2,t) &= K_{s2}\cdot(z_{pre2}-z_2) \quad ; \quad (z_{pre2}-z_2)\geq 0 \\ F_{s2}(z_2,t) &= 0 \quad ; \quad (z_{pre2}-z_2)<0 \end{aligned} \tag{5.9}$$

The suspension spring force $F_{s1}(z_1,t)$ is related to its linear spring rate K_{s1} in the following manner:

$$\begin{aligned} F_{s1}(z_1,t) &= K_{s1}\cdot(z_{pre1}-z_1) \quad ; \quad (z_{pre1}-z_1)\geq 0 \\ F_{s1}(z_1,t) &= 0 \quad ; \quad (z_{pre1}-z_1)<0 \end{aligned} \tag{5.10}$$

The friction forces in the quarter-car simulator, F_{c1} and F_{c3}, are attributed to the journal bearings that guide the unsprung mass relative to the sprung mass, and the sprung mass relative to the road input, respectively. These friction forces are represented as follows, assuming ideal characteristics:

$$F_{ci}(z_i, t) = F_{coul_i} \cdot \mathrm{sgn}(\dot{z}_i) \qquad ; \qquad i=1,3 \qquad (5.11)$$

where F_{coul_i} is the magnitude of the friction force and $\mathrm{sgn}(\dot{z}_i)$ characterizes the sign of the relative velocity $\dot{z}_i$.

The analytical model developed of the quarter car simulator differs from a more realistic representation of a race car, due primarily to the design considerations of the simulator. An improved quarter-vehicle model of a race car, used in the parametric variation study, is illustrated in Figure 5.2. The primary difference between this analytical model and the quarter-car simulator model is the additional friction element between the sprung mass and input. This friction force component is caused by the bushings mounted between the sprung mass and the input, which is not present in a vehicle suspension model. Although the automotive tires yield only small amount of damping, the damping due to tires used in racing vehicles becomes more significant due to relatively high stiffness of the suspension and tires. The damping due to tire is thus integrated within the quarter car analysis model, as a light viscous damper. The laboratory simulator, however, was developed assuming negligible tire damping. Furthermore, the magnitude of Coulomb friction between the sprung and unsprung masses of a race car is significantly lower due to the usage of low friction spherical bearings, as opposed to the journal bearings found in the simulator.

The analytical model may be further enhanced to incorporate the kinematics and dynamics of the suspension links, which can affect the damping and spring forces in a significant manner. Warner and Rathwell [70] investigated the kinematic performance of a road racing motorcycle suspension linkage shown in Figure 5.3. The results of the

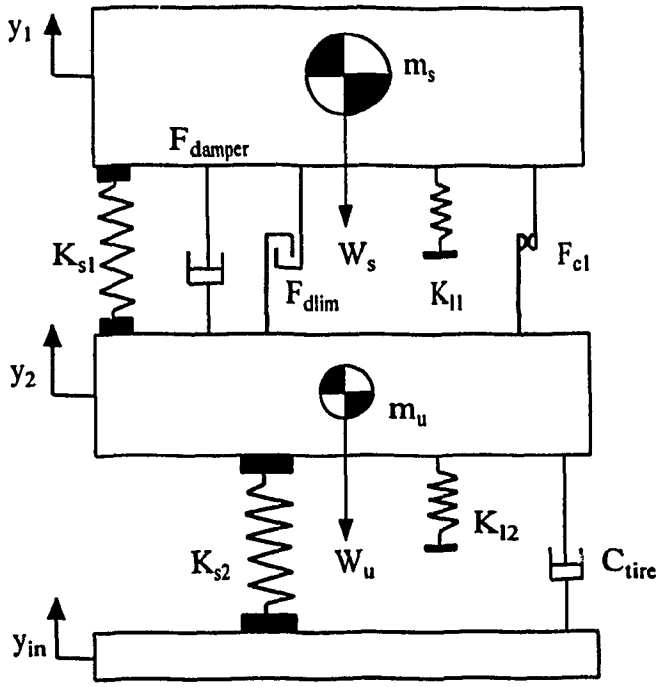

Figure 5.2 Schematic of the quarter car analytical model.

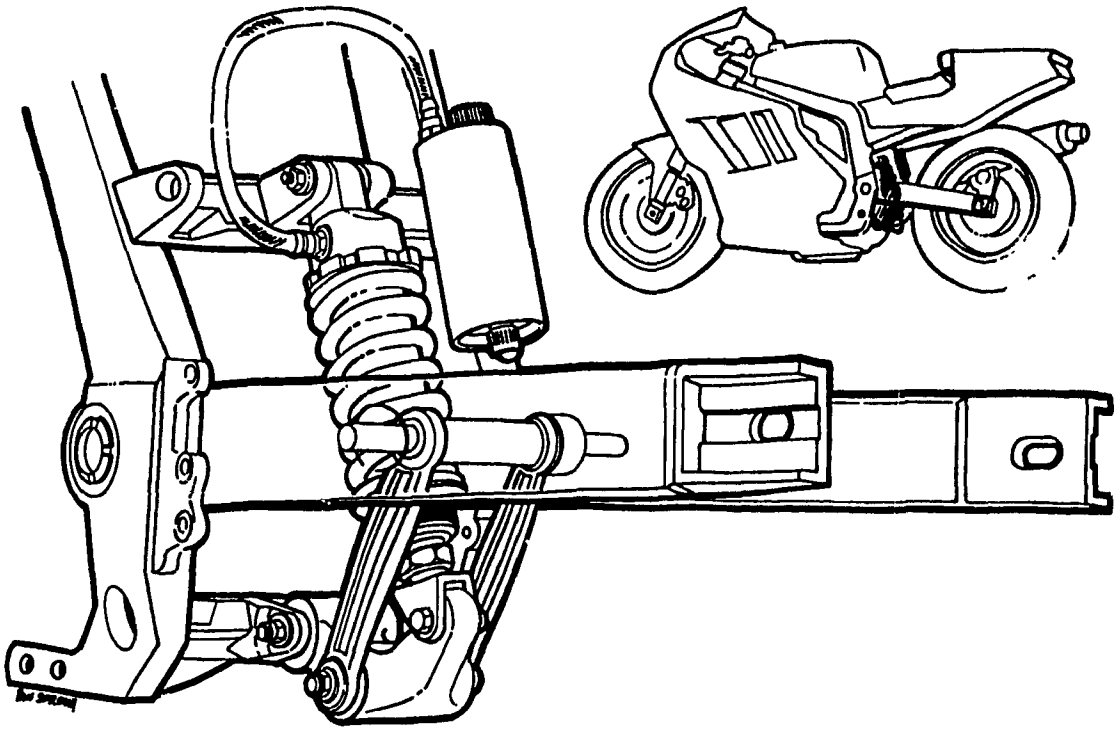

Figure 5.3 Motorcycle rear suspension linkage [70].

study demonstrated significant influence of the linkage design on the suspension forces depending upon the leverage ratio (ratio of change in axle force to the change in suspension force). In this study however, it is assumed that the linkage ratio is 1:1, and hence, the linkage affects can be neglected.

The equations of motion for the two-DOF quarter car analysis model are:

$$(\ddot{y}_1 + g)\cdot m_s + F_{damper} + F_{dlim} + F_{c1} + F_{l1} + F_{s1} = 0 \qquad (5.12)$$

$$(\ddot{y}_2 + g)\cdot m_u - F_{damper} - F_{dlim} - F_{c1} - F_{l1} - F_{s1} + F_{l2} + F_{s2} + F_{dtire} = 0 \qquad (5.13)$$

where F_{dtire} is the damping force due to the tire, given by:

$$\begin{aligned} F_{dtire} &= C_{tire}\cdot \dot{z}_2 \quad ; \quad z_2 < Z_{pre2} \\ F_{dtire} &= 0 \quad ; \quad z_2 \geq Z_{pre2} \end{aligned} \qquad (5.14)$$

where C_{tire} is the equivalent viscous damping coefficient of the tire model

5.3 IDENTIFICATION OF QUARTER CAR SIMULATOR FRICTION

The friction forces caused by the journal bearings used to guide the sprung and unsprung masses of the quarter-car simulator are identified through laboratory measurements. The candidate damper was removed from the simulator in order to characterize the friction force due to journal bearings alone. The undamped quarter-car simulator comprising the sprung and unsprung masses, and suspension and tire springs is subject to a step displacement excitation in the laboratory, and the displacement response characteristics of the sprung and unsprung masses were measured. The measured data was analyzed for its rate of decay and the magnitude of friction force.

Figure 5.4 illustrates the step response of the sprung and unsprung mass of the quarter-car simulator subject to a 1.5 cm step displacement excitation. The measured response characteristics exhibit oscillations with nearly linear decay caused by Coulomb

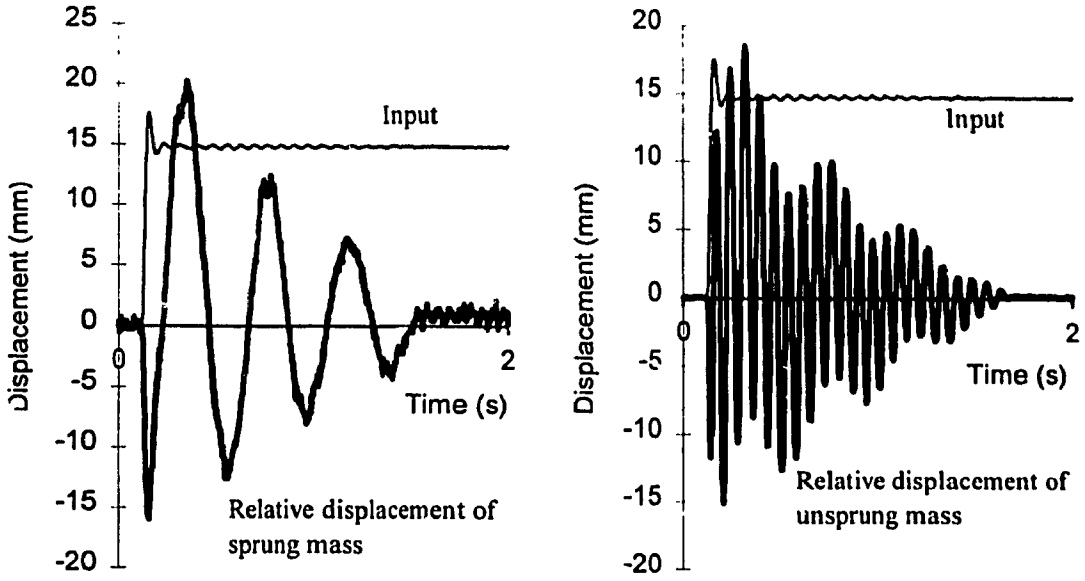

Figure 5.4 Undamped sprung and unsprung mass responses of quarter car simulator (15 mm step).

friction. The results also exhibit oscillation at the sprung mass natural frequency of 2.4 Hz. The corresponding step response of the unsprung mass, exhibits oscillations predominant around the natural frequency of the unsprung mass (14 Hz), while the oscillations are enveloped by the sprung mass resonant frequency. Since the sprung mass is considerably larger than the unsprung mass and the suspension spring is significantly softer than the tire spring, the sprung mass exhibits more or less uncoupled response behavior. The decay in displacement response of the sprung mass can thus be related to the magnitude of Coulomb friction force in the following manner [71]:

$$F_{coul} = \frac{\left(Z_1^i - Z_1^{i+1}\right) \cdot K_{sl}}{4} \tag{5.15}$$

where Z_1^i and Z_1^{i+1} are the amplitude of successive oscillations. The above estimate of Coulomb friction is derived assuming entirely uncoupled sprung mass behavior or the step response characteristics of a single-DOF mass-spring-friction system. The potential

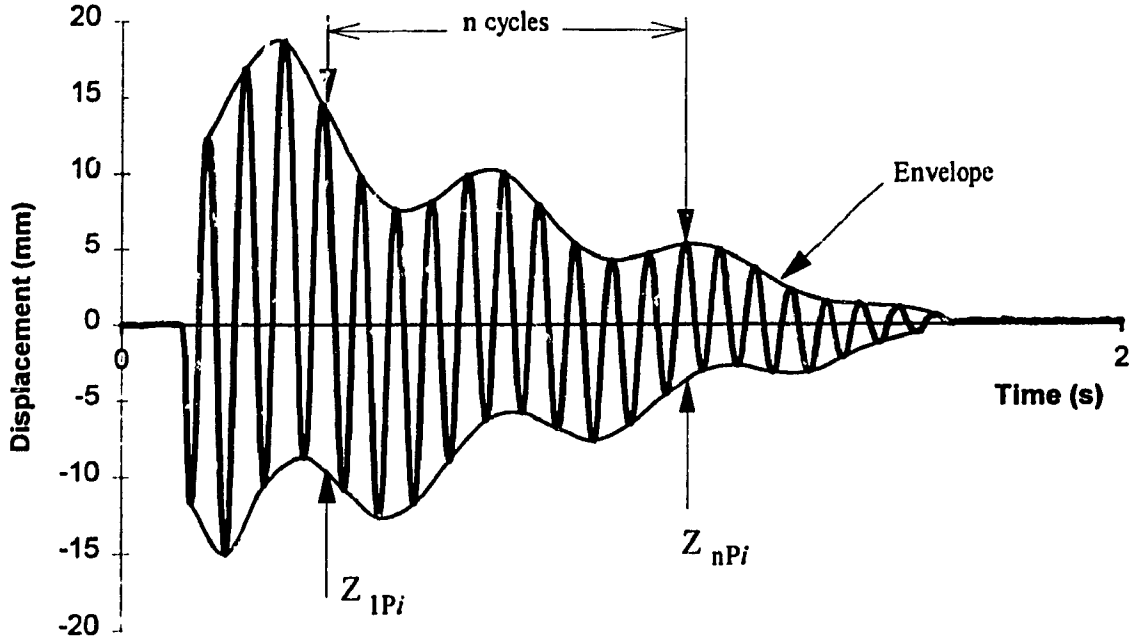

Figure 5.5 Deriving friction from the undamped quarter car simulator unsprung mass response (15 mm step).

errors caused by the coupling between the sprung and unsprung masses, as evident in unsprung mass response, can be reduced through analysis of the width of the envelope of decay. Figure 5.5 illustrates the width of the envelope of decay in unsprung mass displacement response. The change in the width of the envelope of decay is also measured after a number of cycles (n) to reduce the magnitude of the error, which may arise from measuring two successive peaks with only slight variations in the magnitude. The Coulomb friction force is then estimated from:

$$F_{coul\,i} = \frac{(Z_{1Pi} - Z_{nPi}) \cdot K_{si}}{8 \cdot n} \tag{5.16}$$

where Z_{1Pi} and Z_{nPi} are the measurements of the envelope width at the first and n number of cycles.

5.4 ANALYSIS AND EXPERIMENTAL VALIDATION OF THE QUARTER CAR SIMULATOR MODEL

The quarter-car simulator model is verified by comparing the model results with those attained from the laboratory tests. The simulator is fabricated and installed on a electro-hydraulic vibration exciter. Although the internal linear variable differential transformer (LVDT) within the hydraulic cylinder provided a good measure of the excitation, a delay of approximately 4 ms was observed due to the signal conditioning and filtering. Accelerometers are mounted to monitor the response of the sprung and unsprung masses relative to the input. The acceleration signals, however, included excessive noise due to pump (nearly 160 Hz) and friction effects. Low pass filters were, therefore, employed to acquire the acceleration signals. In view of the low signal to noise ratio of the accelerometer response, external LVDT and linear velocity transducers (LVT) were installed to measure the displacement and velocity excitation, and relative response of the sprung and unsprung masses. While the LVDT's with ± 0.25 m full scale range provided low signal to noise ratio, the LVT's provided the most consistent measurements with high signal to noise ratio. Table 5.1 summarizes the different sensors used in the quarter-car simulator, together with their respective gains. Since the LVDT's and LVT's

TABLE 5.1
GAINS OF MEASUREMENT TRANSDUCERS USED WITH QUARTER CAR SIMULATOR

	Input	Unsprung Mass	Sprung Mass
LVT (m/s/V)	0.396	0.378	0.166
External LVDT (m/V)	0.0649	0.0131	.0699
Internal LVDT (m/V)	0.0112		
Accelerometer ($m/s^2/V$)	10.09	9.99	10.19
Damper Force Sensor (N/V)	1032		

are installed to measure the relative displacement and velocity response characteristics of the sprung and unsprung masses with respect to the excitations, these data are primarily used to validate the simulator model.

5.4.1. Measurements of Friction Forces

The tests are initially performed on the quarter-car simulator without a damper under step displacement excitations of varying amplitudes, and the measured data analyzed to estimate the magnitude of Coulomb friction forces (F_{c1} and F_{c3}), as described in section 5.3. The tests were performed for varying magnitudes of displacement excitations to identify the possible variations in the friction properties as a function of the direction and amplitude of excitation. The magnitudes of friction forces attained under different step excitations are summarized in Table 5.2. Although the results show variation of friction force for variations in the magnitude and direction of step excitation,

TABLE 5.2
MAGNITUDE OF COULOMB FRICTION FORCES DERIVED FROM THE STEP RESPONSE

	Magnitude of Friction Force	
Step Displacement (cm)	Sprung Mass to Input (N)	Sprung to Unsprung Mass (N)
+1.5	94.5	69.9
-1.5	81.9	73.5
+2.6	144.2	117.3
-2.6	124.2	99.4
+5.1	122.5	129.9
-5.1	123.9	103.1
Average Friction Force (N)	115.0	98.8

a clear trend cannot be established. The results further show that the friction force acting on the unsprung mass is considerably lower then that acting on the sprung mass, irrespective of the magnitude of step displacement. The averaged values of the friction forces are thus derived and used in the quarter car simulator model.

5.4.2. Validation of the Quarter-Car Simulator Model

The two-DOF model of the undamped quarter-car simulator is analyzed and the response characteristics are compared with those derived from the experimental data. The simulator model based upon the averaged friction values listed in Table 5.2 resulted in response behavior with slightly larger damping than the measured response. The analytical model was thus tuned by slightly lowering the values of friction forces in an iterative manner until a satisfactory correlation between the simulation and experimental results, based on the best compromise under different levels of excitation, was achieved. The magnitudes of friction forces between the sprung mass and the input, and between sprung and unsprung masses were selected as 90 N and 65 N, respectively. These lower values of friction forces, when compared to the averaged values in Table 5.2, are attributed to the coupled behavior of the two-DOF simulator.

The analytical response characteristics of the sprung mass of the simulator, subject to positive 1.5, 2.6, 5.1 cm and negative 2.6 cm step displacement excitations, are compared to those derived from the measured data, as shown in Figure 5.6. The model response exhibits relatively rapid decay, specifically for 1.5 cm and 5.1 cm step excitations. The model response, however, reveals very good correlation for the positive 2.6 cm, and relatively slower decay for the negative 2.6 cm step excitations. Although the model response exhibits trends very similar to those observed with the experimental data, the model exhibits damping slightly larger than the experimental data for the 1.5 and 5.1 cm, and lower for the negative 2.6 cm excitations. The analytical and experimental response characteristics exhibit a slight bias prior to application of the

excitation and after the response is settled, which may be attributed to the lockup behavior of the simulator.

The response characteristics of the unsprung mass of the simulator model, subject to the same step excitations, are compared with those established from the experimental data, as shown in Figure 5.7. A good correlation is observed between the analytical and experimental results. The sprung mass response of the analytical model, however, exhibits relatively rapid decay when compared to that obtained from the experimental response, for 1.5 cm and 5.1 cm step excitations, and slower decay for the negative 2.6 cm step excitation. The results show improved correlation with the experimental data for the positive 2.6 cm step excitation, as observed for the sprung mass. A comparison of response characteristics of the simulator, subjected to positive and negative 2.6 cm step excitations, reveals that both the model and experimental results decay faster for the negative excitation. This nonlinear effect is attributed to the gravitational force opposing the motion under positive step excitation, adding potential energy to the system. From the results presented in Figures 5.6 and 5.7 it is evident that the experimental friction values differ from one test to the next. The experimental studies further reveal that the friction values vary between two applications of successive step inputs. The values of friction used in the computer simulation are thus selected as a compromise from the analysis of different experimental results.

The analytical and experimental results reveal excellent agreement in view of the natural frequencies of the simulator. The bounce and wheel hop mode undamped frequencies of the simulator derived from the analytical model are compared with the measured damped natural frequencies in Table 5.3. While the bounce mode natural frequency of the model is very close to the measured data, the wheel hop is considerably larger than the measured data. The discrepancies between the wheel hop frequencies may be attributed to low unsprung mass and relatively high damping due to the coupling effect, as seen in Figure 5.7. A comparison of the damped and undamped frequencies

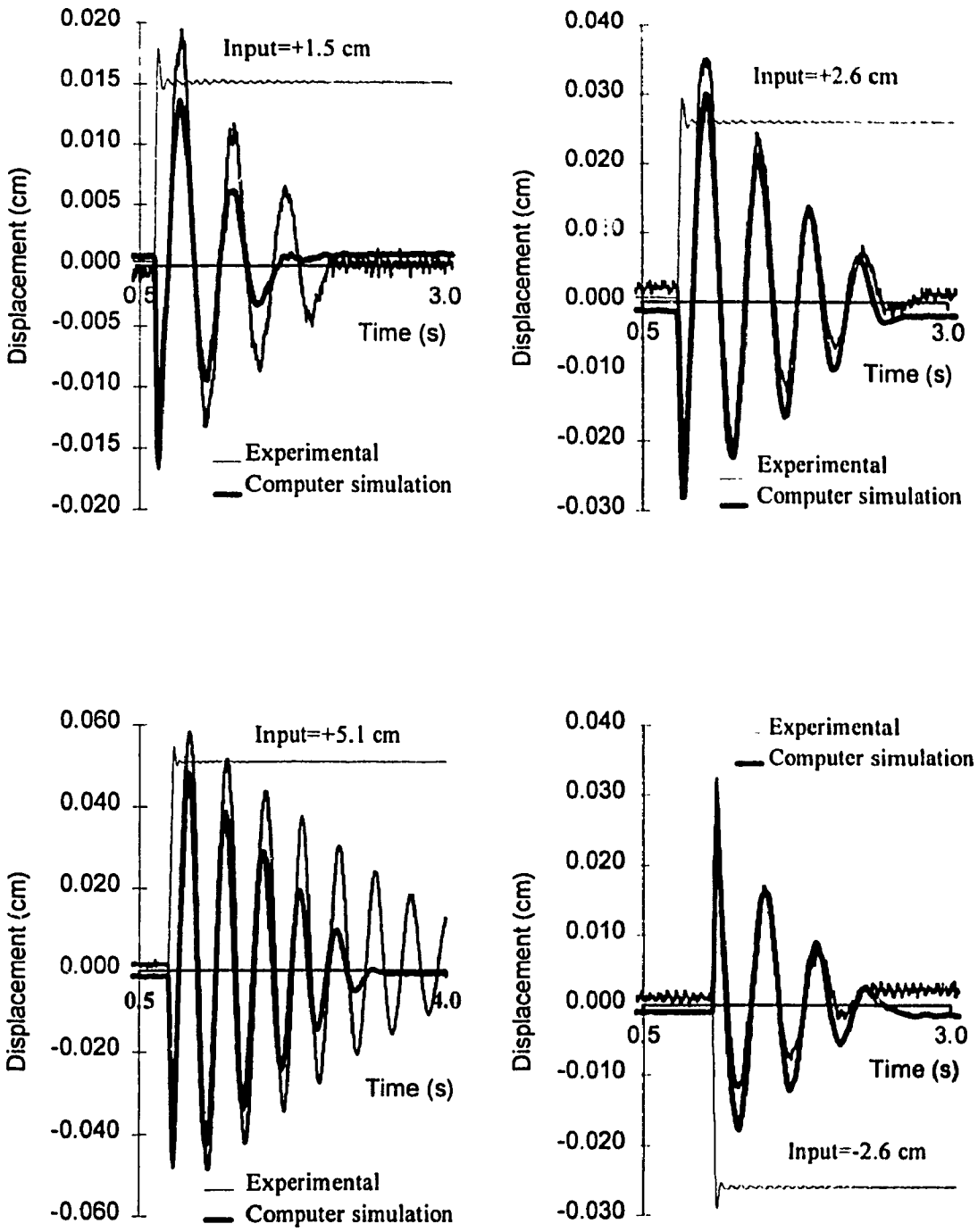

Figure 5.6 Comparison of the step response of the sprung mass of the undamped quarter-car simulator model with the experimental response.

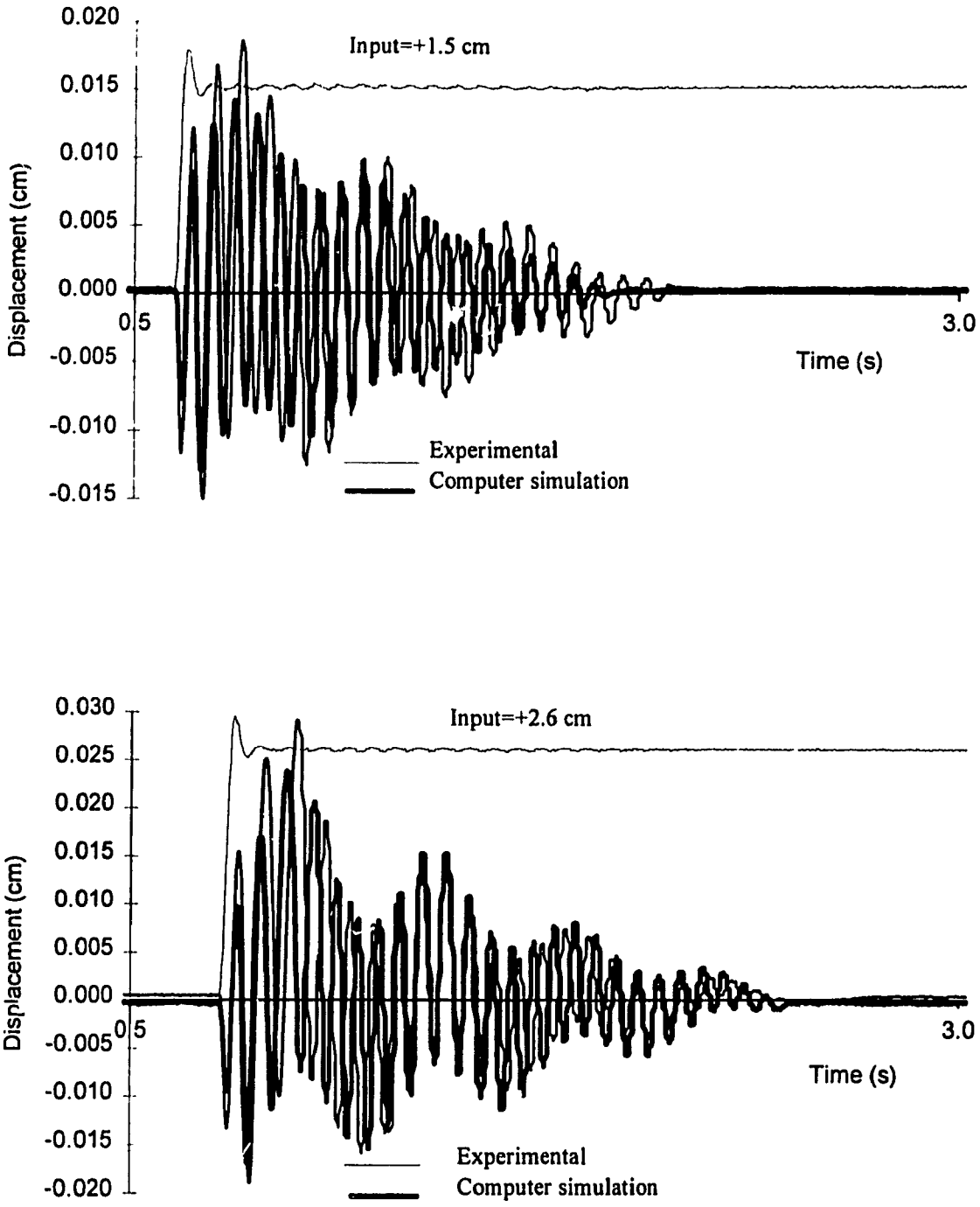

Figure 5.7 Comparison of the step response of the unsprung mass of the undamped quarter-car simulator model with the experimental response.

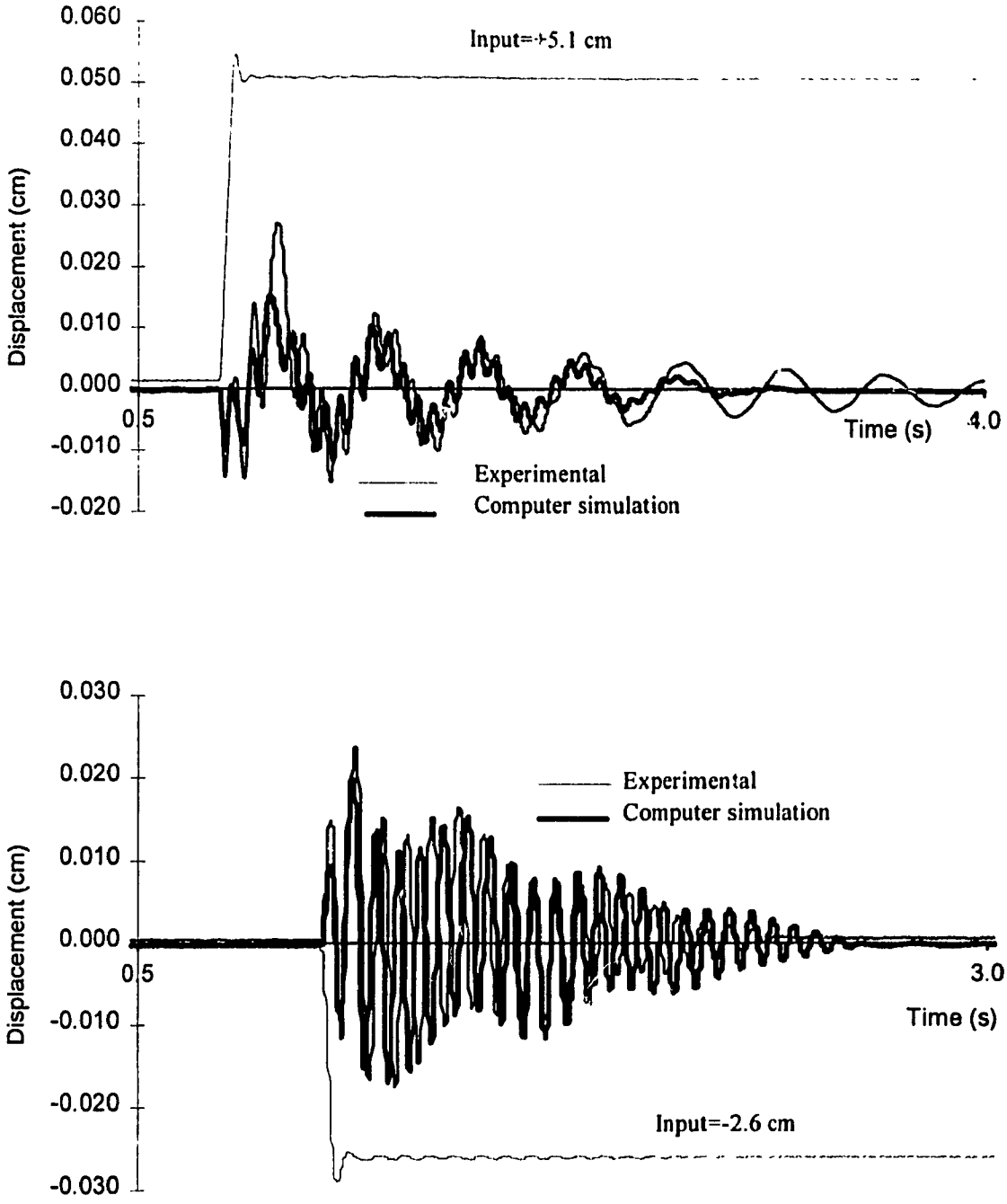

Figure 5.7 Comparison of the step response of the unsprung mass of the undamped quarter-car simulator model with the experimental response.

TABLE 5.3
COMPARISON OF ANALYTICAL AND EXPERIMENTAL NATURAL FREQUENCIES

Mode	Theoretical	Experimental	Percent Error
Bounce; Hz	2.41	2.4	0.4
Wheel Hop; Hz	14.10	13	7.8

listed in Table 5.3 yields damping ratios of 0.09 and 0.39, respectively, associated with bounce and wheel hop modes.

5.4.3 Frequency Response of the Undamped Simulator

The frequency response characteristics of the undamped two-DOF simulator model are compared with those established from the laboratory tests, to demonstrate the validity of the simulator and the wheel-hop models for different amplitudes of harmonic excitations, in the 1 to 20 Hz frequency range. The response is expressed in terms of rms (root mean squared) velocity transmissibility, peak velocity response, normalized tire force and average ride height.

The rms velocity transmissibility yields a comparison of the mean response behavior, while the response characteristics in compression and rebound are evaluated from the peak velocity curves. The normalized tire force provides an understanding of the wheel-hop behavior, which occurs quite frequently with undamped vehicle models. Although the tests were performed in 1 to 20 Hz frequency range, the experiments could not be performed in the vicinity of the resonant frequencies due to excessive oscillations of the undamped simulator. The operation in a band around the resonant frequencies resulted in excessive motion of the sprung and/or unsprung mass, and the width of this band increased with the increase in the amplitude of excitation. Similar behavior was also observed with the analytical results. Figure 5.8 illustrates the tire force response of

the simulator model, subject to 0.32 cm amplitude excitation at a frequency of 12 Hz in the vicinity of the wheel-hop frequency. The tire force reaches zero in most of the cycles due to wheel-hop motion, and the peak tire force approaches a magnitude as high as four times the static tire force.

The duration of loss of contact of the tire during one cycle is analyzed in terms of normalized wheel lift-off, expressed as the ratio of duration of loss of contact to the period of oscillation. Figure 5.8 illustrates the normalized wheel-lift off as a function of the excitation frequency derived from the analytical and experimental studies. The analytical and experimental results reveal total contact at frequencies up to 12 Hz, and 12.2 Hz, respectively, when subject to 0.32 cm peak displacement excitation. The laboratory experiments were not performed in the frequency range of 12.3 to 17.0 Hz, to ensure the safety of the experiment. The experimental results exhibit wheel lift in the 17 to 18.5 Hz frequency range, while the analytical model reveals wheel lift off only up to 18 Hz.

The rms velocity transmissibility and the peak velocity response characteristics of the sprung and unsprung masses are presented in Figure 5.9. The rms transmissibility response of the model exhibits good correlation with the experimental data except in the vicinity of the resonant frequencies. The analytical and experimental sprung mass responses exhibit lock-up to a frequencies around 2 Hz, where a distinct break-away occurs. The experiments were performed at excitation frequencies around the sprung mass resonant frequency, but not at the peak response in order to ensure the safety of the instrumentation and the apparatus, explaining why the peak response derived from the analytical model is observed to be considerably larger than the experimental data at the resonant frequency. The velocity ratio response of the unsprung mass correlates very well with the experimental results up to frequencies of 12.2 Hz, as shown in the Figure. While the tests were not performed in the wheel-hop frequency range (12.3 - 17 Hz), the model response in this frequency range resulted in excessive and inconsistent oscillatory

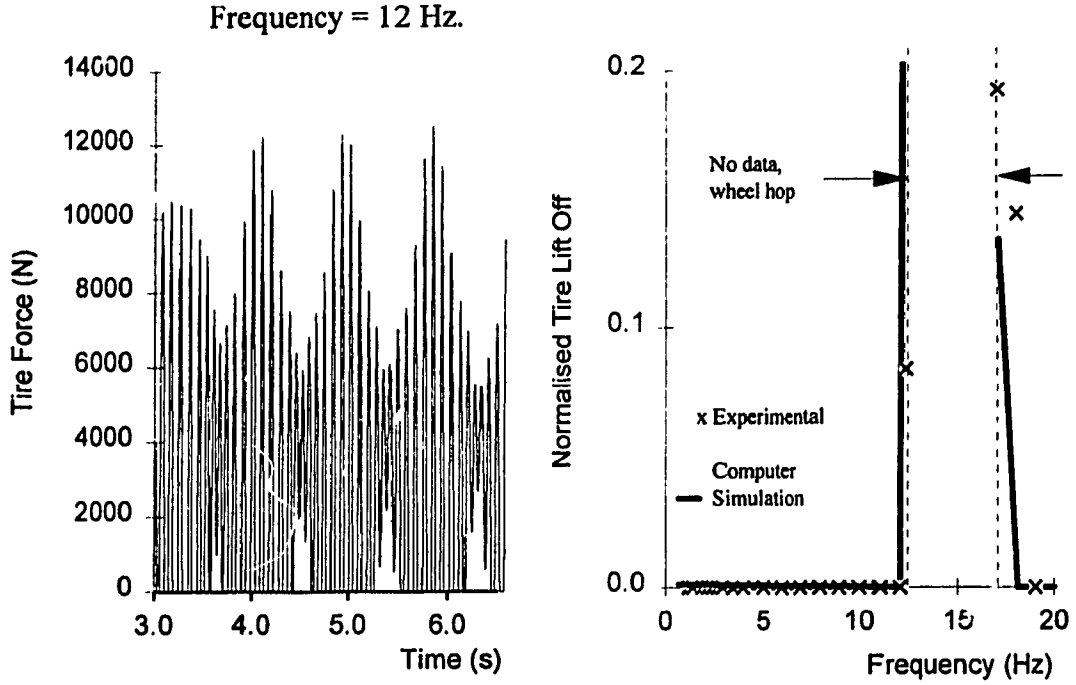

Figure 5.8 Tire force and normalized tire-lift-off response of the undamped quarter-car simulator subject to 0.32 cm peak displacement excitation.

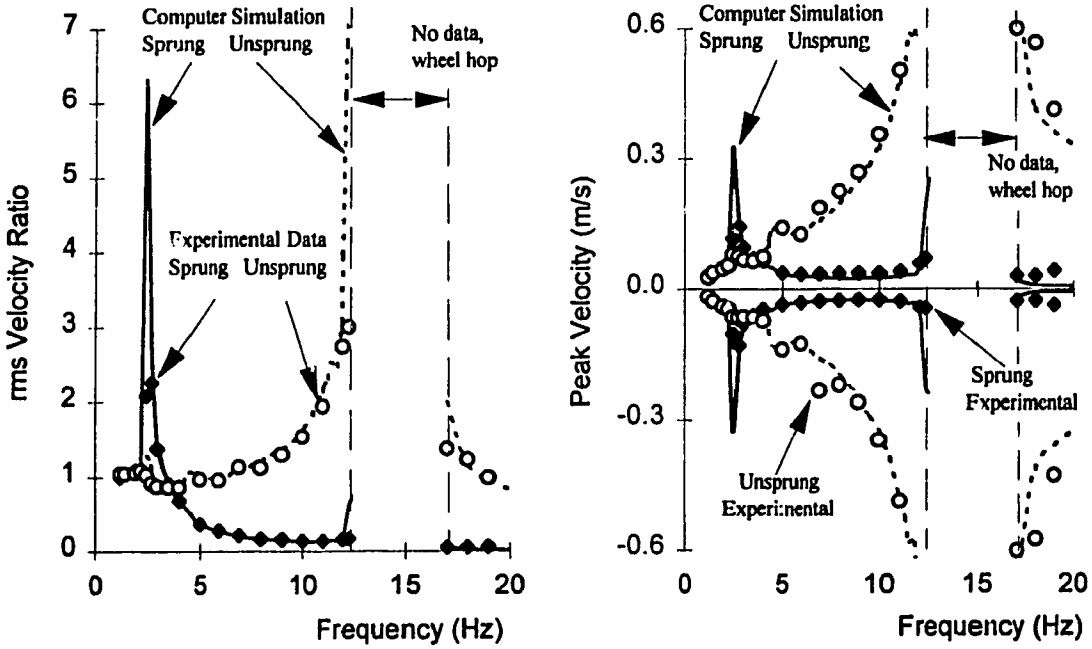

Figure 5.9 rms velocity transmissibility and peak velocity characteristics of the undamped quarter-car simulator subject to 0.32 cm peak displacement excitation.

response as illustrated in Figure 5.8. No attempts therefore were made to identify the response in this frequency range.

Figure 5.10 illustrates a comparison of analytical and experimental velocity response characteristics of the undamped simulator subject to 1.27 cm peak displacement excitation. The results are presented only up to excitation frequencies of 9.5 Hz, due to excessive wheel-hop encountered at higher frequencies. The quarter-car simulator also revealed excessive wheel-hop motion in the vicinity of sprung mass resonant frequency, as evident from the normalized tire lift-off shown in Figure 5.11. It was, therefore, not possible to acquire experimental data in the 2 to 3 Hz frequency range. The frequency response characteristics reveal considerable increase in the response with increase in the excitation amplitude, specifically in the vicinity of the resonant frequency. Furthermore, the breakaway is observed to occur at considerably lower frequencies, due to increased acceleration of excitation. A comparison of Figures 5.9 and 5.10 reveals that the unsprung mass is subject to considerably larger motion near the sprung mass frequency, when the amplitude of excitation is increased. This increase in the unsprung mass velocity is primarily attributed to wheel-hop motion in this frequency range, as shown in Figure 5.11. Figure 5.10 further reveals that the peak velocity response of the unsprung mass at the sprung resonant frequency is larger then that of the sprung mass, while the rms velocity ratio response of the unsprung mass is lower then that of the sprung mass. This response behavior of the simulator can be attributed to the system's strong nonlinearities.

5.5 SUMMARY

In this chapter, two quarter car simulator models are developed to study the damper performance under more realistic excitations. While one of the models is developed to characterize the quarter-car simulator test stand, the second model is derived to represent the race car vertical dynamics. The quarter car simulator model, incorporating sprung

and unsprung masses, coulomb friction, linear tire and suspension spring models, tire lift off and deflection limits is validated by the reasonable correlation between the analytical and experimental response characteristics. The friction due to guiding mechanisms was observed to be highly inconsistent, hence a compromise value was selected based on various laboratory measurements. The previously validated damper models are integrated within the validated quarter-car models to study the damper performance in the following chapter.

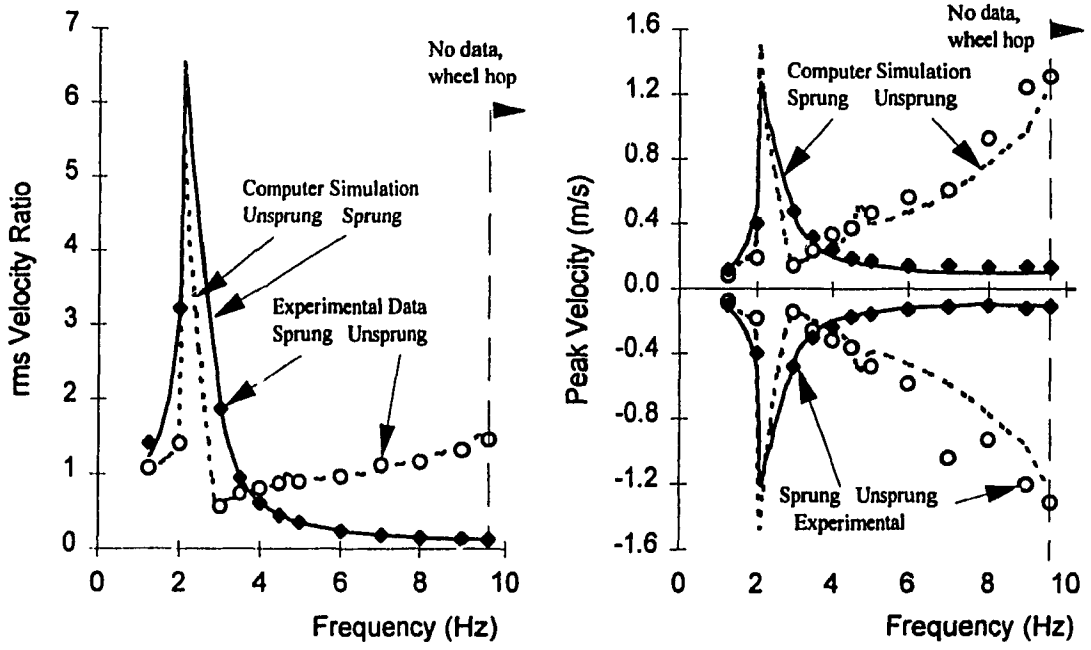

Figure 5.10 rms velocity transmissibility and peak velocity characteristics of the undamped quarter-car simulator subject to 1.27 cm peak displacement excitation.

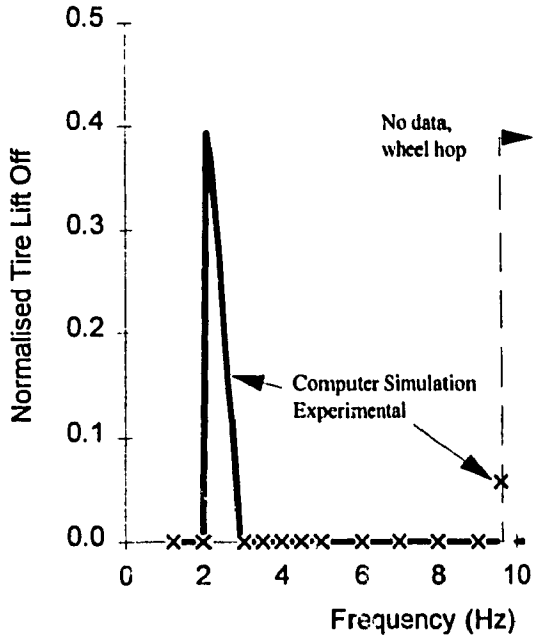

Figure 5.11 The normalized tire-lift-off response of the undamped quarter-car simulator subject to 1.27 cm peak displacement excitation.

CHAPTER 6

ANALYSIS OF CANDIDATE DAMPERS IN A QUARTER CAR CONFIGURATION

6.1 INTRODUCTION

The damping characteristics of the suspension play an important role in the handling performance of vehicles particularly for racing vehicles. While the experimental studies of dampers mounted on a conventional test stand provide a convenient and effective means to evaluate the damping characteristics, they do not evaluate the affect that the damper performance has, under realistic excitations, on the performance of the vehicle. As the ride, handling and road-holding ability of a vehicle are predominantly related to vertical motions encountered at different wheel and suspension assemblies, the performance characteristics of dampers can be conveniently evaluated through consideration of uncoupled quarter-car dynamics assuming negligible contributions due to variations in roll and pitch motions.

In this dissertation research, the comprehensive analytical models of the candidate dampers, developed in Chapter 3, are integrated within the quarter-car models described in Chapter 5, allowing further validation of the damper and quarter car models, under transient as well as harmonic excitations, and at different operating conditions. Typically the performance characteristics of the dampers are analyzed in terms of sprung mass acceleration, rattle space and dynamic tire deflection. The sprung mass acceleration yields a measure of the ride comfort, while the dynamic tire deflection is an indication of the road holding capability. The rattle space is the limits of the relative displacement between the sprung and unsprung masses and is limited by the design constraints. Although the sprung mass acceleration determines the ride and thus the fatigue reduced performance of the driver [ISO-2631], this measure is considered to be of secondary

importance for racing vehicles in comparison to the tractive forces developed at the tire-road interface.

The tractive effort generated by the tires of a race car is frequently classified into two categories of grip or traction: *(i)* mechanical grip, the traction available without aerodynamic downforce, which is a function of the normal load acting on the tire, the tires orientation relative to the track surface (effect of suspension geometry), tire and suspension properties and spring/damper tuning; and *(ii)* aerodynamic grip, the tractive force developed due to aerodynamic down force, which is a function of the ride height and aerodynamic lift force. The traction component due to mechanical grip is frequently quantified in terms of rms tire deflection [27,72,73], which does not indicate the occurrence or severity of tire lift-off. Fukushima et al. [74] utilized the tire ground contact rate (defined as the percent of time the wheel is in contact with the ground) and load fluctuation rate (rms value of tire load fluctuation normalized by the static load) to characterize the mechanical grip or the road-holding. In this study the minimum dynamic tire load is used as a performance indicator of road holding, since it describes the best performance the vehicle can provide under steady state conditions without driver corrections. Further, the minimum dynamic tire load of zero describes the loss of tire-road contact. To measure the performance during tire lift-off, a modified form of the tire-ground contact rate presented by Fukushima et al. [74] is evaluated.

The traction component related to aerodynamic grip increases with increase in vehicle speed, and is normally assumed to be negligible at low speeds. As an example of the possible contribution of aerodynamic downforce, to the normal load acting on the tires, it has been documented that the aerodynamic downforce can contribute 22 kN at a speed of 75 m/s for 1978 and 1979 Formula One race cars, which is 3 times the static weight of the car [75]. Where permitted by racing organizations, the most significant contributor to downforce is the flow of air under the race car and the pressure difference developed along the vertical axis. The pressure drop under the car yields a downforce

acting on the tire which is commonly referred to as the "ground effects". At a constant angle of pitch, the magnitude of downforce increases as the distance between the undersurface of the race car and the ground is decreased until the underbody air flow diminishes. In practice the race vehicles are also designed to achieve minimal ground clearance or ride height between the undersurface and the road surface in order to achieve a lower height of the center of gravity and thus reduced roll and dynamic load transfer. The suspension performance is thus evaluated in terms of the ride height (distance between the ground and a reference point on the undersurface of the sprung mass). The change in the ride height, due to dynamic inputs and suspension performance, affects the aerodynamic grip in a considerable manner due to variations in the venturi effect.

6.2 VALIDATION OF THE QUARTER-CAR MODEL

Equations (3.1) to (3.63), developed to describe the damper forces, were combined with the quarter-car simulator model, equations (5.1) to (5.16), to derive the total quarter-car model. The nonlinear coupled differential equations of motion of the two-DOF system was solved using a numerical integration technique based upon Hammings modified predictor-corrector method. The response characteristics of the three candidate dampers in a quarter-car configuration were evaluated for step displacement excitations of different amplitudes, and sinusoidal excitations in the 1 to 20 Hz frequency range. The analytical results were compared with those established from the experimental studies performed in the laboratory. The transient response characteristics of the quarter-car model was evaluated in terms of the damper force, and the relative displacement between the input and the sprung and unsprung masses. The steady-state response characteristics are presented in terms of rms velocity ratio and peak velocities of the sprung and unsprung masses, the average ride height, minimum tire load and the normalized tire lift-off.

6.2.1 Validation Under Step Excitations

The analytical model of the quarter-car comprising the models of three candidate dampers is evaluated for step excitations of 2.5 cm and 5.1 cm displacements amplitudes. The response characteristics of the sprung and unsprung masses of the simulator with each damper model are compared with the experimental results to demonstrate the validity of the total model.

Quarter-Car Simulator With Koni Damper

The relative displacement response characteristics of the sprung and unsprung masses of the simulator model including the Koni damper, subject to 5.1 cm step displacement excitations, show excellent correlation with the corresponding results derived from the experimental study in Figure 6.1. The relative motion of both the masses, with respect to the excitation, tends to decay in approximately 0.45s. The experimental relative displacement response of the sprung mass, does not return to its initial static equilibrium position, which may be attributed to the friction of the guiding mechanism. A further application of the step excitation at a later instance results in settling of the sprung mass near its static equilibrium, as shown in Figure 6.2. The results demonstrate the lock-up due to friction and possible variations in magnitude of friction along the guides. It should be noted that the relative displacement response of the sprung mass, with respect to the unsprung mass, forms the excitation for the damper. As shown in Figure 6.3 the damper force from the analytical quarter-car simulator model correlates very well with the experimentally measured force with only slight errors in the peak force, and the force near the zero-crossing. The errors near the zero crossing are attributed to the backlash in the bearings, which is evident from the rapid change in the damper force (from 0 to approximately 50 N) at t = 0.24 s.

The influence of asymmetric properties of the damper on the quarter-car model response are demonstrated by the results attained under positive and negative step

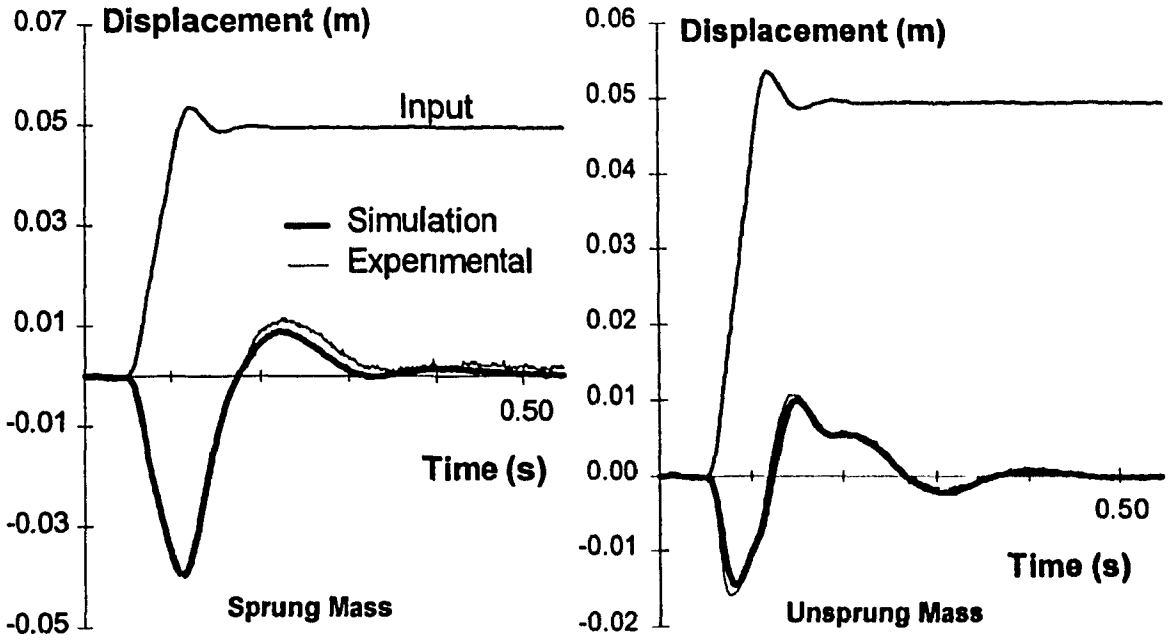

Figure 6.1 Analytical and experimental relative displacement response of the sprung and unsprung masses of the quarter-car simulator (Damper: Koni; Excitation: +5.1 cm step).

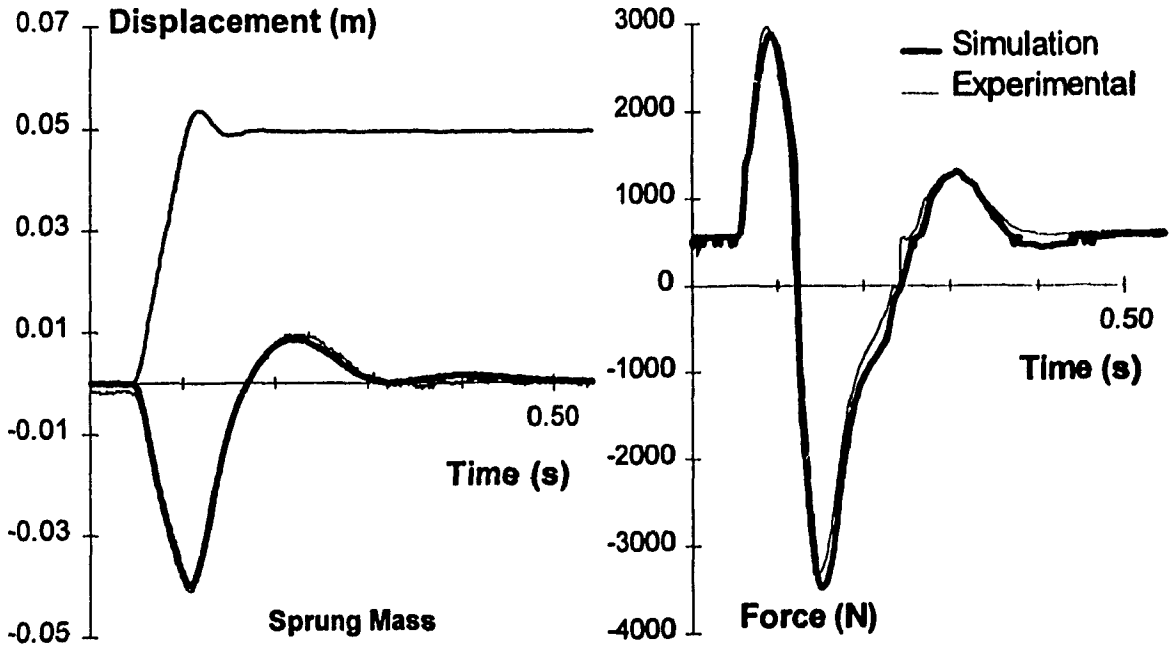

Figure 6.2 Analytical and experimental response of the sprung mass of the quarter-car simulator, at a latter time (Damper: Koni: Excitation: +5.1 cm step).

Figure 6.3 Analytical and experimental damper force of the quarter-car simulator (Damper: Koni: Excitation: +5.1 cm step).

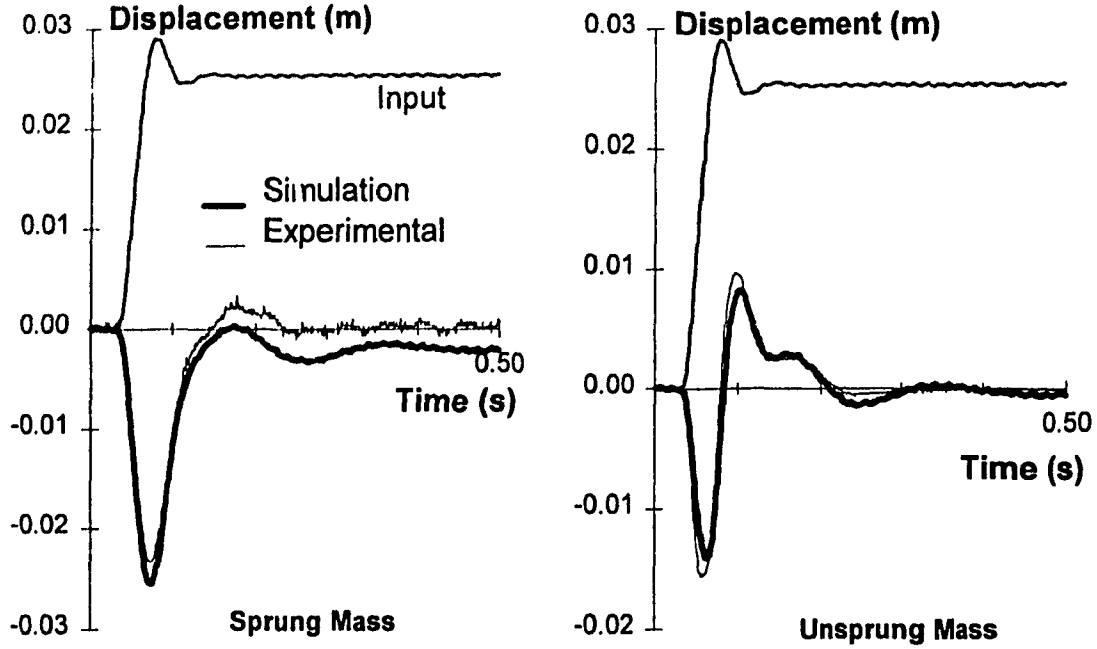

Excitation: + 2.5 cm step.

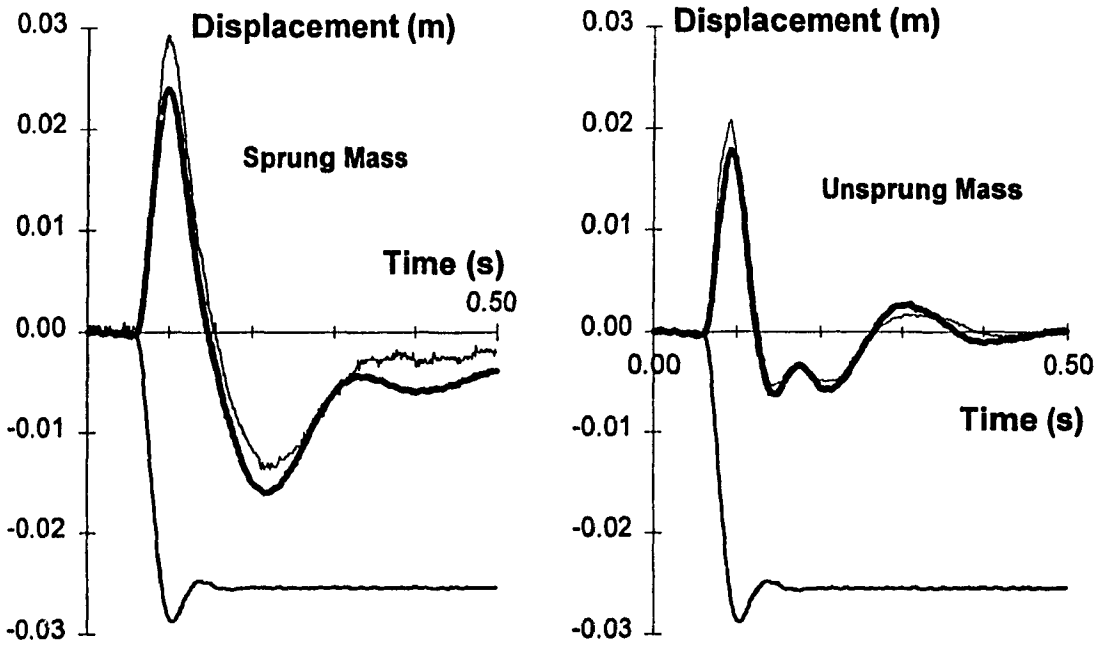

Excitation: - 2.5 cm step.

Figure 6.4 Comparison of relative displacement response characteristics of the sprung and unsprung masses of the simulator subject to positive and negative step displacement excitation (Damper: Koni).

excitations of 2.5 cm displacement. The analytical response characteristics of the sprung and unsprung masses are compared with the experimental data as shown in Figure 6.4. A comparison of the response characteristics attained under +2.5 and -2.5 cm step displacement excitations clearly demonstrates the influence of asymmetric damping properties in compression and rebound. Both the sprung and unsprung masses exhibit considerably faster decay in response under positive excitation, which is contrary to the response behavior of the undamped simulator presented in Figures 5.6 and 5.7. Application of a negative step input results in sudden change in position of the masses, and the potential energy is converted into kinetic energy resulting in relatively larger overshoot in the sprung mass response. The response of the unsprung mass, which is substantially lighter and is supported on stiff tire springs, exhibits considerably less overshoot for the negative step than that observed under a positive step excitation due to higher damping and resultant tire lift-off. The high rebound damping tends to impede the transfer of potential energy of the suspension spring into kinetic energy resulting in tire lift off during the time interval of 0.07 to 0.107 s. The sprung and unsprung masses move out-of-phase during this interval, in which the velocity of the unsprung mass increased at a faster rate than that of the sprung mass. Upon regaining contact with the base, the kinetic energy of the unsprung and sprung masses approach peak values at t = 0.145 and t = 0.215, respectively, and is transferred into the tire spring. Since the sprung mass attains peak kinetic energy at a considerable delay relative to the unsprung mass, the tire spring experiences relatively less deflection. In case of a positive step excitation, this time delay is considerably smaller (maximum kinetic energy transfer occurring at 0.07 seconds for the sprung mass and at 0.06 seconds for the unsprung mass), resulting in increased energy transfer to the tire spring. The results presented in Figure 6.4, in general, exhibit good correlation between the analytical and experimental relative displacement response of the sprung and unsprung masses. The peak analytical response, however, is smaller than the measured response under -2.5 cm step input and slightly larger under +2.5 cm step input.

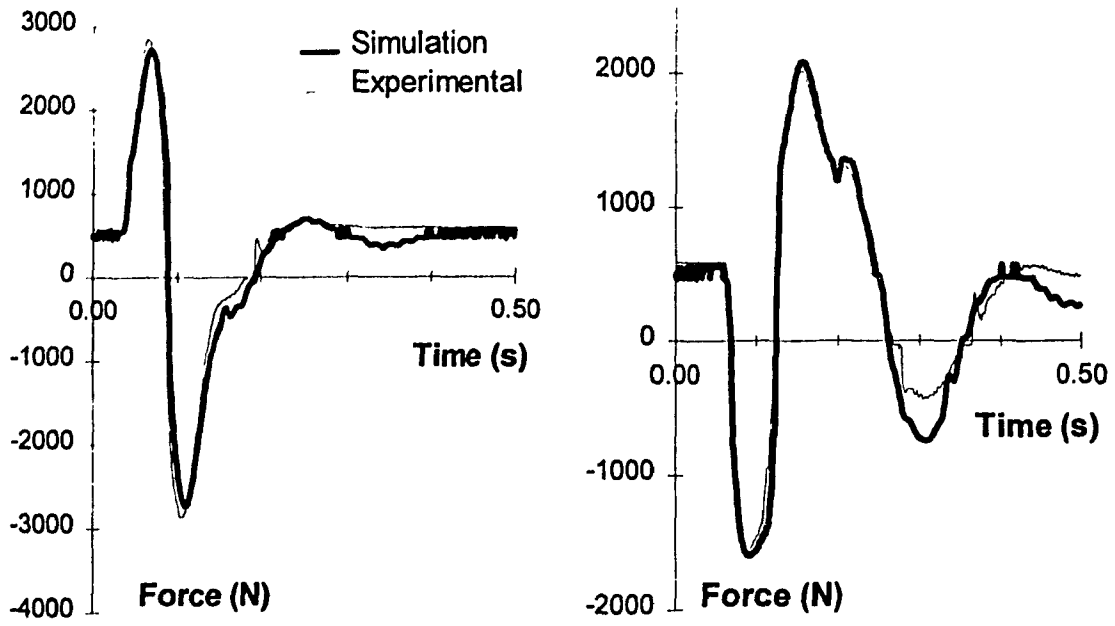

Figure 6.5 Comparison of analytical and experimental damper force of the quarter-car simulator subject to positive and negative step displacement excitation (Damper: Koni).

The settling times of the sprung mass of the simulator subject to +2.5 and -2.5 cm step displacement excitation are considerably different due to the asymmetric damping in compression and rebound. The damper force time-histories developed under the two step inputs is illustrated in Figure 6.5, for both the computed and the measured damper forces. Under the application of a +2.5 cm step displacement the damper is subject to compression, which is followed by extension, while this sequence is reversed under application of a -2.5 cm step input. During the initial compression stroke, when subject to the +2.5 step displacement, the suspension spring stores considerably more energy than the tire spring, due to relatively light resistance (damping and spring) to motion of the suspension, when compared to that of the tire. The energy stored in the suspension spring is rapidly dissipated during the extension stroke, due to high rebound damping resulting in rapid decay of the system response. Under the application of a -2.5 cm step displacement, the heavy damping in extension results in relatively higher increase of

energy in the tire spring than in the suspension during the first part of the response. The higher energy stored in the tire spring must be transferred to the suspension spring and damper, resulting in increased oscillations in the sprung mass response.

Quarter-Car Simulator With Mechformance Damper

The relative damping properties of the three candidate dampers are examined in order to enhance an understanding of their affect on the response characteristics of the quarter-car simulator. The damping forces in compression and rebound are evaluated corresponding to a velocity of 0.3 m/s realized by 1.27 cm displacement harmonic excitation at a frequency of 4 Hz. The rebound and compression damping forces, together with the ratio of rebound to compression damping forces evaluated from the conventional test stand described in Chapter 2, are summarized in Table 6.1. The mean damping coefficients of each damper is also evaluated as the ratio of mean damper force to velocity. The results summarized in the table reveal highest values of mean damping coefficient for the Mechformance damper, with considerable larger rebound damping force then the other units.

The relative displacement response characteristics of the sprung and unsprung masses of the simulator model comprising the Mechformance damper are evaluated for

TABLE 6.1
DAMPING FORCES AND MEAN DAMPING COEFFICIENTS
OF THE TEST DAMPERS (velocity = 0.3 m/s)

	Damping Force (kN)		Rebound force/	Mean Damping
	Compression	Rebound	Compression force	Coefficient (kNs/m)
Koni	1.20	2.20	1.83:1	5.7
Mechformance	1.43	5.56	3.90:1	11.6
Fox (heavy damping)	0.60	3.72	6.23:1	7.2
Fox (light damping)	0.49	1.71	3.46:1	3.7

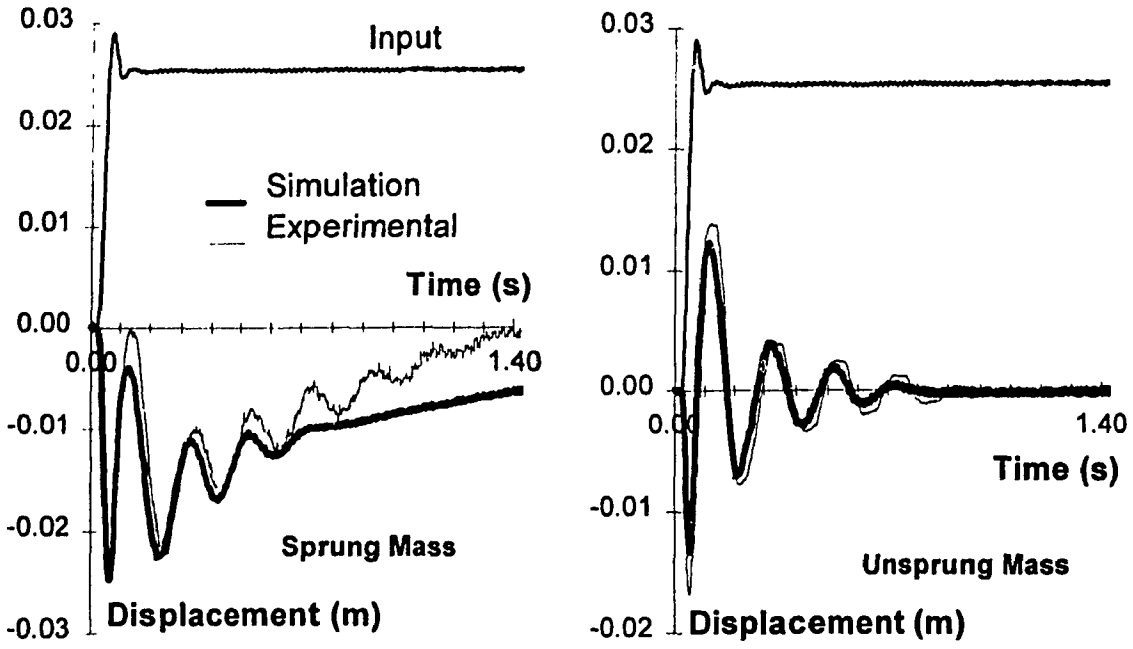

Figure 6.6 Comparison of analytical and experimental relative displacement response of the sprung and unsprung masses of the quarter-car simulator subject to +2.5 step displacement excitation (Damper: Mechformance).

+2.5 cm step displacement excitations. The response characteristics are compared to those derived from the experimental data, as shown in Figure 6.6.

A comparison of Figures 6.1 and 6.6 reveals considerably different response of the masses with the Koni and Mechformance dampers. The response of the quarter-car model with the Koni damper decays considerably faster when compared to that with the Mechformance damper, due to the latter's high damping. The compression and rebound damping forces of the Mechformance damper are respectively, 19% and 150% greater than those of the Koni damper. The highly asymmetric Mechformance damper yields high relative deflections of the sprung and unsprung masses in compression, as evident from Figure 6.7. The potential energy stored in the suspension spring during the compression stroke is dissipated during extension in an overdamped manner. Such suspension response behavior is commonly referred to as "packing or jacking down", which is further evidenced in the frequency response of the system presented in later

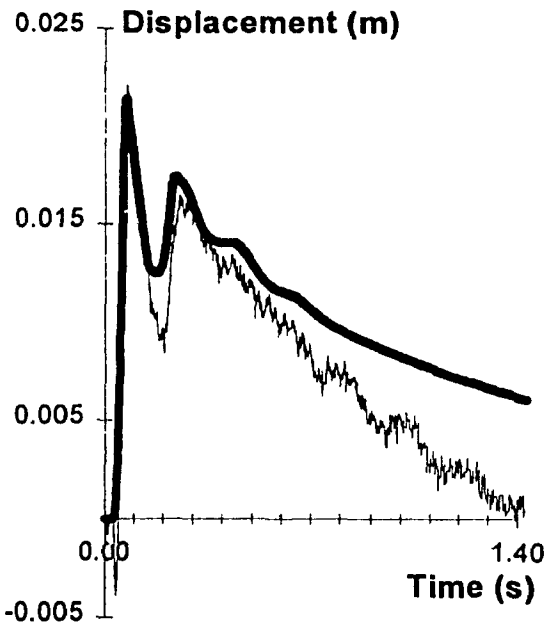

Figure 6.7 Comparison of analytical and experimental relative damper displacement response of the quarter-car (Damper: Mechformance; Excitation: +2.5 cm step).

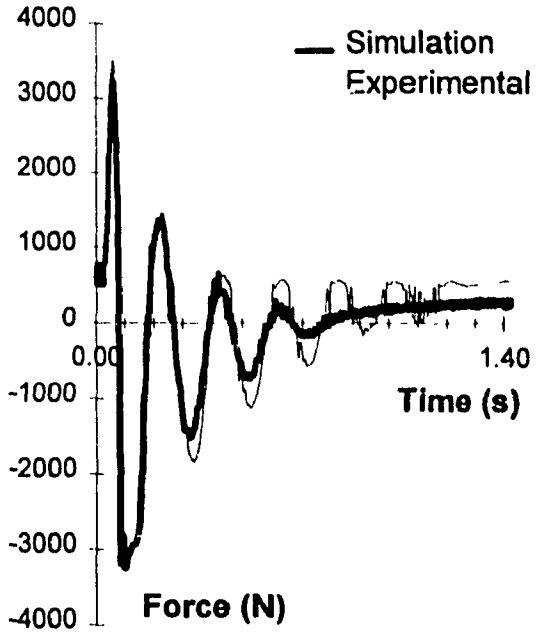

Figure 6.8 Comparison of analytical and experimental damper force response of the quarter-car simulator (Damper: Mechformance; Excitation: +2.5 cm step).

sections of this Chapter. The high damping properties (approximately 2 times greater than that for the Koni) also yield increased oscillations of the tire, since the kinetic energy of the system is not effectively dissipated. The frequencies of oscillation of the sprung and unsprung masses are observed as 5 and 5.3 Hz respectively, which approach the natural frequency, 5.46 Hz, of a single-DOF system, with mass equal to the combined sprung and unsprung mass, and spring stiffness equal to that of the tire.

The results presented in Figure 6.6 demonstrate reasonably good correlation between the analytical and experimental response characteristics of quarter-car simulator equipped with Mechformance damper. The analytical displacement response characteristics of the sprung and unsprung masses, however, exhibit slightly rapid decay of oscillations than observed with the experimental data. The measured response of the sprung mass also tends to approach the static equilibrium at a faster rate. These discrepancies between the analytical and experimental response characteristics indicate

relatively higher damping of the model. The damper force time-history derived from the analytical model is further compared with the measured force, as shown in Figure 6.8, to demonstrate the validity of the analytical model. The damper response, derived from the analytical model, decays at a faster rate than that observed with the measured force. The analytical and experimental damper forces, however, correlate very well during the first two oscillations. The measured force exhibits rapid variations in the damper force of approximately 250-300 N magnitude. The magnitude of rapid reversal of damper force is close to the magnitude of friction force indicating the presence of stick-slip phenomena, which was not incorporated within the analytical model.

Quarter-Car Simulator With Fox Damper

The relative displacement response characteristics of the sprung and unsprung masses of the two-DOF simulator, equipped with Fox damper, are evaluated under +2.5 cm step displacement excitation. The response characteristics are evaluated for both the light and heavy damping settings, and are compared with those established from the laboratory tests, as shown in Figure 6.9. It should be noted that the Fox damper with the light setting yields rebound damping 3.46 times the compression damping, which is similar to that for the Mechformance damper, although its overall damping is the lowest among all the dampers. The heavy damping setting yields considerably higher rebound to compression damping force ratio of 6.23, while the mean damping value lies between those for the Koni and Mechformance dampers, as summarized in Table 6.1. The relative displacement response of the quarter-car simulator with Fox heavy damper is thus quite similar to that observed with the Mechformance damper. The relative displacement response of the simulator masses with Fox damper, however, decay at a faster rate as shown in Figure 6.9. Although the analytical and experimental sprung mass characteristics exhibit identical trends and similar rate of decay, the model response is considerable larger than the experimental response. The error between the analytical and

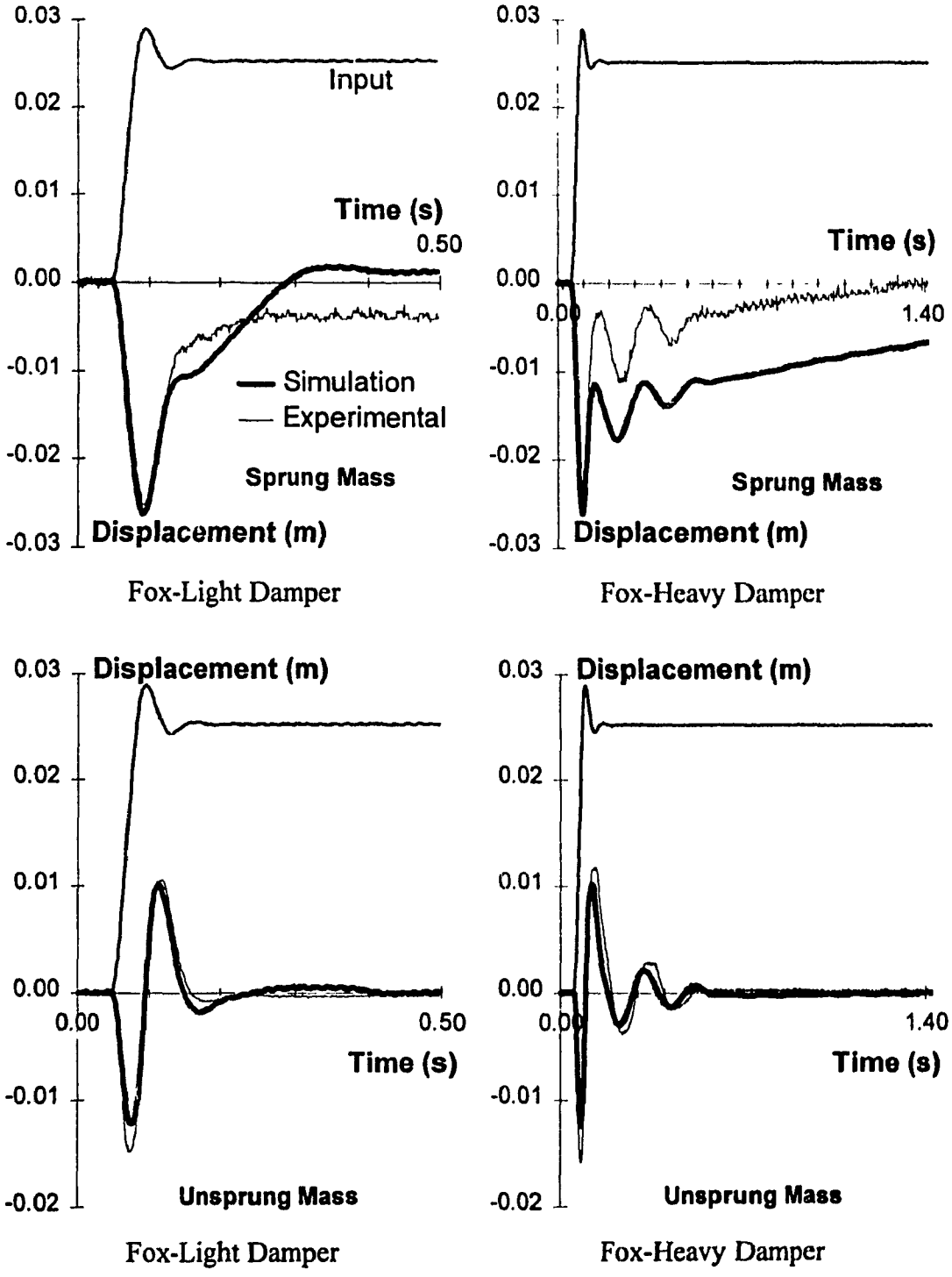

Figure 6.9 Comparison of analytical and experimental relative displacement response of the quarter-car simulator (damper Fox; Excitation: +2.5 cm step).

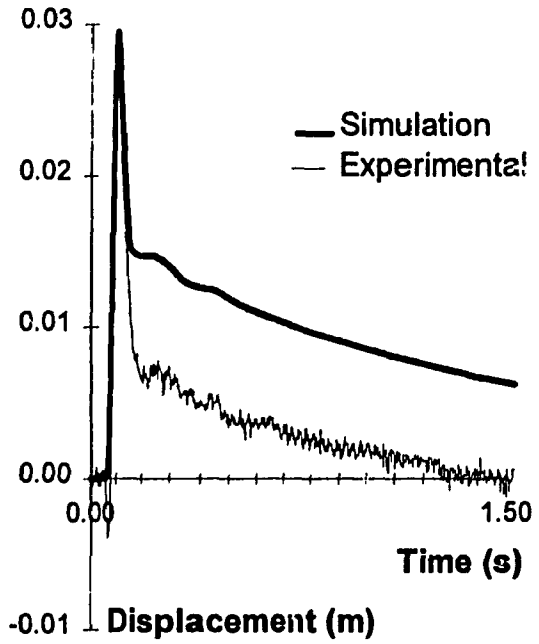

Figure 6.10 Comparison of analytical and experimental relative damper displacement response of the quarter-car (Damper: Fox-Heavy; Excitation: +2.5 cm step).

experimental displacements remains nearly constant throughout the simulation period after the initial oscillation.

For the Fox with heavy damping, the experimental relative displacement response, of the sprung mass with respect to the unsprung mass, as presented in Figure 6.10, shows that the damper tends to extend by nearly 4 mm, immediately after application of the step displacement, which may be attributed to the variations in breakaway friction or the slip-stick mechanism. The error between the analytical and experimental displacement response of the sprung mass is attributed to these factors. The sprung mass displacement response of the model with light damping compares well with the experimental data. The unsprung mass displacement response characteristics of the model with the light and heavy dampers also correlate very well with the experimental data, as shown in Figure 6.9.

Although the Fox-light damper yields damping properties, that are lower then those of the Mechformance or Koni dampers in both compression and rebound, its ratio of rebound to compression damping is significantly higher then that of the Koni damper and is similar to that of the Mechformance. The displacement response of the sprung mass of the simulator with Fox damper thus exhibits overdamped behavior during extension.

6.2.2 Summary of Step Response of the Quarter-Car Models

The step response characteristics of the quarter-car simulator with different candidate dampers are evaluated for different magnitudes of positive and negative displacement excitation. The response characteristics are analyzed in terms of percent overshoot, defined as the ratio of the peak displacement magnitude to the magnitude of the steady state displacement response and settling time, defined as the time required for the response to approach 90 % of its steady state value. Table 6.2 summarizes the comparison of analytical and experimental response behavior of the quarter-car simulator, equipped with the Koni damper. An excellent correlation is observed between the analytical and experimental results in terms of % overshoot and settling time. The response characteristics of the sprung and unsprung masses exhibit peak errors of 8.5% and 6%, respectively, in overshoot and 6.7% and 5% in the settling time. The results further show that the settling time, in general, increases with the magnitude of positive step excitation. The sprung mass response, specifically, exhibits considerable increase in settling time when the step displacement is increased from 2.5 to 5.1 cm. The damping associated with the sprung mass mode of vibration thus decreases at a faster rate with increase in excitation amplitude, when compared to that associated with the unsprung mode.

An examination of results obtained for +2.5 and -2.5 step displacement excitation reveals that % overshoot and the settling time of the sprung mass response are considerably larger under negative excitation. The percent overshoot of the unsprung

TABLE 6.2
COMPARISON OF OVERSHOOT AND SETTLING TIME OF THE ANALYTICAL AND EXPERIMENTAL RESPONSE OF QUARTER CAR SIMULATOR WITH KONI DAMPER

Step Excitation (cm)	% Overshoot			Settling Time (s)		
	Experimental	Analytical	% Error	Experimental	Analytical	% Error
Sprung Mass						
+5	23	17	4.4	0.218	0.214	1.8
+5	19	17	2.0	0.225	0.210	6.7
+2.5	9	1	8.5	0.085	0.088	3.5
-2.5	52	63	7.7	0.241	0.227	5.8
Unsprung Mass						
+5	23	20	2.8	0.171	0.171	0.0
+5	23	20	2.8	0.176	0.176	0.0
+2.5	41	33	6.0	0.087	0.089	2.3
-2.5	20	24	3.3	0.179	0.188	5.0

mass, however, decreases when negative step displacement is applied. The increase in settling time and overshoot of the sprung mass response under -2.5 step excitation is attributed to high rebound damping. The unsprung mass response exhibits lower overshoot and higher settling time under negative excitation, which is attributed to higher rebound damping and tire lift-off.

The percent overshoot and settling time of the response characteristics of the simulator with different candidate dampers are summarized in Table 6.3. The following relative performance observations can be made from the results presented in the Table.

- The displacement response for the unsprung mass exhibits higher overshoot than that of the sprung mass for all the dampers.

TABLE 6.3
COMPARISON OF OVERSHOOT AND SETTLING TIME OF THE ANALYTICAL AND EXPERIMENTAL DISPLACEMENT RESPONSE OF THE QUARTER CAR SIMULATOR (+2.5 cm Step)

Candidate Damper	Settling Time (s) Experimental	Analytical	% Error	% Overshoot Experimental	Analytical	% Error
Sprung Mass						
Koni	0.085	0.088	3.5	9	1	8.5
Mechformance	1.05	1.86	77.1	0	0	0.0
Fox-heavy	0.63	1.95	209	0	0	0.0
Fox-light	0.145	0.219	50.9	0	2.2	24.3
Unsprung Mass						
Koni	0.087	0.089	2.3	41	33	6.0
Mechformance	0.51	0.42	17.6	70	63	4.4
Fox-heavy	0.31	0.26	16.1	46	41	3.1
Fox-light	0.087	0.093	6.9	46	48	2.1

- The displacement response of the sprung and unsprung masses with the Koni damper reveals rapid decay, while the unsprung mass response exhibits larger overshoot.
- The Fox damper with light settling yields a slightly overdamped sprung mass response, while the unsprung mass response is very similar to that with the Koni. The sprung mass response with the stiff dampers (Fox with high setting and Mechformance) reveals overdamped system response, with long settling time and no overshoot, while the unsprung mass response is that of a lightly damped system, with increased settling time.

The results summarized in Table 6.3 reveal good correlation between the analytical and experimental values of peak overshoot, with the exception of the sprung mass

response with the Fox damper at light settings, which is attributed to the friction and stick-slip mechanism. The settling time of the unsprung mass response derived from the analytical and experimental studies also exhibit good agreement with all dampers, as shown in the table. The analytical model, however, yields considerably larger settling time for the sprung mass response of the system with Fox and Mechformance dampers, when compared to those derived from test data. This larger settling time is mostly attributed to the friction forces. With the exception of errors caused by complexities associated with modeling of friction components, the results presented in Figures 6.1 to 6.10 and Tables 6.2 and 6.3 exhibit very good correlation between the analytical and experimental results.

6.2.3 Frequency Response Characteristic of the Quarter-Car Simulator Model

The nonlinear quarter-car model comprising nonlinear models of the candidate damper is further validated by comparing its frequency response characteristics with those established from laboratory tests. The frequency responses of the quarter-car simulator are evaluated analytically and experimentally for constant displacement amplitude, 0.32 and 1.27 cm, harmonic excitations in the 1.25 to 20 Hz frequency range. The frequency response behavior is expressed in terms of average ride height, the rms velocity transmissibility and peak velocity of the sprung and unsprung masses, and the normalized tire lift-off duration. The response characteristics of the simulator model with different candidate dampers are described below.

6.2.3.1 Frequency Response Characteristics of the Quarter-Car Simulator with Monotube Damper Design (Koni)

Figures 6.11 and 6.12 illustrate the comparison of analytical and experimental rms velocity ratio and peak velocity response characteristics of the simulator masses subject to 0.32 and 1.27 cm peak displacement excitations, respectively. The analytical and

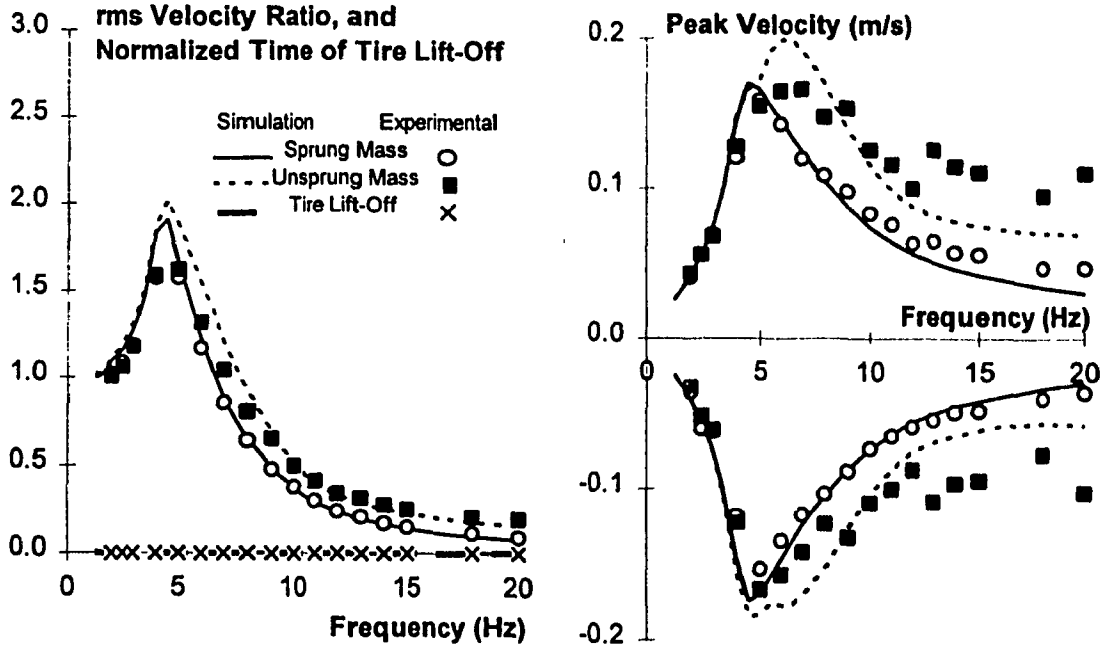

Figure 6.11 Comparison of analytical and experimental response characteristics of the quarter-car simulator (Damper: Koni; Excitation amplitude: 0.32 cm).

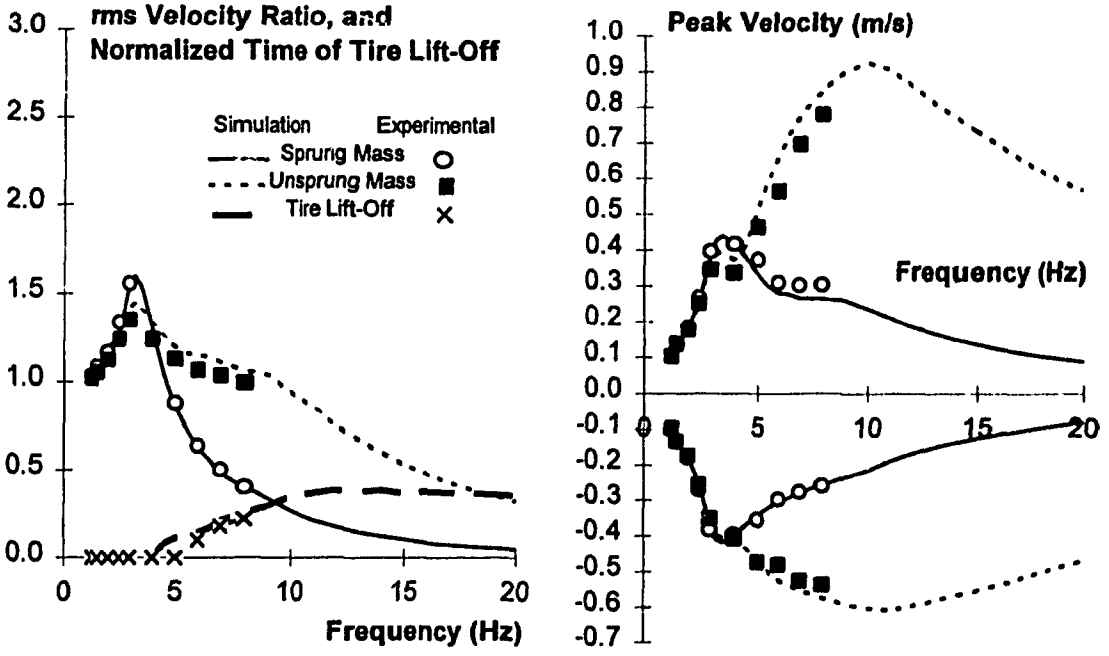

Figure 6.12 Comparison of analytical and experimental response characteristics of the quarter-car simulator (Damper: Koni; Excitation amplitude: 1.27 cm).

experimental studies reveal wheel-hop motion only under 1.27 cm peak displacement excitation, which is also presented in Figure 6.12 in terms of normalized tire lift-off. The results exhibit reasonable correlation between analytical and experimental velocity ratio response in the entire frequency range under 0.32 cm excitation. The analytical velocity ratio and normalized tire lift-off response also agrees well with the measured data up to 8 Hz, above which the tests were not performed due to excessive wheel-hop motion. The analytical results show that tire lift-off approaches a value of 40% at approximately 10 Hz, and remains relatively constant through the higher frequency range. The analytical peak velocity response of the sprung mass correlates well within the experimental data, irrespective of the excitation frequency. The peak velocity response of the unsprung mass exhibits errors in the vicinity of resonant frequencies. The peak velocity response characteristics of the sprung and unsprung masses are observed to be nearly symmetric in compression and rebound.

The rms velocity ratio response of the sprung mass peaks at 3.25 Hz, slightly higher then it's natural resonant frequency of 2.25 Hz. The unsprung mass response also peaks at the same frequency as the sprung mass, under both amplitudes of excitation. The peak velocity and rms velocity response of the unsprung mass reveals high magnitude at higher frequencies due to wheel-hop motion under 1.27 cm excitation. The measured peak velocity response of the unsprung mass also exhibits peak magnitude near the unsprung mass resonance under 0.32 cm excitation. The analytical response, however, does not exhibit this peak, which may be attributed to slight tire spring-hop in the experimental simulator.

The average ride-height frequency response of the quarter-car simulator with the Koni damper is illustrated in Figure 6.13. The results show that the average ride height tends to vary with frequency and excitation amplitude. The magnitude of variation in average ride height increases with increasing frequency up to a peak value, after which it decreases with further increase in the excitation frequency. The frequency at which this

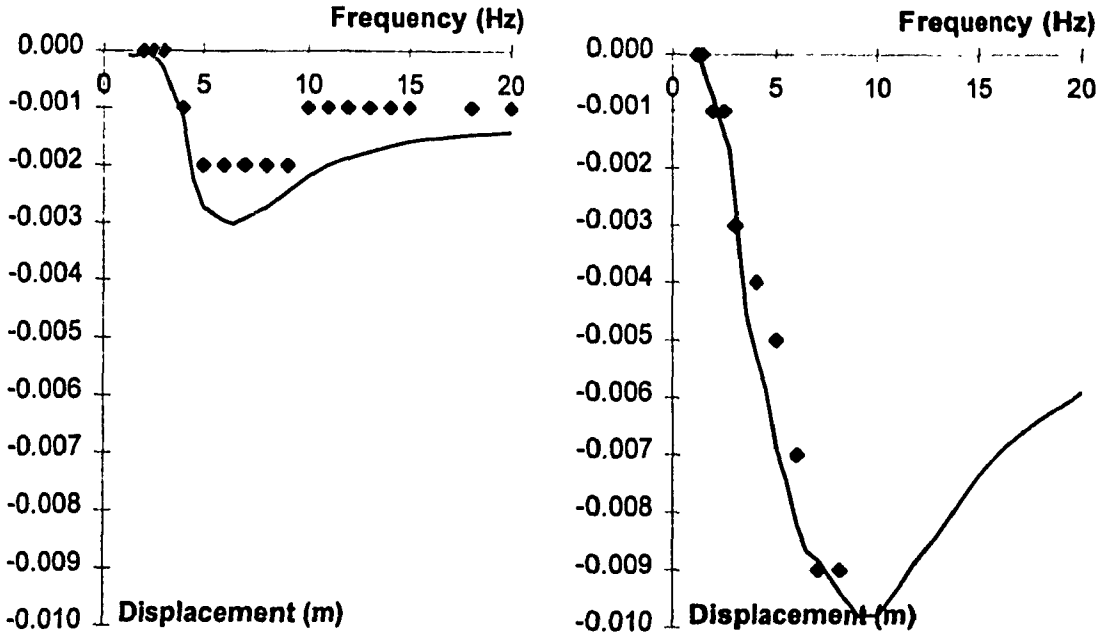

Excitation Amplitude: 0.32 cm

Excitation Amplitude: 1.27 cm

Figure 6.13 Comparison of analytical and experimental average ride height response characteristics of the quarter-car simulator (Damper: Koni).

peak value occurs also increases with increase in the amplitude of excitation. While the analytical results correlate very well with the experimental data under 1.27 cm excitation at frequencies below the wheel-hop frequencies, the correlation is slightly poorer for 0.32 excitation, due in part to experimental measurement resolution. The ride height also increases with increase in the excitation amplitude and the damping ratio, resulting in reduced ground clearance of the sprung mass, up to frequencies of 6 and 10 Hz under 0.32 cm and 1.27 cm excitation, respectively. Although the variations in ride height diminish at higher excitation frequencies, the sprung mass does not return to the static ride height.

6.2.3.2 Frequency Response Characteristics of the Quarter-Car Simulator with Remote Reservoir Dampers

Mechformance Damper

Figures 6.14 to 6.16 illustrate the rms velocity ratio, the peak velocity, normalized time of tire lift-off, and average ride height response of the quarter-car simulator model as a function of excitation frequency and amplitude. The analytical results are compared to those derived from the laboratory test data to demonstrate the validity of the model. The quarter-car simulator revealed excessive wheel-hop motion at considerably lower frequencies (near 3.2 Hz), when compared to the Koni, when subject to 1.27 cm displacement excitation, as shown in Figure 6.15. The laboratory tests were, therefore, not performed at excitation frequencies greater than 3 Hz. The results show very good correlation between the analytical and available experimental data for both excitation amplitudes. The change in average ride height increases with excitation frequency up to 6 Hz and tends to reduce with further increase in the excitation frequency, as observed

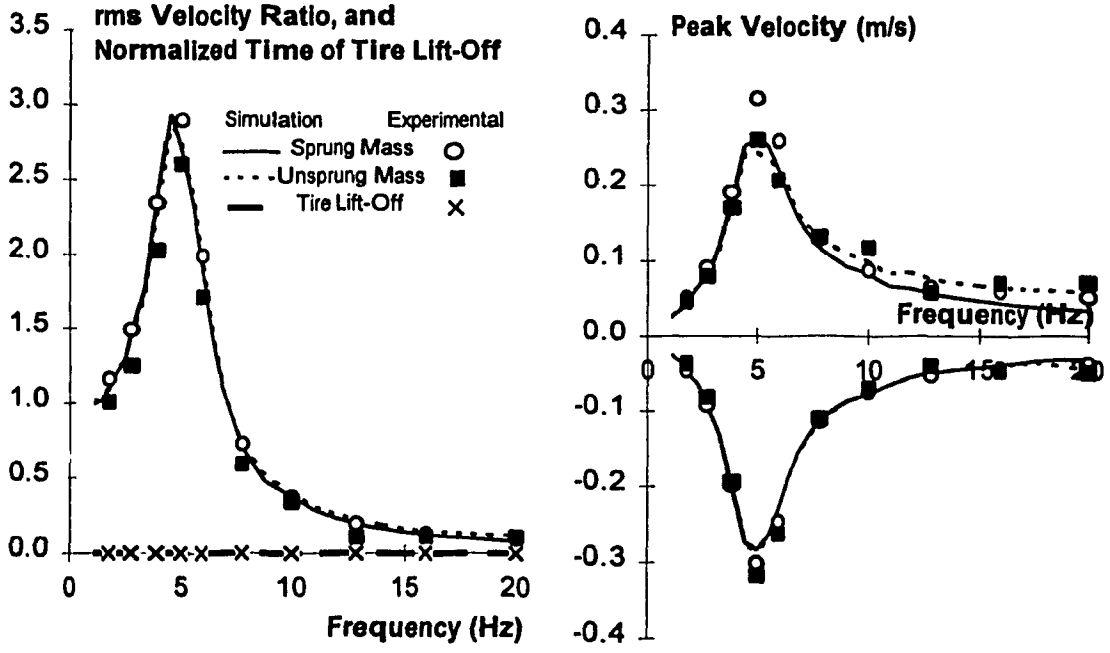

Figure 6.14 Comparison of analytical and experimental response characteristics of the quarter-car simulator (Damper: Mechformance; Excitation amplitude: 0.32 cm).

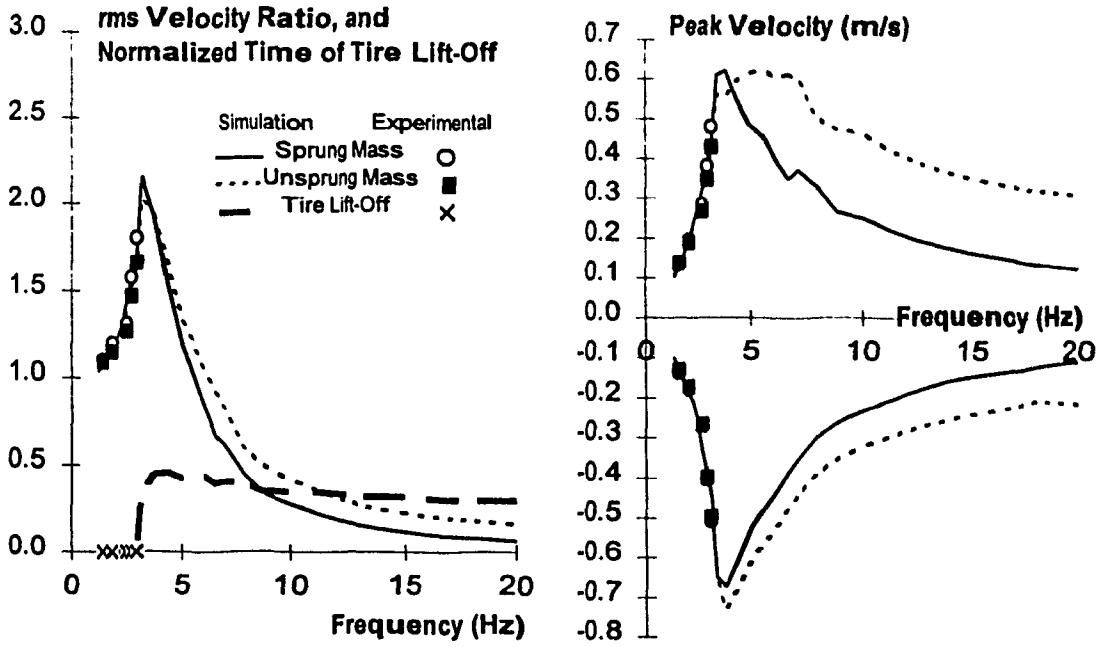

Figure 6.15 Comparison of analytical and experimental response characteristics of the quarter-car simulator (Damper: Mechformance; Excitation amplitude: 1.27 cm).

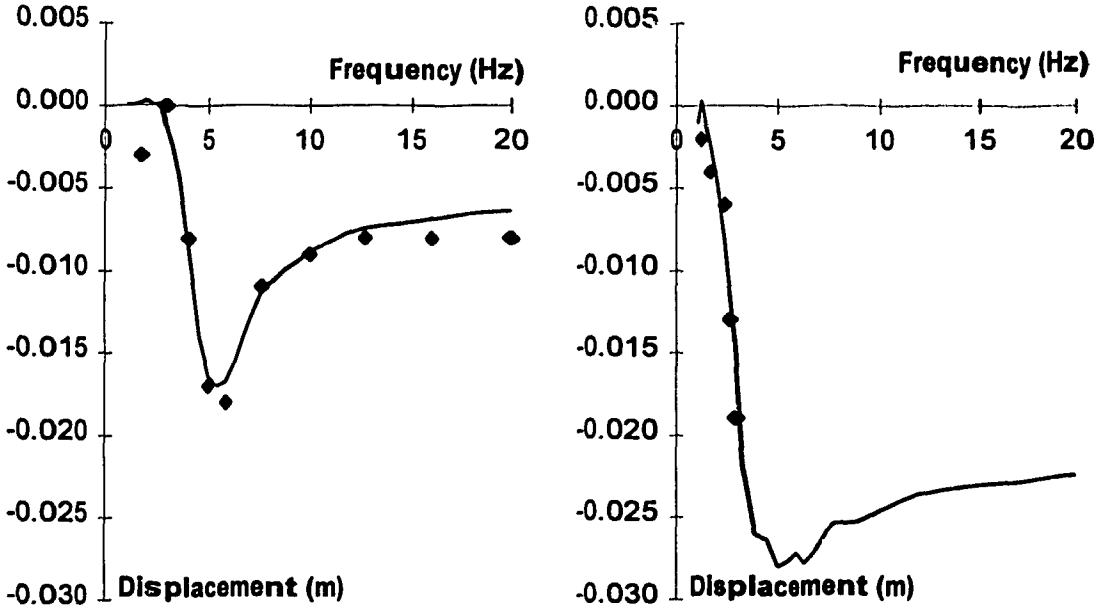

Excitation Amplitude: 0.32 cm

Excitation Amplitude: 1.27 cm

Figure 6.16 Comparison of analytical and experimental average ride height response characteristics of the quarter-car simulator (Damper: Mechformance).

with the Koni damper. The magnitude of average ride height of the sprung mass with the Mechformance damper, however, is considerably larger than that attained with the Koni damper. As is expected with the increase in the ratio of rebound to compression damping, the average ride height increases with the excitation amplitude and does not decrease significantly at higher frequencies, as shown in Figure 6.16.

Fox Damper

Figures 6.17 to 6.19 illustrate the peak velocity, rms velocity ratio, normalized time of tire lift-off, and average ride height response of the quarter-car simulator model with Fox-light damper. The corresponding response characteristics of the model with Fox-heavy damper are presented in Figures 6.20 to 6.22, as a function of excitation frequency and amplitude. A comparison of the responses reveals reasonable correlation between the analytical and experimental response characteristics of the simulator equipped with both dampers.

6.2.3.3 Discussion Of Frequency Response Characteristics

The frequency response characteristics of the quarter-car simulator, comprising monotube and remote reservoir damper models, as presented in Figures 6.11 to 6.22, reveal similar patterns. The magnitude of the sprung and unsprung mass rms transmissibility, peak velocity response, nondimensionalized tire-lift off, and the average ride height response, however, differ considerably with the damper model used. The peak value of velocity ratio response and the corresponding frequency of the quarter-car model equipped with different damper models are summarized in Table 6.4. The frequency ranges of the wheel-hop motion encountered under 1.27 cm excitation with the different damper, models are summarized in Table 6.5. The peak variation in the average ride height of sprung mass and the corresponding excitation frequency are summarized in

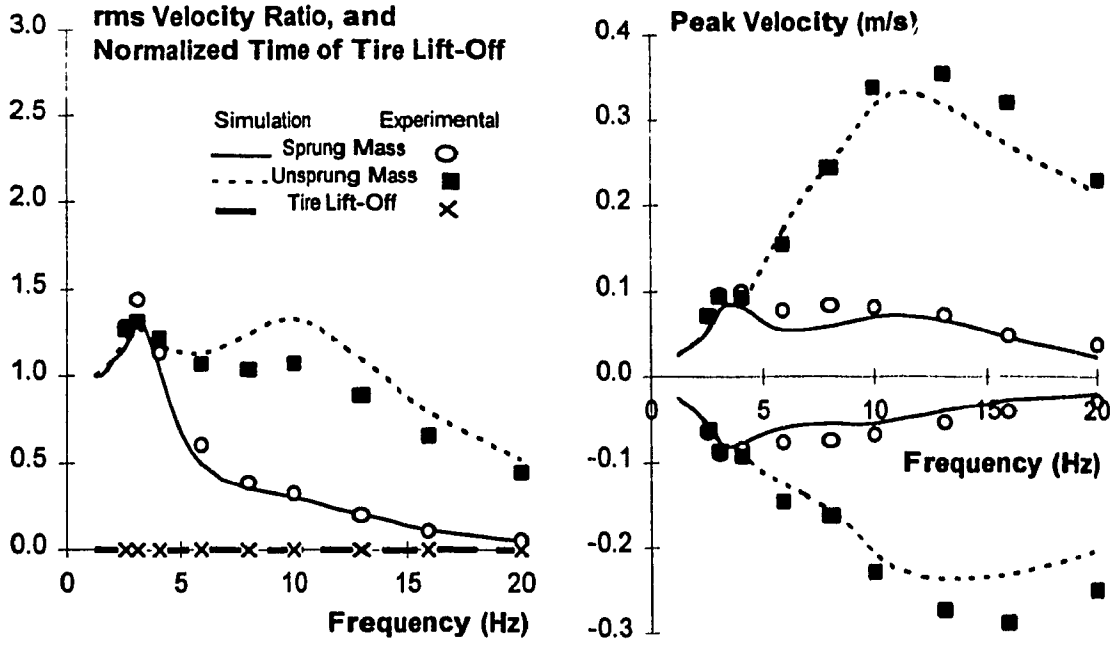

Figure 6.17 Comparison of analytical and experimental response characteristics of the quarter-car simulator (Damper: Fox-Light; Excitation amplitude: 0.32 cm).

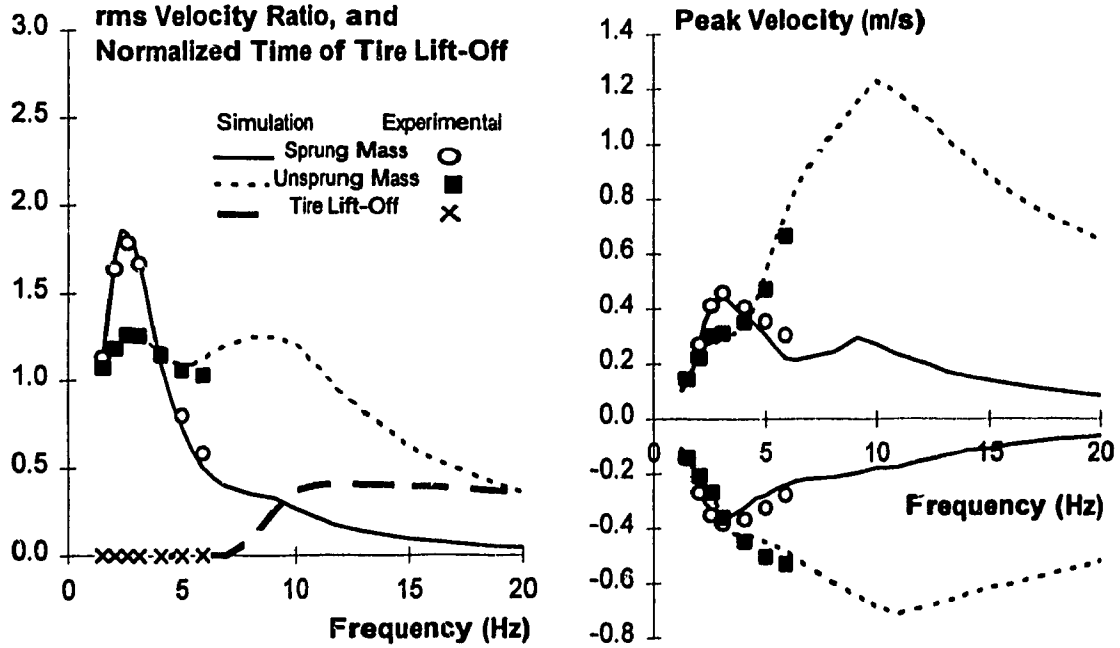

Figure 6.18 Comparison of analytical and experimental response characteristics of the quarter-car simulator (Damper: Fox-Light; Excitation amplitude: 1.27 cm).

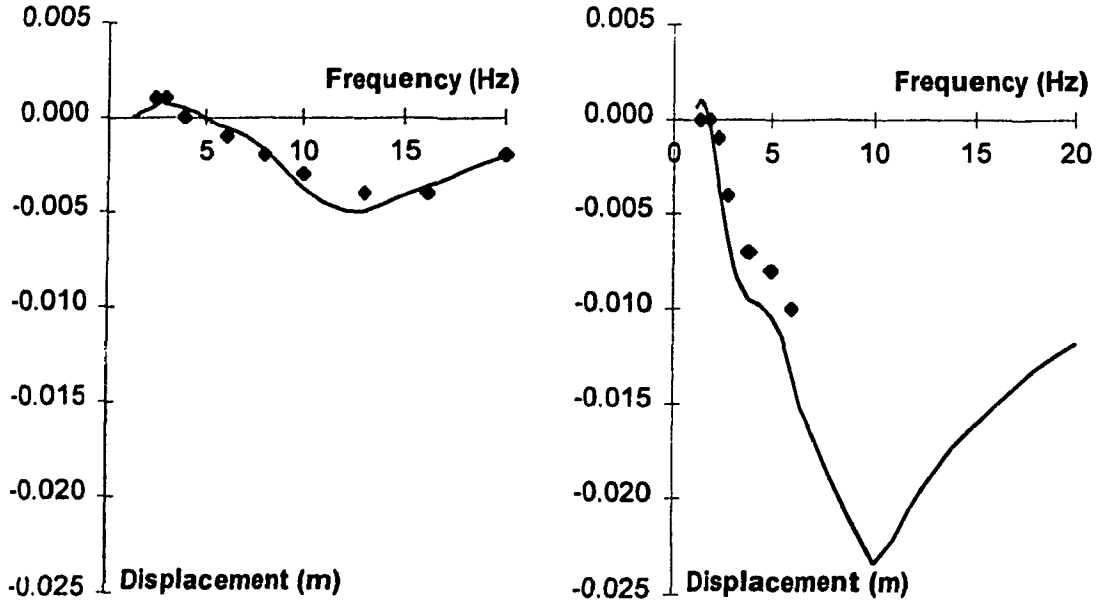

Excitation Amplitude: 0.32 cm

Excitation Amplitude: 1.27 cm

Figure 6.19 Comparison of analytical and experimental average ride height response characteristics of the quarter-car simulator (Damper: Fox-Light).

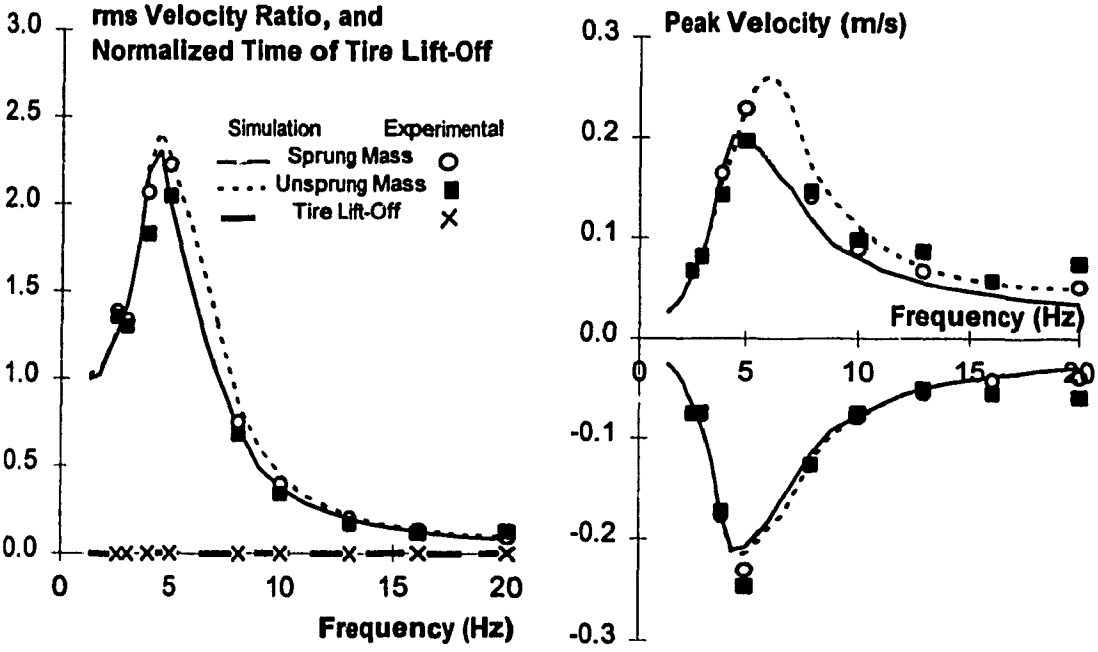

Figure 6.20 Comparison of analytical and experimental response characteristics of the quarter-car simulator (Damper: Fox-Heavy; Excitation amplitude: 0.32 cm).

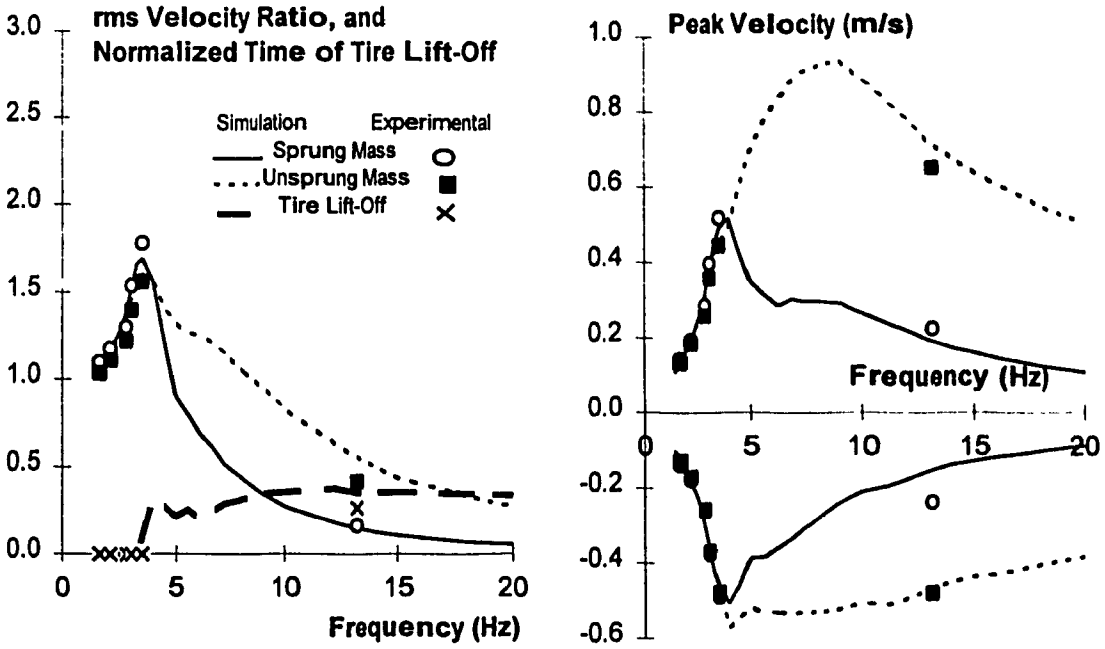

Figure 6.21 Comparison of analytical and experimental response characteristics of the quarter-car simulator (Damper: Fox-Heavy; Excitation amplitude: 1.27 cm).

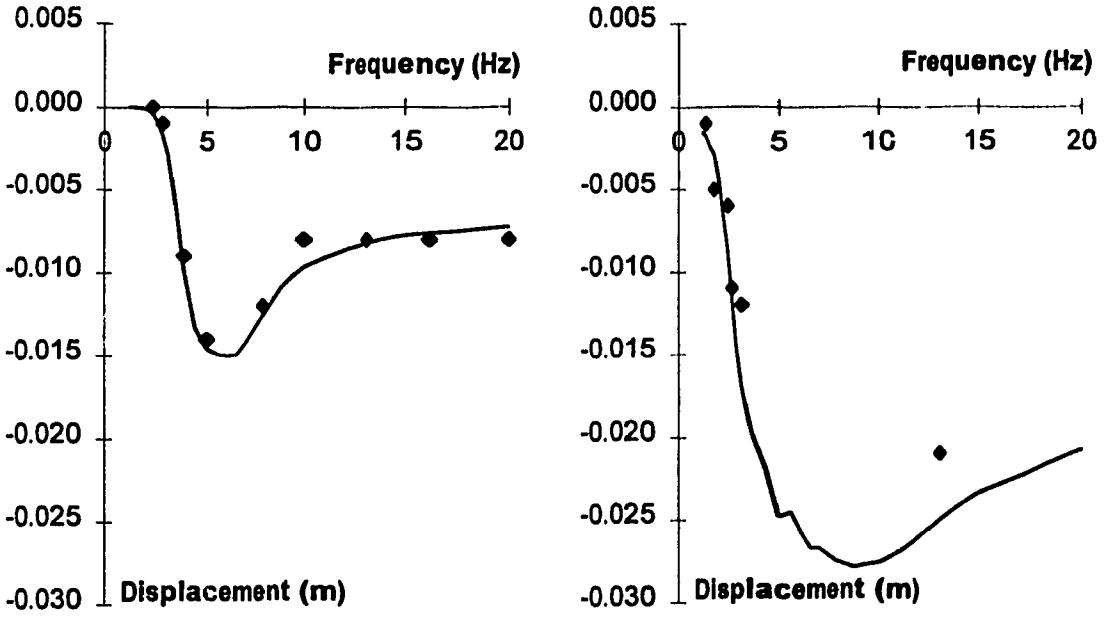

Excitation Amplitude: 0.32 cm

Excitation Amplitude: 1.27 cm

Figure 6.22 Comparison of analytical and experimental average ride height response characteristics of the quarter-car simulator (Damper: Fox-Heavy).

TABLE 6.4
SUMMARY OF PEAK VELOCITY RATIO RESPONSE OF QUARTER-CAR MODEL WITH DIFFERENT DAMPERS

Damper Model	Peak Excitation Amplitude (cm)	Peak Velocity Ratio		Frequency of Peak Velocity Ratio; Hz	
		Sprung	Unsprung	Sprung	Unsprung
Koni	0.32	1.91	2.02	4.5	4.5
	1.27	1.6	1.45	3.25	3.25
Mechformance	0.32	2.93	2.85	4.5	4.5
	1.27	2.16	2.03	3.5	3.5
Fox-heavy	0.32	2.3	2.41	4.5	4.5
	1.27	1.69	1.60	3.5	3.5
Fox-light	0.32	1.32	1.33	3.0	10
	1.27	1.86	1.29	2.25	2.75

TABLE 6.5
RANGE OF EXCITATION FREQUENCIES RESULTING IN WHEEL-HOP MOTION
(Excitation Amplitude: 1.27 cm)

Damper Model	Frequency; Hz
Koni	4.5-20
Mechformance	3.5-20
Fox-heavy	3.5-20
Fox-light	5.0, 7-20

TABLE 6.6
PEAK AVERAGE RIDE HEIGHT RESPONSE OF THE SPRUNG MASS WITH DIFFERENT DAMPER MODELS

Damper Model	Excitation Amplitude (cm)	Peak Change in Average Ride Height (cm)	Frequency of Peak Variation; Hz
Koni	0.32	-0.3	6.5
	1.27	-1.0	9
Mechformance	0.32	-1.7	5.5
	1.27	-2.8	5.0
Fox-heavy	0.32	-1.5	6.0
	1.27	-2.79	9
Fox-light	0.32	-0.5	12
	1.27	-2.34	10

Table 6.6. An examination of the results presented in Tables 6.4 to 6.6, and Figures 6.11 to 6.22, revealed the following important trends in the frequency response characteristics:

- The frequency response characteristic of the sprung and unsprung masses, in-general, exhibit large amounts of coupling ,and are similar to those of a Single-DOF system due to high damping properties of the damper, with the exception of the Fox damper with light setting. The frequency response characteristics of the unsprung mass of the simulator comprising the Fox-light damper model exhibits two distinct resonant frequencies.
- An increase in the excitation amplitude yields the peak response occurring at a lower frequency. The peak value of rms velocity response ratio also decreases with increase in the excitation amplitude, with the exception of the sprung mass response with the Fox-light damper.
- The magnitude of the peak response tends to increase with the increase in damping.

- The peak values of normalized tire lift-off ranges from 0.4 to 0.45 for all cases.
- The peak velocity response of the sprung mass is approximately symmetric about zero. The velocity response of the unsprung mass, however, exhibits higher velocity in compression, specifically under 1.27 cm excitation.
- The magnitude of deviation in average ride height increases with excitation frequency up to a frequency at which the variations approach a peak value. The magnitude of change in ride tends to decrease at higher excitation frequency. The sprung mass ride height, however, does not approach its static value.
- The magnitude of deviation in average ride height increases with increased damping and excitation amplitude. At higher excitation frequencies the rate of change of the ride height decreases with increase in excitation amplitude, which is most apparent in case of the Mechformance damper.
- A comparison of the response characteristics of the quarter-car simulator model, with and without damper, reveals that the wheel-hop motion is considerably reduced with the damper. The on-set of wheel-hop motion occurs at considerably larger levels of excitation, when damping is introduced. However, increasing damping above an optimal value results in tire lift-off occurring at lower excitation frequency. Further wheel-hop motion encountered at relatively large amplitudes of excitation, increases with high damping. Tire lift-off can thus be minimized through selection of optimal damping properties. The Fox-light damper with the remote reservoir design resulted in minimal tire lift-off.
- An increase in rebound to compression damping ratio yields larger variations in the ride height performance. The monotube Koni damper resulted in least variation in the ride height. Higher rebound to compression damping ratio in all cases tends to pack down the system.

The high damping properties of the Mechformance and Fox-heavy dampers yield increased motion of the sprung mass. The Koni and Fox-light dampers with relatively

low damping and low rebound to compression damping ratio are considered suited to achieve best traction performance.

6.3 PARAMETRIC SENSITIVITY ANALYSIS

From the analytical and experimental response characteristics of the candidate dampers, presented in Chapter 4, it is evident that the damper performance is strongly related to various design and operating parameters. While the most probable variations in operating conditions include temperature, excitation amplitude and frequency, the damping properties are mostly affected by the variation in valving, friction, gas spring and the fluid compressibility. The influence of variations in these design and operating variables on the performance characteristics is investigated using the validated models of the candidate dampers and quarter-car simulator. The performance characteristics of the damper models are evaluated in terms of the following:

(i) Change in average ride height, a measure of the aerodynamic grip.

(ii) Normalized tire lift-off duration and minimum tire load, measures of the mechanical grip.

(iii) rms velocity response ratio of the sprung mass, a measure of the ride quality.

The analyses are performed using the modified quarter-car model, derived upon eliminating the friction between the sprung mass and the input, as discussed in Chapter 5. This modified model is selected to represent the quarter-car more accurately. The elimination of friction force between the sprung mass and the input, however, results in undamped tire spring model. Since race car suspensions are generally stiff, the tire damping is often an important factor. A viscous tire damping term is thus introduced in Equation 5.14, with an uncoupled unsprung mass mode damping ratio of 5%, as proposed by Barek [76]. The friction force caused by the guidance mechanism between the sprung and unsprung masses is also reduced to a value representing the low friction spherical bearings used in race car suspensions. The magnitude of this friction is thus reduced

from 65 N to 15 N. The influence of variations in design and operating parameters is investigated for two different amplitudes of harmonic displacement excitations: 0.32 and 1.27 cm. The equation of motion for the modified two DOF quarter-car simulator, Equations (5.12) and (5.13), are solved for harmonic excitations, and response characteristics are analyzed to highlight influence of variations in design and operating variables.

The parametric study is performed for only one of the candidate dampers, (monotube Koni), and the results of the study are described below.

6.3.1 Influence Of Variation In Damping Coefficients

The performance characteristics of dampers are strongly dependent upon the valving and thus the damping coefficients. Typical dampers, however, may comprise different valving in compression and rebound. Furthermore each of the valves is considered effective only in a specific velocity range. The velocity response across the damper of the modified quarter-car model is thus investigated to examine the effective velocity ranges of the response for different inputs. Figure 6.23 illustrates the peak damper velocity response in compression and rebound, when subject to harmonic displacement excitations of 0.32 cm and 1.27 cm amplitude. The results show that the peak velocity response in compression is larger than the peak rebound velocity response in almost entire frequency range. The difference between the peak velocities in compression and rebound tends to increase considerably with increase in excitation amplitude. The asymmetric velocity response across the damper is attributed to its asymmetric damping properties, the lower magnitude of velocity response in rebound is due to the high rebound to compression ratio of the Koni damper. The peak compression and rebound velocity response approaches its highest value near 6 Hz, when subject to 0.32 cm displacement excitation. This frequency, however, increases to nearly 9 Hz when excitation amplitude is increased to 1.27 cm. The results provide an understanding

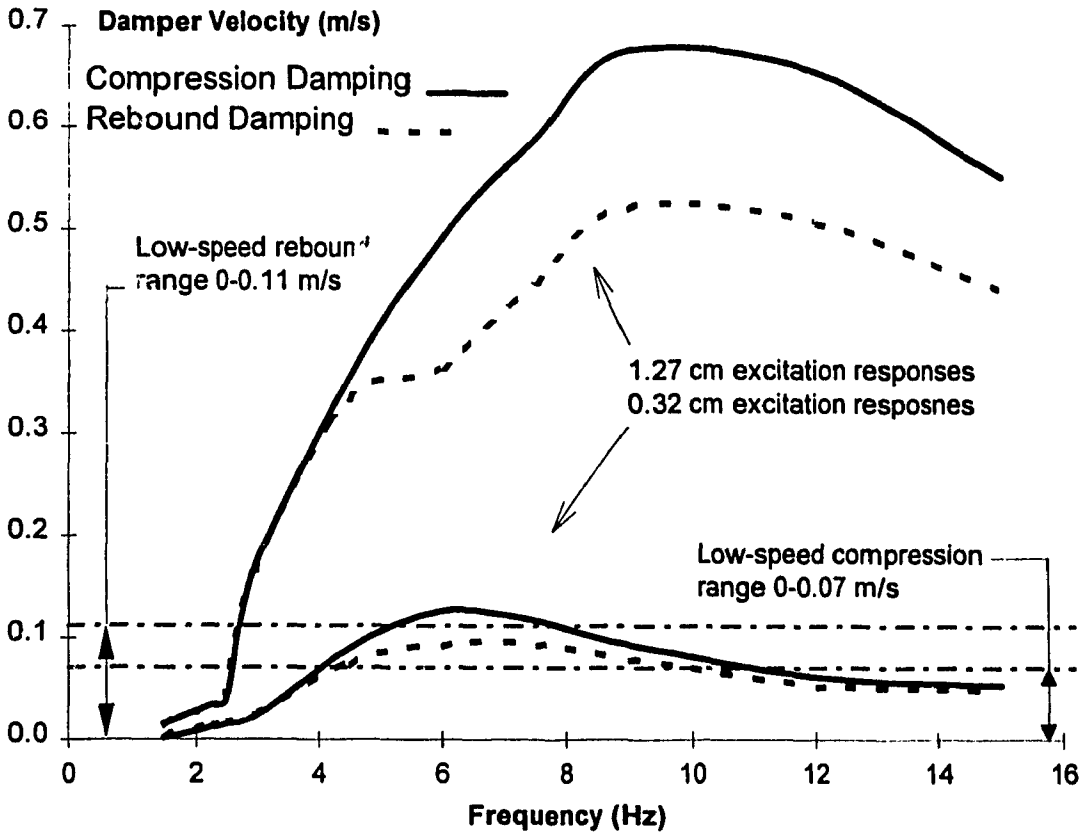

Figure 6.23 Relative peak velocity response across the damper of the quarter-car model.

of the effectiveness of the different damper valving. Under 0.32 cm excitation, the damper response is primarily determined by the low speed valving, due to relatively low velocity across the damper. The response of the damper to the 1.27 cm excitation, however, is controlled by the mid speed valving; although, the contributions of the low speed valving most also be considered. The frequency response characteristics of the quarter-car model with the Koni damper further revealed rapid decay of oscillations below excitation responses of 3 Hz and above 15 Hz. The study is thus limited to the excitation frequencies ranging from 3 to 15 Hz. The results clearly show considerable variations in the response behavior with variation in the excitation frequency and amplitude. The influence of variation in different rebound and compression valving on

the performance criteria is thus investigated to enhance an understanding of the damper behavior in varying speed ranges.

Variation in Low Speed Compression Damping

The results of the analytical and experimental studies performed on the monotube Koni damper design (presented in Chapter 4) revealed that the low speed compression damping is most effective in the 0 to 0.07 m/s range. The influence of variation in the low speed compression damping parameter is investigated by varying the nominal values, identified in Chapter 4, to 50% and 200% of the nominal values.

The response characteristics are presented in terms of: average ride height, which relates to the aerodynamic grip; the minimum tire force normalized with respect to the static load, which relates to minimum mechanical grip; rms velocity ratio of the sprung mass normalized with respect to that obtained with the nominal damper parameters. Figures 6.24 to 6.26 illustrate the influence of variations in low speed compression damping on the average ride height, normalized minimum tire load, normalized tire lift-off, and normalized sprung mass rms velocity ratio response, respectively, for two different amplitudes of excitation. An increase in compression damping tends to reduce the potential energy being stored in the suspension springs, resulting in increased average ride height, as shown in Figure 6.24. The damper velocity response under low levels of excitations predominately lies around the low speed compression damping speed range, as evident in Figure 6.23. The variation in low speed compression damping thus affects the damper response under lower excitation amplitude (0.32 cm) more significantly, particularly when the damper velocity is low (below 4 Hz and above 10 Hz). Although an increase in the low speed compression damping yields smaller variation in the ride height for both excitation amplitudes, the variations are more pronounced for 0.32 cm excitation. The minimum tire force tends to increase in the vicinity of sprung and unsprung mass resonant frequencies, when low speed compression damping is increased,

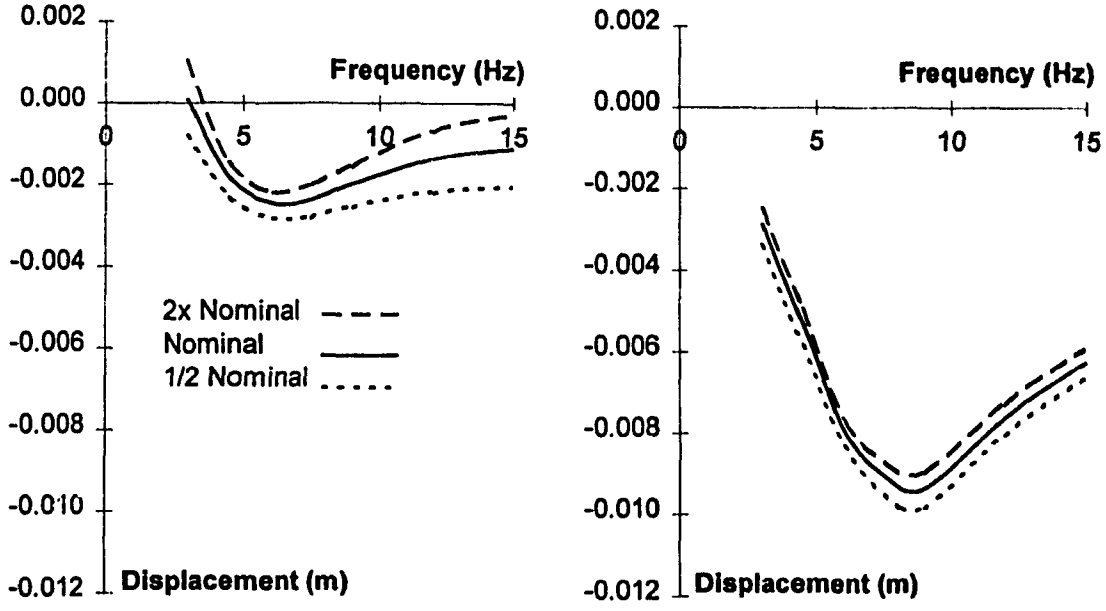

Excitation Amplitude: 0.32 cm

Excitation Amplitude: 1.27 cm

Figure 6.24 Influence of variations in low-speed compression damping on the average ride height response.

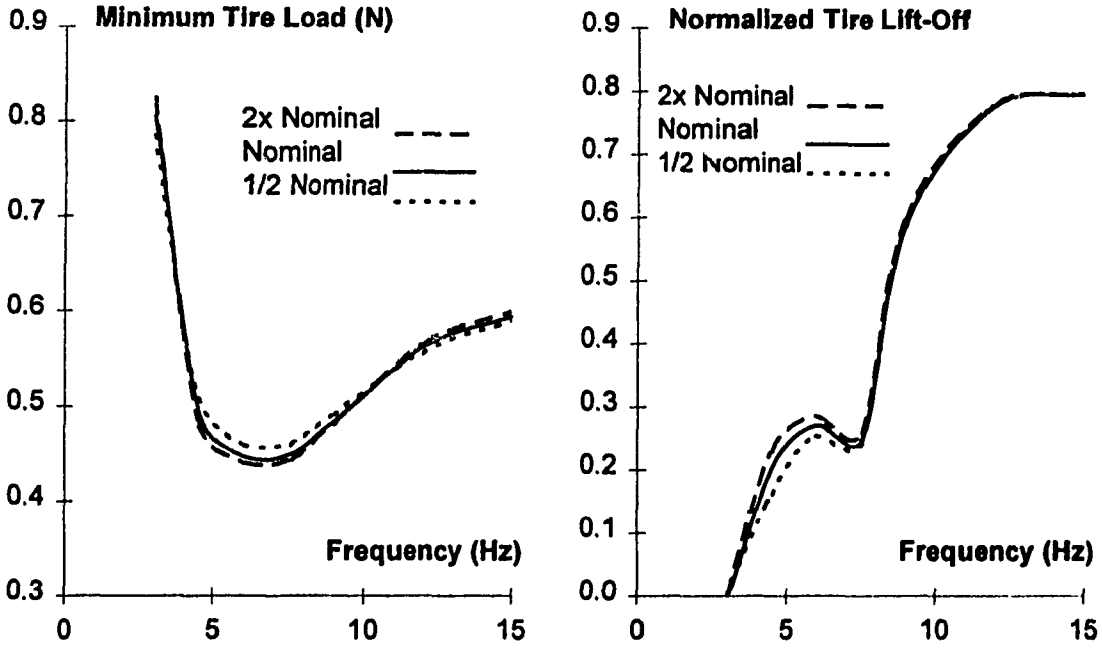

Excitation Amplitude: 0.32 cm

Excitation Amplitude: 1.27 cm

Figure 6.25 Influence of variations in low-speed compression damping on the minimum tire load and normalized tire lift-off.

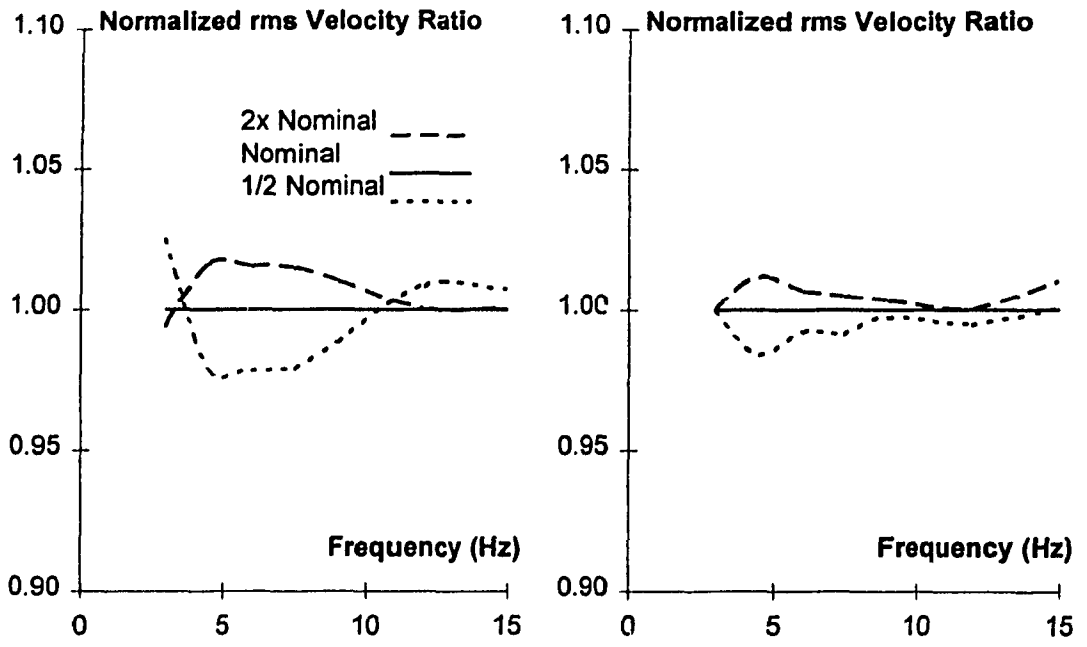

Figure 6.26 Influence of variations in low-speed compression damping on the normalized rms velocity ratio response of the sprung mass.

as shown in Figure 6.25. Under low levels of excitation, an increase in compression damping reduces the minimum tire force in the frequency range between the resonance's, 4 to 11 Hz. The quarter-car model exhibits wheel lift-off near the sprung mass resonance and reduction in low speed compression damping reduces the magnitude of wheel-hop up to approximately 8 Hz. At higher excitation frequencies, the effect of low speed compression damping on the normalized tire lift-off is insignificant due to high damper velocities. Lower compression damping results in increased sprung mass velocity response near the resonant frequencies and in improved isolation between the two resonant frequencies (4 to 11 Hz) under low amplitude excitation, as shown in Figure 6.26. Under higher levels of excitation, where the contribution due to low speed compression damping is not as significant, a reduction in compression damping yields slightly improved isolation of the sprung mass. The variation in the normalized rms velocity response of the sprung mass, however, are well below 2%.

Variation of Mid Speed Compression Damping

Flow through mid-speed compression valving occurs when the damper velocity exceeds 0.07 m/s. Variations in mid speed compression damping thus mostly affect the performance of the quarter-car model, when subject to high levels of excitation. Figure 6.27 to 6.29 illustrate the influence of variations in mid-speed compression damping on the average ride height, normalized minimum tire force and normalized rms velocity response of the sprung mass, respectively, for two different amplitudes of excitation. The results clearly show that the variations in mid-speed compression damping affect the quarter-car model response significantly for 1.27 cm displacement excitation. The variations affect the system response under 0.32 cm excitation only in the 4 to 10 Hz frequency range, where the damper velocity slightly exceeds the low speed valve limit. The average ride height of the sprung mass increases with increase in the compression damping, as shown in Figure 6.27. The variations in the average ride height are quite significant for high displacement amplitude excitation (1.27 cm), with a peak variation of approximately 60% occurring at the excitation frequency of 9 Hz.

As observed earlier in Figure 6.25 for variations in the low speed compression damping, the mechanical grip of the tires under low level of excitation tends to decrease with the increase in mid-speed compression damping. A comparison of Figures 6.25 and 6.28 clearly illustrates the minimal contributions of the mid-speed compression damping under low amplitude excitation. The normalized tire lift-off and thus the mechanical grip improves at higher excitation levels, when mid-speed compression damping is decreased. The normalized tire lift-off, however, decreases near and above the wheel-hop frequency with increased mid-speed damping. From the comparison of Figures 6.25 and 6.28, it is evident that lower mid-speed compression damping yields considerably enhanced mechanical grip. The decrease in mid-speed compression damping also results in enhanced vibration isolation of the sprung mass, as shown in Figure 6.29. The variations in mid-speed damping affect the sprung mass velocity response in the 3 to 8 Hz

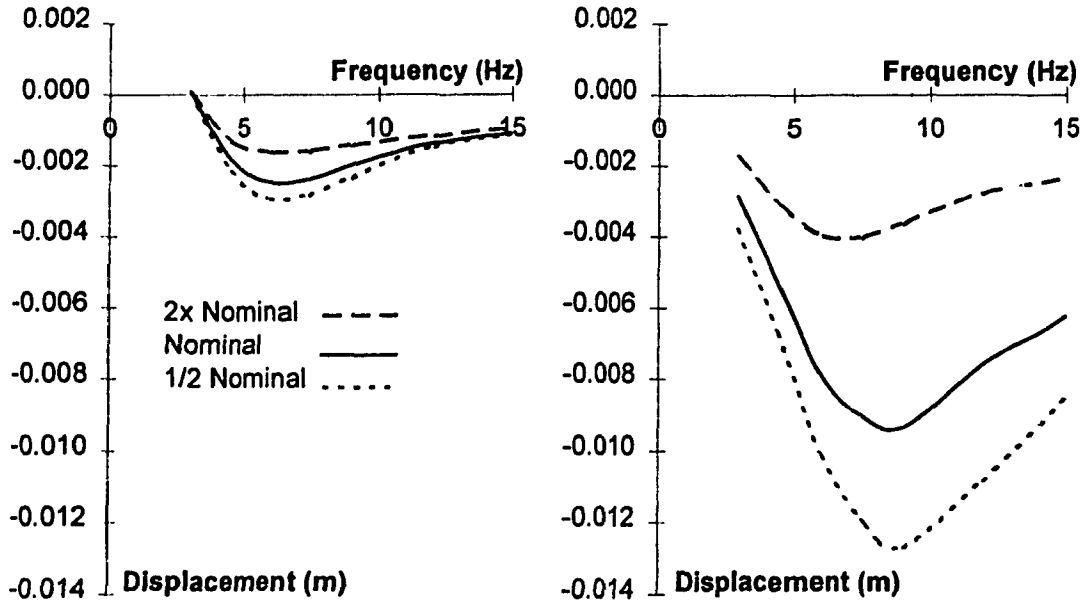

Excitation Amplitude: 0.32 cm Excitation Amplitude: 1.27 cm

Figure 6.27 Influence of variations in mid-speed compression damping on the average ride height response.

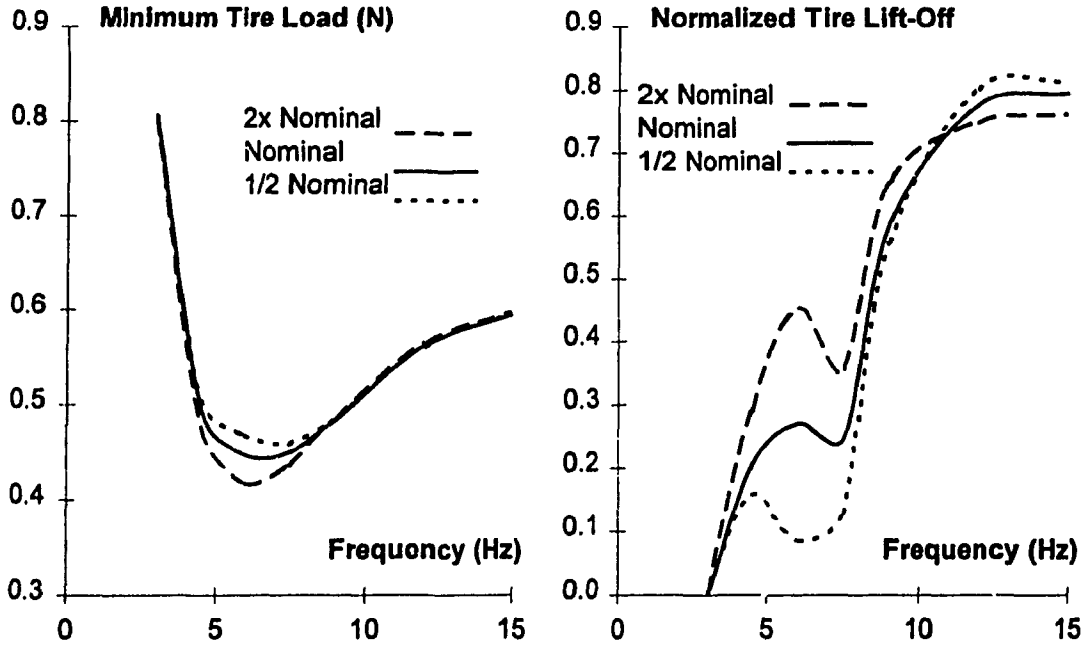

Excitation Amplitude: 0.32 cm Excitation Amplitude: 1.27 cm

Figure 6.28 Influence of variations in mid-speed compression damping on the minimum tire load and normalized tire lift-off.

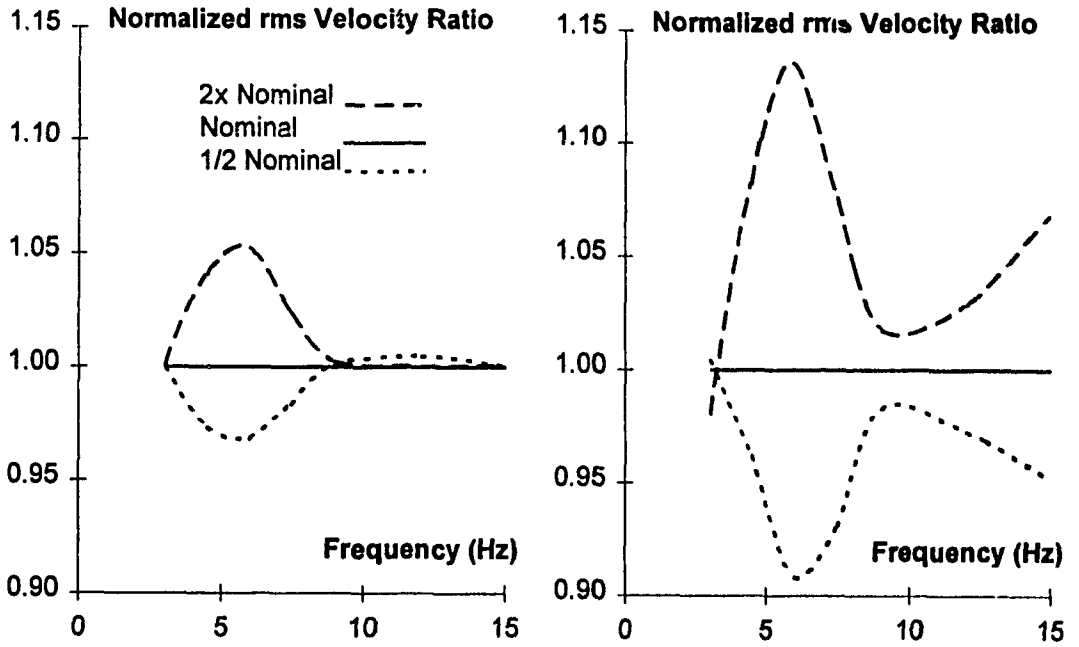

Figure 6.29 Influence of variations in mid-speed compression damping on the normalized rms velocity ratio response of the sprung mass.

frequency range, when the quarter-car model is subject to 0.32 cm displacement excitation. The sprung mass rms velocity ratio increases by approximately 5% near 6 Hz when the damping is selected as twice the nominal value. The corresponding increase in the rms velocity is observed as 14% under high excitation amplitude. The reduction in mid-speed compression damping (0.5 times nominal) yields nearly 3% and 9% reduction in the rms velocity ratio at 6 Hz under 0.32 and 1.27 cm excitation, respectively.

Variation of Low Speed Rebound Damping

From the analytical and experimental studies of the Koni damper, the low speed rebound valving range of 0 to -0.11 m/s was identified. The influence of variation in the low speed rebound damping is more pronounced under excitation amplitude of 0.32 cm, as shown in Figures 6.30 to 6.32. An increase in the damping causes a decrease in the

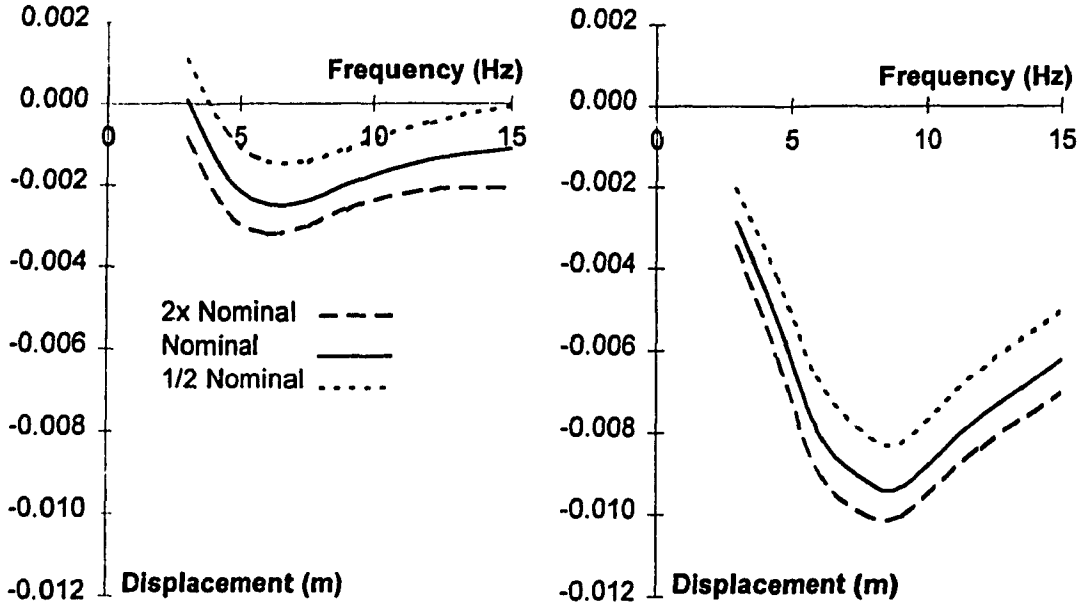

Excitation Amplitude: 0.32 cm Excitation Amplitude: 1.27 cm

Figure 6.30 Influence of variations in low-speed rebound damping on the average ride height response.

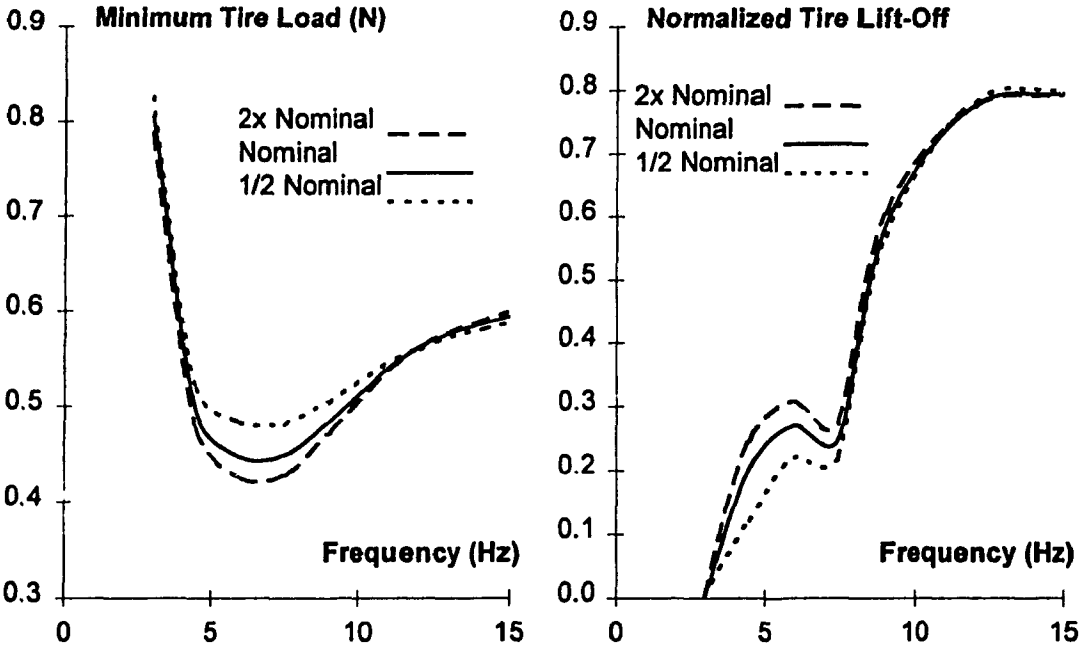

Excitation Amplitude: 0.32 cm Excitation Amplitude: 1.27 cm

Figure 6.31 Influence of variations in low-speed rebound damping on the minimum tire load and normalized tire lift-off.

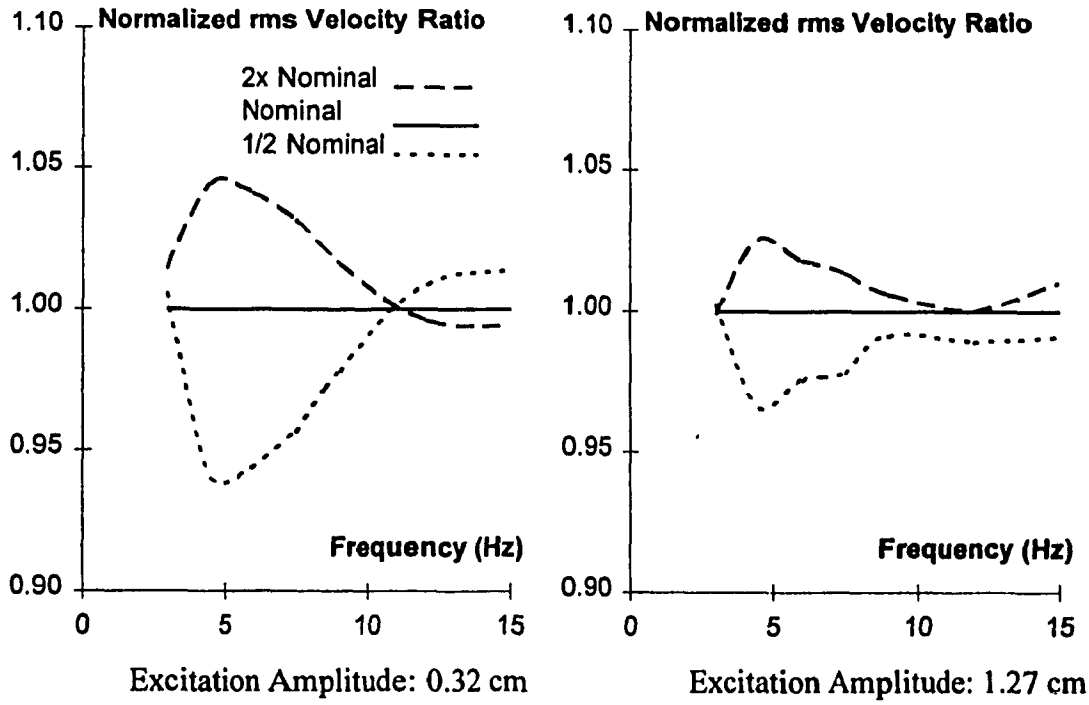

Figure 6.32 Influence of variations in low-speed rebound damping on the normalized rms velocity ratio response of the sprung mass.

average position of the sprung mass, as shown in Figure 6.30. Increasing the low-speed rebound damping by a factor of 2 yields an approximate change of 1 mm in the average ride height throughout the frequency range, for both amplitudes of excitation. A comparison of the results obtained for variation in low-speed compression and rebound damping (Figures 6.24 and 6.30) reveal that low-speed rebound damping affects the average ride height performance in a significant manner. The normalized minimum tire force and thus the mechanical grip of tire reduces with increased low speed rebound damping for low amplitude excitation, as observed earlier with variations in low speed compression damping (Figure 6.25). The effect of variations in rebound damping shown in Figure 6.31, however, is more pronounced due to higher speed range of the rebound valving and its high nominal value. Under high amplitude excitation, the normalized tire lift-off increases with the increase in rebound damping, as observed earlier with the low-speed compression damping, specifically, in the 4 to 8 Hz frequency range. A reduction

in low-speed rebound damping yields improved vibration isolation of the sprung mass, specifically in the 4 to 11 Hz frequency range under 0.32 cm excitation, as shown in Figure 6.32.

Variations in Mid Speed Rebound Damping

The fluid flows through mid-speed rebound valves occur when the damper velocity in rebound exceeds 0.11 m/s. The mid-speed rebound damping thus affects the suspension performance most significantly at relatively high velocities. Figures 6.33 to 6.35 illustrate the influence of variations in the mid-speed rebound damping on the average ride height, normalized minimum tire force and tire lift-off, and the normalized rms velocity ratio response of the sprung mass, respectively. The average ride height of the sprung mass is observed to be most sensitive to variations in the mid-speed rebound damping, as shown in Figure 6.33. The magnitude of changes in average ride height

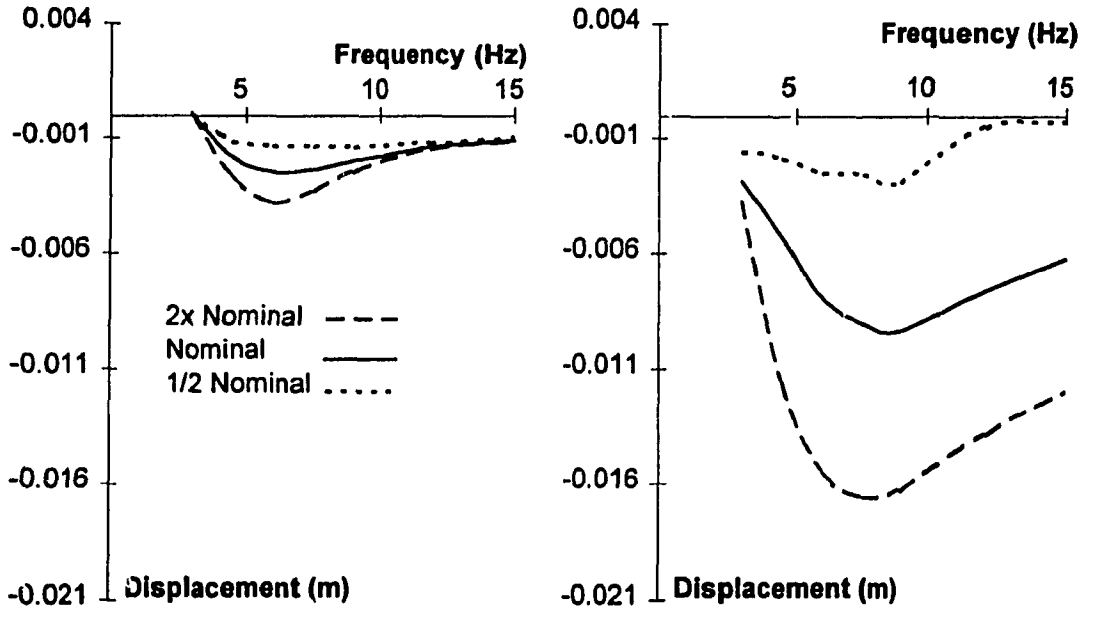

Excitation Amplitude: 0.32 cm Excitation Amplitude: 1.27 cm

Figure 6.33 Influence of variations in mid-speed rebound damping on the average ride height response.

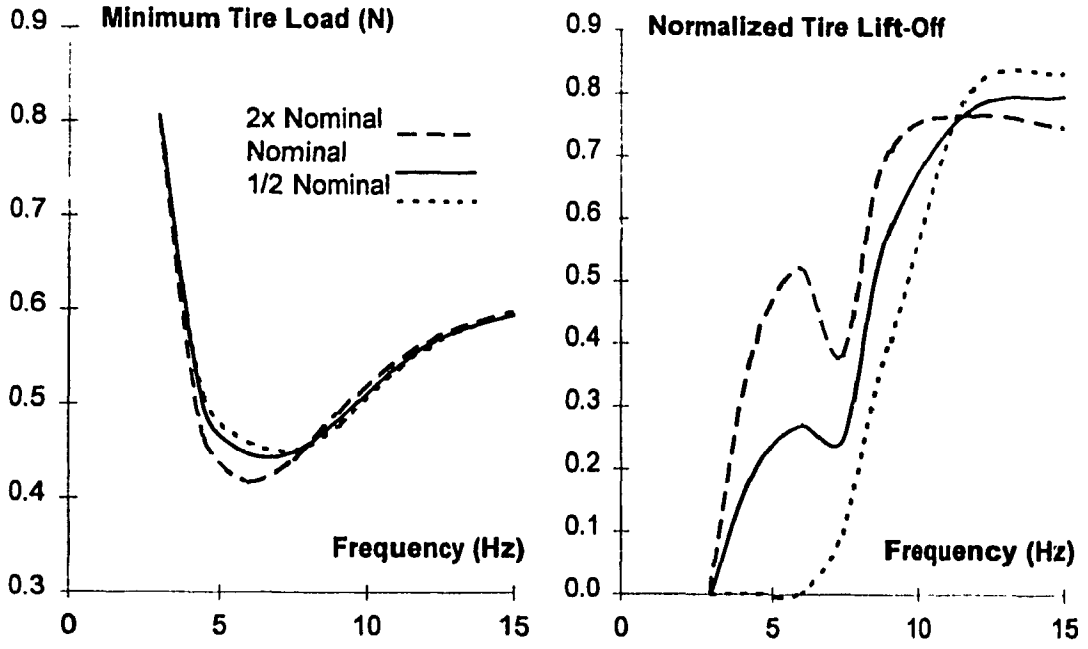

Excitation Amplitude: 0.32 cm Excitation Amplitude: 1.27 cm

Figure 6.34 Influence of variations in mid-speed rebound damping on the minimum tire load and normalized tire lift-off.

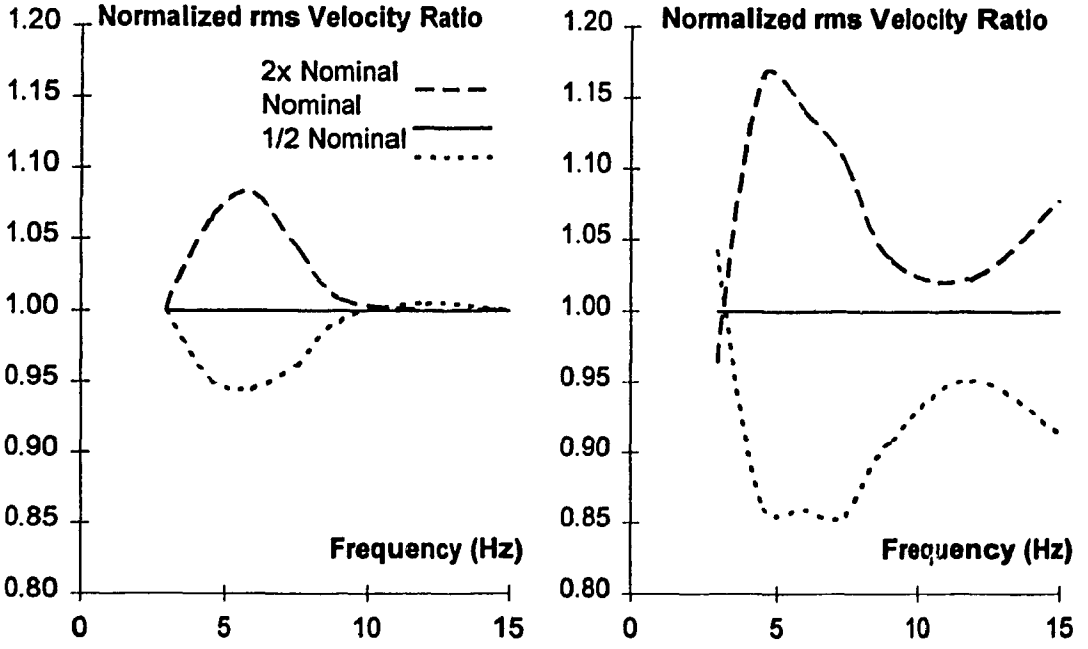

Excitation Amplitude: 0.32 cm Excitation Amplitude: 1.27 cm

Figure 6.35 Influence of variations in mid-speed rebound damping on the normalized rms velocity ratio response of the sprung mass.

increases considerably with the increase in rebound damping, for both excitation amplitudes. A reduction in rebound damping yields improved ride height performance, irrespective of the excitation amplitude. This response behavior is attributed to excessive rebound damping, which further reduces the minimum tire force in the 4 to 8 Hz range under low level excitations as shown in Figure 6.34. The normalized tire lift-off and thus the loss of mechanical grip, under high amplitude excitation, occurs considerably latter when the damping is decreased. The high rebound damping deteriorates the sprung mass vibration isolation performance, in almost the entire frequency range, as shown in Figure 6.35. The high damping, however, improves the vibration attenuation performance in the vicinity of the sprung mass resonant frequency.

6.3.2 Influence of Variations in Magnitude of Friction

The influence of friction force on the quarter-car model response is similar to that observed for variations in the low speed compression and rebound damping. Friction force yields high equivalent damping at very low velocities and extremely low damping at higher velocities. Since the magnitude of friction force is small, the equivalent damping at lower speeds is comparable to those developed by low-speed compression and rebound valves. The influence of Coulomb friction on the system response at higher speeds is almost negligible due to low equivalent damping. The influence of friction force on the average ride height is insignificant, since the average ride height is less sensitive to variations in low speed damping. Furthermore, symmetric damping properties of the ideal friction model further yield only insignificant variations in the average ride height. The influence of variations in the minimal tire damping force and normalized tire lift-off is also quite small due to the low damping corresponding to the wheel-hop motions, as shown in Figure 6.36. The sensitivity of normalized minimum tire force and the normalized tire lift-off to variations in friction is similar to that observed for low speed damping. The increase in friction force, similar to the damping, results in poor

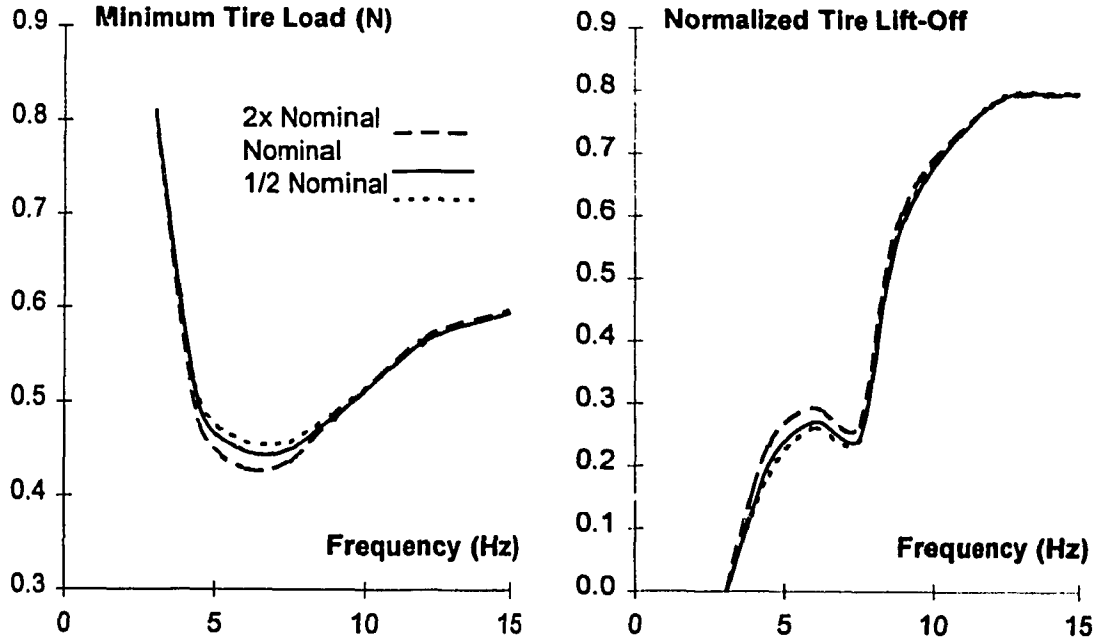

Figure 6.36 Influence of variations in friction on the minimum tire load and normalized tire lift-off.

vibration isolation performance of the sprung mass, specifically under low level excitation. The high damper velocity response caused by high amplitude excitation results in only minimal damping due to Coulomb friction and thus only small variations in the rms velocity ratio response of the sprung mass, as shown in Figure 6.37.

6.3.3 Variations in the Fluid Compliance

From the experimental and analytical results, presented in Chapter 3 and 4, it is evident that the damper performance at higher mass acceleration is strongly affected by fluid compliance. The influence of variations in fluid compliance on the quarter-car model response thus becomes evident only when the inertia forces predominate at relatively higher excitation frequencies. Figures 6.38 to 6.40 illustrate the influence of variations in fluid compliance on the average ride height, minimum tire load and normalized tire lift-off, and normalized sprung mass rms velocity response, respectively.

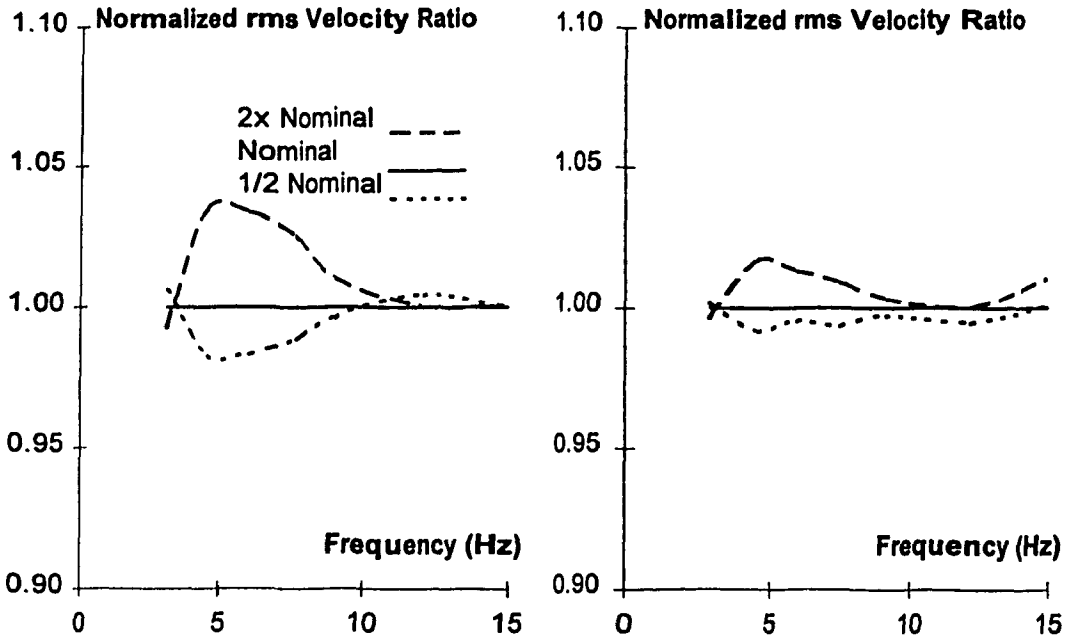

Excitation Amplitude: 0.32 cm Excitation Amplitude: 1.27 cm

Figure 6.37 Influence of variations in friction on the normalized rms velocity ratio response of the sprung mass.

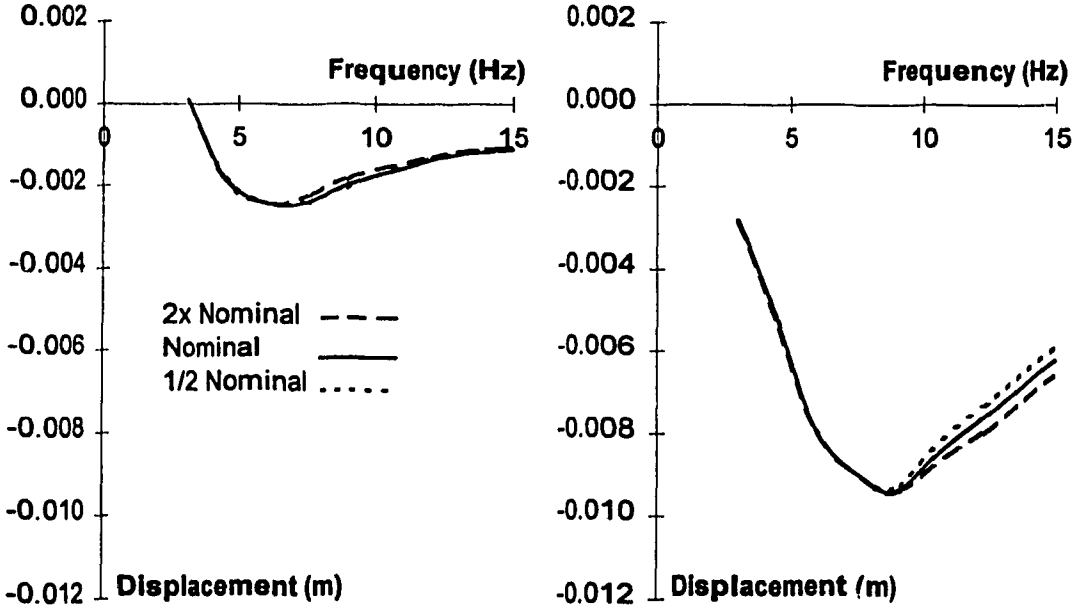

Excitation Amplitude: 0.32 cm Excitation Amplitude: 1.27 cm

Figure 6.38 Influence of variations in fluid compliance on the average ride height response.

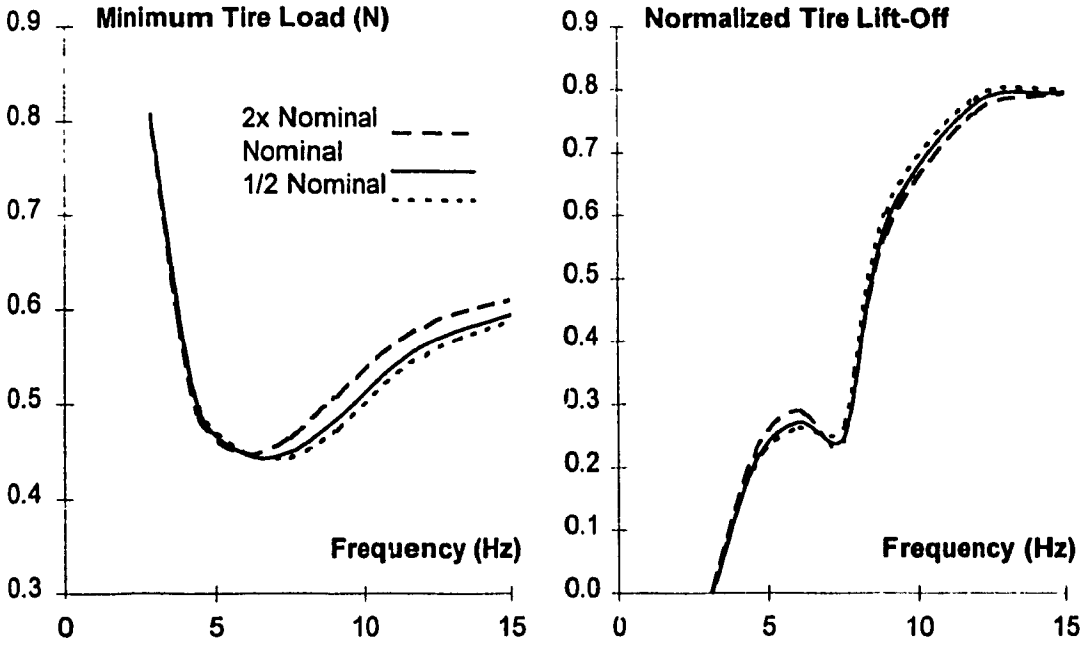

Excitation Amplitude: 0.32 cm Excitation Amplitude: 1.27 cm

Figure 6.39 Influence of variations in fluid compliance on the minimum tire load and normalized tire lift-off.

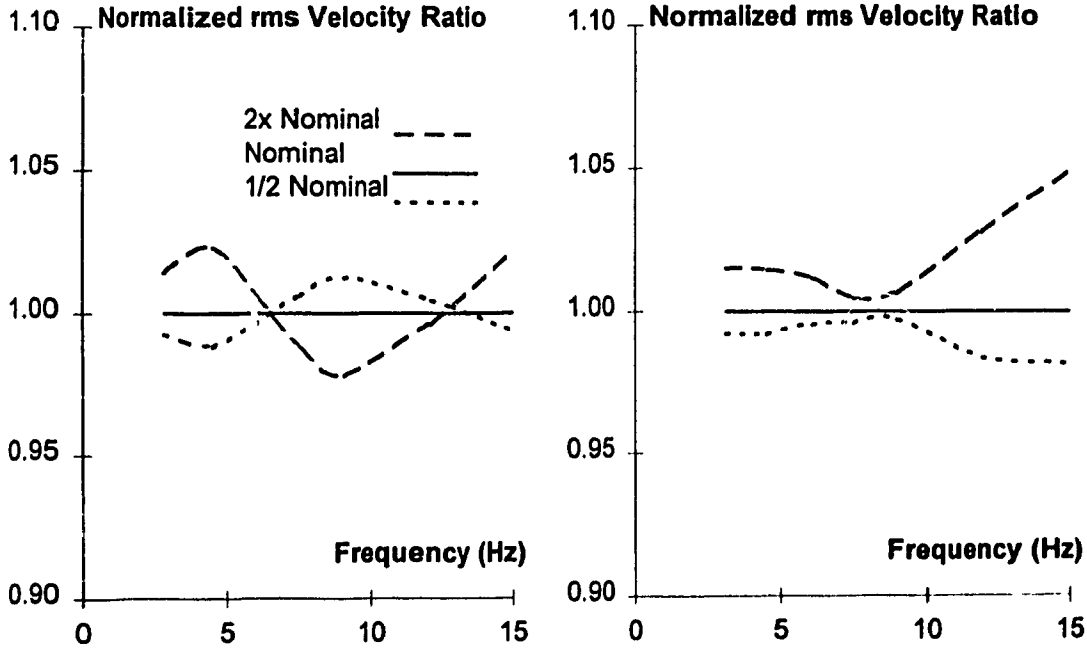

Excitation Amplitude: 0.32 cm Excitation Amplitude: 1.27 cm

Figure 6.40 Influence of variations in fluid compliance on the normalized rms velocity ratio response of the sprung mass.

The influence of variations in the fluid compliance on the average ride height is only minimal, except at higher frequencies and excitation levels, when mass acceleration approaches a high value. An increase in fluid compliance tends to enhance minimum tire force for low amplitude high frequency excitations, normalized tire lift-off and the sprung mass vibration isolation in the 7 to 12 Hz frequency range, when the quarter-car model is subject to 0.32 cm excitation, as shown in Figure 6.40. The rms velocity response of the sprung mass, however, increases near the wheel-hop frequencies and at frequencies below 6 Hz. The rms velocity response under 1.27 cm excitation exhibits poor vibration isolation and considerable amplification near the wheel-hop frequency, when fluid compliance is increased.

6.3.4 Influence of Variations in Operating Temperature

Variations in the operating temperature typically produce considerable affect on the gas spring, and smaller variations in damping and frictional characteristics of the damper, as discussed earlier in Chapter 3 and 4. The performance characteristics of the quarter-car model are thus strongly influenced by variation in the damper temperature. An increase in the damper temperature tends to increase the gas spring force and hence the ride height, while damping and friction forces decrease. The baseline damper model is considered to operate at a temperature of 90 °C, and the influence of temperature is investigated by varying the temperature to 45 °C and 180 °C. An increase in the damper temperature yields an increased bias due to gas spring and thus the ride height, as shown in Figure 6.41. The ride height increases considerably with the increase in temperature, irrespective of the excitation frequency and amplitude. It should be noted that the variations in the ride height response are somewhat less significant at different excitation frequencies. Such response behavior is similar to that obtained with reduced low-speed damping as is the effect on the normalized minimum tire load and rms velocity response, shown in Figures 6.42 and 6.43. An increase in operating temperature results in lower

minimum tire load under 1.27 cm excitation and improved vibration attenuation of the sprung mass due to lighter damping. The minimal tire force under lower amplitude of excitation, however, increases with an increase in operating temperature. This trend is similar to that observed with variations in the low-speed damping shown in Figures 6.28 and 6.32.

6.3.5 Highlights of Parametric Variation Study

The performance characteristics of a damper in a quarter-car configuration is related to various design and operating parameters of the damper, and response characteristics of the quarter-car model. The damper performance is strongly dependent upon the damping coefficients and the velocity response of the vehicle or the quarter-vehicle model. The damping valves or the coefficients are thus frequently adjusted to suit the vehicle response and excitations by the user, while the variations in operating

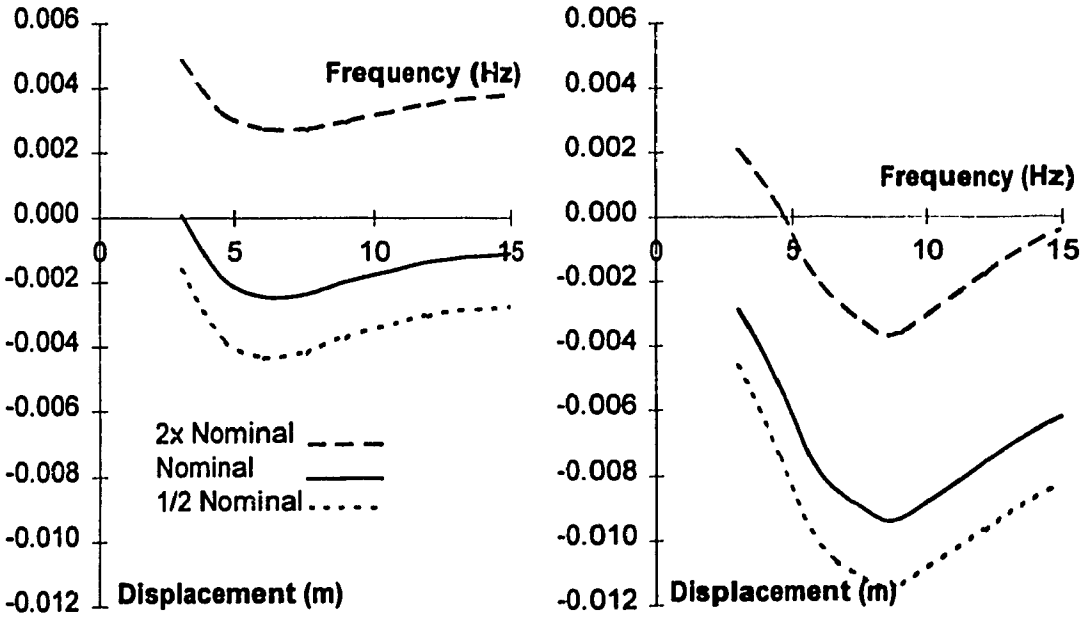

Figure 6.41 Influence of variations in damper temperature on the average ride height response.

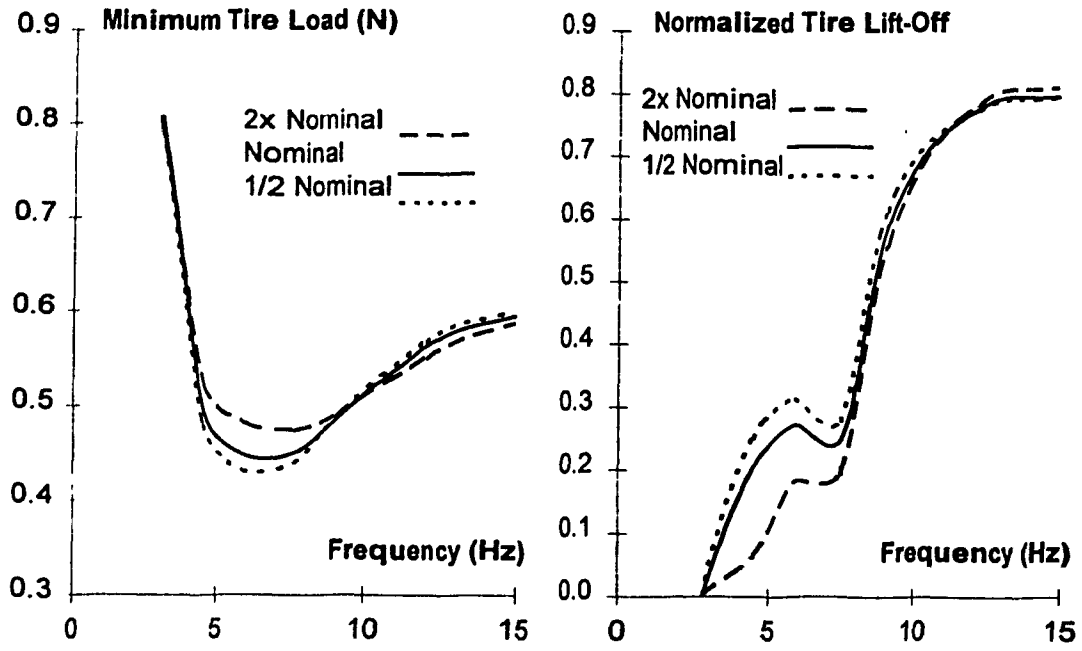

Excitation Amplitude: 0.32 cm Excitation Amplitude: 1.27 cm

Figure 6.42 Influence of variations in damper temperature on the minimum tire load and normalized tire lift-off.

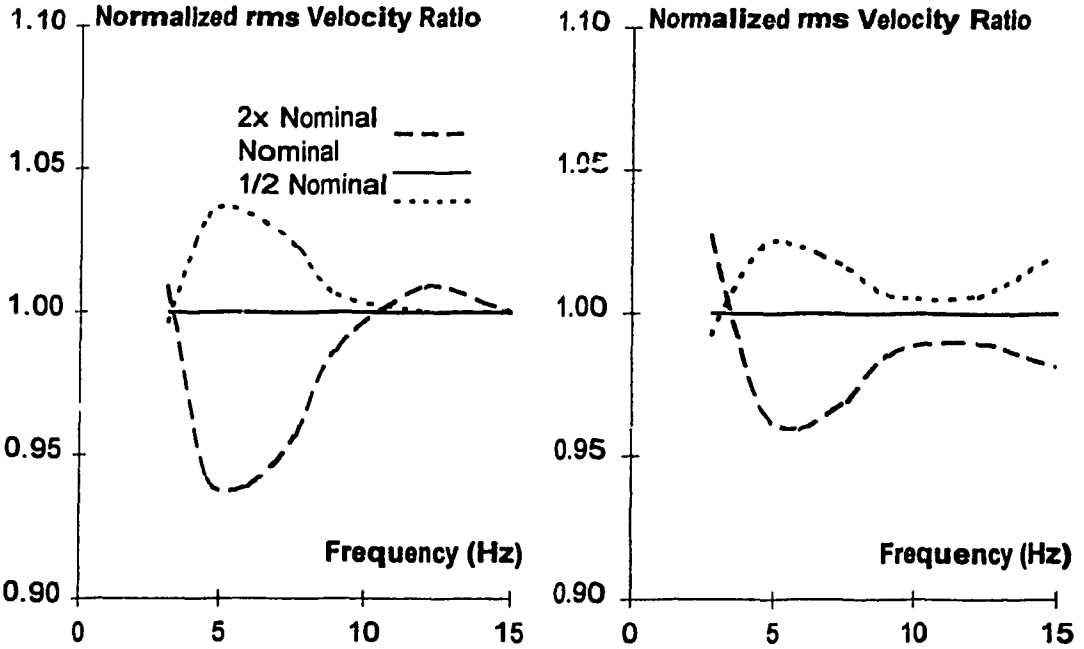

Excitation Amplitude: 0.32 cm Excitation Amplitude: 1.27 cm

Figure 6.43 Influence of variations in damper temperature on the normalized rms velocity ratio response of the sprung mass.

cannot be easily modified by the user. The performance characteristics of the coupled damper-vehicle model, as influenced by these design variables are summarized below.

- The average ride height of the sprung mass primarily depends upon the compression to rebound velocity response, and increases with the increase in compression and/or decrease in rebound velocity. Changes in either low-speed compression or rebound damping causes nearly consistent changes in the ride height in the entire frequency range, while changes in either mid speed compression or rebound damping result in considerable variations in the ride height at higher damper velocities. Furthermore, an increase in the mid speed compression damping and/or a decrease in the mid speed rebound damping reduces the magnitude of variations in the average ride height with frequency. Variations in high rebound damping yield considerably larger variations in ride height than those caused by proportional changes in the compression damping.
- The minimum tire force at the tire-load interface is strongly affected by variations in damping in the range of higher damper velocities (4 to 10 Hz). A reduction in damping results in increased minimum tire load at the tire-load interface. Changes in the low speed rebound damping affect the minimum tire load in a most effective manner. The variation in the tire load caused by variations in the low-speed rebound damping is nearly twice that caused by the variation in the mid speed compression damping as measured at 6 Hz. Variations in the low speed compression damping yield the lowest effect on the minimum tire load.
- The normalized tire-lift off of the two-DOF quarter-car model reduces, with reduction in damping, except when near the natural wheel hop frequency, where the reduction of damping in both the mid speed compression and rebound results in slight increase in the lift off. The reduction in mid speed compression or rebound damping greatly decreases the tire lift off below the wheel hop frequency.
- The velocity response of the sprung mass is primarily dependent upon the damping coefficients. A reduction in low- and mid-speed damping yields improved

attenuation of sprung mass vibration in the frequency range between the two resonant frequencies. The lower damping, however, results in a slight increase of the sprung mass velocity response in the vicinity of the resonant frequencies, when subject to low amplitude excitation. Under high amplitude excitation, there is no cross over frequency and a decrease in damping yields improved performance throughout the frequency range. The low speed damping tends to be more effective at lower excitation amplitudes, while the response under higher excitation amplitudes is mostly influenced by the mid-speed damping.

- The variations in low speed damping, in general, yield a smaller but more consistent influence on all the performance indicators, while the variations in the mid speed damping result in larger variations of response characteristics
- The influence of variations in damper friction force on the response behavior is similar to that caused by variations in low speed damping, except in the case of average ride height.
- The symmetric nature of ideal friction model yields only slight variations in the ride height. Although, an increase in friction force yields enhanced ride height performance, the increase in equivalent low speed damping and the breakaway frequency deteriorate the overall performance. Friction force reduces the repeatability of the measurement of the static ride height of the car, which is often a critical reference for suspension tuning. An increase in friction force also increases the jerk of the masses, and interferes with the driver perception of the road holding properties of the tire.
- The average ride height and mechanical grip performance of the damper can be enhanced by increasing the fluid compliance. The vehicle ride quality, however, deteriorates with increased compliance. The fluid compliance further causes a time lag between the excitation and response, which affects transient response behavior and driver perception of the vehicle-road interactions.

- The variations in operating temperature result in substantial changes in the average ride height. Such effects thus need to be considered when tuning the suspension. An increase in temperature reduces the effective damping, resulting in enhanced mechanical grip and sprung mass vibration isolation.

6.4 ANALYSIS OF SIMPLIFIED DAMPER MODELS

In view of the complexities associated with characterization of friction, gas spring and damping forces, dynamic response characteristics of vehicle and suspension systems are frequently analyzed using a symmetric linear damping models [13,23-26,77]. Such simplified models often represent mean values of compression and rebound damping, and neglect the influences of gas spring, friction, and asymmetry in damping forces. Alternatively, simplified asymmetric piecewise linear damping models have been reported in a few published studies [56,78]. These simplified models are based upon peak force-peak velocity response characteristics of the dampers, while the contribution due to friction, fluid compliance and gas spring forces are considered negligible. In this study two simplified asymmetric models are developed using the measured characteristic curve for the Monotube Koni damper. In the first model (model I), asymmetric damping with constant rebound and compression damping coefficients, identified from the measured peak force-peak velocity data of the Koni damper, are used. The damping force, F_{d1}, is thus expressed as:

$$\begin{aligned} F_{d1} &= c_1 \dot{z}_1 \quad ; \quad \dot{z}_1 \geq 0 \\ F_{d1} &= c_2 \dot{z}_1 \quad ; \quad \dot{z}_1 < 0 \end{aligned} \tag{6.1}$$

where c_1 and c_2 are damping constants in compression and rebound, derived from the measured data. In the second model (model II), the damping coefficients corresponding to low- and mid-speeds in compression and damping are identified from the measured data. The damping force, F_{d2}, is then expressed as:

TABLE 6.7
SIMPLIFIED ASYMMETRIC DAMPER MODEL COEFFICIENTS

Model	Mode	Damping Coefficients (Ns/m)		Transition velocity (m/s)	R^2
		Low-speed	Mid-speed		
I	Compression	3421	3421	-	0.513
	Rebound	6434	6434	-	0.861
II	Compression	10510	1777	0.0727	0.975/0.995
	Rebound	11661	4369	-0.1129	0.917/0.998

$$
\begin{aligned}
F_{d2} &= c_1 \dot{z}_1 && ; \quad 0 \le \dot{z}_1 \le \alpha_c \\
F_{d2} &= c_1 \alpha_c + c_3 (\dot{z}_1 - \alpha_c) && ; \quad \dot{z}_1 > \alpha_c \\
F_{d2} &= c_2 \dot{z}_1 && ; \quad \alpha_e \le \dot{z}_1 \le 0 \\
F_{d2} &= c_2 \alpha_e + c_4 (\dot{z}_1 - \alpha_e) && ; \quad \dot{z}_1 < \alpha_e
\end{aligned}
\tag{6.2}
$$

where c_1 and c_2 are the low-speed compression and rebound damping coefficients, respectively; c_3 and c_4 are the respective mid-speed damping coefficients; α_c and α_e are the transition velocities in compression and rebound, respectively, at which low speed damping changes to mid-speed damping. The values of the damping coefficients derived from the measured data and the linear regression analysis are summarized in Table 6.7, together with corresponding R^2 values. Figure 6.44 illustrates a comparison of force-velocity characteristics of the two models with the measured data. The results presented in Figure 6.44 and Table 6.7 reveal that the model characterizes the damping curve more accurately.

The quarter-car simulator model comprising the simplified damper models are formulated as described in Chapter 5. The frequency response characteristics of the simplified models are evaluated for 0.32 cm displacement harmonic excitation, and compared with those derived from the comprehensive monotube damper model and the

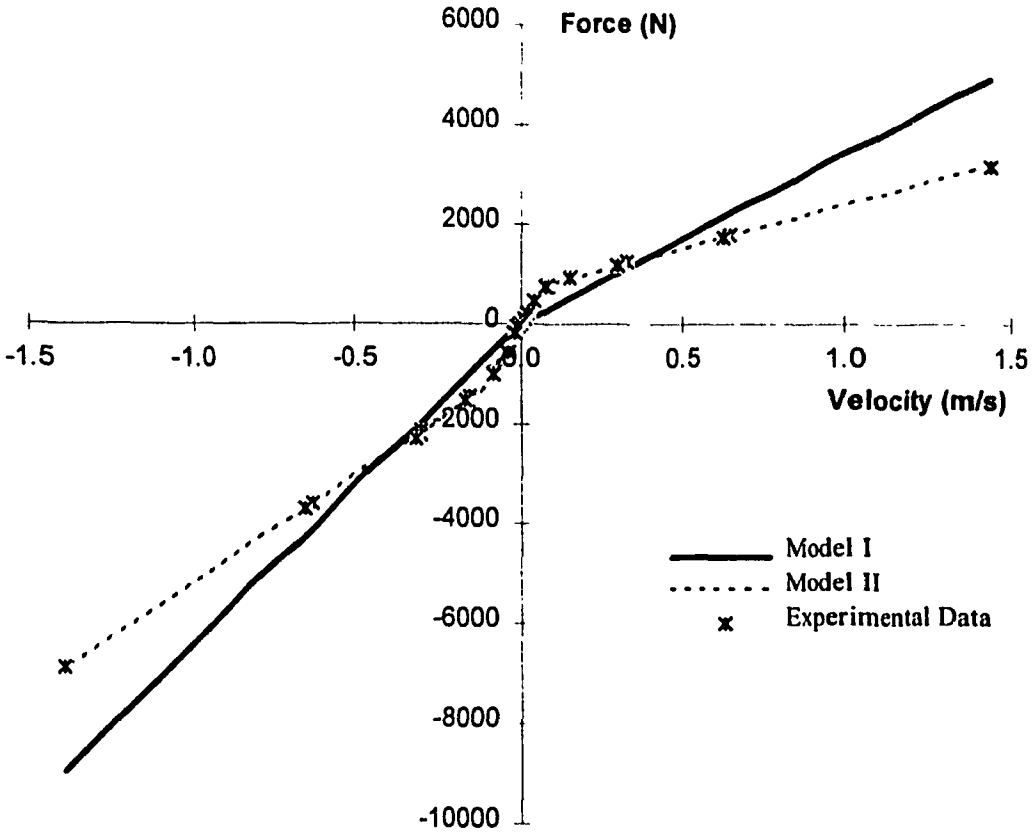

Figure 6.44 Comparison of force-velocity characteristics of the simplified damper models with experimental peak force-velocity data.

test data. Figure 6.45 illustrates the comparison of the average ride height response of the two simplified models with the measured data and that of the comprehensive model. It is evident that both simplified models yield considerable error in the average ride height response, specifically in the bias, which is primarily attributed to the gas spring effects. Model II, however, yields a pattern similar to that of the comprehensive model. The addition of bias due to gas spring force to the simplified model II can certainly enhance its accuracy.

The rms velocity ratio response of the sprung and unsprung masses of the simplified and comprehensive models are compared with the measured data in Figure 6.46. The velocity ratio response of both models deviate considerably from those of the comprehensive model. The simplified model I yields considerable deviations in the

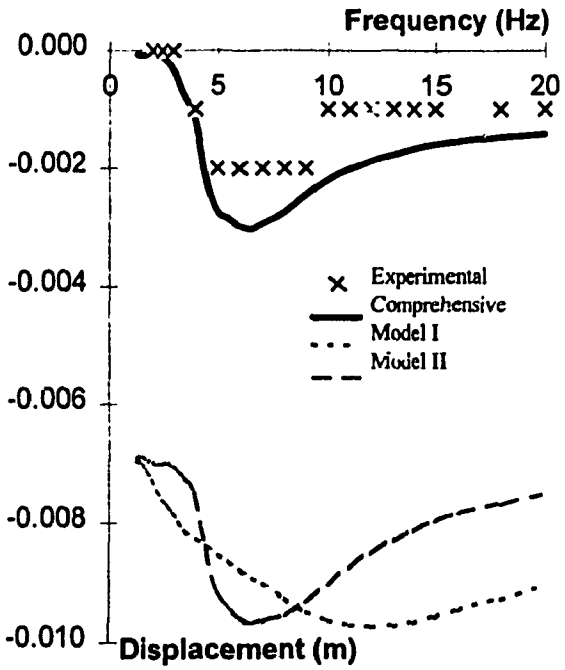

Figure 6.45 Comparison of average ride height response of the simplified and comprehensive damper models, and the experimental data.

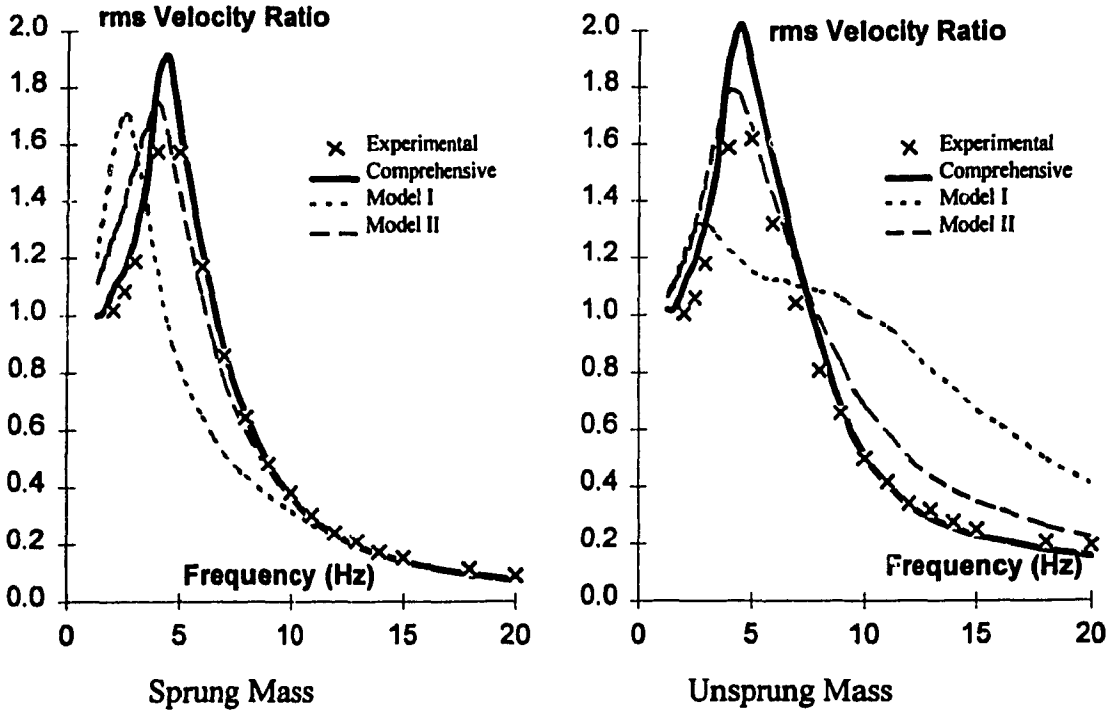

Figure 6.46 Comparison of response of the simplified and comprehensive damper models, and the experimental data.

sprung mass resonant frequency due to poor characterization of the low-speed and mid-speed damping. While the model II yields improved correlation of the natural frequencies and velocity response characteristics, the magnitude of error remains considerable.

From the results presented in Figures 6.44 to 6.46, it is evident that the representation of the damper force curve is paramount to achieving good correlation between the analytical and experimental results. The appropriate consideration of the gas spring force in the model, however, is vital to characterize the effects on the bias of the sprung mass. The effects of friction and fluid compliance are not readily noticeable in the results, which concurs with the observations made from the results of the parametric study. The influence of operating temperature, which is quite significant, can not be represented through the simplified models.

6.5 SUMMARY

The quarter-car model comprising the candidate damper model is validated using the experimental data for varying amplitudes of step and harmonic displacement excitation. A reasonably good correlation was obtained between the analytical and experimental response characteristics affecting the ride height, mechanical grip and ride quality performance. The results revealed poor performance due to high damping of Mechformance and Fox-heavy dampers. A performance criteria to assess the ride, handling, and traction performance of racing car dampers was formulated to study the influence of low- and mid-speed, compression and rebound damping, and temperature variations. The influence of variations in the friction force and fluid compliance on the performance criteria was observed to be less significant. Finally two simplified asymmetric damper models were developed and their validity was investigated under harmonic excitation. A comparison of response characteristics derived from simplified and comprehensive models demonstrated the significance of the comprehensive model

for accurate characterization. The simplified model comprising asymmetric low- and mid- speed damping constants, however, showed considerable potentials in estimating the rms velocity response.

CHAPTER 7

CONCLUSIONS AND RECOMMENDATIONS FOR FURTHER WORK

7.1 GENERAL

The lateral and longitudinal accelerations developed by a race vehicle constitute its primary performance measure. These accelerations, attributed to the road-holding ability of the vehicle, are dependent upon the performance characteristics of the suspension spring and dampers.

Although considerable developments in suspension dampers have been realized during the past few decades through repetitive field trials and tuning, the effective analytical models of the modern high performance dampers do not yet exist to perform the design and tuning in a cost effective manner. In this dissertation, analytical models of monotube and remote reservoir design of modern high performance dampers are developed through systematic component identification, laboratory experiments and parameter identifications.

The primary objectives of the study included: (i) development of various component models to enhance an understanding of the contributions due to gas spring, friction force, thermal expansion, fluid compliance, and low- and mid-speed asymmetric valving; (ii) development and analysis of total damper models to study the overall performance characteristics of dampers; (iii) development and analysis of damper models in a quarter-car configuration to investigate the influence of damper design parameters on the performance measures of a race-car; (iv) experimental study of candidate dampers and parameter identification; and (v) validation of analytical models under varying excitations arising from conventional test stand and quarter-car simulator. The major highlights of the study and the conclusion drawn are discussed in the following sections.

7.2 MAJOR HIGHLIGHTS OF THE INVESTIGATION

This dissertation research describes the methodologies for developing comprehensive dampers models based on the experimental data, for usage in vehicle models. Analytical models of different damper designs were developed and validated using the experimental data derived from a traditional test and a quarter vehicle simulator. The analytical models comprising various coefficients identified from the test data allow for an exact characterization of the dampers and their interactions with the vehicle. The methodology involves initial development of the damper models from the fundamental laws, and simplifications and refinements based upon validated assumptions to facilitate the determination of coefficients from the experimental data. The analytical models thus developed include the nonlinearities due to multi-stage asymmetric damping; friction force dependent upon the sign of velocity, operating temperature and displacement; gas spring forces as a function of initial volume and pressure, operating temperature and the variations in the effective volume of the oil; variations in the damping force caused by thermal expansion of the oil; fluid compressibility as a function of the pressure; and displacement limits.

A quarter-vehicle simulator is developed to validate the analytical model and to investigate the role of damper on the road-holding, and the dynamics of the sprung and unsprung masses. The friction properties of the guiding mechanism is identified and incorporated into the model. Nonlinearities arising from the displacement limits of the suspension and the tire lift off are also incorporated into the model. Four candidate damper models are thoroughly validated using the experimental data obtained under a wide range of excitations.

The major highlights and contributions of this investigation are summarized below:

1) A static test methodology is developed to determine the initial gas spring pressure and volume, and static breakaway friction properties of a damper. The proposed method

provides an highly accurate identification of the above parameters, and does not require the disassembly of the damper. The analytical model of the gas spring is further derived using the ideal gas laws.

2) A test methodology and the algorithms are developed to determine the effective volumetric change in the damper with variations in the operating temperature, which affects the gas spring and dynamic breakaway friction in a considerable manner. The proposed methodology is based upon experiments performed at low speeds. The effective volumetric change with variations in the operating temperature is analytically derived upon identifying the various coefficients of thermal expansion.

3) A methodology to determine the thermal sensitivity of the damping model is derived based on variations in density and thermal expansion of the fluid.

4) Analytical models of the hydraulic flows through multistage asymmetric valving are derived, incorporating the effects of fluid compliance, and the dampers coefficients are identified from the experimental data using an iterative procedure. A methodology to estimate the starting values for the analytical model is proposed, assuming incompressible flow at low levels of acceleration. A compliance model as a function of pressure is developed, for cases where a constant value is found to be inadequate.

5) Analytical models of the monotube and remote reservoir dampers are developed by comparing the model response with the experimental data obtained for a wide range of excitation frequencies and amplitudes, and varying thermal conditions.

6) A quarter car model, incorporating nonlinearities due to wheel lift-off, friction, displacement limits, and the damper is developed and a parameter identification is performed using the test data. Performance criteria are proposed in relation to the race cars average dynamic ride height variation, normalized time of tire contact and minimum tire load. The damper models in the quarter-car configuration are thoroughly validated using the experimental data obtained under different harmonic and step excitations.

7) Component models are analyzed under varying operating temperature conditions and excitations to demonstrate the thermal sensitivity of the damper, friction and gas spring forces. A comprehensive parametric study is performed using the quarter-car model to highlight the influence of various damper design and operating parameters on the performance criteria.

8) Two simplified asymmetric damper models are further developed in an attempt to reduce the complexities associated with identifying the displacement, friction and temperature dependence of the dampers. The response characteristics of the comprehensive model are compared with those of the simplified models to highlight their validity and significance of the different components.

7.3 CONCLUSION

The major conclusions drawn from the analytical and experimental studies are summarized below:

- The initial gas volume and pressure can be accurately determined from the static measurements, assuming ideal gas process. Under dynamic excitation the polytropic exponent of 1.38 resulted in very good correlation between the experimental and analytical gas spring force response in the range of working pressures of a high performance damper.
- The dynamic force developed by a suspension and damper is strongly influenced by the variations in operating temperature. The gas spring, in particular, is highly sensitive to temperature changes, an increase in temperature of 56°C results in a change of the magnitude of gas spring force of 250 N, and a 0.94 to 1.88 mm change in the ride height. The variations in gas spring pressure are attributed to: i) thermal expansion of the gas; and ii) the loss of gas volume due to expansion of the oil and damper components. In-general temperature variations result in relatively smaller variations in the damping force, the same 56°C change results in a 4.26% reduction in

rebound damping. The variations in the damping force with changes in the temperature are primarily due to changes in the fluid density.

- The assymetric multi-stage valving integrated into the high performance damper in-general yields different damping characteristics in three distinct speed ranges: low, mid and high. Low speed valving typically provides an orifice type flow with a high damping coefficient and can be accurately modeled by one of three models: i) orifice flow; ii) compensating valve flow; or iii) combined flow. Mid-speed damping yields a relatively low damping coefficient, based on flow through a compensating valve. High-speed valving is also orifice type flow, however, in-general it is effective at velocities that are outside the normal operating range of the race-car damper.
- The change in fluid pressure (gas and oil) caused by motion and the thermal expansion affects the friction, increase in pressure tends to increase the magnitude of friction.
- Coulomb friction force in-general is strongly dependent upon the sign of velocity and relative damper displacement. The frictional force is further influenced by the variations in temperature particularly for dampers with aluminum bodies and steel pistons.
- Variations in fluid compressibility influence the hydraulic flows through the valves and thus the damping and gas spring forces in an interrelated manner. The effects of compressibility increase with magnitude of acceleration. Furthermore the fluid compressibility becomes sensitive to the operating pressure, when the valving restriction is decreased to obtain high damping.
- The response characteristics of the undamped quarter-car simulator and the simulation model under a step excitation revealed strong influence to the direction and magnitude of the excitation, attributed to the spring preload and the gravitational effects.

- The percent overshoot of the sprung mass response and the settling time of the sprung and unsprung mass response are considerably larger under negative step excitation when compared to those obtained under positive excitation. This is attributed to the assymetric damping properties and tire-lift off. The settling time increases with increase in the magnitude of positive step excitation. Furthermore, the unsprung mass response exhibits larger overshoot than that of the sprung mass response for all the dampers.
- While the sprung and unsprung mass step response characteristics with the Koni damper reveal rapid decay, the Fox-light damper yields a slightly overdamped sprung mass response. The sprung mass response of the simulator with the stiff dampers (Fox with high setting and Mechformance) is similar to that of an overdamped S-DOF response, with long settling time and no overshoot, while the unsprung mass response is that of a lightly damped system, with increased settling time.
- The analytical models of the dampers and the simulator correlate very well with the experimental data. The errors between the two are attributed to the inconsistencies in friction.
- An increase in the harmonic excitation amplitude resulted in lower frequency for the peak response and decreased rms velocity response ratio, with the exception of the sprung mass response with the Fox-light damper. The magnitude of the peak response increased with an increase in the damping.
- The wheel-hop motion is reduced considerably with the installation of a damper, for which it only occurs at considerably large levels of excitation. The wheel hop motion, however, increases with high damping at higher amplitudes of excitation, indicating that tire lift-off can be reduced through selection of optimal damping properties. The Fox-light damper with the remote reservoir design resulted in minimal tire lift-off. The peak values of normalized tire lift-off ranged from 0.4 to 0.45 for all dampers.

- While the peak velocity response of the sprung mass is almost symmetric about zero, the magnitude of the unsprung mass velocity response is considerably higher in compression.
- The average ride height decreases with excitation frequency up to a frequency at which the variations approach a minimum, after which the ride height increases though it does not reach the static value. The variation in ride height increases with increase in damping and excitation amplitude. An increase in rebound to compression damping ratio yields larger variations in the ride height performance. With high rebound to compression damping ratio for the candidate dampers, the system packed down.
- Assymetric, multi-stage damping provides certain flexibility to tune the suspension based on the magnitude and direction of excitation. Variations in low-speed compression or rebound damping resulted in nearly consistent changes in the ride height over the entire frequency range, while the changes in mid-speed damping resulted in considerable variations in the ride height at higher damper velocities. The variations in rebound damping yields considerably larger variations in the ride height than those caused by proportional changes in the compression damping.
- The minimum tire force is strongly affected by variations in damping in the range of higher damper velocities (4 to 10 Hz). A reduction in damping results in increased minimum tire load at the tire-road interface. An increase in the low speed rebound damping affects the minimum tire load in a most effective manner. The variations in the minimum tire force caused by changes in the low-speed rebound damping are twice the magnitude of variation caused by proportional variations in the mid speed compression damping. The influence of variations in the low speed compression damping on the minimum tire load is relatively insignificant.
- The variations in the low speed damping, in general, yield a smaller but more consistent influence on all the performance indicators, while the variations in the mid

speed damping result in excessive variations in the response characteristics. The influence of variations in damper friction force on the response behavior is similar to that caused by variations in low speed damping, except in the case of average ride height.

- A reduction in low- or mid-speed damping yields improved vibration isolation of the sprung mass subject to low amplitude excitations in the frequency range between the two resonant frequencies, with a slight increase in the response in the vicinity of the resonant frequencies. Under high amplitude excitations, a decrease in damping yields improved performance throughout the frequency range.
- The characterization of fluid compliance and damper friction are extremely important to achieve good correlation between the analytical results and experimental data obtained from traditional test stands. The role of these factors, however is less significant when studying the response of a quarter-car model.
- The two simplified damper models yield considerable error in the average ride height response, specifically in the bias, which is primarily attributed to the gas spring effects. The model II, however, yields a pattern similar to that of the comprehensive model.
- The rms velocity ratio response of the sprung and unsprung masses of both simplified models deviate considerably from those of the comprehensive model. Model I yields considerable deviations in the sprung mass resonant frequency due to poor characterization of the low-speed and mid-speed damping. While model II yields improved correlation of the natural frequencies and velocity response characteristics, the magnitude of error remains considerable.
- In general, for the quarter car response, representation of the damper force curve is paramount to achieving good correlation between the analytical and experimental results. The appropriate consideration of the gas spring force in the model, however, is vital to characterize the effects on the bias of the sprung mass. The effects of

friction and fluid compliance are not readily noticeable in the results, which concurs with the observations made from the results of the parametric study. The influence of operating temperature, which is quite significant, can not be represented through the simplified models.

7.4 RECOMMENDATIONS FOR FUTURE WORK

Recommended further studies on the design and characterization of suspension dampers can be classified in two categories: those recommended to enhance the scope of the dissertation research, and those recommended to enhance the studies on the total vehicle suspension. The following efforts are recommended to enhance the scope of the dissertation research:

1) Enhance the damping models to increase the accurately characterize the transition from low to mid speed damping. The model would allow variation in the transition in order to achieve more accurate representation of the measured response.

2) Identify or develop instrumentation or signal amplification to better define the low speed forces, specifically, the friction and gas spring forces.

3) Develop friction force models for the damper and the quarter-car simulator to characterize the friction forces as a function of the velocity, and internal damper pressure.

4) Develop a more effective quarter-car simulator with reduced guiding friction to study the vertical dynamics of the suspension and the vehicle under more realistic conditions.

5) Replace the valving models used in this investigation by models of the generic valves to permit the study of different designs.

6) A hardware-in-the-simulation test and analysis tool is highly desirable to investigate the interactions of different dampers with the vehicle models in an efficient manner. This tool would further facilitate the tuning of the suspension in the laboratory.

The models developed can be incorporated into such tools as the damper model for hardware-in-the-simulation test of other suspension components.

The following further studies are recommended to enhance the performance characteristics of the total vehicle suspension:

1) Develop analytical models of the suspension and damper incorporating the mechanical advantage between the wheel and damper-spring assembly in a quarter vehicle model.

2) Investigate the role of the damper on the overall race-car performance through development and analysis of multi-DOF full scale vehicle models, allowing the study of the influence of dampers and the temperature sensitivity on the traction, ride and cornering performance.

3) Response analysis of the vehicle and suspension damper under stochastic road excitation is vital to evaluate the performance behavior of different designs.

REFERENCES

1. Smith, C., "Tune to Win", Osprey Publishing Limited, London, 1987.

2. Puhn, F., "How to Make Your Car Handle", HP Books, Tucson, AZ, 1981.

3. Van Valkenburg, P., "Race Car Engineering and Mechanics", Paul Van Valkenburgh, Seal Beach, CA, 1992.

4. Staniforth, A., "Competition Car Suspension", Haynes Publishing Group, Somerset, England, 1988.

5. Smith, C., "A Quiet Evolution", RACECAR ENGINEERING, Vol. 2, No. 4, 1992, pp. 20-26.

6. Crahan, T., "Modeling Steady-State Suspension Kinematics and Vehicle Dynamics of Road Racing Cars-Part I: Theory and Methodology", SAE Technical Paper No. 942505, SAE Publication P-287, Presented at the '1994 Motor Sports Engineering Conference and Exposition', Dearborn, December 5-8, 1994, pp. 179-212.

7. Crahan, T., "Modeling Steady-State Suspension Kinematics and Vehicle Dynamics of Road Racing Cars-Part II: Examples", SAE Technical Paper No. 942506, SAE Publication P-287, Presented at the '1994 Motor Sports Engineering Conference and Exposition', Dearborn, December 5-8, 1994, pp. 213-234.

8. Jonasch, R., "Computer-Aided Vehicle Design Synthesis for Handling and Stability", Master Thesis, Concordia University, Montreal, Quebec, 1991.

9. Milliken, W.F., Milliken, D., L., "Race Car Vehicle Dynamics", SAE, R-146, Warrendale,. Pa., Ch 1, 1994, p. 811.

10. Morris Nunn, Chief Engineer Uno Racing, interviewed at P.I.R., " Speed Week", T.S.N., Feb.9, 1991.

11. Patrick Head, Chief Engineer Williams Grand Prix Racing, Personnel conversation, Montreal, June 9 1990.

12. Wright, P.G., "The Influence of Aerodynamics on the Design of Formula One Racing Cars", International Journal of Vehicle Design, 3(4), pp. 383-397, 1982.

13. Kasprzak, J. L., Floyd, R. S., "Use of Simulation to Tune Race Car Dampers", SAE Technical Paper No. 942504, SAE Publication P-287, Presented at the '1994 Motor Sports Engineering Conference and Exposition', Dearborn, December 5-8, 1994, pp. 171-178.

14. Simanaitis, D., "Shock Absorbers", Automotive Engineering, November 1976, pp. 34-39.

15. Jackson, G.W., "Fundamentals of the Direct Acting Shock Absorber", SAE Technical Paper No. 37R, Presented at the 'SAE National Passenger Car, Body and Materials Meeting', March 16-18, 1959.

16. Yukimasa T., et al., "Comments on Oil Seals for Gas Pressurized Shock Absorbers of Automotive Suspensions", SAE Technical Paper No. 850333, 1985, pp. 85-94.

17. Lang, H.H., "A Study of the Characteristics of Automotive Dampers at High Stroking Frequencies", Ph.D. Thesis, University of Michigan, Ann Arbor, Michigan, 1977.

18. Segel, L., and Lang, H.H., "The Mechanics of Automotive Hydraulic Dampers at High Stroking Frequencies", IAVSD Extensive Summaries, Vehicle System Dynamics, pp. 82-85,(Proceedings of the 7th IAVSD Symposium), 1981.

19. Anderson, R. J., and Fan, Y., "Dynamic Testing and Modeling of a Bus Shock Absorber", SAE paper no. 902282

20. Karadayi, R., Masada, G. Y. ,"A Nonlinear Shock Absorber Model", Proceedings of SCGVTS, ASME Winter Annual Meeting, Dec., 1986, Anaheim, Cal., pp 149-165.

21. Moline, D., et al., "Simulation and Evaluation of Semi-Active Suspensions", SAE Technical Paper No., 1994.

22. Reybrouck, K., "A Non Linear Parametric Model of an Automobile Shock Absorber", SAE Technical Paper No. 940869, 1994.

23. Sharp, R. S., and Hassan, S. A., "The Relative Performance Capabilities of Passive, Active and Semi-Active Car Suspension Systems", Proceedings of the Institution of Mechanical Engineers, Vol. 200, No. D3, pp. 219-228, 1986.

24. Horton, D. N. L., and Crolla, D. A., "Theoretical Analysis of a Semi-Active Suspension Fitted to an Off-Road Vehicle", Vehicle System Dynamics, 15, pp. 351-372, 1986.

25. Crolla, D. A., Horton, D. N. L., Pitcher, R. H., and Lines, J. A., "Active Suspension Control for an Off-Road Vehicle", Proceedings of the Institution of Mechanical Engineers, Vol. 201, No. D1, pp. 1-10, 1987.

26. Hendrick, J. K., and Butsuen, T., "Invariant Properties of Automotive Suspensions", Proceedings of the Institution of Mechanical Engineers, Vol. 204, Part D: Journal of Automobile Engineering, pp. 21-27, 1990.

27. Sharp, R. S., and Hassan, S. A., "An Evaluation of Passive Automotive Suspension Systems with Variable Stiffness and Damping Parameters", Vehicle System Dynamics, 15, pp. 335-350, 1986.

28. Hall, B. B., and Gill, K. F., "Performance of a Telescopic Dual-tube Automotive Damper and the Implications for Vehicle Ride Prediction", Proceedings of the Institution of Mechanical Engineers, Vol. 200, No. D2, pp. 115-123, 1986.

29. Rakheja, S., Su, H., and Sankar, T. S., "Analysis of a Passive Sequential Hydraulic Damper for Vehicle Suspension", Vehicle System Dynamics, 19, pp. 289-312, 1990.

30. van Vliet, M., "Computer Aided Analysis & Design of Off-Road Motorcycle Suspensions", Ph.D. Thesis, Concordia University, Montreal, Quebec, 1983.

31. van Vliet, M., Sankar, S., "Computer-Aided Analysis and Experimental Verification of a Motorcycle Suspension", Transactions of the ASME, Journal of Vibration, Stress, and Reliability in Design, Vol. 105, No. 1, January, 1983. pp. 120-131.

32. van Vliet, M., Sankar, S., Bapat, C., "Frequency and Time Domain Analysis of Off-Road Motorcycle Suspension", Shock and Vibration Bulletin, Vol. 53, No. 3, May 1983, pp. 35-49.

33. Joo, F., "Dynamic Analysis of a Hydropneumatic Suspension System", Master Thesis, Concordia University, Montreal, Quebec, 1991.

34. Yabuta, K., Hidaka, K., Fukushima, N., "Effects of Suspension Friction on Vehicle Riding Comfort", IAVSD Extensive Summaries, Vehicle System Dynamics, pp. 85-91,(from the Proceedings of the 7th IAVSD Symposium), 1981.

35. Ilosvai, L., Szucs; B., "Random Vehicle Vibrations as Effected by Dry Friction in Wheel Suspensions", Vehicle System Dynamics, 1, pp. 197-209, 1979.

36. Sano, S., "Evaluation of Motor Vehicle Handling", International Journal of Vehicle Design, 3(2), pp. 171-189, 1982.

37. Loos, H., and Dodlbacher, G., "A Mathematical 'Prototype' of the Vehicle to Describe Vehicle Handling Behavior", IAVSD, Extensive Summaries, Vehicle System Dynamics, pp. 61-68,

38. Morman, K. N., and Giannopoulos, F., "Recent Advances in the Analytical and Computational Aspects of Modeling Active and Passive Vehicle Suspensions", in; Computational Methods in Ground Transportation Vehicles, M. M. Kamal and J. A. Wolf Jr., Eds., ASME AMD Vol. 50, American Society of Mechanical Engineers, New York, 1983.

39. Sharp, R. S., and Crolla, D. A., "Road Vehicle Suspension System Design - a Review", Vehicle System Dynamics, 16, pp. 167-192, 1987.

40. Bernard, J., Vanderploeg, M., and Shannan, J., "Recent Developments in Vehicle Dynamics", Journal of Shock and Vibration Digest, Vol. 19, No. 4, April, pp. 10-16, 1987.

41. Rakheja, S., van Vliet, M., Sankar, S., "A Discrete Harmonic Linearization Technique for Simulating Nonlinear Mechanical Subsystems", Journal of Sound and Vibration, 100(4), pp. 511-526, 1985.

42. Ibid. 9, Ch 1.

43. Lizell, M., "Dynamic Leveling for Ground Vehicles", Ph.D. Thesis, Royal Institute of Technology, Stockholm, Sweden, p.20, 1990.

44. Satchel, T. S., Indy Race Car Engineer, Telephone Interview, December 13 1995.

45. Rathwell, D., Race Engineer, Yamaha Motorsports USA, Telephone Interview, March 28 1994.

46. Mitchell, W., "Shock Tactics", On Track, Vol. 11, No. 2, p.60, February 8, 1991.

47. "Shock Absorber/McPerson Strut Manual", Arvin Ride Control Products, January 1995.

48. Japanese Automobile Standards Organization, "Telescopic Shock Absorbers for Automobiles", C 602-83, rev. March 17, 1983, Society of Automotive Engineers of Japan, Inc.

49. Hancock, D., Product Design Engineer, Chrysler Corporation, Personnel Interview, December 12 1995.

50. Warner, B., Sankar, S., "Influence of Temperature Variations on the Performance Characteristics of Shock Absorbers-An Experimental Approach", Proceedings CSME Forum SCGM 1992, Vol.1, pp. 87-92, 1992.

51. Warner, B., "Adjustable Damper Means for Shock Absorber", United States Patent No. 4872537, October 10 1989.

52. Hanselmann, H., "Hardware-in-the -Loop Simulation as a Standard Approach for Development, Customization, and Product Test", SAE Technical Paper No. 930207, Presented at the 'International Congress and Exposition, March 1-5, 1993.

53. Rakheja, S., Director, CONCAVE Research Centre, Concordia University, Telephone Interview, December 12 1995.

54. Ivers, D. E., Lane, R. M., "Experimental Comparison of Passive, Semi-Active On/Off, and Semi-Active Continuous Suspensions", SAE Technical Paper No. 892484.

55. Rengarajan, S., "An Analytical and Experimental Investigation on the Vibration Isolation Performance of Semi Active Suspension", Master Thesis, Concordia University, Montreal, Quebec, 1991.

56. Ahmed, A. K. W., Rakeja, S., Richard, M. J., "Frequency Response Analysis of Symmetric and Asymmetric Vehicle Suspensions", Proceedings CSME Forum SCGM 1992, Vol.1, pp. 134-139, 1992.

57. Bastrow, D., "Friction in Suspensions", Proceedings of the Institution of Mechanical Engineers, Vol. 188, Part (D): Journal of Automobile Engineering, pp. 21-24, 1974.

58. Otis, D. R., Pourmovahed, A., "An Algorithm for Computing Nonflow Gas Processes in Gas Springs and Hydropneumatic Accumulators", Transactions of the ASME, Journal of Dynamic Systems, Measurement and Control, Vol. 107, March 1985, pp. 93-95.

59. Els, P. S., Grobbelaar, B., "Investigation of the Time- and Temperature Dependency of Hydro-Pneumatic Suspension Systems", SAE Technical Paper No. 930265, International Congress and Exposition, March 1-5, 1993.

60. Kuhns, J., Senior Engineer, Arvin Ride Control Products, Personnel Interview, January, 1995.

61. "Product Information Lubricants and Specialties", 5th ed., Esso Petroleum Canada, 1985.

62. Ibid. 17, p.89.

63. Ibid. 17, pp. 20-23.

64. Su, H., "An Investigation of Vibration Isolation Systems Using Active, Semi-Active and Tunable Passive Mechanisms With Applications to Vehicle", Ph.D. Thesis, Concordia University, Montreal, Quebec, 1990.

65. Hanly, F. J., "Fluids for High-Pressure Industrial Hydraulic Systems", SAE Technical Paper No. 670697, 1967.

66. Mayne, R. W., "The Effects of Fluid and Mechanical Compliance on the Performance of Hydraulic Shock Absorbers", Transactions of the ASME, Journal of Engineering for Industry, February 1974. pp. 101-106.

67. Wahi, M. K., "Oil Compressibility and Polytropic Air Compression Analysis for Oleopneumatic Shock Struts", Journal of Aircraft, Volume 13, Number 7, 1976, pp. 527-530.

68. Ibid. 33, p 43.

69. Sharp, R. S., and Hassan, J. H., "Performance Predictions for a Pneumatic Car Suspension System", Proceedings of the Institution of Mechanical Engineers, Vol. 202, No. D4, pp. 243-250, 1988.

70. Warner, B., Rathwell, D., "Computer-Aided Engineering of Championship Winning Linkage Suspension", SAE Technical Paper No. 942511, SAE Publication P-287, Presented at the '1994 Motor Sports Engineering Conference and Exposition', Dearborn, December 5-8, 1994, pp. 251-258.

71. Thomson, W. T., "Theory of Vibration With Applications", 2nd ed., Prentice-Hall, Englewood Cliffs, N.J., 1981.

72. Ibid. 9 p. 811.

73. Thompson, A. G., "Suspension Design for Optimum Road Holding", SAE Technical Paper No. 830663, International Congress and Exposition, February 28-March 4, 1983.

74. Fukushima, N., Hidaka, K., and Iwata, K., "Optimum Characteristics of Automotive Shock Absorbers Under Various Driving Conditions and Road Surfaces", Int. J. of Vehicle Design, vol. 4, no. 5, 1983, pp. 463-472.

75. Dominy, J. A., and Dominy, R. G., "Aerodynamic Influences on the Performance of the Grand Prix Racing Car", Proceedings of the Institution of Mechanical Engineers, Vol. 198, Part D, No. 7, pp 87-93, 1984.

76. Barek, P., "Magic Numbers in Design of Suspensions for Passenger Cars", SAE Technical Paper No. 911921, Passenger Car Meeting and Exposition, Nashville, TN., Sept. 16-19, 1991.

77. Floyd, R. S., Law, H. E., "Simulation and Analysis of Suspension and Aerodynamic Interactions of Race Cars", SAE Technical Paper No. 942537, SAE Publication P-287, Presented at the '1994 Motor Sports Engineering Conference and Exposition', Dearborn, December 5-8, 1994, pp. 341-352.

78. Woodrooffe, J., "Heavy Truck Suspension Damper Performance for Improved Road Friendliness and Ride Quality", SAE Technical Paper No. 952636, SAE Publication P-1128, 1995, pp. 49-54.